ESTIMATION OF THERMAL PROPERTIES IN A MEDIUM WITH CONDUCTION AND RADIATION HEAT TRANSFER

by

Jerome Hamilton Guynn

Thesis submitted to the Faculty of the

Virginia Polytechnic Institute and State University

in partial fulfillment of the requirements for the degree of

MASTER OF SCIENCE

in

Mechanical Engineering

APPROVED: Claire P Scott

Dr. Elaine P. Scott, Chairperson

J R Mahan

Dr. J. R. Mahan

James R. Thomas

Dr. J. R. Thomas

July, 1996
Blacksburg, Virginia

Keywords: Parameter Estimation, Heat Transfer, Conduction, Radiation, Foam

ESTIMATION OF THERMAL PROPERTIES IN A MEDIUM WITH CONDUCTION AND RADIATION HEAT TRANSFER

by

Jerome H. Guynn

Committee Chairperson: Dr. Elaine P. Scott
Mechanical Engineering

ABSTRACT

The simultaneous estimation of multi-mode heat transfer properties, conductive and radiative, is investigated for materials that include significant heat transfer by radiation. The focus is on insulative type materials with a relatively large optical thickness. Two basic models were developed for the combined conduction and radiation heat transfer: a diffusion solution and a more exact absorbing and isotropically scattering solution. Both solutions were written for one-dimensional heat transfer in gray, isotropically scattering materials. Different experimental setups were compared through a sensitivity analysis of the parameters to determine the best experiment for estimating the properties.

An experiment was performed to collect real data to verify estimation procedures. The material used for the experiment was Styrofoam and the experiment consisted of a heat flux supplied by a thin film heater on one boundary and a constant temperature on the other boundary. The thermal capacitance of the heater proved to have an effect on the temperature measurements at the heated surface and had to be incorporated into the model.

The estimation procedure involved the use of two methods, the modified Box-

Kanemasu algorithm and a genetic algorithm. Difficulties were encountered in simultaneously estimating all the properties due to correlation between the thermal conductivity and the radiation parameters, as well as some correlation between the heat capacity of the Styrofoam and the heat capacity of the heater. However, the genetic algorithm did provide fairly narrow and well-defined property ranges and confirmed that radiation transfer was significant in the Styrofoam.

Acknowledgments

I would like to thank the following people for their assistance in achieving this degree:

Dr. Elaine Scott, my advisor, for her help, advice, and overall guidance in obtaining my Masters degree. I especially appreciate the freedom and responsibility she has given me in performing this research; it has been a pleasure working with her.

Dr. J. R. Mahan and Dr. J. R. Thomas for serving on my committee, reviewing my thesis, and giving suggestions on my work.

Sandrine Garcia, for helping me with the genetic algorithm and for her discussions and suggestions on my research.

Jim, Greg, and all the people at the lab for their help with the data acquisition and the computers.

My parents, Patricia Hamilton and Jesse Guynn, for the support they have given me throughout my engineering education.

And last, but foremost, my wife, Elizabeth, for all her love and understanding. Thank you for your support, your patience during my writing, and for the photographs of the Styrofoam.

Table of Contents

List of Tables

List of Figures

Nomenclature

a	absorption coefficient (m^{-1})
b	constant for radiation portion of k_{eff}, $16\sigma/3\beta$, (W/mK^4)
b	estimated parameter matrix
c	volumetric heat capacity, ρc_p, (KJ/m^3K)
c_p	specific heat (KJ/kgK)
D	thickness of layer (m)
$E_n(x)$	exponential integral function, $\equiv \int_0^1 \mu^{n-2} \exp\left(\frac{-x}{\mu}\right) d\mu$
G	scalar factor for Box-Kanemasu estimation
h	scalar interpolation factor for Box-Kanemasu estimation
I'	dimensionless source function
I'	radiation source function (W/m^2)
k	thermal conductivity (W/mK)
k_{eff}	effective thermal conductivity, $k + bT^3$, (W/mK)
K	kernel of a Fredholm integration equation
M	number of quadrature points
n	total number of measurements
N	number of x locations or mesh points
N_r	conduction-radiation parameter

p	total number of parameters
$\boldsymbol{P}$	Gaussian estimation vector, $\boldsymbol{X}^T\boldsymbol{X}$ for OLS estimation
q	energy flux (W/m^2)
q_c	heat flux due to conduction (W/m^2)
q_r	heat flux due to radiation (W/m^2)
q_a	applied heat flux (W/m^2)
q_r	radiative flux (W/m^2)
q_{r0}	radiative flux at x = 0 (W/m^2)
r	root mean squared (RMS) residual, $\sqrt{S/n}$
S	sum of squares
t	time (s)
T	temperature (K)
TC	thermocouple
T_r	reference temperature (K)
w	Gauss-Legendre weight functions
x	direction across layer (m)
$\boldsymbol{X}$	sensitivity coefficient matrix
X^+	dimensionless sensitivity coefficient
X^*	semi-dimensionless sensitivity coefficient, $p\frac{\partial \eta}{\partial p}$
Y	measured independent variable
$\mathbf{Y}$	measured independent variable vector
z	under-relaxation factor

Greek

α	grouping of parameters for heat flux B.C., $4N_r/(1-\Omega)\kappa_D$
β	extinction coefficient, $(a + \sigma_s)$, (m^{-1})
β_p	general parameter in estimation
β_p	parameter matrix
ϵ	emissivity
κ	optical thickness, $(a+\sigma_s)x$
η	dimensionless coordinate
η_p	calculated dependent variable
η_p	calculated dependent variable vector
Ω	scattering albedo, $\sigma_s/(a+\sigma_s)$
σ	Stephan-Boltzman constant
σ_s	scattering coefficient (m^{-1})
τ	grouping of time-related parameters
Θ	dimensionless temperature, T/T_r

Subscripts

0	at beginning of layer, x = 0
1	first x location; first quadrature point
a	applied
D	at end of layer, x = D
h	heater

I ith x location; ith measurement; incoming

m mth quadrature point

n nth quadrature point

o outgoing

p pth parameter

r reference

Superscripts

k kth iteration in estimation

l lth iteration in numerical heat transfer solution

p pth time step

Chapter 1

Introduction

Radiation can be a major source of heat transfer within certain materials, most noticeably porous materials, such as insulations, and glass materials, including ceramics. In the former, the radiation is absorbed and scattered by cell walls or fibers and is transmitted across gas spaces within the material, while the latter is transparent to certain radiation wavelengths. Heat conduction is proportional to the temperature difference, but radiation is proportional to the temperature to the fourth power, resulting in cases where radiation through a medium is not only significant, but dominant. An analysis which ignores the radiation component could give erroneous temperature histories and inaccurate heat fluxes.

The mechanism of this energy transfer is fairly well understood, and with the advent of digital computers numerous methods of solution have been developed. However, much less is known regarding the specific radiation properties of materials; while tables of radiative surface properties exist in the literature, few references exist for properties relating to radiation transfer through a material. Semi-transparent materials appear in many areas of advanced technologies, such as insulation for re-entry vehicles, ceramic components for

engines, and fibrous composites for a variety of high temperature applications. Furthermore, new materials for these applications are continuously being created and all the thermal properties, including conduction properties, are unknown. Finally, it would be an advantage to estimate the properties using a relatively simple heat transfer experiment without resorting to spectral analysis that requires use of equipment that is costly, complicated, and in many cases unavailable to the practicing engineer. The scope of this research was simultaneously estimating conductive and radiative thermal properties in a low thermal conductivity medium with combined conduction and radiation heat transfer.

This research focused on gray materials largely without anisotropic scattering. The goal of the research was to investigate the feasibility of simultaneously estimating both conductive and radiative thermal properties in such a material, and the specific objectives were to:

1) develop a simple but realistic model for combined conduction and radiation transfer in a gray, absorbing and isotropically scattering medium,

2) analytically investigate the optimization of experiments and estimation of properties using sensitivity analyses for insulative-type materials with radiation heat transfer,

3) perform a one-dimensional experiment to obtain temperature histories in an

actual material, Styrofoam, for use in estimating properties,

4) and estimate the following properties of Styrofoam: thermal conductivity, volumetric heat capacity, absorption coefficient, and scattering coefficient.

The first objective involves the application of suitable models to determine the temperature solution in the material. Radiation calculations can be extremely complicated due to wavelength dependence, temperature dependence, the importance of geometry, and the integral nature of radiation. Simplifications are generally made, relying on the semi-opaque nature of the medium, but over-simplification can miss the physics of the problem and lead to inaccuracy. Two different, basic models were examined. The materials considered were for the most part optically thick, though some analysis is presented for optically thin media that meet the assumptions used to derive the models.

The second objective was the investigation of an optimal experiment to estimate the properties. An optimum experiment is one that provides the most information about the properties from the measurements and allows the properties to be estimated with a minimum of uncertainty. The boundary conditions, method of heating, sensor location, and other experimental parameters can greatly influence the accuracy of the estimates, or indeed, can prevent them from being made at all.

Thirdly, an experiment was developed to collect a temperature history for use in estimating the properties. The experiment consisted of a one-dimensional, transient setup

with an applied heat flux at one boundary and a constant temperature at the opposite boundary. The temperatures were measured using thermocouples and the data collected via a digital data acquisition system connected to a personal computer.

Finally, the data were used to estimate the four properties by employing two estimation algorithms: the modified Box-Kanemasu method and a genetic algorithm. Simultaneously estimating several properties is not only efficient, but estimating only one property entails developing an experiment that does not depend on other unknown properties. Often, however, it can be difficult for a parameter estimation algorithm to find a unique set of properties, resulting in high uncertainty and estimates that do not converge. The Box-Kanemasu failed to provide estimates for this case, but the genetic algorithm succeeded due to the robustness of the method.

Chapter 2

Literature Review

The purpose of this study was to investigate the simultaneous determination of thermal properties in a medium that has combined conduction and radiation heat transfer. The investigation consisted of developing a heat transfer solution, finding optimal experiments, performing an experiment with a test material, and estimating parameters. The test material consisted of a layer of molded polystyrene beads (Styrofoam). Each of these areas has been reviewed and summarized here.

2.1 Combined Conduction and Radiation Heat Transfer

The problem of combined conduction and radiation transfer in a participating medium is quite complex due to the coupling of the conduction and radiation, the integral nature of radiation, and the wavelength dependence of radiation. Simplifications are generally made, but care must be taken to capture the physics of the problem. The advent of the digital computer has made numerical solution of complex equations possible and numerous methods exist for solving the one-dimensional problem, as well as more complex geometries. Formulations of the problem of combined heat transfer in a medium can be

found in Özişik (1973) and Siegel and Howell (1992), and the latter contains a comprehensive review of current solution methods.

One of the more restricted models is the diffusion model, detailed in Siegel and Howell (1992), which assumes an optically thick medium and basically reduces the problem to an effective thermal conductivity composed of a constant term and a term that depends on the temperature to the third power. The radiation is reduced to one parameter, the extinction coefficient, that describes the attenuation of the radiation in the medium. The diffusion solution assumes a temperature-independent mean extinction coefficient and diffuse radiation. These restrictions limit the applicability of the model to regions away from the boundaries. Caps et al. (1984) performed extensive analytical and experimental work on glass fibre papers that utilized the diffusion solution. They calculated a Rosseland mean extinction coefficient from both a spectral extinction coefficient, calculated using Mie theory, and spectral transmittance and reflectance measurements. Good agreement was found between theory and experiment. They also performed Monte Carlo simulations which demonstrated that the diffusion solution could be applied to an anisotropically scattering medium and could be applied very close to the boundaries, provided the spectral nature of the extinction coefficient and the first moment of the scattering phase function are known and used to compute the mean extinction coefficient.

Hamaker (1947) developed a two-flux model that idealized the radiation as propagating in the forward and backward directions, for a gray, non-absorbing material and steady-state conditions. Larkin and Churchill (1959) utilized this method in examining the heat transfer in Fiberglass, Styrofoam, and Foamglas. Linford et al. (1974) extended this

model to four fluxes, which took into account the dependence of the scattering on the temperature of the two surfaces of a slab. They used this model and spectral measurements of transmittance and reflectance to investigate the thermal conductivity of fibrous insulations. These two- and four-flux models have the disadvantage, in addition to considering only steady state, of only predicting the heat flux through the material and not the temperature distribution. However, extensions have been made to utilize *n*-flux models in transient problems and obtain temperature distributions, such as the use of a two-flux model by Tong et al. (1986) for combined conduction and radiation in porous insulating materials.

Viskanta (1962) numerically solved the steady-state combined conduction and radiation problem exactly for a planar, gray, absorbing and emitting, but nonscattering medium between two isothermal plates using an iterative method and compared the results to both the diffusion solution and the Milne-Eddington approximation for the radiation intensity. This solution was extended by Viskanta (1965) for scattering as well as absorbing media. Ho and Özişik (1987) solved the steady-state problem for a two-layer, gray, absorbing and isotropically scattering planar medium with nonzero reflectivities on both sides of the interface. Siewert and Thomas (1990) used the P_N, or spherical harmonics, method to develop a solution for steady-state heat transfer in a planar medium that included anisotropic scattering and specularly or diffuse reflecting boundaries. The scattering phase function was represented by a finite Legendre polynomial and the solution was solved numerically using an iterative process. Siewert (1995) improved on the iteration scheme using a form of Newton's method; this improvement allowed the solution to converge for

some particular cases for which it previously diverged.

Hazzah and Beck (1970) investigated transient one-dimensional transient heat transfer for a gray, absorbing, isotropically scattering medium. The solution involved reducing the integral formulation of the radiation terms to fourth-order nonlinear differential equations, reducing the complexity of the problem. The differential equations were solved using implicit finite differences. Lii and Özişik (1972) solved a similar case with reflective boundaries using a Case normal-mode expansion technique for the radiation. Tsai and Nixon (1986) solved the transient temperature distribution in a multi-layer wall for a gray, absorbing, nonscattering planar medium exposed to a heat flux on one surface and convection on both surfaces. A finite-difference was used for the space variable, a fourth-order Runge-Kutta method for the time variable, and Simpson's method combined with a Gauss-Seidel matrix solution for the radiation equations. Siegel (1992) utilized a finite-difference solution to solve the transient cooling of a gray, nonscattering, semi-transient layer in a vacuum.

2.1.1 Heat Transfer in Foams

Skochdopole (1961) found that a significant portion of the heat transfer in foams was due to radiation and that convection was negligible for cell sizes less than 4 mm. Valenzuela (1981) also showed that convection was negligible and that most previous models had underestimated the radiative heat transfer of foams.

A great deal of research has been done at the Massachusetts Institute of Technology on determining the heat transfer through polyurethane foams. Glicksman and Schuetz (1984)

found that the general assumption of opaque cell walls was invalid and that polyurethane foams behave approximately gray at large (5-30 μm) wavelengths. Furthermore, they reported the foams were largely absorbing and scattered radiation only moderately anisotropically. They used spectral transmission measurements to determine a mean extinction coefficient and concluded that a diffusion approximation could be used to model the radiation transfer with only 10 to 15 percent loss in accuracy. Radiation was determined to account for about 25 percent of the heat transfer in foams at room temperature. Glicksman et al. (1986) compared detailed measurements of transmissivity and scattering in foams and fiber glasses. It was found that for foams of large optical thickness (approximately 10 or greater), the scattering albedo had a small effect on the solution and the medium could be analyzed with the diffusion solution. Foam extinction coefficients were accurately determined using conventional spectrometers, but fiberglass required the use of hemispherical collection systems due to the much larger scattering contribution.

2.2 Optimization of Experiments

The design of an experiment can be influenced to provide greater accuracy through the choice of design parameters. A well designed experiment will provide property estimates with a higher degree of certainty and confidence.

Beck and Arnold (1977) list several optimization techniques, which are designated by letters. These techniques all deal with the sensitivity coefficient matrix and the determinant of its transpose, $|\mathbf{X}^T\mathbf{X}|$, which is a component of the covariance matrix of the

estimate vector. The D-optimal criterion attempts to maximize the determinant of $\mathbf{X}^T\mathbf{X}$, the C-optimal method maximizes the minimum eigenvalue of $\mathbf{X}^T\mathbf{X}$, and the A-optimal method maximizes the trace of $\mathbf{X}^T\mathbf{X}$.

The D-optimal method was used by Beck (1969) to optimize an experiment for measuring heat capacity and thermal conductivity and by Taktak et al. (1991) to optimize the number of sensors, the sensor locations, and the heating time for estimating thermal properties in carbon-fiber/epoxy-matrix materials. Moncman (1994) used this criterion to develop experiments for measurements of directional-dependent thermal conductivities in composites and her work was verified experimentally by Hanak (1995). Both of these references provide an extensive review of experimental optimization for determination of heat capacity and thermal conductivity.

2.3 Simultaneous Estimation of Parameters

Parameter estimation is a broad discipline that seeks to determine the properties or parameters of a system given a valid model and a set of measurements. Estimation algorithms seek to minimize an objective function, generally the sum of squares, which compares calculated data to measured data. Beck and Arnold (1977) give a review of some of the more common methods.

Gauss linearization is one of the simplest techniques of nonlinear estimation that works well on problems with well defined minima and reasonable initial estimates. An

improvement on both the speed and robustness of convergence was made by Box and Kanemasu (1972) by adjusting the step size of the parameter adjustment. This method was further modified by Bard (1975) to include the requirement that the sum of squares function continually decrease. This is known as the modified Box-Kanemasu method.

The Gauss and Box-Kanemasu methods have been used successfully in heat transfer to estimate thermal properties. Loh and Beck (1991) used the Gauss method to estimate the volumetric heat capacity and thermal conductivity in two directions. The Box-Kanemasu method has been used by Moncman (1994) and Hanak (1995) to find thermal properties in composites, though the latter had some difficulty in simultaneously estimating thermal conductivities in the normal and planar directions due to correlation. Copenhaver (1996) attempted to use the modified Box-Kanemasu method to estimate face sheet thermal capacitance, core thickness, and emissivity in a honeycomb structure. He found that the emissivity and capacitance were correlated and that the modified Box-Kanemasu method would not converge to the estimates. A penalty function method that allowed constraints to the estimation was implemented instead.

The one drawback of almost all current parameter estimation techniques is their inability to account for variance in the "known" parameters. Other parameters in the problem, such as thickness, heat flux, or initial temperature, are assumed to be known exactly, which is never true in an actual experiment. A recent paper by Fadal et al. (1995) outlined one method of including parameter uncertainties in the objective function and used the method to find the thermal conductivity of a slab using simulated data. Unfortunately, the method used to estimate the thermal conductivity was a direct search and while a

Newton-Raphson type method is proposed for multiple parameters, no attempt was made to determine the speed or robustness of such a method. Due to time constraints and uncertainties in implementation, this method was not included in the present study.

2.3.1 Genetic Algorithms

Genetic algorithms (GAs), developed by Holland (1975), are optimization algorithms based on biological and evolutionary laws. They are essentially intelligent probabilistic methods that combine random selection with a ranking system. Each design variable represents a gene, and strung together they represent a particular design, or genetic code. The best designs, ranked according to the objective function, are used as parents to create children with new genetic codes, and mutations, or random selections, are used to introduce new "blood". The children then become the parents of the next generation and the process is repeated until the optimization criteria are met. Genetic algorithms have several advantages over other optimization algorithms. They do not use gradient methods and therefore do not require a continuous objective function and avoid local minima. They can also contain constraints, such as minimum and maximum values for optimized parameters. An excellent overview of GAs and their advantages over other optimization methods is given by Goldberg (1989).

Genetic algorithms have traditionally been programmed using binary coding, but Furuya and Haftka (1993) have shown that integer coding works as well or better. They used GAs to optimize the locations of actuators on a complicated space structure. Belegundu et al.(1994) modified GAs to optimize several problems with multiple,

competing objective functions. Garcia and Scott (1996) applied GAs to the optimization of experiments for thermal properties using the cases of Moncman (1994) and Hanak (1995) and utilizing the same D-optimal criteria as the objective function. The GA proved to be more efficient and to provide better experimental parameters than the parametric studies. In addition, Garcia (1996) used GAs for property estimation of Hanak's (1995) problem and was able to simultaneously find correlated normal and planar thermal conductivities that were unattainable using the Box-Kanemasu method. Carroll (1996) used GAs to find five parameters in a chemical laser model by comparing predicted and measured power. The algorithm was compared to a parametric study and found to be more efficient.

2.4 Estimation of Conductive-Radiative Properties

Tong et al. (1986) showed that a two-flux radiation model and a one-dimensional, transient experiment could be used to model the heat transfer in fiberglass insulations. The parameters they examined were thermal conductivity, absorption and scattering coefficients, and back-scattered fraction coefficient. The experiment consisted of a screen heater between two samples bounded by isothermal plates. However, known values were used for the radiative parameters and their estimation of thermal conductivity consisted of simply adjusting the value until a reasonable curve fit was obtained. No attempt was made to explicitly solve for a unique set of properties or determine confidence bounds.

Thomas (1989) developed a model for the same flat screen tester and fibrous insulations that incorporated a P_N solution of the radiative transfer equation, with anisotropic

scattering represented through a 20-term Legendre polynomial, and an implicit finite-difference for the energy equation. The results were checked against data from samples with known properties, though the extinction coefficient of the samples was not well known. Through trial and error, extinction coefficients were found that allowed the transient solution to be matched within ±1.2°C over the experimental time, approximately one hour.

Mann and Viskanta (1992) found the true thermal conductivity and true specific heat in float glass by taking transient measurements of the temperature of the glass as it cooled from a high initial temperature to ambient conditions.

Nicolau et al. (1994) attempted to determine six radiation parameters, including optical thickness, in an anisotropic scattering medium by exposing fibrous insulations to a known radiation flux and measuring the radiation transmitted and reflected in all directions. They performed a sensitivity analysis of the parameters and found that for large optical thicknesses ($\tau_o > 12$), the parameters were highly correlated. However, if optical thickness was left out of the estimation, an optically thick material was better for simultaneously estimating the other five parameters. In addition, the forward anisotropy had a very small sensitivity coefficient for all optical thicknesses and prevented convergence for five parameters. As a result, they first found the optical thickness through a simple transmission experiment, then fixed the forward anisotropy factor to a value representative of the expected phase function, and finally simultaneously estimated the final four parameters using the Gauss linearization method.

Neto and Özişik (1995) developed an inverse analysis for the simultaneous estimation of optical thickness, single scattering albedo, and the coefficients of the phase

function for an anisotropically scattering, planar medium if the exit distribution of radiation intensity is known (measured). Four theoretical cases were studied with 5-8 phase function coefficients. The Levenberg-Marquardt parameter estimation algorithm was successfully used to estimate the properties, though accurate values for the phase coefficients were found only if the higher index coefficients were neglected. In general, the number of phase coefficients that could be estimated was two or three less than the number used to simulate the data. This was not a problem, however, as these coefficients contributed less to the radiation transfer. The simulated data used had 2-6 percent error; error higher than 10 percent resulted in poor estimates.

Chapter 3

Theory and Mathematical Analysis

The following section deals with the development of heat transfer solutions and the optimization and estimation algorithms and procedures.

The radiative transfer in the medium was considered to be gray and isotropically scattering, so that the radiation terms did not depend on wavelength or incident angles. Two temperature solutions were investigated for this problem; a simplified diffusion solution and an absorbing and isotropically scattering integrodifferential formulation, both of which had to be solved numerically due to nonlinearity of the equations.

The use of sensitivity coefficients and the D-optimal criteria for experimental optimization are presented, as well as two estimation methods, the modified Box-Kanemasu and a genetic algorithm. A brief overview of confidence intervals is also given.

3.1 Steady-State Diffusion Solution

The diffusion solution for radiation assumes an optically thick medium where the radiation is absorbed or scattered within a short distance and the radiation intensity depends on local conditions. In this case, for one dimension, the radiative flux through the medium

reduces to (Siegel and Howell (1992))

$$q_r = -\frac{16\sigma T^3}{3\beta}\frac{\partial T}{\partial x} \tag{3.1}$$

where β is a mean extinction coefficient and σ the Stephan-Boltzman constant. Note that since β is in the denominator, the smaller its value, the more radiation transfer in the medium. This equation is in a gradient form similar to conduction and the two can be combined to give, for steady state

$$q = q_c + q_r = -k\frac{\partial T}{\partial x} - \frac{16\sigma T^3}{3\beta}\frac{\partial T}{\partial x} = -\left(k + \frac{16\sigma T^3}{3\beta}\right)\frac{\partial T}{\partial x} . \tag{3.2}$$

Assuming k and β are constant, this equation can be integrated from 0 to D for two constant-temperature boundaries in the following manner

$$\int_0^D q\,dx = -\int_{T_0}^{T_D}(k+bT^3)\,dT \quad , \quad b \equiv \frac{16\sigma}{3\beta} , \tag{3.3}$$

$$qD = -\left[k(T_D - T_0) + \frac{b}{4}(T_D^4 - T_0^4)\right] , \tag{3.4}$$

and

$$q = k\frac{(T_0 - T_D)}{D} + b\frac{(T_0^4 - T_D^4)}{4D} . \tag{3.5}$$

Note that equation (3.2) could also be integrated from 0 to x to find the temperature distribution in the medium. The resulting equation is a polynomial in x that can be solved numerically using Newton's method.

3.1.1 Mean Radiation Coefficients

The question of what, exactly, β represents is not a trivial one. The extinction coefficient is a combination of the absorption and scattering coefficients, a and σ_s, and for a purely absorbing medium is simply the absorption coefficient. It describes the ability of the medium to attenuate radiation over a unit of length and has units of inverse length. The lower the extinction coefficient, the less attenuation and the more radiation is transferred.

The extinction coefficient is a mean quantity, representing some weighted average over wavelength based on the length of the medium. Several different coefficients are described in Siegel and Howell (1992) and two of the most common are described here, using absorption only for simplicity.

The first is the Plank mean, which is the mean of a spectral absorption coefficient weighted by the Plank black body emission spectrum

$$a_P(T,P) = \frac{\int_0^\infty a_\lambda(\lambda,T,P)\, e_{\lambda b}(\lambda,T)\, d\lambda}{\sigma T^4} \tag{3.6}$$

where a_λ is the wavelength-dependent absorption coefficient and $e_{\lambda b}$ is the spectral emissive power of a black body.

The second is the Rosseland mean

$$a_R(T,P) = \frac{1}{\int_0^\infty \frac{1}{a_\lambda(\lambda,T,P)} \frac{\partial e_{\lambda b}(\lambda,T)}{\partial e_b(T)} d\lambda}, \tag{3.7}$$

which includes the assumption that the local flux depends only on the local a_λ and the local gradient of $e_{\lambda b}$. This assumption is also made in the development of the diffusion solution and the Rosseland mean is generally used with the diffusion solution.

A medium cannot be characterized as optically thick from the mean absorption coefficients; it must be optically thick for each wavelength. In a nongray medium that is still optically thick at each wavelength, the correct procedure is to divide the spectrum into more or less equal bands and apply the mean coefficient over each band.

The Rosseland mean is, strictly speaking, only accurate within an isotropically scattering material. However, Caps et al. (1984) used a weighted extinction coefficient that includes a scattering factor

$$\beta^* = \beta(1 - \bar{\mu}) \qquad \textit{where} \qquad \bar{\mu} \equiv \overline{\cos\Theta} = \frac{1}{2}\int_{-1}^{1} p(\mu)\,\mu\, d\mu \tag{3.8}$$

where Θ is the scattering angle, μ is $\cos(\Theta)$, and $p(\mu)$ is the phase function. This extinction coefficient was found to be fairly accurate even for highly anisotropic scattering. Glicksman et al. (1987) describe a similar approach called the *P-1* approximation that also gave reasonable results.

In a gray medium, all the coefficients are equivalent

$$a_P(T,P) = a_R(T,P) = a(T,P)\ . \tag{3.9}$$

In this study, a gray medium is assumed and the absorption and scattering coefficients are assumed temperature independent.

3.2 Transient Diffusion Solution

Equation (3.1) can be incorporated into the transient energy equation for conduction, neglecting energy sources, to give

$$\rho c_p \frac{\partial T}{\partial t} = -\frac{\partial}{\partial x}\left(\left(k + \frac{16\sigma T^3}{3\beta}\right)\frac{\partial T}{\partial x}\right) = -\frac{\partial}{\partial x}\left(k_{eff}\frac{\partial T}{\partial x}\right) . \qquad \textbf{(3.10)}$$

This equation is non-linear due to the T^3 term and cannot be solved exactly using closed-form analytical methods. However, it is a straightforward equation to solve numerically, as it is simply the heat conduction equation with a temperature-dependent thermal conductivity. This allows the diffusion solution to be incorporated into almost any existing numerical code.

In the first part of this research, the finite element language EAL (Engineering Analysis Language, Whetstone, 1983) was utilized to provide solutions utilizing the diffusion approximation. A table of effective thermal conductivities was created for a range of temperatures and read into the EAL programs. A sample EAL program for heat flux and constant temperature boundaries is given in Appendix A. This program includes two materials layered together, but is basically the same for one material.

It later became more convenient to have a finite difference solution implemented in a FORTRAN program that could run on a PC, as well as on a workstation. This also allows the solution to be incorporated into the genetic algorithm estimation program, which is written in FORTRAN. The solution is developed using the volume integration method, where the variable conductivity is handled by integrating the energy equation over a nodal "area",

($x_m - \Delta x/2$, $x_m + \Delta x/2$), m being a node and T_m being the temperature of the nodal "area". The time differential is represented by a forward difference from time p to time $p+1$.

The left hand side of equation (3.10) becomes

$$\int_{x_m-\frac{\Delta x}{2}}^{x_m+\frac{\Delta x}{2}} \frac{\partial}{\partial x}\left(k_{eff}\frac{\partial T}{\partial x}\right) dx = k_{eff}\frac{\partial T}{\partial x}\Big|_{x_m-\frac{\Delta x}{2}}^{x_m+\frac{\Delta x}{2}} \approx k_m^+\left(\frac{T_{m+1}-T_m}{\Delta x}\right) - k_m^-\left(\frac{T_m - T_{m-1}}{\Delta x}\right) \qquad \textbf{(3.11)}$$

$$k_m^+ = k_{eff}\left(\frac{T_m + T_{m+1}}{2}\right) \quad , \quad k_m^- = k_{eff}\left(\frac{T_{m-1}+T_{m+1}}{2}\right)$$

while the right hand side is

$$\int_{x_m-\frac{\Delta x}{2}}^{x_m+\frac{\Delta x}{2}} \rho c_p \frac{\partial T}{\partial t} dx \approx \rho c_p \frac{\partial T}{\partial t}\Big|_{x_m} \Delta x \approx \rho c_p \frac{T_m^{p+1} - T_m^p}{\Delta t}\Delta x \ . \qquad \textbf{(3.12)}$$

Defining the Fourier number at each node m as

$$fo_m^+ \equiv \frac{k_m^+ \Delta t}{\rho c_p \Delta x^2} \qquad \textbf{(3.13)}$$

and combining terms and rearranging gives

$$-fo_m^- T_{m-1}^{p+1} + (1 + fo_m^+ + fo_m^-) T_m^{p+1} + f_{om}^+ T_{m+1}^{p+1} = T_m^p \ . \qquad \textbf{(3.14)}$$

This results in a tri-diagonal system of equations for $m=1,M$ nodes that can be solved using the well known Thomas algorithm. The Ts used to calculate k^+ and $\bar{k}$ should be the temperatures at time $p+1$; however, these are not known and so T^p must be used to find T^{p+1}, then T^{p+1} used to recalculate k^+ and k^- and new T^{p+1} values found. This procedure is iterated until the difference between T^p and T^{p+1} is less than some small value.

The boundary conditions also need to be discretized. The boundary condition at $m=M$ $(x=D)$ is simply a fixed temperature, T_D. The temperature gradient at $m=1$ $(x=0)$ is replaced with a second-order forward difference, as given by Grossman (1991),

$$q_a = -k\frac{\partial T}{\partial x}\bigg|_{x=0} = k_0^+\left(\frac{-T_3 + 4T_2 - 3T_1}{2\Delta x}\right) . \qquad \textbf{(3.15)}$$

This can be rearranged to yield an equation for T_1

$$T_1 = \frac{4}{3}T_2 - \frac{1}{3}T_3 + \frac{2\Delta x}{3k_0^+}q_a . \qquad \textbf{(3.16)}$$

The number of mesh points and the time increment were determined by examining temperatures at the heated surface for different values of Δt and M. Values of T_0 for $t=30s$ are plotted in Figure 3.1 for different mesh sizes. This figure clearly shows convergence for decreasing mesh size, with a value in the range of 40-50 sufficient. Temperatures at the same time and position are plotted in Figure 3.2 for different time increments and the temperature reveals a linear dependence on the time step. A value of 0.5 s places the temperature within 0.08 K of the extrapolated temperature as the time step becomes infinitely small ($\Delta t \rightarrow 0$), which is about the precision limit of the data acquisition system.

The diffusion program, HCVK.FOR, with some modifications discussed later, is listed in Appendix B.

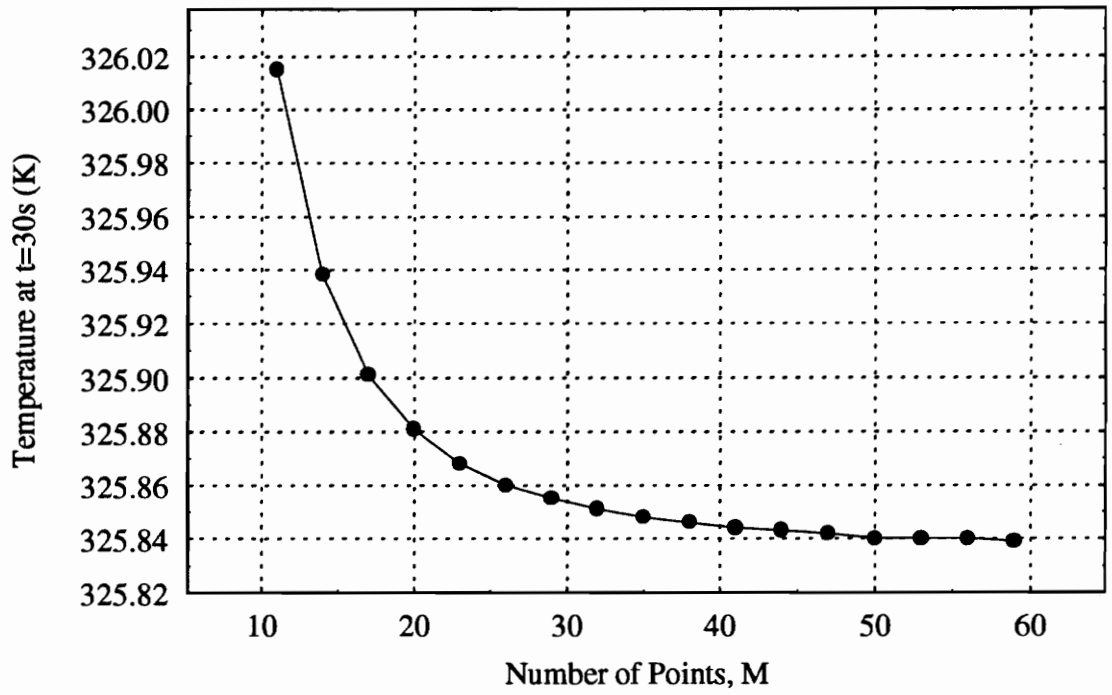

Figure 3.1 Change in Diffusion Solution with an Increase in Mesh Points.

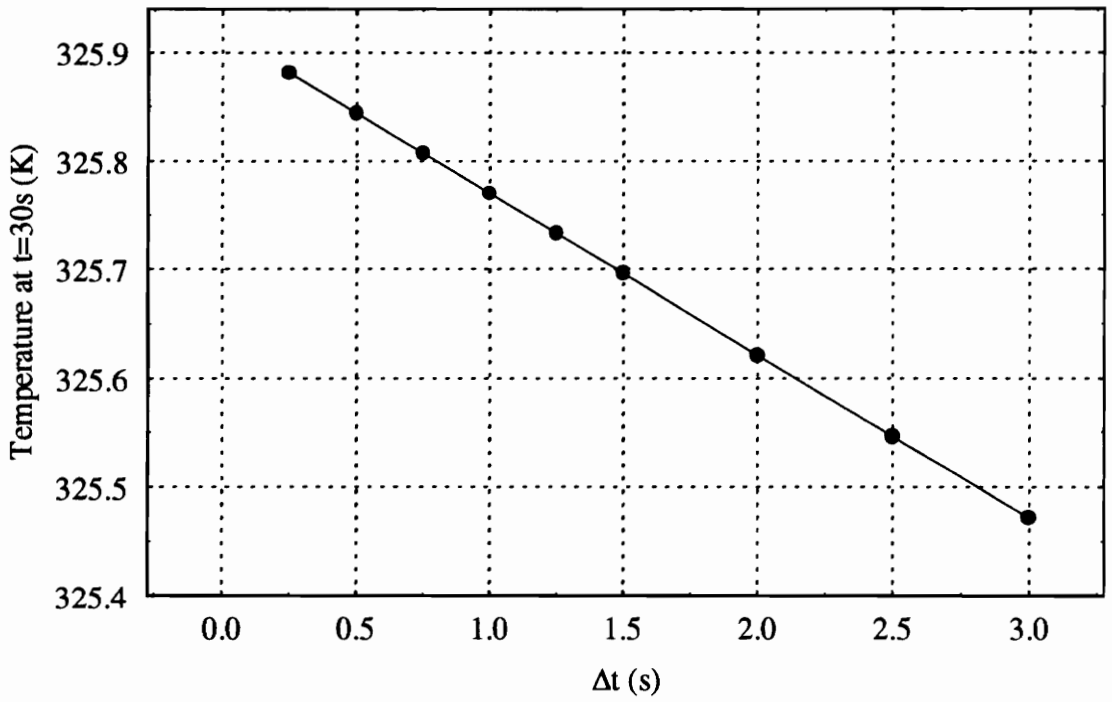

Figure 3.2 Change in Diffusion Solution with a Decrease in Δt.

3.3 Transient Absorbing and Isotropically Scattering Solution

A more complex and general solution than the diffusion model was desired, one which is valid near the boundaries and which could be used to examine the effects of absorption versus scattering. An attempt was made to use EAL in the analysis, but the program language was only able to model radiation at boundaries and could not handle radiation in a participating medium. Instead, a numerical solution was developed for the one-dimensional case and implemented using FORTRAN. The numerical solution involves a finite-difference representation for the derivatives and a Gaussian numerical integration for the radiation integrals. An iterative scheme is used since the equation is nonlinear.

3.3.1 Assumptions, Equations, and Boundary Conditions

The assumptions of a gray medium and isotropic scattering were used for simplicity; these assumptions are also valid for the experimental test material (Section 4.11). Black boundaries were also assumed, as these were easier to implement experimentally. The energy equation for the problem considered, from Siegel and Howell (1992), is

$$\rho c_p \frac{\partial T}{\partial t} = k\frac{\partial^2 T}{\partial x^2} - \frac{\partial q_r}{\partial x} \tag{3.17}$$

where

$$\frac{\partial q_r}{\partial x} = 4\frac{a}{\Omega}[\pi I'(\kappa) - \sigma T^4(\kappa)] \quad \text{and} \quad \Omega = \frac{\sigma_s}{a + \sigma_s} . \tag{3.18}$$

The equation for the gradient of the radiative heat flux, q_r, is written in terms of the optical depth, $\kappa=(a+\sigma_s)x$, the scattering albedo Ω, and the absorption coefficient a and includes the temperature and the radiation source function, $I'(\kappa)$. The form of the radiation source function, again from Siegel and Howell (1992), is

$$\pi I'(\kappa) = (1-\Omega)\sigma T^4(\kappa) + \frac{\Omega}{2}\Big[q_{o0}E_2(\kappa) + q_{oD}E_2(\kappa_D-\kappa) + \int_0^{\kappa_D}\pi I'(\kappa^*)E_1(|\kappa^*-\kappa|)d\kappa^*\Big] \tag{3.19}$$

where the $E_n(x)$ terms are the exponential integral functions and κ_D is the optical thickness, $\kappa_D=(a+\sigma_s)D$. The first term on the right hand side of equation (3.19) is the radiation emitted at position κ, the next two terms represent the radiation emitted from each boundary that reaches κ, and the last term is the energy emitted by the rest of the medium that arrives at κ. The q_{o0} and q_{oD} are outgoing radiation fluxes from the boundaries that arrive at κ. Since the boundaries are black, the emissivities at each boundary, ϵ_0 and ϵ_D, are unity and

$$q_{o0} = \epsilon_0\sigma T_0^4 + (1-\epsilon_0)q_{iD} = \sigma T_0^4 \tag{3.20}$$

and

$$q_{oD} = \epsilon_D\sigma T_0^4 + (1-\epsilon_D)q_{i0} = \sigma T_D^4 \ . \tag{3.21}$$

The temperature, distance, and radiation intensity are placed in dimensionless form using the transforms

$$\Theta \equiv \frac{T}{T_r} \ , \qquad \eta \equiv \frac{x}{D} \ , \text{ and } \qquad i' \equiv \frac{\pi I'}{\sigma T_r^4} \tag{3.22}$$

where T_r is the reference temperature, usually a constant boundary temperature. The time variable was kept dimensional for clarity and convenience in dealing with the experimental data.

Substituting the appropriate terms, the energy and radiative source equations become

$$\rho c_p T_r \frac{\partial \Theta}{\partial t} = \frac{kT_r}{D^2}\frac{\partial^2 \Theta}{\partial \eta^2} - \frac{a}{\Omega}\left[4\sigma T_r^4 \Theta^4(\eta) - 4\sigma T_r^4 i'(\eta)\right] \tag{3.23}$$

and

$$\sigma T_r^4 i'(\eta) = (1-\Omega)\sigma T^4(\eta) + \frac{\Omega}{2}\left[\sigma T_0^4 E_2(\kappa_D \eta) + \sigma T_D^4 E_2(\kappa_D(1-\eta)) + \kappa_D \int_0^1 \sigma T_r^4 i'(\eta^*) E_1(\kappa_D|\eta^* - \eta|)\, d\eta^*\right]. \tag{3.24}$$

The equations can be further reduced by defining the conduction-radiation parameter

$$N_r \equiv \frac{ka}{4\sigma T_r^3} \tag{3.25}$$

and collecting some time-related terms

$$\tau \equiv \frac{\rho c_p}{4a\sigma T_r^3}. \tag{3.26}$$

The conduction-radiation parameter represents an approximate ratio of conduction to radiation heat transfer. As N_r approaches infinity, the heat transfer approaches pure conduction, while as N_r approaches zero, the heat transfer approaches pure radiation. Dividing the energy and source equations through by σT_r^4 and collecting terms leads to the final equations

$$N_r \frac{\partial^2 \Theta}{\partial \eta^2} = \tau \kappa_D^2 \frac{\partial \Theta}{\partial t} + \frac{\kappa_D^2}{\Omega}\left[\Theta^4(\eta) - i'(\eta)\right] \tag{3.27}$$

and

$$i'(\eta) = (1-\Omega)\Theta^4(\eta) + \frac{\Omega}{2}\Big[\Theta_0^4 E_2(\kappa_D \eta) + \Theta_D^4 E_2(\kappa_D(1-\eta)) + \kappa_D \int_0^1 i'(\eta^*) E_1(\kappa_D|\eta^* - \eta|)\, d\eta^*\Big] . \tag{3.28}$$

The conduction boundary conditions for equation (3.27) are an applied heat flux at one surface and a constant temperature at the other surface. The heat flux boundary condition, including radiation, is simply

$$q_a = -k \frac{\partial T}{\partial x}\bigg|_{x=0} . \tag{3.29}$$

The nondimensional conduction gradient is then

$$\overline{q_a} \equiv \frac{q_a}{\sigma T_r^4} = -k \frac{\partial T}{\partial x} \frac{1}{\sigma T_r^4} = -\frac{k}{\sigma T_r^3 D} \frac{\partial \Theta}{\partial \eta} = \frac{4}{(a+\sigma_s)D} \frac{ka}{4\sigma T_r^3} \frac{(a+\sigma_s)}{a} \frac{\partial \Theta}{\partial \eta}$$
$$= -\frac{4N_r}{\kappa_D(1-\Omega)} \frac{\partial \Theta}{\partial \eta} = -\alpha \frac{\partial \Theta}{\partial \eta} . \tag{3.30}$$

3.3.2 Discretization and Numerical Solution of the Equations

The energy equation derivatives are replaced with finite differences: a second-order central difference in space and a first-order forward difference in time. This results in the following discretized form of equation (3.27) for each interior mesh point, assuming constant

properties

$$N_r\left(\frac{\Theta_{i+1}^{p+1} - 2\Theta_i^{p+1} + \Theta_{i-1}^{p+1}}{\Delta\eta^2}\right) = \tau\kappa_D^2\left(\frac{\Theta_i^{p+1} - \Theta_i^{p}}{\Delta t}\right) + \frac{\kappa_D^2}{\Omega}\left(\Theta_i^{4(p+1)} - i_i^{p+1}\right) . \qquad (3.31)$$

This equation cannot be solved for Θ^{p+1} because of the nonlinear radiation terms on the right. Therefore, the radiation terms are first evaluated at time step *p*, the equations are solved for Θ^{p+1}, and then the radiation terms are re-evaluated using the new Θ^{p+1}, as detailed in the flow chart of Figure 3.3. The process is iterated until Θ^{p+1} converges to a static value and then moves to the next time step. Equation (3.31) is rearranged to produce the algebraic equation

$$-\Theta_{i-1}^{p+1} + \left(2 + \frac{\tau\kappa_D^2\Delta\eta^2}{N_r\Delta t}\right)\Theta_i^{p+1} - \Theta_{i+1}^{p+1} = \frac{\tau\kappa_D^2\Delta\eta^2}{N_r\Delta t}\Theta_i^{p} + \frac{\kappa_D^2\Delta\eta^2}{N_r\Omega}\left(\Theta_i^{4l} - i_i^{l}\right) \qquad (3.32)$$

where *l* denotes the *l*th iteration. These equations are written for each interior node *I*, resulting in *N-2* equations with *N-2* unknowns. The coefficient matrix is tri-diagonal and is easily inverted using the well-known Thomas algorithm.

The radiative source integral equation must also be solved for each iteration. This equation is in the form of a Fredholm equation of the second kind,

$$i'(\eta) = \lambda\int_a^b K(\eta,\eta^*)\,i'(\eta^*)\,d\eta^* + g(\eta) , \qquad (3.33)$$

$$\text{where} \quad \lambda = \frac{\Omega\kappa_D}{2} \quad , \quad K(\eta,\eta^*) = \int_0^1 E_1(\kappa_D|\eta^* - \eta|)d\eta^* \qquad (3.34)$$

$$\text{and} \quad g(\eta) = (1-\Omega)\Theta^4(\eta) + \frac{\Omega}{2}\left[\Theta_0^4 E_2(\kappa_D\eta) + \Theta_D^4 E_2(\kappa_D(1-\eta))\right] . \qquad (3.35)$$

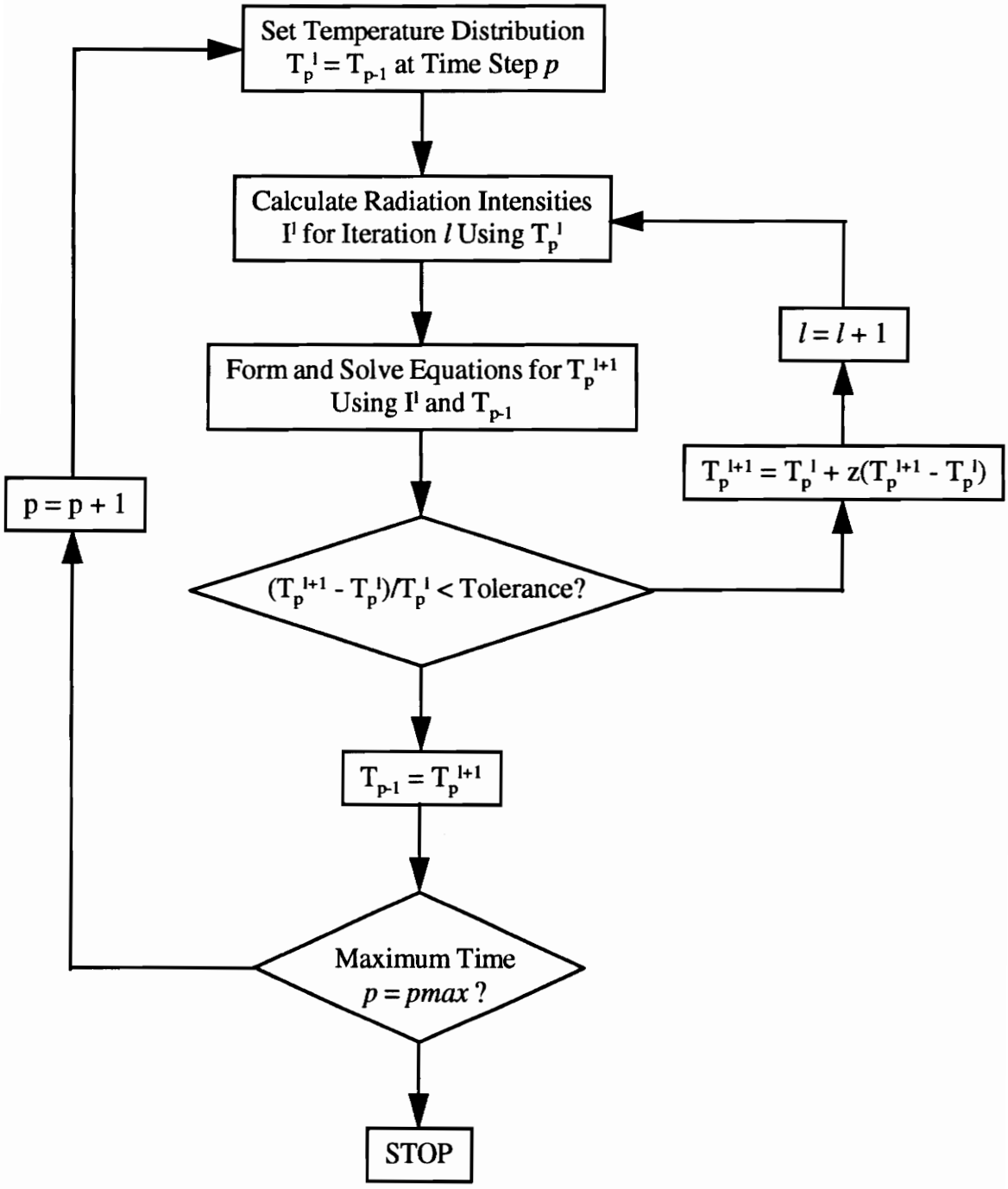

Figure 3.3 Iterative Process for Conduction/Radiation Solution.

$$i'(\eta_n) = \lambda \sum_{m=1}^{M} w_m K(\eta_n, s_m) i'(s_m) + g(\eta_n) \ , \qquad \textbf{(3.36)}$$

The function $K(\eta,\eta^*)$ is the Kernel of equation (3.33). The numerical solution can be obtained, as outlined in Press et al. (1992), by the Nystrom method, which replaces the integral with a quadrature rule, for $n = 1$ to M equations. The quadrature weights, w_m, are found using the Gauss-Legendre quadrature rule. These equations can then be solved using standard algorithms for matrices (note that the system is not tri-diagonal). The program uses an LU decomposition method combined with a back substitution subroutine.

This method must be modified, however, due to a singularity in the kernel. The kernel consists of the term $E_1(\kappa_D|s-\eta|)$, which results in $E_1(\kappa_D|s_m-\eta_n|)$ in the quadrature rule. On the diagonal, when $m=n$, this becomes $E_1(0)$, which goes to infinity. This problem is resolved by subtracting the singularity from the equation and then the singular integral is evaluated analytically as

$$\int_a^b K(t,s)[f(s) - f(t)]\,dt + \int_a^b K(t,s) f(t)\,ds = \int_a^b K(t,s)[f(s) - f(t)]\,dt + r(t) f(t) \qquad \textbf{(3.37)}$$

and

$$i_n = \lambda \sum_{\substack{m=1 \\ m \neq n}}^{M} w_m K_{nm}[i_m - i_n] + \lambda r_n i_n + g_n \quad \text{where} \quad r_n = \int_a^b K(s_n, t_n) \ . \qquad \textbf{(3.38)}$$

For this case

$$r_n = \int_0^1 E_1(\kappa_D|s - \eta_n|)ds = \frac{1}{\kappa_D}\left[2E_2(0) - E_2(\kappa_D \eta_n) - E_2(\kappa_D(1-\eta_n))\right] . \qquad \textbf{(3.39)}$$

Note that the N quadrature points *are not the same* as the M finite difference grid points. Since the source equation depends on the temperature distribution, and vice-versa, an interpolation routine must be used to find the temperature at the quadrature points for the Nostrum method and to find the radiation source values at the grid points for the finite difference matrix. A cubic spline was implemented for this task and should not introduce a significant loss of accuracy, since the temperature and radiative source functions for this problem are relatively smooth and well behaved.

The boundary conditions also need to be placed in discretized form. The boundary condition at $x=D$ is simply Θ_D. The temperature gradient at $x=0$ is written similar to the diffusion solution, using equation (3.15),

$$\overline{q_a} = -\alpha\left(\frac{-\Theta_3 + 4\Theta_2 - 3\Theta_1}{2\Delta\eta}\right) , \tag{3.40}$$

which can be rearranged to yield an equation for Θ_1

$$\Theta_1 = \frac{4}{3}\Theta_2 - \frac{1}{3}\Theta_3 + \frac{2\Delta\eta}{3\alpha}\left(\overline{q_a}\right) . \tag{3.41}$$

3.3.3 Addition of Non-Black Boundary

At one point in the analysis, it was desired to have a non-black (reflecting) boundary. Though more algebraically complex, it is a relatively simple matter to add this to the solution. Using the non-black boundary form of q_{oD} from equation (3.21), nondimensionlizing, and adding to equation (3.28) gives

$$i'(\eta) = (1-\Omega)\Theta^4(\eta) + \frac{\Omega}{2}\left[\left(\epsilon_0\Theta_0^4 + (1-\epsilon_0)\frac{q_{i0}}{\sigma T_0^4}\right)E_2(\kappa_D\eta) + \Theta_D^4 E_2(\kappa_D(1-\eta))\right.$$
$$\left. + \kappa_D\int_0^1 i'(\eta^*)E_1(\kappa_D|\eta^*-\eta|)d\eta^*\right]. \qquad \textbf{(3.42)}$$

The expression for q_{i0} in nondimensional form is

$$q_{i0} = 2\Theta_D^4 E_3(\kappa_D) + 2\kappa_D\int_0^1 i'(\eta^*)E_2(\kappa_D\eta^*)d\eta^* . \qquad \textbf{(3.43)}$$

Collecting terms and combining the two integrals, the radiation source equation can again be written in the form of a second-order Fredholm equation, equation (3.33), where $g(\eta)$ is

$$g(\eta) = (1-\Omega)\Theta^4(\eta) + \left[\frac{\epsilon_0\Omega}{2}\Theta_0^4 + (1-\epsilon_0)\Omega\Theta_D^4 E_3(\kappa_D)\right]E_s(\kappa_D\eta)$$
$$+ \frac{\Omega}{2}\Theta_D^4 E_2(\kappa_D(1-\eta)) \qquad \textbf{(3.44)}$$

and the kernel, K(η,η*), is

$$\lambda\int_0^1 K(\eta,\eta^*)i'(\eta^*)d\eta^* = \frac{\Omega}{2}\int_0^1\left[2(1-\epsilon_0)\kappa_D E_2(\kappa_D\eta)E_2(\kappa_D\eta^*)\right.$$
$$\left. + \kappa_D E_1(\kappa_D|\eta^*-\eta|)\right]i'(\eta^*)d\eta^* . \qquad \textbf{(3.45)}$$

Equation (3.32) for the boundary is the same.

3.3.4 Convergence and Grid Size

As mentioned, the solution for Θ^{p+1} is iterated until Θ^{p+1} converges. The convergence

criterion is

$$\left|\frac{(\Theta^{J+1} - \Theta^{J})}{\Theta^{J}}\right| < tolerance \tag{3.46}$$

and tolerance is a small number, such as 10^{-4}. Generally, the solution is well behaved. However, as the radiation contribution increases (i.e. low k or a), the solution requires more iterations to converge and eventually diverges.

This behavior seems to be common to numerical solutions for radiation in a participating medium, as it is mentioned in Viskanta (1962), Ho and Özişik (1987), and Siewert and Thomas (1990). Siewert (1995) modified the latter work to use an iteration scheme based on Newton's method that greatly improved the convergence. The divergent behavior may be due to the temperature to the fourth power in the radiation portion of the solution. The difference in temperature from one iteration to the next is based on the results of solving the linear conduction matrix; that difference is magnified in the radiation portion, causing the solution of the radiation source term to oscillate and the temperature to diverge.

To compensate, an under-relaxation factor was used when updating the new temperature

$$\Theta^{J+1} = \Theta^{J} + z(\Theta^{J+1} - \Theta^{J}) \tag{3.47}$$

The more radiation contributes to the solution, the lower the z factor should be; the best value is a matter of trial and error. Most of the problems considered here could use a factor of one.

After analyzing some of the output, it was noticed that halfway to steady state small irregularities occurred in the solution. These irregularities were small enough to be

unnoticeable in dealing with the temperature output, as they were on the order of 0.001 °C, but when sensitivity coefficients were calculated, they led to significant oscillations in the values. Further analysis revealed that a minimum of two iterations eliminated the irregularities and produced a smoother sensitivity coefficient curve. Therefore, at least two iterations were performed in the program.

The same analysis was performed for mesh size and time step as for the transient diffusion solution. Figure 3.4 reveals almost the same linear dependence on time step that was observed for the diffusion solution. A time step of 0.5 s was again chosen, as this is fairly close to the precision of the data acquisition and a time step of 0.25 s would require twice as long to run for a minor gain in accuracy.

This solution actually has two sets of grid points to choose, the number of mesh points, M, for the finite difference and the number of quadrature points, N, for the Gaussian integration. Of the two, the quadrature points are the more important from a time standpoint. The finite difference equations result in a tri-diagonal matrix that is solved quickly and efficiently using the Thomas algorithm. Unfortunately, the numerical solution of the radiation source equation results in a dense matrix that must be solved using a slower LU decomposition method. This matrix is the primary source of CPU time in the program.

The temperature at the heated surface for $t=30\ s$ is shown in Figure 3.5 and clearly shows convergence. The value chosen was $M=81$, as an increase to $M=101$ would result in a change in the temperature less than the error of the data acquisition system. The case for N, Figure 3.6, is unexpected and more difficult. The temperature oscillates as N increases and

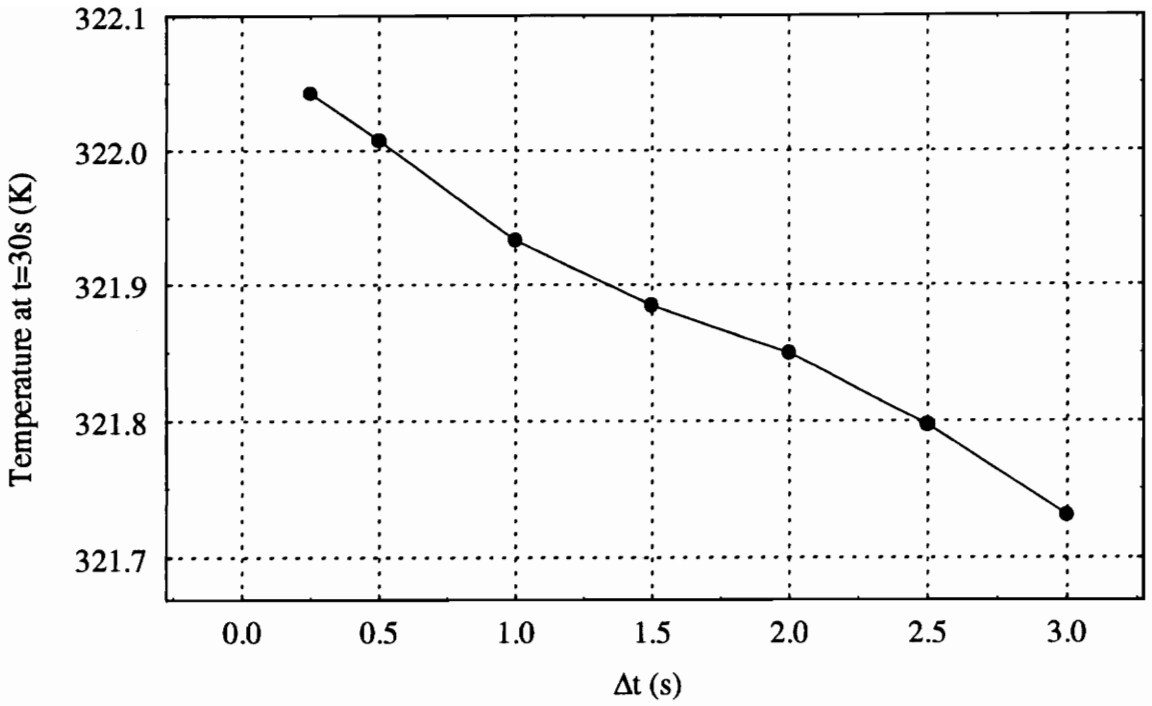

Figure 3.4 Change in Absorbing and Scattering Solution with a Decrease in Δt.

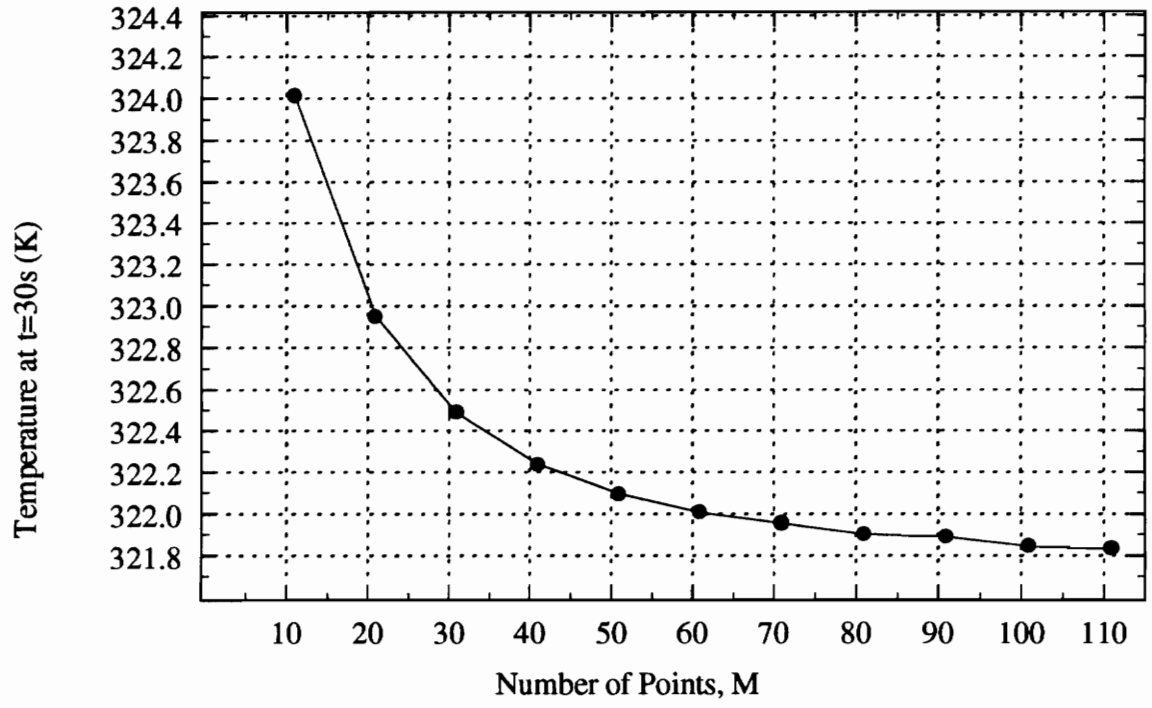

Figure 3.5 Change in Absorbing & Scattering Solution with an Increase in Mesh Points.

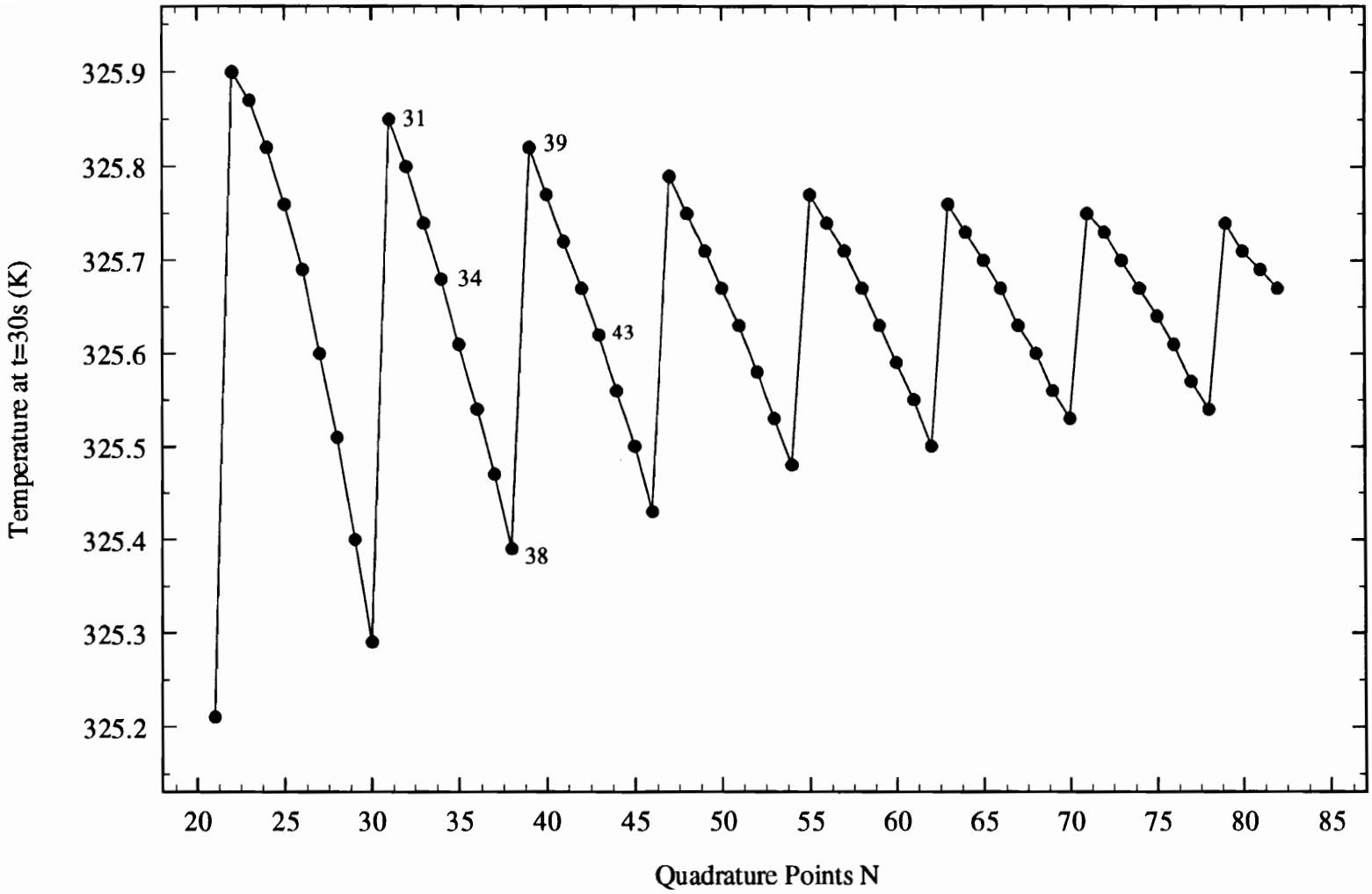

Figure 3.6 Change in Absorbing and Scattering Solution with a Change in N Quadrature Points.

while the oscillations die down, they do so very slowly. This behavior was observed for different temperatures at different times and for different parameters. In addition, the relative positions of the temperature for each N did not change for any problem if the value of M was the same, i.e. $T(N=31) > T(N=34) > T(N=38)$, etc. for $M=61$. It is presumed that the temperatures in Figure 3.6 oscillate about the value that a very large number of quadrature points would converge to, somewhere between 325.6 K and 325.7 K in this case. After thoroughly examining the quadrature routine and running some experimental programs, it is believed the behavior is a result of the interpolation between the mesh points and the quadrature points. Though both the temperature and radiation functions are smooth, there appears to be some interaction between the two sets of points that causes the behavior in Figure 3.6. Using the quadrature routine to numerically integrate other, complicated functions, it was found that very few points were needed, generally less than 10. The variance in temperature due to N has more to do with where the quadrature points happen to fall relative to the mesh points rather than with the number used. The program produced an erroneous temperature solution with less than 21 points. Comparing an optically dense case between the diffusion solution and the absorbing and scattering solution, whose results should be about the same, $N=43$ was found to be a reasonable value for the quadrature points and this was used in the analysis.

The program, RCB.FOR, with a non-black boundary and some modifications discussed later, is listed in Appendix C.

3.3.5 Solutions

Some solutions from the programs are shown in Figures 3.7 through 3.10. Figure 3.7 is a comparison of the temperature at the heated surface for heat flux and constant temperature boundaries as computed by EAL, the diffusion solution, and the absorbing and scattering solution using the parameters in Table 3.1, which are the nominal values for Styrofoam. The parameters are for an optically thick medium and the plots show good agreement for this case. Figure 3.8 plots the temperature distribution in the material for both HCVK (diffusion solution) and RCB (absorbing and scattering solution) at various times for the same parameters and boundary conditions and also shows good agreement. Figure 3.9 is a comparison of a temperature distribution from an RCB solution that has reached steady state, which is effectively a steady-state solution for two constant temperature boundaries,

Table 3.1 Preliminary Styrofoam Parameters.

Parameter	Value
Thermal Conductivity, k	0.028 W/mK
Volumetric Heat Capacity, ρc_p	19.2 kJ/m^{3}K
Absorption Coefficient, a	1200 m^{-1}
Scattering Coefficient, σ_s	300 m^{-1}
Emissivity of Boundaries, ϵ_0, ϵ_D	1.0
Thickness, D	0.01815 m
Applied Heat Flux, q_a	100 W/m^2
Initial Temperature, $T_i = T_D$	298 K

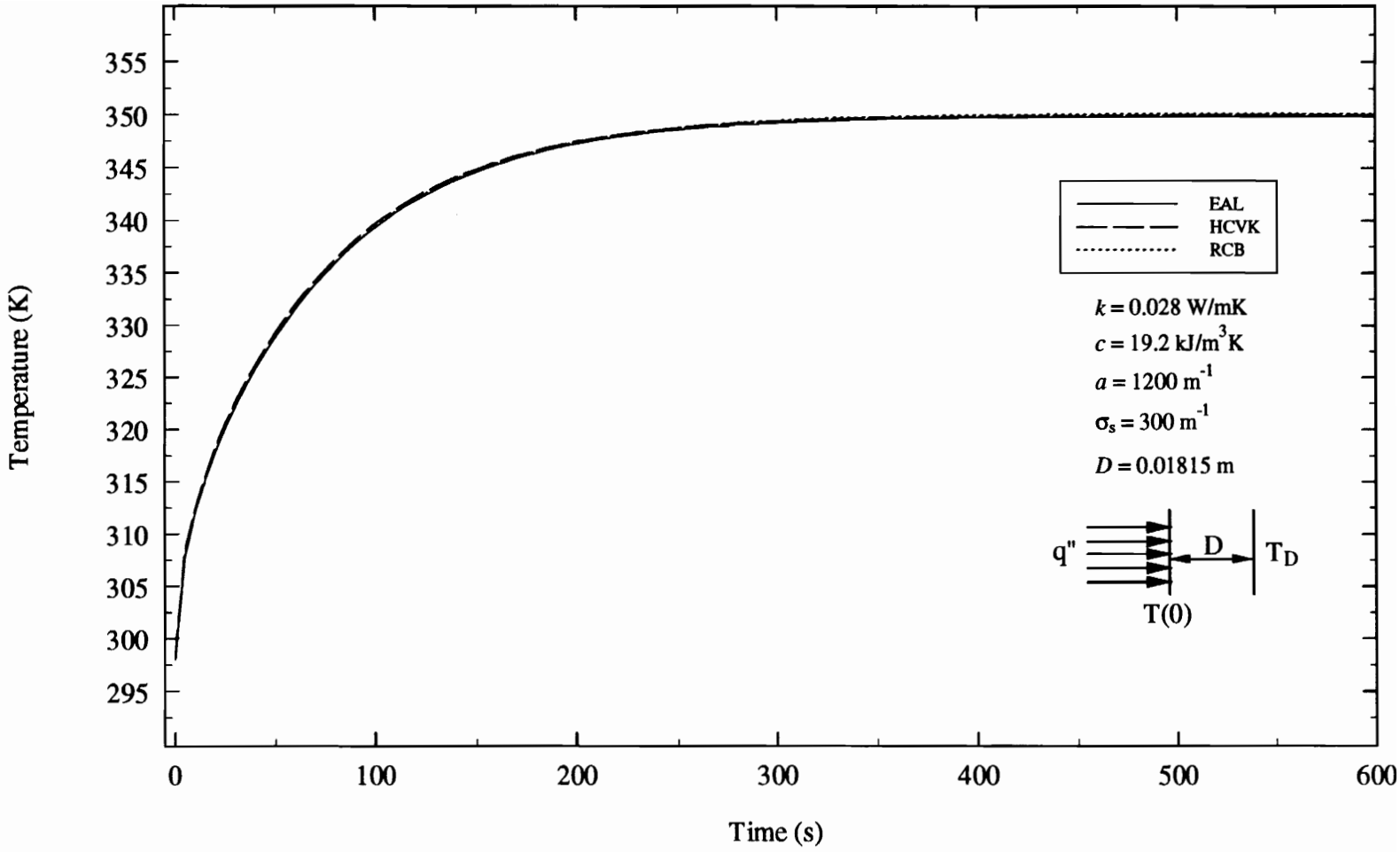

Figure 3.7 Comparison of Temperature at $x=0$ for EAL, HCVK.FOR, and RCB.FOR Using a 100 W/m^2 Heat Flux and an Initial and Boundary Temperature of 298K.

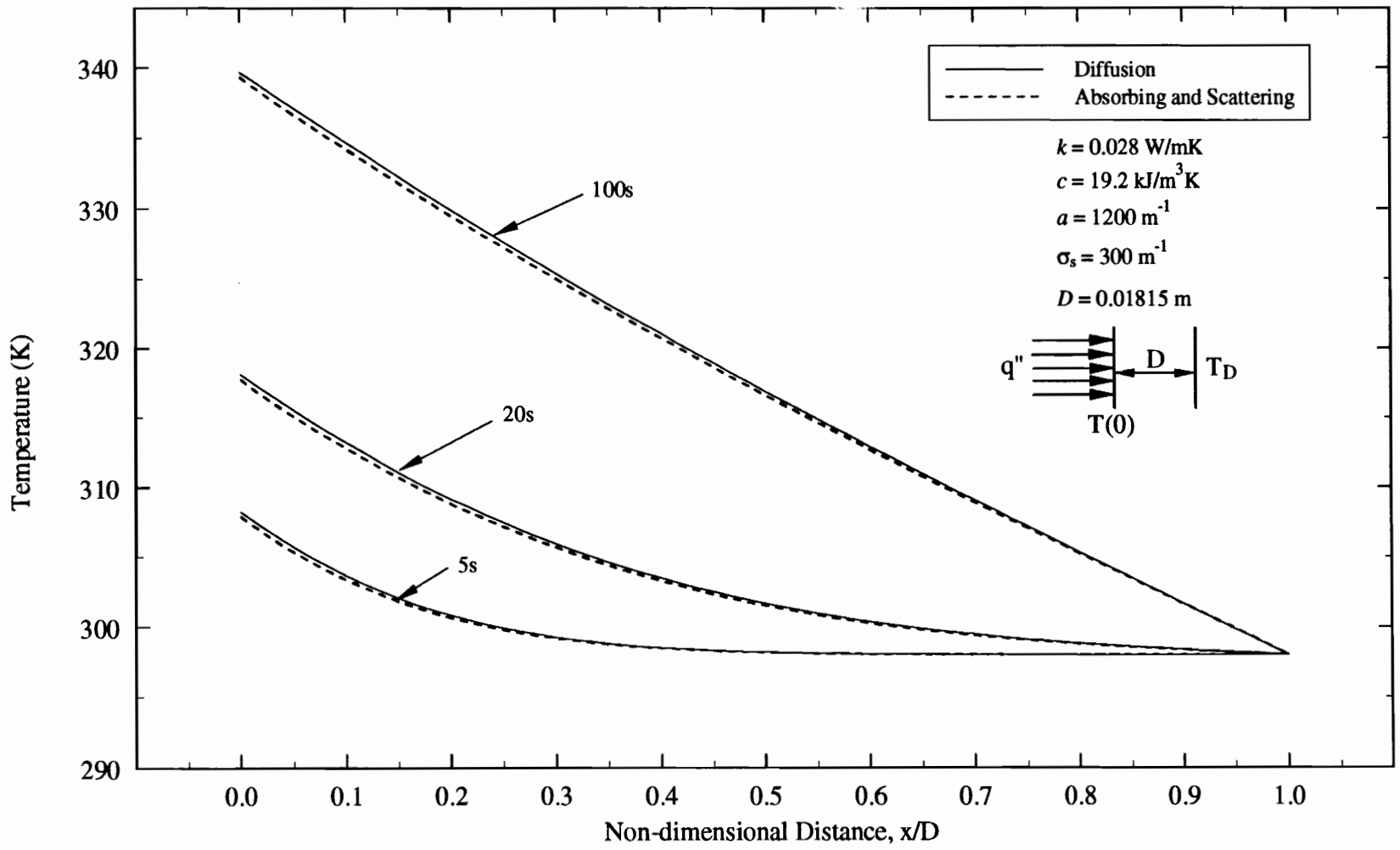

Figure 3.8 Comparison of Diffusion Temperature Distributions to Absorbing and Scattering Solution Using a Heat Flux of 100 W/m^2 and an Initial and Boundary Temperature of 298K.

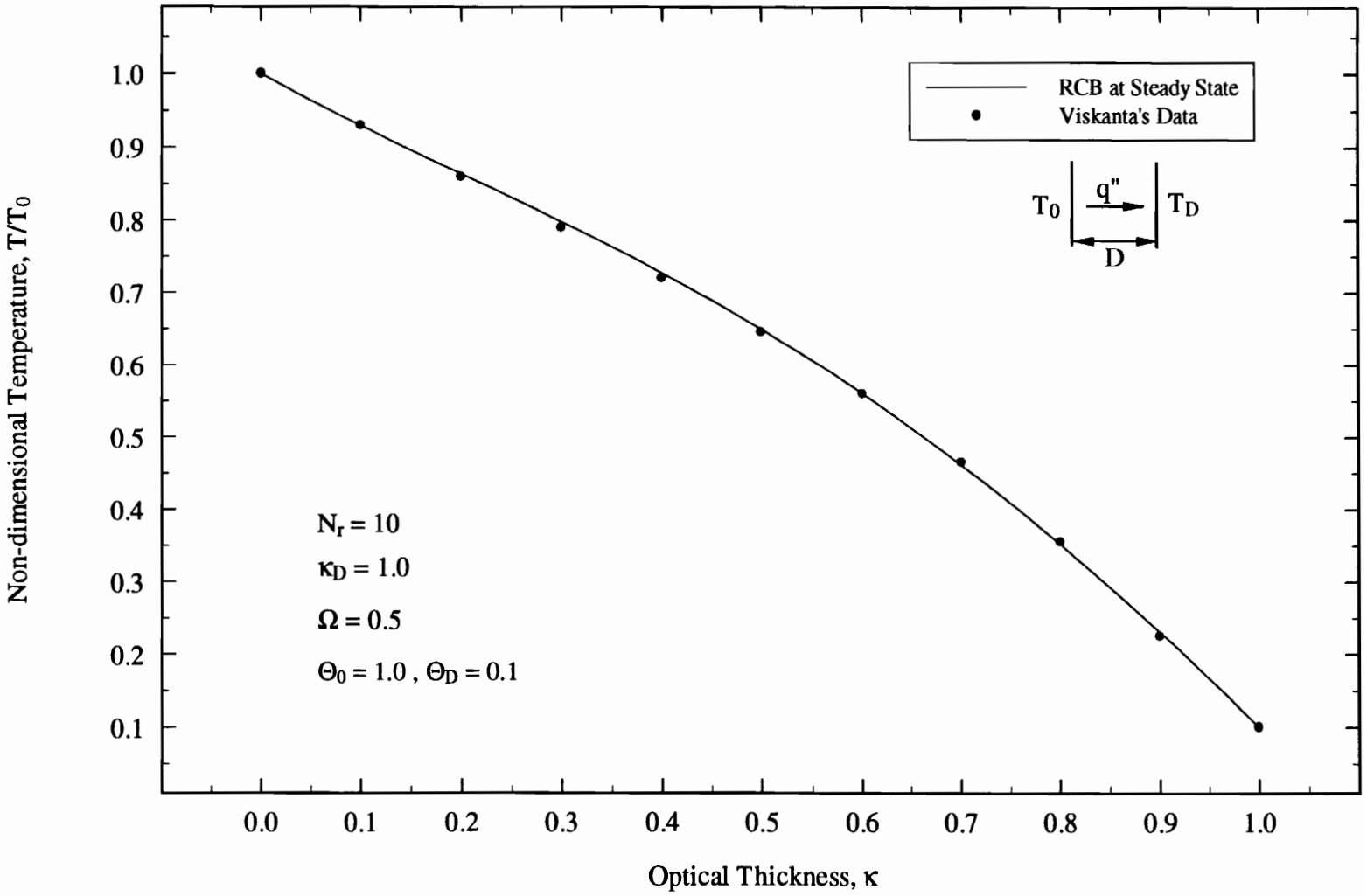

Figure 3.9 Comparison of RC Temperature Distribution at Steady State to Data from Viskanta (1965).

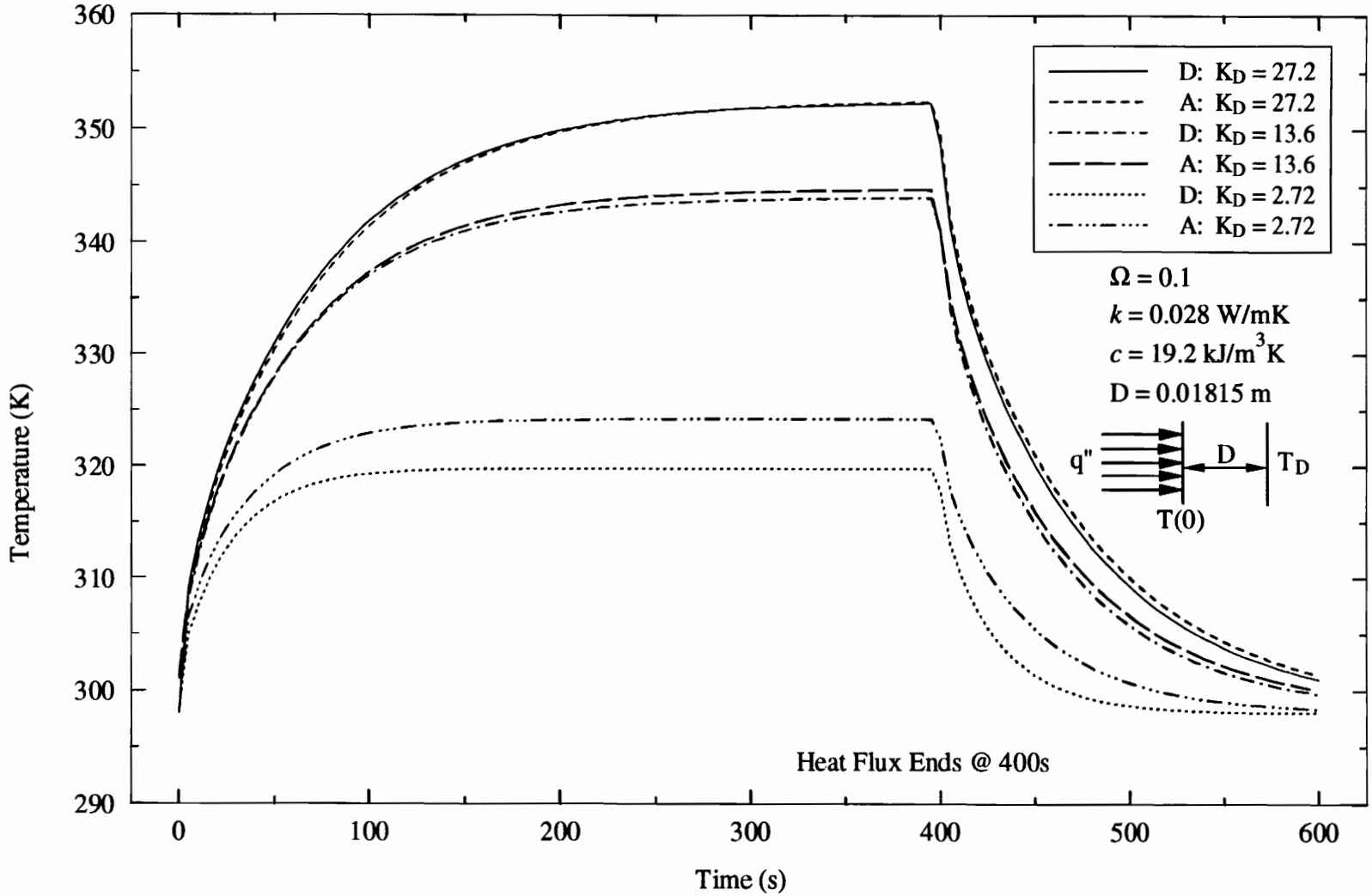

Figure 3.10 Comparison of Diffusion (D) and Absorbing and Scattering (A) Solutions for Different Optical Thicknesses with a Heat Flux of 100 W/m^2 and an Initial and Boundary Temperatue of 298K.

with the steady-state temperature distribution from Viskanta (1965). The RCB solution shows excellent agreement with the latter. Finally, Figure 3.10 compares the results of HCVK to RCB for several optical thicknesses and reveals major differences in the temperature for optically thin cases.

3.4 Optimization and Estimation Algorithms

Experimental optimization seeks to find the experiment that provides the most information concerning the parameters or properties and leads to the estimate with the most certainty, or smallest confidence interval, e.g. $k = 5.00 \pm 0.05$ versus $k = 5.00 \pm 1.00$. Parameter estimation attempts to determine the unknown parameters of a system given a valid model of the system and experimental measurements using the system. Estimation algorithms proceed by trying to minimize an objective function that is a measure of how close the calculated solution matches the experimental solution. Generally, the sum of squares function is used in parameter estimation. If there is more than one property or parameter to be found, it is most efficient to run only one experiment and determine all the properties from those results. This is known as simultaneous parameter estimation.

3.4.1 Sensitivity Coefficients and Correlation

The sensitivity coefficients are very important in parameter estimation. They are defined as the change in the dependent variable with respect to a change in a parameter and indicate

how sensitive the dependent variable is to the parameters. Mathematically:

$$\textit{Sensitivity Coefficient} \quad X_p \equiv \frac{\partial \eta_p}{\partial p} \quad , \quad \text{e.g.} \quad X_k = \frac{\partial T}{\partial k} \tag{3.48}$$

Sensitivity coefficients give an idea of how much information the measurements contain for each unknown parameter. For example, if temperature is being measured, the sensitivity coefficient for any parameter at a constant temperature boundary will always be zero; the parameters have no influence on the temperature at that point and could be anything. The sensitivity coefficients should be maximized when designing an experiment to obtain the most accurate estimate of the parameters. However, there is often a trade-off, as maximizing one parameter's sensitivity coefficient may decrease another.

One of the biggest problems in simultaneous parameter estimation is correlation. Correlation in parameter estimation occurs when the sensitivity coefficients are linearly dependent; that is, one can be written as a constant times another. This correlation is a result of two or more parameters having the same effect on the solution. If this is the case, the two properties cannot be simultaneously determined.

Consider the following equation: $\eta_p = 2ax + bx$, where $X_a = 2x$ and $X_b = x$. The sensitivity coefficients for a and b are not the same, but differ only by the constant factor of two; they are linearly dependent. The equation can be rewritten as: $\eta_p = (2a + b)x = cx$. Obviously, given values of x and η, the only information obtainable is $(2a + b)$, or c, and any combination of a and b that produces c will satisfy the equation.

In practice, estimates that are not exactly correlated, but nearly linearly dependent, are

also difficult to estimate simultaneously. In these cases, the particular algorithm chosen to estimate the properties is important, as some may be able to handle a higher degree of correlation than others. In actuality, all the estimates are somewhat dependent on one another, but it is the degree of the dependence that determines if they are correlated. If the sensitivity coefficients are exactly linearly dependent, the choice of estimation algorithms is irrelevant.

It is important to remember that in parameter estimation, correlation is a statistical phenomenon, not a physical phenomenon. The actual properties are not correlated and are independent of one another, if the model is correct. It is the estimates that are correlated and the value of one will affect the value of another.

Correlation of the estimates can be affected by the boundary conditions of a system or the particular experiment chosen. Often, correlation can be avoided through careful design of the experiment. In some cases, properties simply cannot be estimated concurrently. This occurs in the heat conduction equation with density and specific heat

$$\frac{\partial}{\partial x}\left(k\frac{\partial T}{\partial x}\right) = \rho c_p \frac{\partial T}{\partial t} \tag{3.49}$$

In any heat conduction experiment, only the volumetric heat capacity, ρc_p, can be determined. The density must be found from other independent experiments.

3.4.2 Modified Box-Kanemasu Estimation

The Modified Box-Kanemasu is a derivative of the Gauss linearization method, both of

which are frequently used estimation algorithms. A complete and detailed derivation of both methods can be found in Beck and Arnold (1977), but a brief overview will be given here. In the following analysis, ordinary least squares (OLS) estimation is assumed, which requires no known information about the errors.

As mentioned, the goal of parameter estimation is to minimize the sum of squares function, written here in matrix notation for OLS,

$$S = [Y - \eta_p(\beta_p)]^T[Y - \eta_p(\beta_p)] \ , \tag{3.50}$$

where Y is the observation vector (measured temperatures), η_p is the modeled vector (calculated temperatures), and β_p is the parameter vector, which contains the parameters to be estimated. In scalar notation, the sum of squares function results in the familiar expression

$$S = \sum_{i=1}^{n} [Y_i - \eta_p(\beta_p)]^2 \tag{3.51}$$

where n is the number of measurements. One of the requirements of the minimum of S is that the derivative of S with respect to the parameters is zero

$$\nabla_\beta S = 2[-\nabla_\beta \eta_p^T(\beta_p)][Y - \eta_p(\beta_p)] = 0. \tag{3.52}$$

Note that $\nabla_\beta \eta_p$ is the matrix of the sensitivity coefficients. The sensitivity matrix is defined as

$$X(\beta_p) \equiv [\nabla_\beta \eta_p^T(\beta_p)]^T \quad , \quad \text{where} \quad X_{ij} = \frac{\partial \eta_{pi}}{\partial \beta_{pj}} \ . \tag{3.53}$$

Equation (3.52) is difficult to solve for β_p, especially for problems that are non-linear *in the parameters*. In parameter estimation, a model is linear if it can be written as

$$\eta_{pi} = \beta_{p1} x_{1i} + \beta_{p2} x_{2i} + \ldots \tag{3.54}$$

where x are independent variables. Note that in accordance with this definition, even a linear heat conduction equation is nonlinear in the parameters. To simplify equation (3.56), two approximations are made. First, the exact parameter vector, $\boldsymbol{\beta}_p$, is replaced with the estimate vector, $\boldsymbol{b}$, and secondly, $\boldsymbol{\eta}_p(\boldsymbol{\beta}_p)$ is approximated with the first two terms of a Taylor series. Equation (3.52) can now be rewritten as

$$\boldsymbol{b}^{(k+1)} = \boldsymbol{b}^{(k)} + \boldsymbol{P}^{(k)}[\boldsymbol{X}^{T(k)}(\boldsymbol{Y} - \boldsymbol{\eta}_p^{(k)})] \tag{3.55}$$

where

$$\boldsymbol{P}^{(k)} \equiv [\boldsymbol{X}^{T(k)}\boldsymbol{X}^{(k)}]^{-1}, \tag{3.56}$$

which is the Gauss linearization method. Note that it is an iterative method, where $k+1$ represents the next iteration and $\boldsymbol{b}$, hopefully, converges to specific values. Also note that it requires an initial guess of the parameters, $\boldsymbol{b}^{(0)}$, and that the efficiency of the algorithm is somewhat dependent on the soundness of the initial estimates.

Many methods have been proposed to improve convergence, as well as the rate of convergence, and the following is by Box and Kanemasu {1972}. The method has been modified to include a check that the sum of squares function continually decreases to the minimum, ensuring the minimum is not overstepped.

Generalize equation (3.55) to

$$\boldsymbol{b}^{(k+1)} = \boldsymbol{b}^{(k)} + h^{(k+1)}\Delta_g \boldsymbol{b}^{(k)} \tag{3.57}$$

and

$$\Delta_g \boldsymbol{b}^{(k)} = \boldsymbol{P}^{(k)}[\boldsymbol{X}^{T(k)}(\boldsymbol{Y} - \boldsymbol{\eta}_p^{(k)})] \tag{3.58}$$

where $h^{(k+1)}$ is an iteration dependent scalar factor. This factor is determined through approximating S and β_p (see Beck and Arnold (1977)), leading to

$$h^{(k+1)} = G^{(k)}\alpha^2[S_\alpha^{(k)} - S_0^{(k)} + 2G^{(k)}\alpha]^{-1} \quad \textbf{(3.59)}$$

and

$$G^{(k)} = [\Delta_g \beta_p^{(k)}]^T(X^{T(k)}X^{(k)})[\Delta_g b^{(k)}] \ . \quad \textbf{(3.60)}$$

The terms S_0 and S_α are found by computing the sum of squares using $h=0$ and $h=\alpha$, respectively. The parameter α is used to ensure S continually decreases; if S increases, α is halved and S recomputed, and the process continued until S decreases. The value of α is initially set to one.

The process is iterative, with $\mathbf{b}^k$ being updated at the end of each iteration with $\mathbf{b}^{k+1}$ until the value of $\mathbf{b}^k$ stops changing significantly. This results in a criterion such as

$$\frac{b^{k+1} - b^k}{b^k} \leq tolerance = 1\times10^{-3}\ ,\ 1\times10^{-4}. \quad \textbf{(3.61)}$$

3.4.3 Genetic Algorithms in Optimization and Estimation

Genetic algorithms have been demonstrated by Garcia and Scott (1996) to be superior to other, more common, optimization algorithms, including the modified Box-Kanemasu, for optimization and estimation. The genetic algorithm was also used by Garcia (1996) to estimate parameters that had a high degree of correlation. These algorithms were used in addition to the modified Box-Kanemasu method to estimate the thermal properties in this study. The actual algorithm was written by Sandrine Garcia and only a brief review of the

method for thermal property estimation is given here.

The genetic algorithm used was an Extended Elitist GA and is outlined in Figure 3.11. In the GA, each parameter is considered a chromosome and each set of parameters is considered a genetic string. At the start, a random population of *n1* strings, or parameter sets, is created by randomly generating chromosomes from the initial parameter ranges input by the user. The strings are ranked according to the objective function, in this case the sum of squares, with the parameter set having the smallest S considered the best, or most fit, string. The chromosomes are selected from an initial range input by the user. A certain number of strings, *nbest*, are kept based on their rank and the process is repeated for a total of *npop* times. The resulting population of $nbest \times npop = n1$ parameter sets is the initial elitist population used to begin the analysis. In order to narrow the ranges when the parameters are not well known, this procedure is first performed with a large *n1* population and the *nbest* are used to determine better inital ranges for the algorithm. In that case, the program is stopped at this point.

In relation to biology, the *n1* strings constitute a "parent" population that is "mated" to create a "child" population, or new set of parameter sets. The child population is made by combining chromosomes, or parameters, from two different parents. In this algorithm, this process was achieved using a single-point crossover operation. In this operation, an integer, k, from one to the number of parameters, n, is randomly selected. Then, k parameters from the first parent and n-k parameters from the second parent are combined to create the child string. In addition, mutations, or random introduction of chromosomes, are performed on the

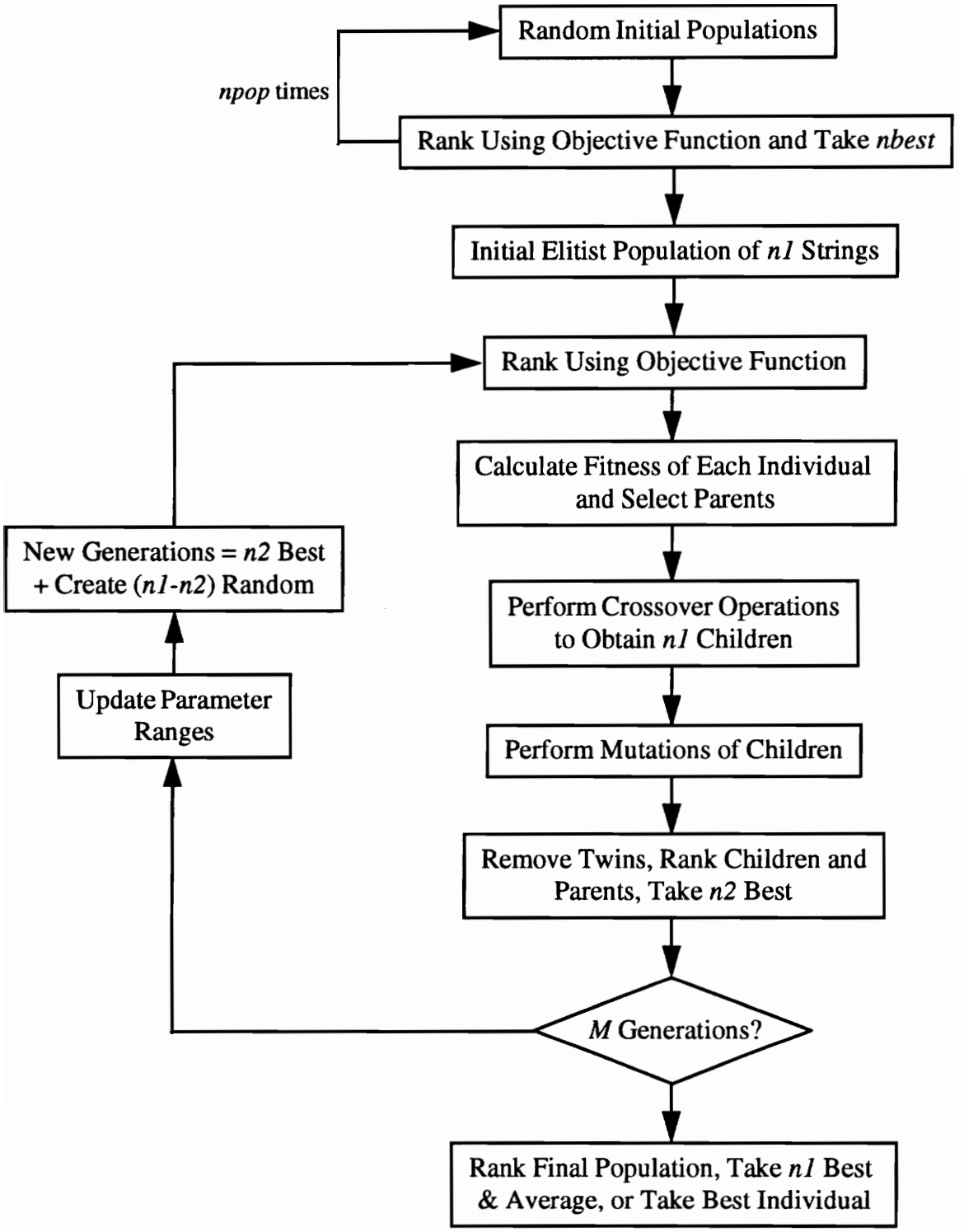

Figure 3.11 Extended Elitist Genetic Algorithm (Garcia, 1996).

children to introduce "new blood" and help prevent selection of a local minimum. The probability of a mutation is set quite small. There is now a population os 2×n1 strings, both parents and children. The best child strings, according to the sum of squares function, will be better than the best parent strings, so that each generation will create a set of estimates that more closely models the data than the previous generation.

Next, twins, or strings that are the same, are removed as redundant, the resulting population is ranked, and the *n2* best are selected for the new population. If this is the final generation, the program stops here and statistics are performed on both the *nbest* and *n1* best strings. If not, the parameter ranges are updated based on the *n3* best of the new population, where $n3 \leq n2$. Then, a new generation is created using the *n2* population and (*ns* - *n2*) random strings and ranked for selection of parents. Note that the random chromosomes are selected from the new parameter ranges, which are always the same as or narrower than the previous ranges. The process is then repeated for *M* generations. If the parameters do not show convergence at the end of *M* generations, another run is made with new parameter ranges and possibly a larger *M*.

3.4.4 Confidence Intervals and Correlation Matrix

Confidence intervals provide an idea of how close the estimated parameter is to the actual parameter. They give the probability that the estimated value is within a certain range of the actual value. The nonlinear OLS confidence interval, from Beck and Arnold (1977), is computed from

$$b_k \pm C.I. = b_k \pm \sqrt{(P_{kk})}\, t_{1-\alpha/2}(\nu) \qquad \textbf{(3.62)}$$

where ν is the degrees of freedom, $\nu = n\text{-}p$, $\alpha = 1\text{-}0.95 = 0.05$, and t is the t-distribution. This expression is approximate, with the approximation being better the more linear the problem. It also includes the ideal statistical assumptions of additive, zero mean, normal errors in Y and errorless independent variables. In this study a 95 percent probability is used for the confidence intervals. For a 95 percent probability and large degrees of freedom, $t_{.975}(>120) = 1.96$.

An approximate correlation matrix can also be formed using the **P** matrix. From Beck and Arnold (1977)

$$r_{ij} = P_{ij}(P_{ii}P_{jj})^{-1/2} \qquad \textbf{(3.63)}$$

where **r** is the approximate correlation matrix. Generally, if the absolute values of the off-diagonal elements are greater than 0.90, the estimates are correlated. Note that the diagonal elements represent the correlation between an estimate and itself and are always 1.0.

Chapter 4

Experimental Optimization

The developed heat transfer solutions were used to compare different experimental setups by analyzing the sensitivity coefficients for a variety of boundary conditions. Steady-state and transient experiments were considered for the diffusion solution. The steady-state case was examined for two constant-temperature surfaces, where the applied heat flux is the independent variable, and several possible experimental setups were considered for the transient experiments.

The absorbing and scattering solution was examined for an actual transient experiment that was conducted. The experiment consisted of a test sample with an applied heat flux on one surface and a constant temperature maintained on the opposite surface. The temperature being measured was that of the heated surface.

4.1 Materials and Properties

In order to optimize experiments and analyze the sensitivity coefficients, nominal values must generally be chosen for the material properties. This research was originally based on the properties of an aluminum oxide compound, Saffil, a fibrous, insulating material.

These nominal properties were used in the investigation of steady-state and transient diffusion solutions and the values are presented in Table 4.1. However, as this material was not available for testing, the transient solutions for absorbing and scattering media and the experiments were based on molded polystyrene, or Styrofoam.

4.1.1 Styrofoam

The material chosen to experimentally verify the parameter estimation procedure was Styrofoam, technically known as polystyrene. Styrofoam offers several advantages for this study. First of all, it has a significant amount of radiative heat transfer at low temperatures (Larkin and Churchill (1959) reported it to be around 20 percent), allowing for an experiment using available equipment. Secondly, Schuetz and Glicksman (1984) have shown that foams in general can be treated as isotropically scattering and are dominated by absorption. Schuetz, et al. (1987) also determined that for foams with small cell sizes, such as commercial foams, the foam can be assumed gray. Therefore, Styrofoam fits the assumptions used for the development of the heat transfer mode. Finally, Styrofoam is readily obtainable and some information is available on the effective thermal conductivity and heat capacity for this material, thus providing initial parameter values and validation for the experimental results.

The particular Styrofoam used consists of molded polystyrene beads in sheets approximately 3/4 in. (1.905 cm) thick. Measurements with calipers produced a thickness of 1.815 cm $\pm$ 0.03 cm. The beads are an average of 3-4 mm in diameter, with an average of 5 beads spanning the layer. Two pictures of the sample are shown in Figures 4.1 and 4.2.

Table 4.1 Nominal Saffil Property Values for Diffusion Sensitivity Analysis.

Effective Thermal conductivity:	[1] $k_{eff} = a + bT^3$
Constant term of effective thermal conductivity, a:	0.05 W/mK
Cubic term of effective thermal conductivity, [2]b:	3.6278×10^{-11} W/mK[4]
Extinction coefficient, β:	8340 m^{-1}
Heat capacity, c_p:	900.0 J/kg*K
Density, ρ:	30 kg/m^3
Thickness, D:	5.08 cm
[3]Optical thickness, κ_D:	423.7
Effective thermal conductivity @ 300K:	0.05098 W/mK
Effective thermal conductivity @ 600K:	0.05996 W/mK
Constant temperature at $x=0$, T_0:	650 K
Constant temperature at $x=D$, T_D:	300 K
Initial temperature, T_i:	300 K
Heat flux through material, [4]q":	380 W/m^2

[1] The temperature used in the k_{eff} equation must be absolute (R or K).
[2] $b = (16\sigma T^3)/(3\beta)$.
[3] The material is optically thick ($\kappa_D >> 1$).
[4] This was chosen to be equal to the q" for steady state with the given T_0 and T_D.

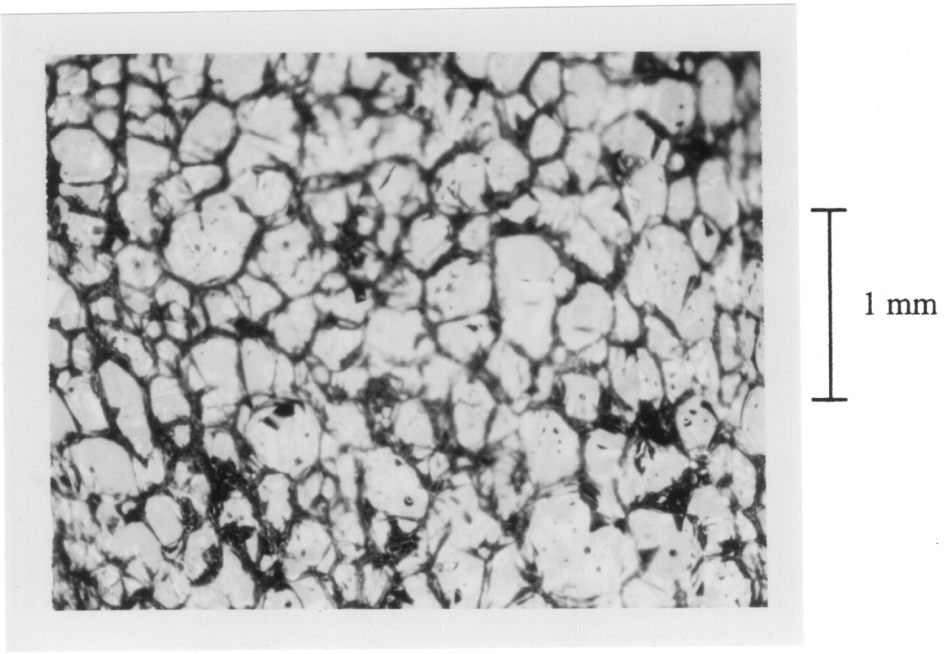

Figure 4.1 Photograph of Styrofoam Showing Center of a Bead.

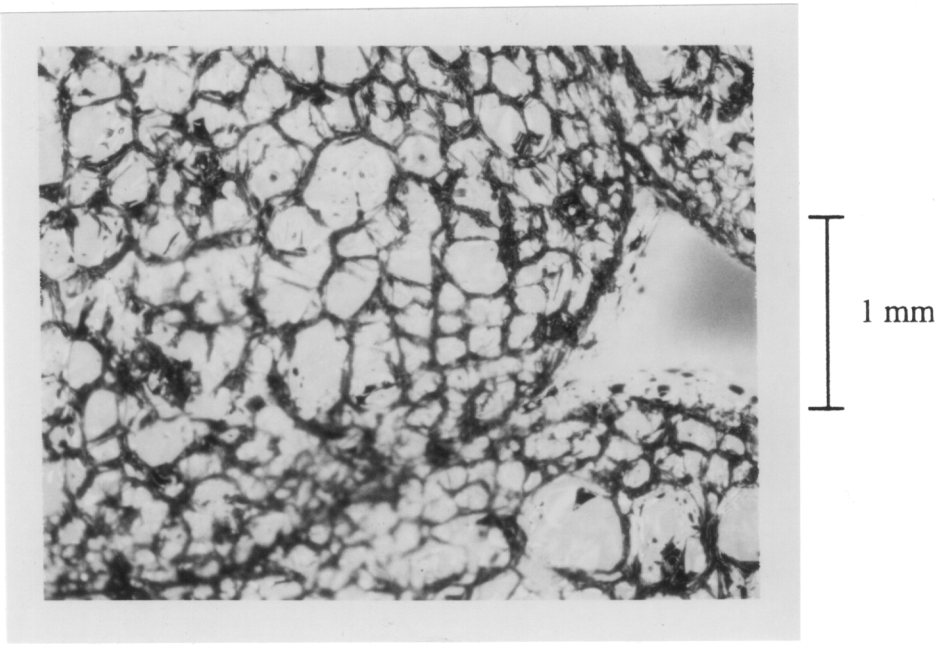

Figure 4.2 Photograph of Styrofoam Showing Junction of Three Beads.

Figure 4.1 is the inside of a bead and reveals a fairly uniform cell diameter of 0.1-0.2 mm. Figure 4.2 shows the junction of three beads, which creates a small gas space. The bubbles are also smaller near the outside of the bead, on the order of 0.08 mm. The radiation is transported through the material by transmission through the thin cell walls, absorption and emission by the cell walls across the gas spaces, and scattering and reabsorption. The cell size is small enough to regard the foam as homogeneous and the cell membrane thickness small enough to allow significant transmission.

Some typical properties for this type of material, from Incropera and DeWitt (1990), are given in Table 4.2.

Table 4.2 Nominal Styrofoam Conduction Properties.

Density	Specific heat	Thermal conductivity, (W/m·K)			
(kg/m^3)	(J/kg·K) @ 300 K	255 K	270 K	285 K	300 K
16.0	1200.0	0.035	0.036	0.038	0.040

The one disadvantage of Styrofoam is a low maximum serviceable temperature of about 350 K; above this temperature the material will start to degrade and melt. This maximum temperature limits the maximum heat flux that can be applied, and, consequently, the maximum sensitivity of the measurements.

Values for the absorption and scattering coefficient were not found. However, Schuetz and Glicksman (1984) determined some extinction coefficients for polyurethane

foams and these values were used as a starting point for the parameter estimation. The amount of scattering was simply a "best guess" based on the knowledge that Styrofoam is largely absorbing. The nominal values, and their corresponding scattering albedo and optical thickness (based on 1.815 cm), are presented in Table 4.3. Note that with an optical thickness of 27.23, the Styrofoam is optically thick, assuming it is a gray medium.

Table 4.3 Nominal Styrofoam Radiation Properties.

Absorption coefficient, a	Scattering coefficient, σ_s	Optical thickness, κ_D	Scattering albedo, Ω
1200 m^{-1}	300 m^{-1}	27.23	0.2

4.2 Steady-State Diffusion

The steady state experiment considered was one dimensional with each surface maintained at a constant temperature. This is equivalent to a constant applied heat flux at one boundary and a constant temperature at the other, since the heat flux through the material is constant for steady state conditions. The measured variable is the heat flux, determined by the power needed to maintain the hot surface at the specified temperature. The solution is given by equation (3.5) and the sensitivity coefficients, computed by equation (3.48), are

$$X_a = \frac{\partial q}{\partial a} = \frac{(T_D - T_0)}{D} \quad , \quad X_b = \frac{\partial q}{\partial b} = \frac{(T_D^4 - T_0^4)}{4D} \; . \tag{4.1}$$

In order to estimate the parameters, at least two measurements must be taken ($n \geq p$) at two different values of the heat flux. The optimal experimental design, as determined from the D-optimal criterion, is examined for the minimum number of measurements ($n=2$) and for a large value of n.

For two heat flux measurements, the D-optimal criterion is to maximize the absolute value of the determinant of $\mathbf{X}^T\mathbf{X}$, which results in

$$\max |X^T X| = \max\left[(X_{1a}X_{2b} - X_{1b}X_{2a})^2\right] . \qquad \textbf{(4.2)}$$

It can be seen that the determinant depends on the thickness of the material and four temperatures, T_0 and T_D for the first measurement and T_0 and T_D for the second measurement. Note that it does not depend on the values of the parameters being estimated; the model is linear in the parameters and can be written in the form $\eta_p = \beta_{p1}X_1 + \beta_{p2}X_2$. This has the very important result that the optimization is independent of the parameters being estimated and will be applicable to any material where the heat transfer can be represented by equation (3.5). Since the insulation comes in prefabricated thicknesses, the thickness was not considered as an experimental parameter that could be optimized.

Though nominal parameters were not required, they were used to normalize the sensitivity coefficients:

$$X_a^* = a\frac{\partial q}{\partial a} = \frac{a(T_D - T_0)}{L} \quad , \quad X_b^* = b\frac{\partial q}{\partial b} = \frac{b(T_D^4 - T_0^4)}{4L} \qquad \textbf{(4.3)}$$

This produces sensitivity coefficients that are easier to understand, as the units are W/m^2, and reduces the magnitude of the determinant to a manageable level. It does not change the

optimization results. The nominal property values for Saffil, Table 4.1, were used for the normalized sensitivity coefficients.

The optimal experiment maximizes the absolute value of the determinant in equation (4.2). Since the sensitivity coefficients are trivial to calculate and taking the derivative of equation (4.2) is complicated and time intensive, a parametric analysis was performed. The determinant was first calculated using a coarse grid of temperature values between 300 K and 650 K. Each of the four temperatures was varied across this range in increments of 25 K, for a total of 15 temperature values and 15^4 = 5,625 determinant values. The 30 largest determinant values are listed in Table 4.4.

Note that all the largest determinants have T_{01} = 300K and T_{D2} = 650K, the minimum and maximum temperatures, respectively. This fact was used to create a finer grid by fixing T_{01} and T_{D2} and varying T_{D1} and T_{02}. This grid had a resolution of one degree and resulted in the following optimal values

$$T_{01} = 300\text{K} \quad T_{D1} = 550\text{K} \quad T_{02} = 437\text{K} \quad T_{D2} = 650\text{K}\,.$$

These temperatures produced a determinant value of 9.7217×10^6. To ensure that T_{01} = 300K and T_{D2} = 650K produced the maximum determinant, the determinant was calculated using T_{D1} = 550K, T_{02} = 437K, T_{01} = 301K, and T_{D2} = 649K. The resulting determinant was less than the optimum. The determinant is plotted as a function of T_{D1} and T_{02} in Figures 4.3 and 4.4.

For the case of an arbitrarily large number of equally-spaced measurements, the experimental parameters to optimize are the ranges of the temperatures, i.e. the minimum and

Table 4.4 Thirty Largest S.S. Diffusion Determinants.

T_{01}	T_{D1}	T_{02}	T_{D2}	Determinant
300	550	425	650	9678000
300	550	450	650	9667000
300	575	450	650	9532170
300	525	425	650	9513420
300	525	400	650	9388070
300	575	475	650	9324670
300	550	400	650	9321840
300	525	450	650	9309690
300	575	425	650	9288970
300	550	475	650	9245610
300	525	375	650	8976820
300	600	475	650	8942060
300	500	400	650	8904120
300	600	450	650	8871390
300	500	425	650	8856920
300	525	475	650	8749140
300	500	375	650	8700720
300	550	375	650	8659120
300	575	400	650	8659120
300	575	500	650	8632040
300	500	450	650	8529310
300	600	500	650	8485110
300	550	500	650	8397040
300	600	425	650	8332120
300	525	350	650	8332120
300	500	350	650	8284760
300	625	475	650	8088170
300	475	400	650	7961170
300	625	500	650	7933350
300	475	375	650	7910820

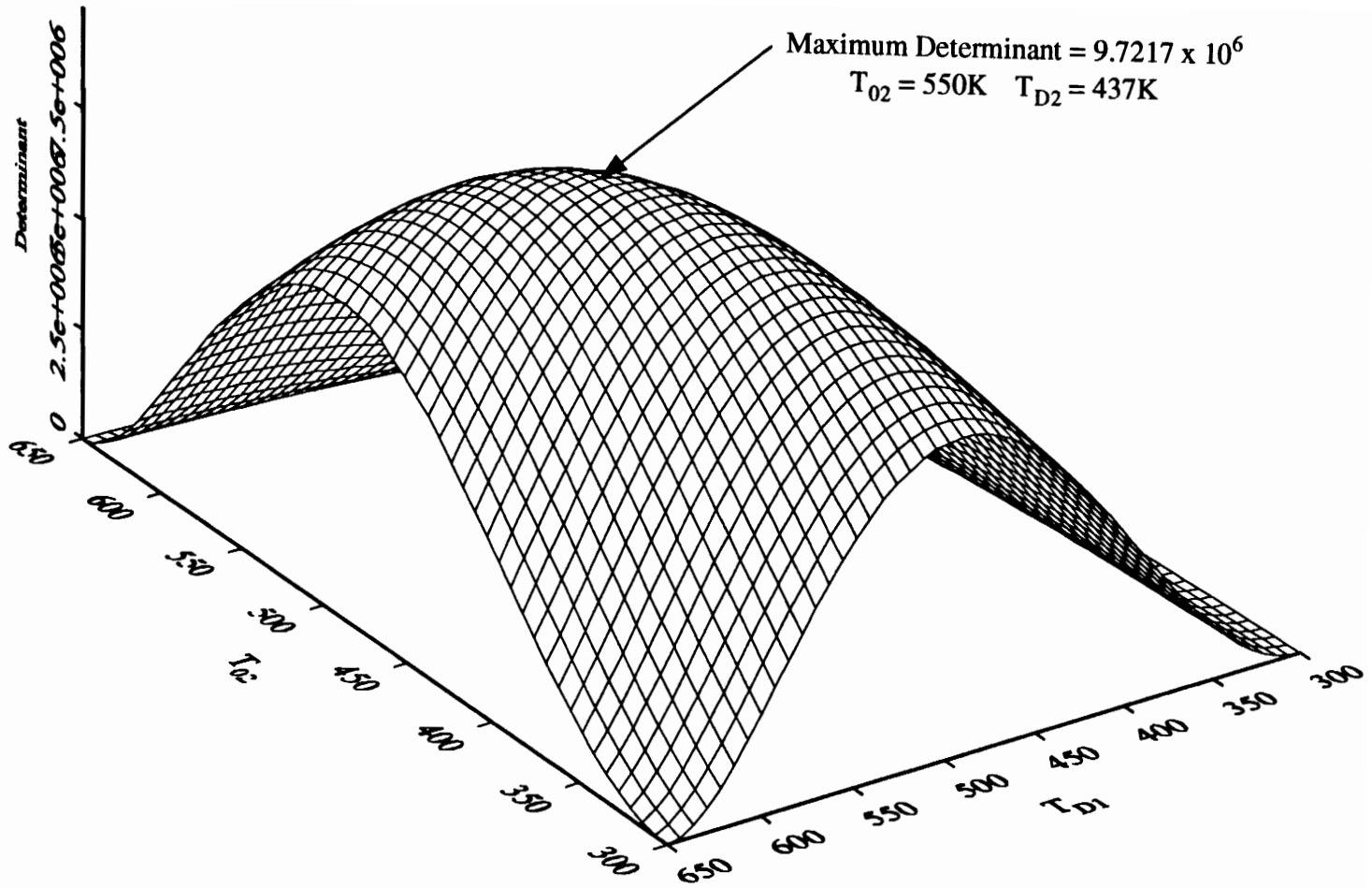

Figure 4.3 One Dimensional Steady State Determinants for Constant T_{01} and T_{D2}.

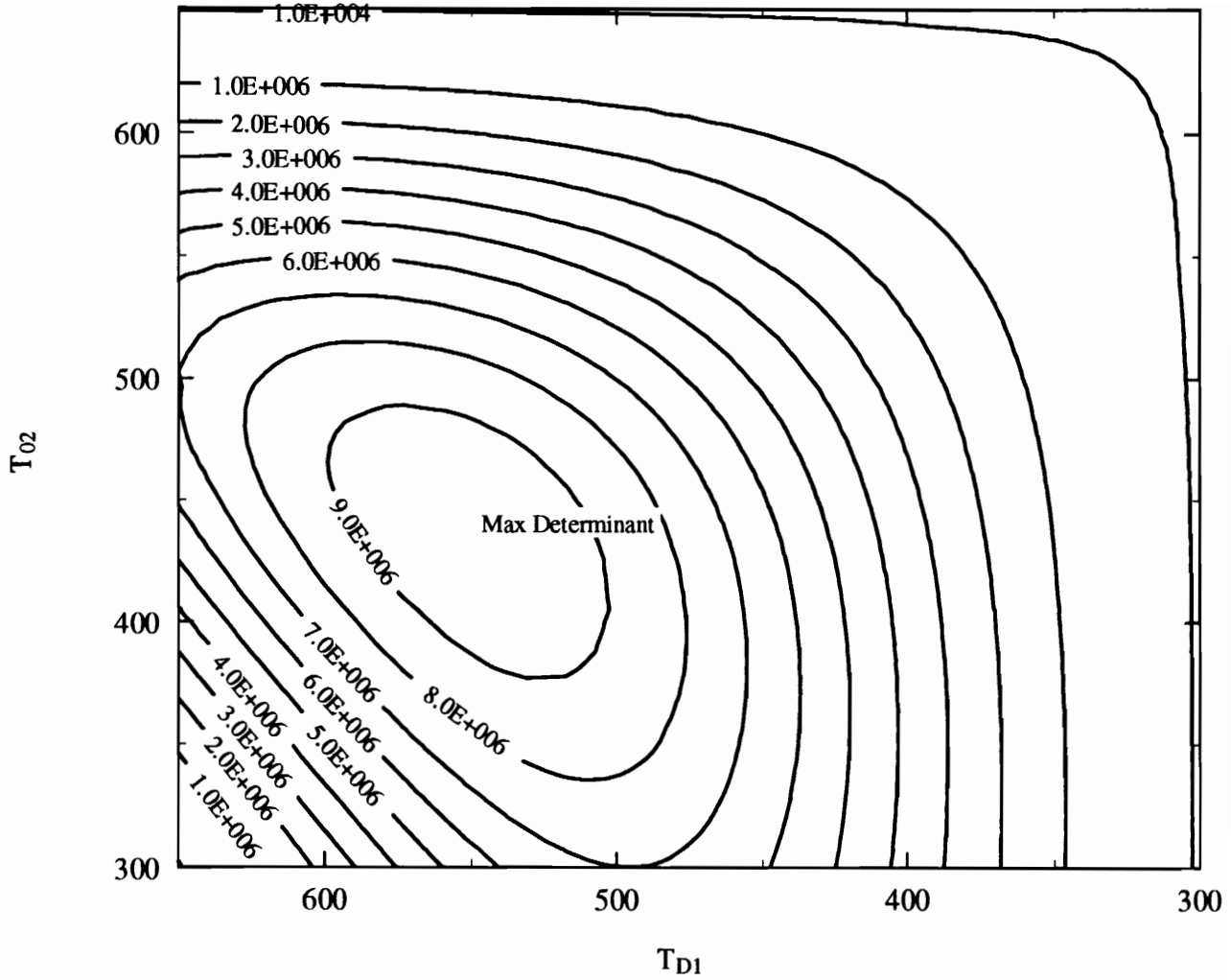

Figure 4.4 Contour Plot of One Dimensional Steady State Determinants.

maximum values for T_0 and T_D. The optimum values for each temperature occur when the sensitivity coefficients are maximized, so plots of the sensitivity coefficients were made for a and b for different T_0 and T_D values. Note that there are always practical constraints on the range of the temperatures, such as the melting point of the material and the highest or lowest temperature achievable in the laboratory.

An inspection of the sensitivity coefficients reveals that they do not have a mathematical maximum. The quantity X_a is a linear function and the quantitiy X_b is a third-order polynomial, both of which go to infinity with T_2 (or ΔT). The sensitivity coefficients are plotted in Figure 4.5, with the arbitrarily chosen temperature range of (300K, 1000K). As a result, the optimum T_2 is the highest practical value, while the optimum T_1 is the lowest practical value. The best experimental setup would be to fix T_1 at the lowest value and then vary T_2 in even increments until the highest value is reached.

The result for many measurements concurs with the two-measurement case, as two of those four optimum temperatures are the minimum and maximum values. Overall, the most important factor is the maximum temperature, or temperature difference, obtainable, which is to be expected since radiation increases strongly with temperature.

4.3 Transient Diffusion

Steady-state conditions generally take several hours to reach and maintaining constant temperature boundaries can be difficult, especially for long periods of time. This can lead to

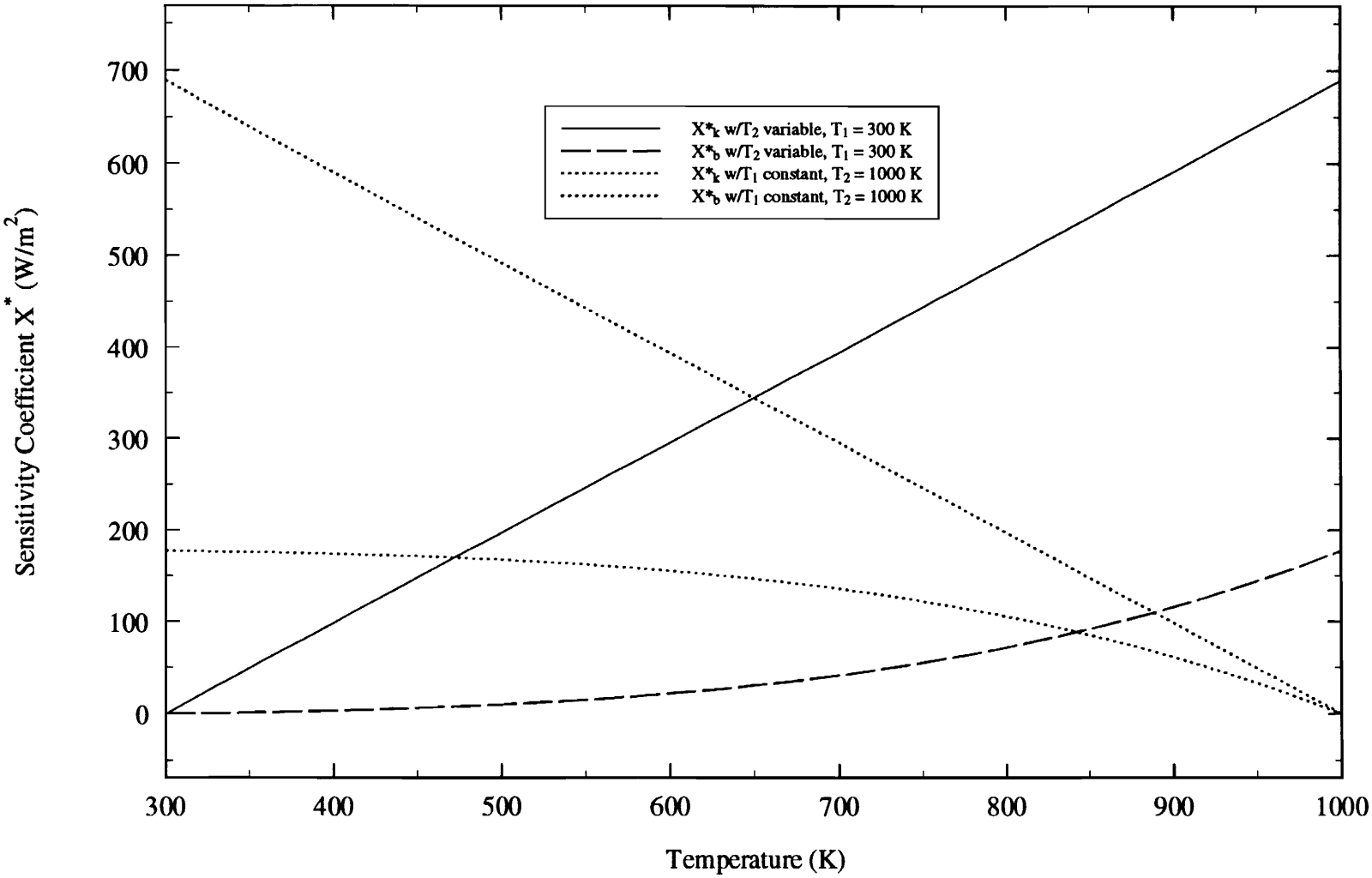

Figure 4.5 Steady-State Diffusion Sensitivity Coefficients for *k* and *b* and Large *n*.

a long, costly experiment. Furthermore, the heat capacity of a material cannot be determined from a steady state-experiment. To overcome these problems, transient experiments are often employed, where the temperature history at a point or points is measured. This section details an analysis of transient experiments for the diffusion solution.

The governing equation is equation (3.10); this is a nonlinear partial differential equation that is also nonlinear in the parameters. There are two consequences from these nonlinearities. First, the sensitivity coefficients and optimization will depend on the values of the properties that need to be estimated. This requires a set of nominal parameters as close to the actual values as can be obtained. If the estimation procedure results in parameter values significantly different from the nominal values, the optimization may have to be performed again using the new estimates.

Secondly, the sensitivity coefficients will have to be determined numerically, since the solution is only known numerically. The sensitivity coefficients were computed using a forward finite difference representation

$$X_a \approx \frac{T(a+\delta a,b,c...) - T(a,b,c...)}{\delta a} \tag{4.4}$$

where δa is a small number. A forward difference was used in place of a central difference due to the length of time to obtain the solution; the latter would require twice as many solutions as the former. A comparison of several sensitivity coefficients calculated using both forward and central differences did not reveal any significant discrepancies in the methods. The sensitivity coefficient actually used is X^*, as in equation (4.3).

The sensitivity coefficients are dependent on all the same parameters that determine the temperature solution. This includes not only the desired properties, but also the position, time, thickness, initial temperature, and boundary conditions. All these can be used to optimize the experiments.

Several types of boundary conditions were considered: applied heat flux, constant temperature, and insulated. The resulting four configurations are illustrated in Figure 4.6. A single and double thickness of insulation were considered and sensitivity coefficients were calculated at four positions: *0*, *D/4*, *D/2*, and *D*. The experimental time was set at 30 min. (1800 s). The initial value and constant temperatures were not varied as the steady-state results indicate the greatest difference between temperatures will give the highest sensitivity coefficients. The same idea applies to the heat flux. The higher the heat flux, the greater the increase in temperature and the higher the sensitivity coefficient, so the heat flux was kept constant. To maintain some degree of commonality between the applied heat flux case and the constant, high temperature case, the heat flux value was set equal to the steady-state heat flux through the material with the two constant temperatures on both sides. The nominal properties and parameters are listed in Table 4.1.

An application of the D-optimal criterion for each experiment and all variables would require considerable computation time for even a few different variables, so only the sensitivity coefficients were calculated and plotted for each case to gain some insight into the best experiment. The experiment which produces the highest sensitivity coefficients will provide the most information for determining the parameters.

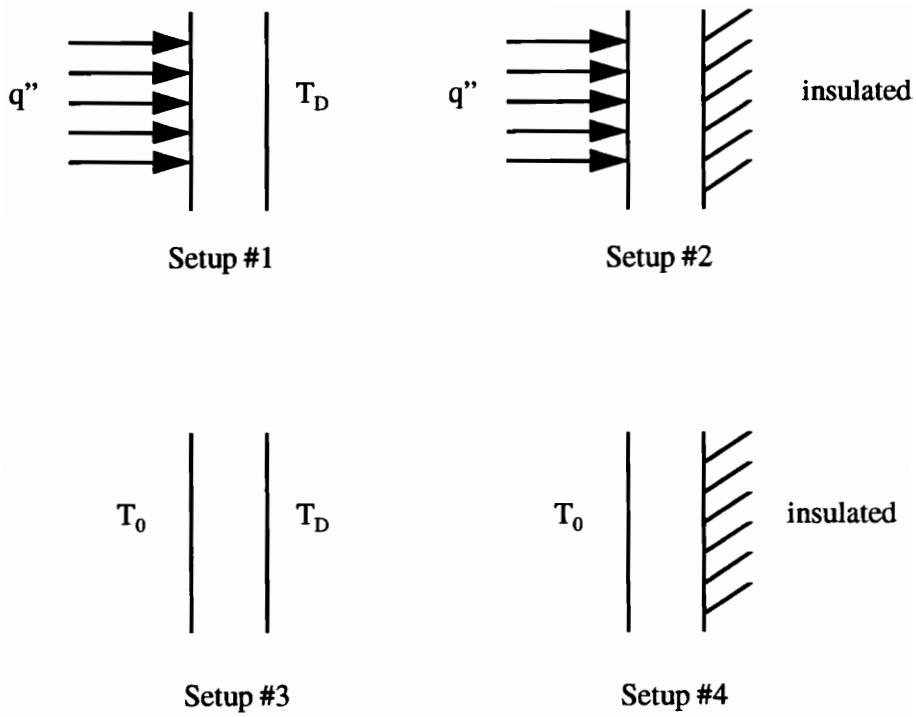

Figure 4.6 Experimental Setups for Transient Diffusion.

The sensitivity coefficients were calculated and are plotted in Figures 4.7 through 4.20. A summary of maximum sensitivity coefficients and their respective times are reported in Table 4.5.

There are several things to note concerning the graphs. First, none of the setups quite reaches steady-state by 1800 s. Secondly, sensitivity coefficients are not given at the constant temperature boundaries; since the temperature does not change, the sensitivity coefficients are zero and no information can be obtained by placing sensors at those locations. Thirdly, note that the volumetric heat capacity and extinction coefficient sensitivity coefficients for the *q", insulated* case are roughly linear and do not seem to level out with time. This is due to the nature of the solution. Ideally, the temperature of a material with a heat flux on one side and an insulated boundary on the other would rise indefinitely, as the energy is unable to dissipate into the surroundings. Since the heat capacity is related to changes in temperature with time and the extinction coefficient is related to changes in thermal conductivity with temperature, as long as the temperature rises, so will these sensitivity coefficients. In reality, the temperature will eventually level off from heat loss through the insulating material and three-dimensional heat loss in the planar direction. Therefore, there will be some practical limit to the length of time for that experimental setup that would have to be determined from a more complex analysis including heat loss at the insulated boundary.

Table 4.5 reveals that the experiment with the most information for k is $q"$, T_D, while for c and β it is *q", insulated.* In all three cases, the highest sensitivity coefficient occurs at the heated surface and at the end of the time period, which may not be practical in order to

Table 4.5 Maximum Sensitivity Coefficients for Transient Diffusion Experiments.

Experimental Setup	Position	Maximum Sensitivity Coefficient	Time (s)
k			
q", T_D	0	-0.680	1800
q", T_D	D/4	-0.537	1800
T_0, insulated	D	0.396	479
q", T_D	D/2	-0.373	1800
T_0, insulated	D/2	0.270	493
q", insulated	0	-0.257	576
T_0, insulated	D/4	0.202	37
T_0, T_D	D/4	0.202	37
T_0, T_D	D/2	0.198	126
q", insulated	D	0.139	718
q", insulated	D/4	-0.095	725
q", insulated	D/2	0.038	239
c			
q", insulated	D	-1.343	1800
q", insulated	D/2	-1.298	1800
q", insulated	D/4	-1.241	1800
q", insulated	0	-1.164	1800
T_0, insulated	D	-0.437	506
T_0, insulated	D/2	-0.303	502
q", T_D	0	-0.269	514
q", T_D	D/4	-0.259	528
T_0, T_D	D/4	-0.225	41
T_0, insulated	D/4	-0.225	41
T_0, T_D	D/2	-0.220	134
q", T_D	D/2	-0.204	538
β			
q", insulated	0	0.065	1800
q", T_D.	0	0.059	1800
T_0, insulated	D	-0.044	667
T_0, insulated	D/2	-0.034	536
q", T_D	D/4	0.032	1800
q", insulated	D	-0.031	1800
T_0, T_D	D/4	-0.027	78
T_0, insulated	D/4	-0.027	85
T_0, T_D	D/2	-0.025	224
q", insulated	D/4	0.021	1700
q", T_D	D/2	0.015	1800
q", insulated	D/2	-0.009	1791

q" - Applied Heat Flux
T_0 - Constant Temperature at $x=0$
T_D - Constant Temperature at $x=D$

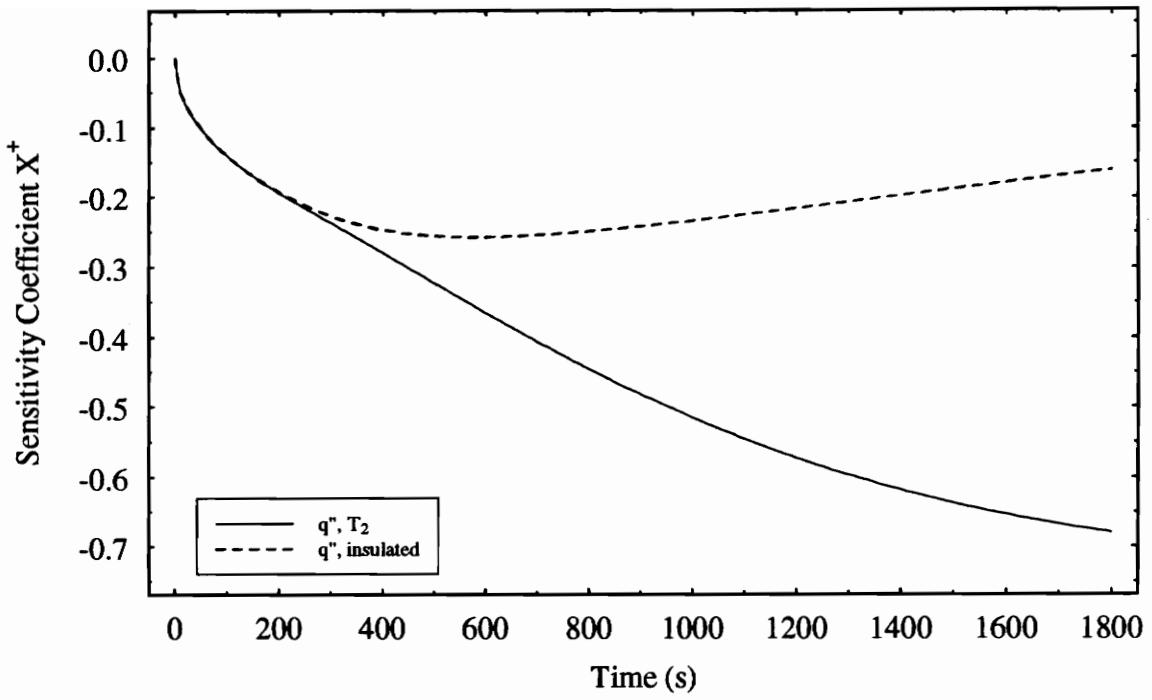

Figure 4.7 Nondimensional Diffusion Sensitivity Coefficients (X^+) at $x=0$ for Thermal Conductivity, k.

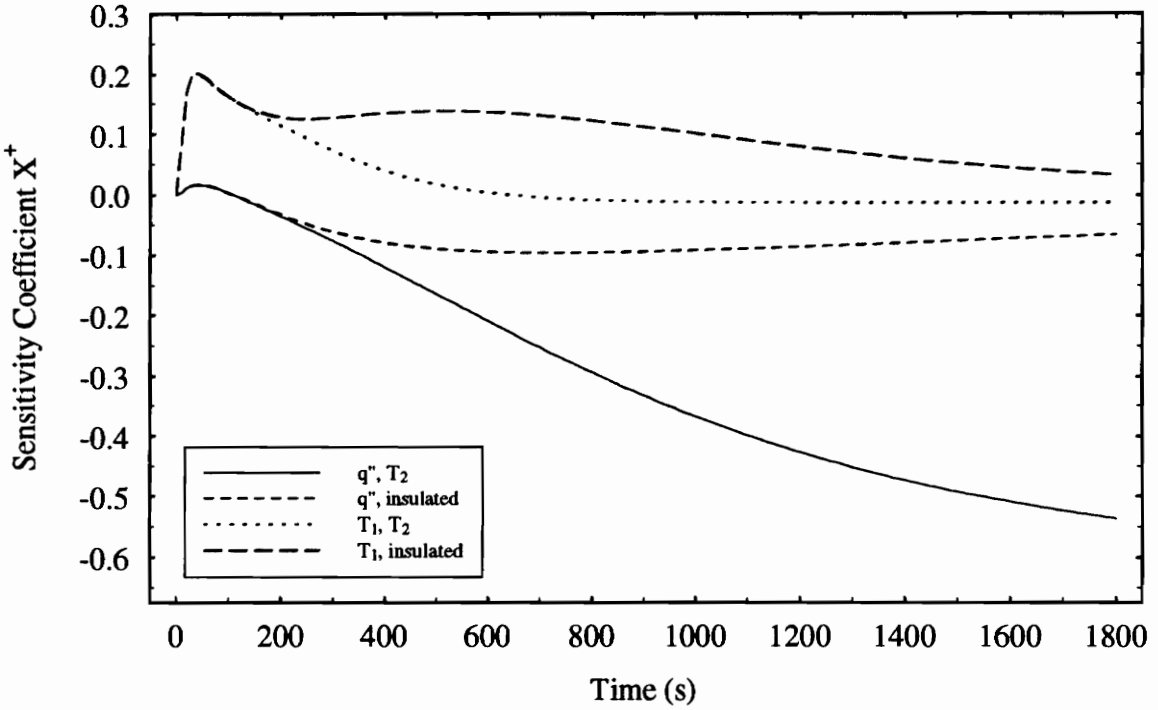

Figure 4.8 Nondimensional Diffusion Sensitivity Coefficients (X^+) at $x=D/4$ for Thermal Conductivity, k.

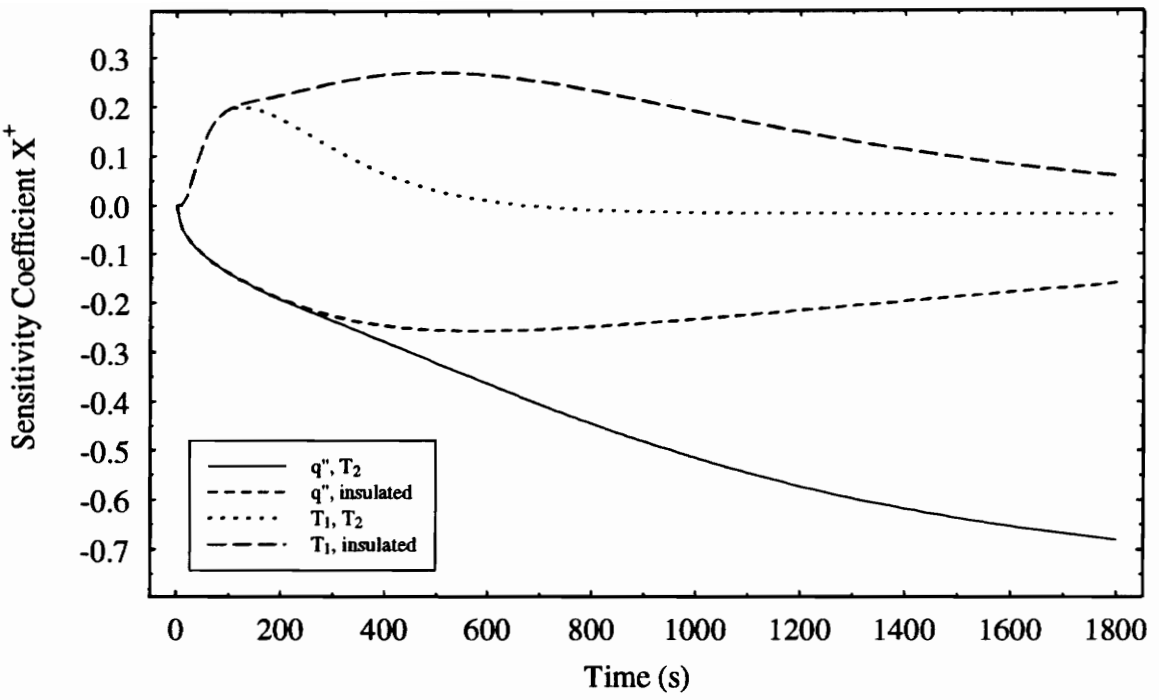

Figure 4.9 Nondimensional Diffusion Sensitivity Coefficients (X^+) at $x=D/2$ for Thermal Conductivity, k.

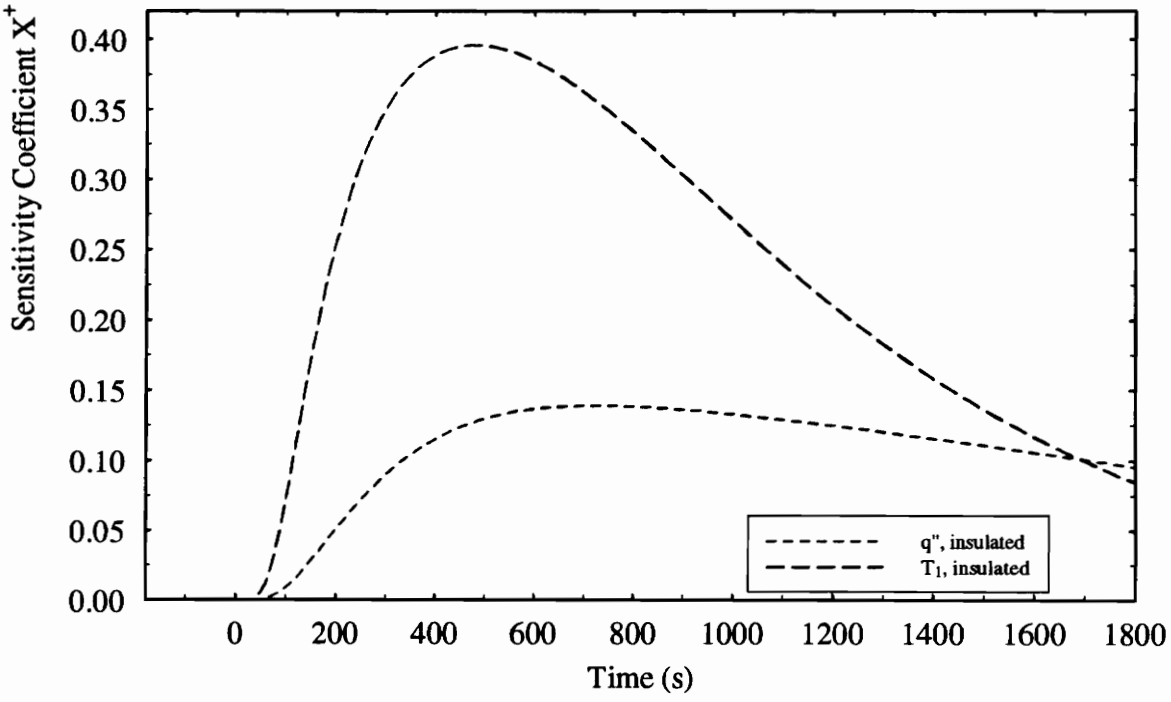

Figure 4.10 Nondimensional Diffusion Sensitivity Coefficients (X^+) at $x=D$ for Thermal Conductivity, k.

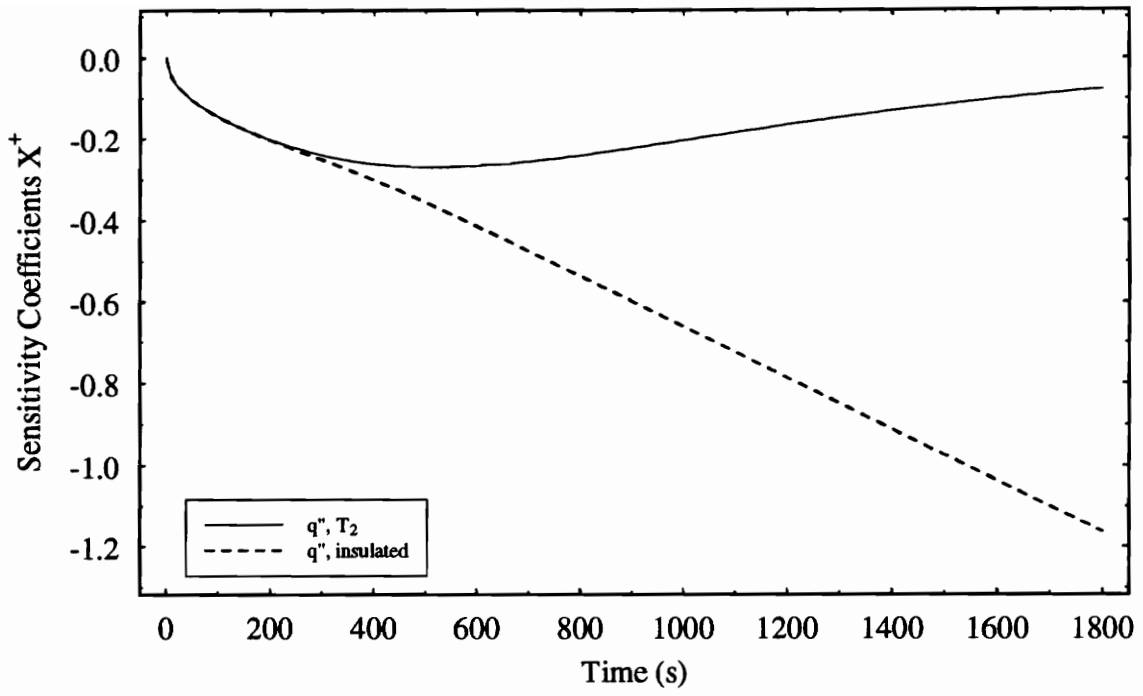

Figure 4.11 Nondimensional Diffusion Sensitivity Coefficients (X^+) at $x=0$ for Volumetric Heat Capacity, c.

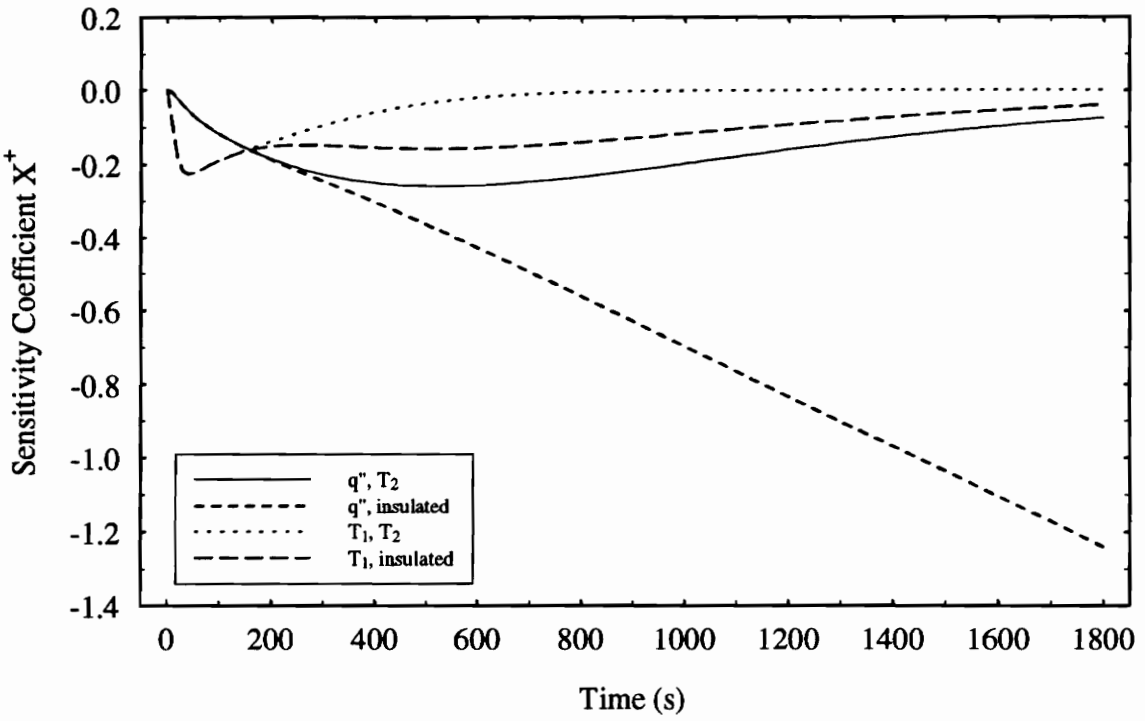

Figure 4.12 Nondimensional Diffusion Sensitivity Coefficients (X^+) at $x=D/4$ for Volumetric Heat Capacity, c.

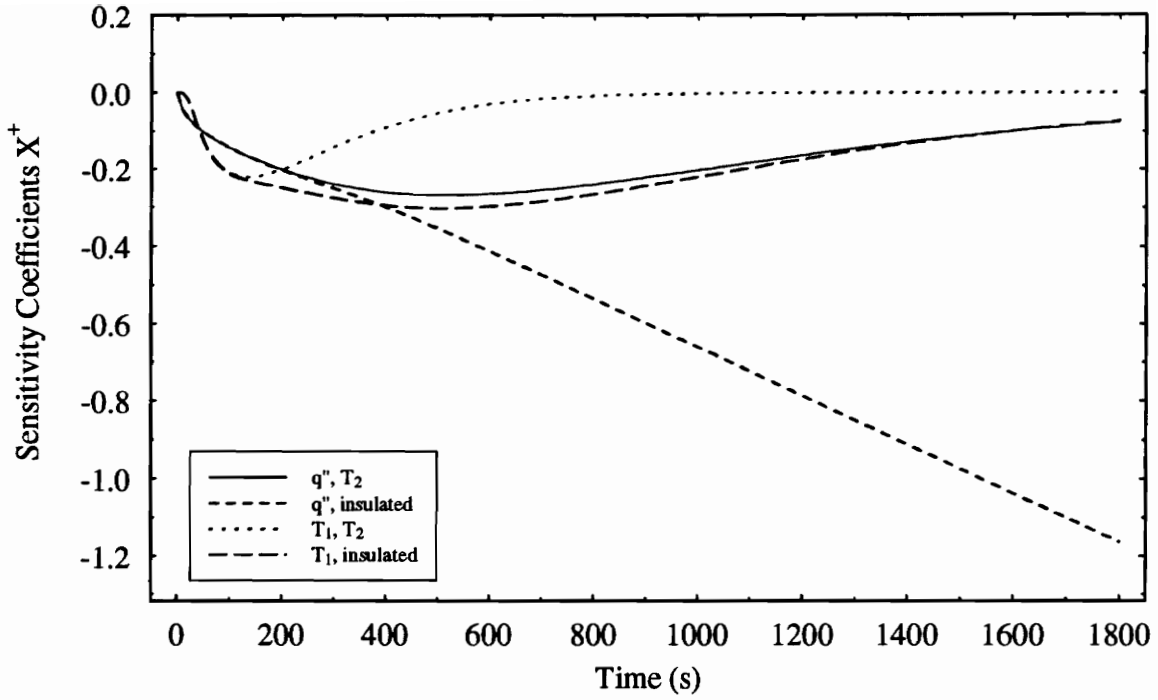

Figure 4.13 Nondimensional Diffusion Sensitivity Coefficients (X^+) at $x=D/2$ for Volumetric Heat Capacity, c.

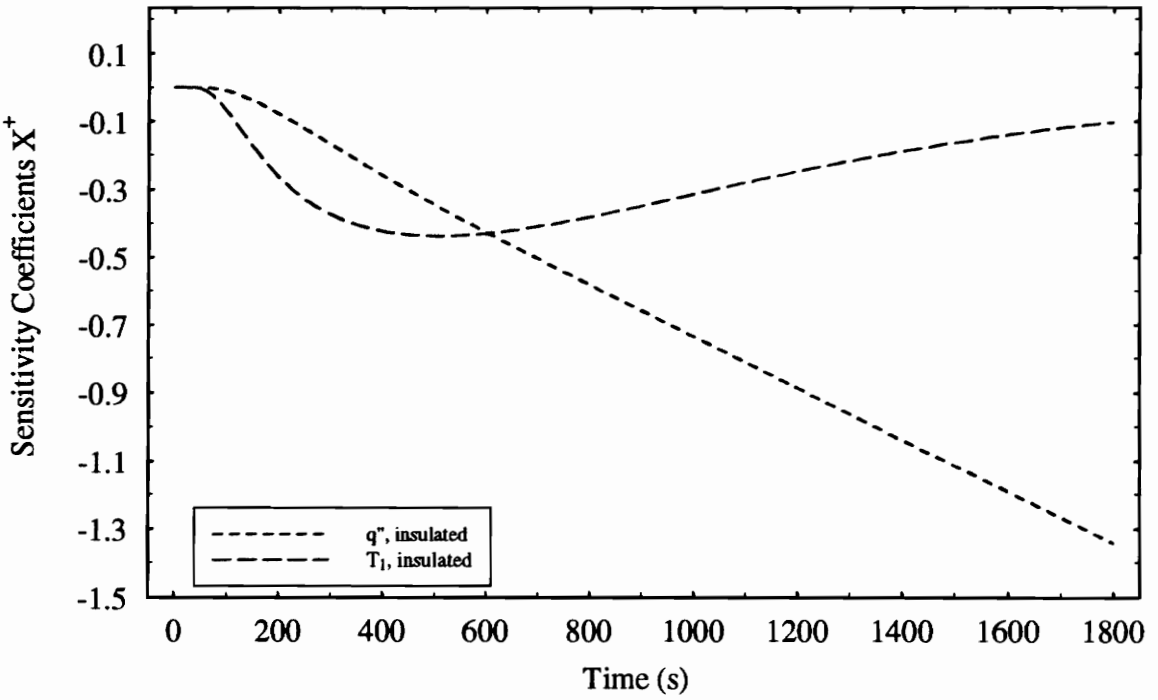

Figure 4.14 Nondimensional Diffusion Sensitivity Coefficients (X^+) at $x=D$ for Volumetric Heat Capacity, c.

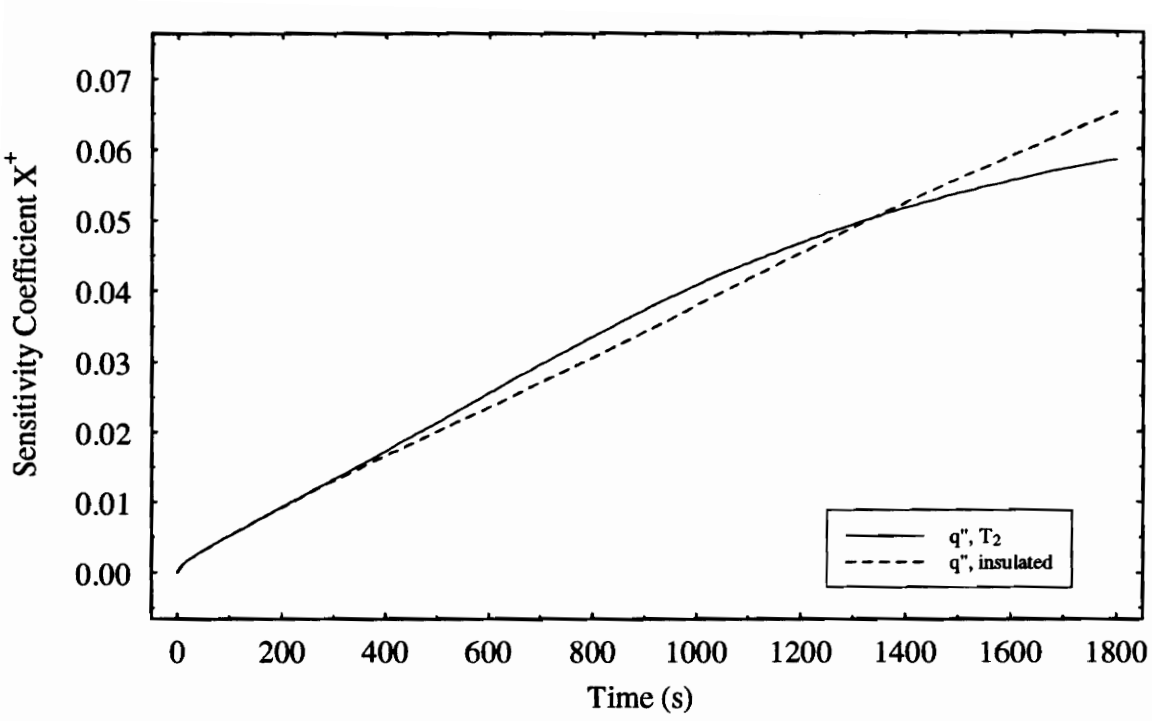

Figure 4.15 Nondimensional Diffusion Sensitivity Coefficients (X^+) at $x=0$ for the Extinction Coefficient, β.

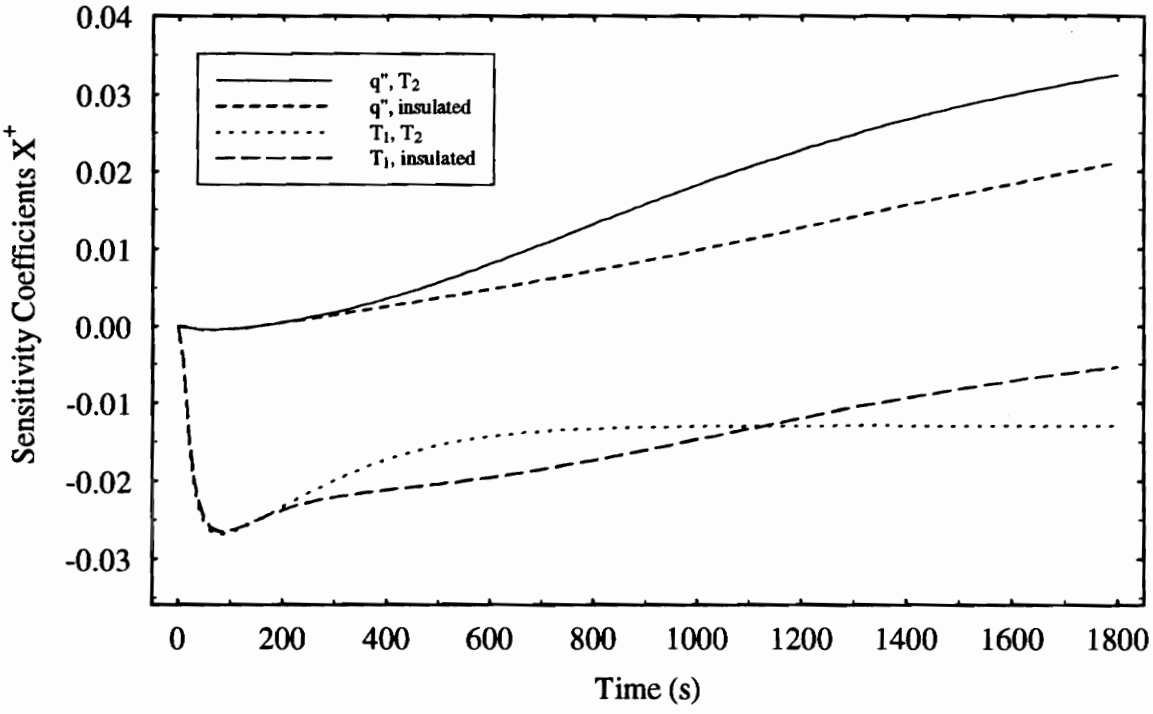

Figure 4.16 Nondimensional Diffusion Sensitivity Coefficients (X^+) at $x=D/4$ for the Extinction Coefficient, β.

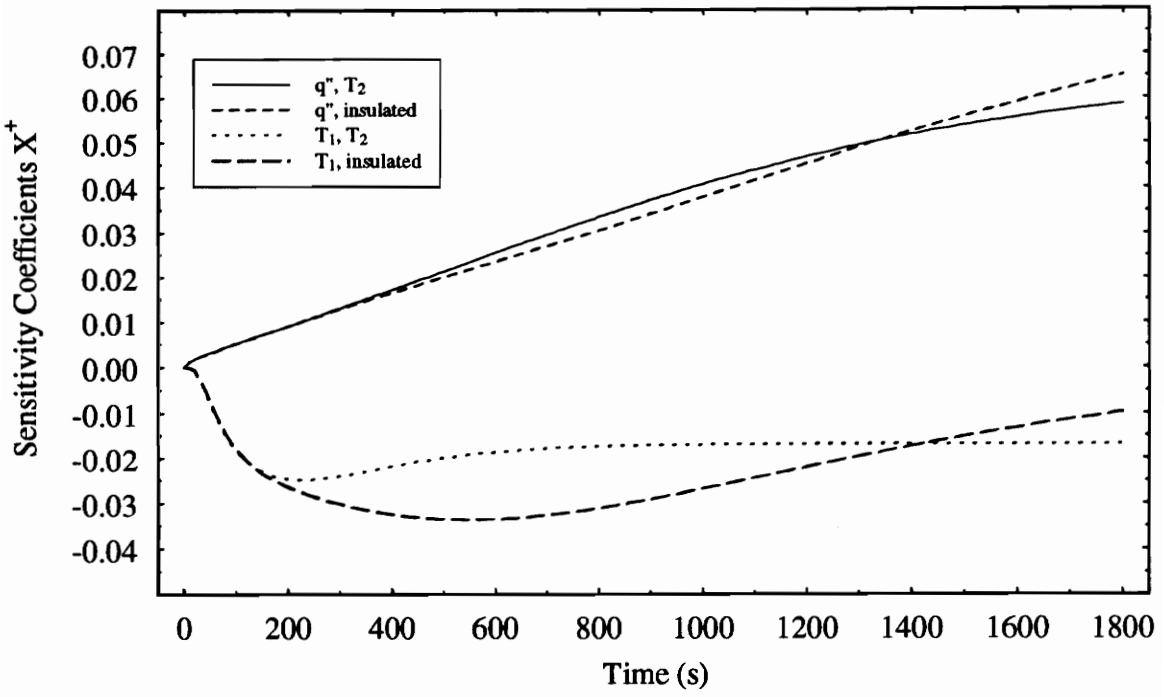

Figure 4.17 Nondimensional Diffusion Sensitivity Coefficients (X^+) at $x=D/2$ for the Extinction Coefficient, β.

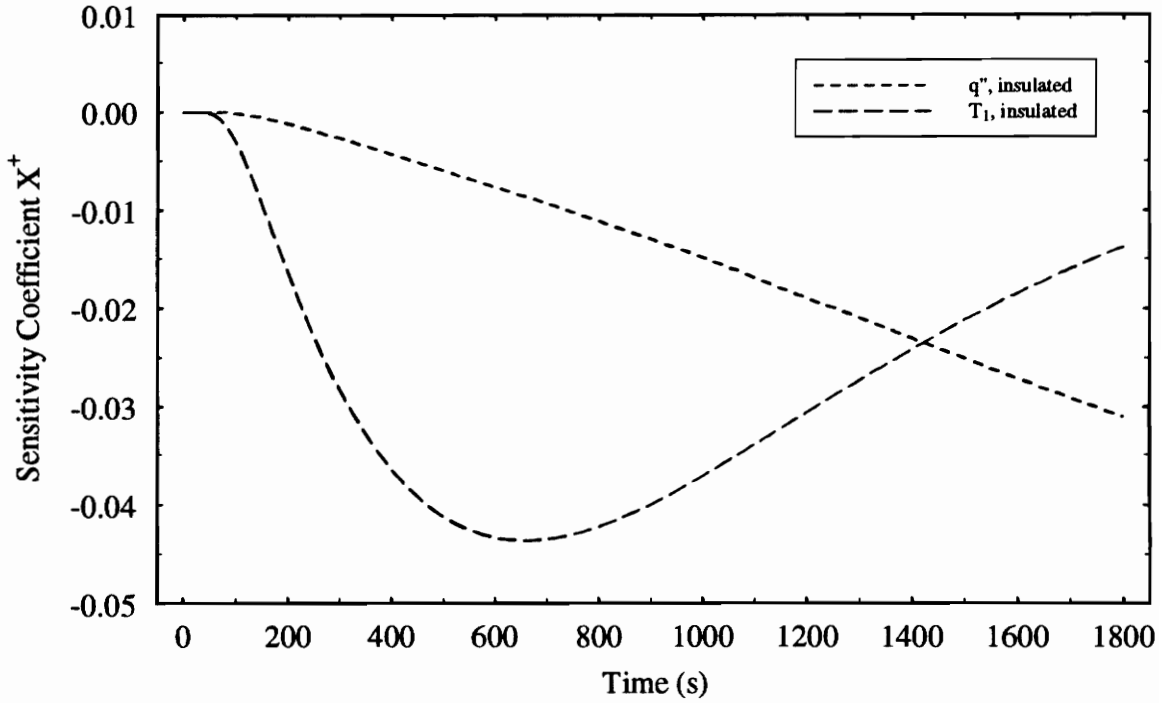

Figure 4.18 Nondimensional Diffusion Sensitivity Coefficients (X^+) at $x=D$ for the Extinction Coefficient, β.

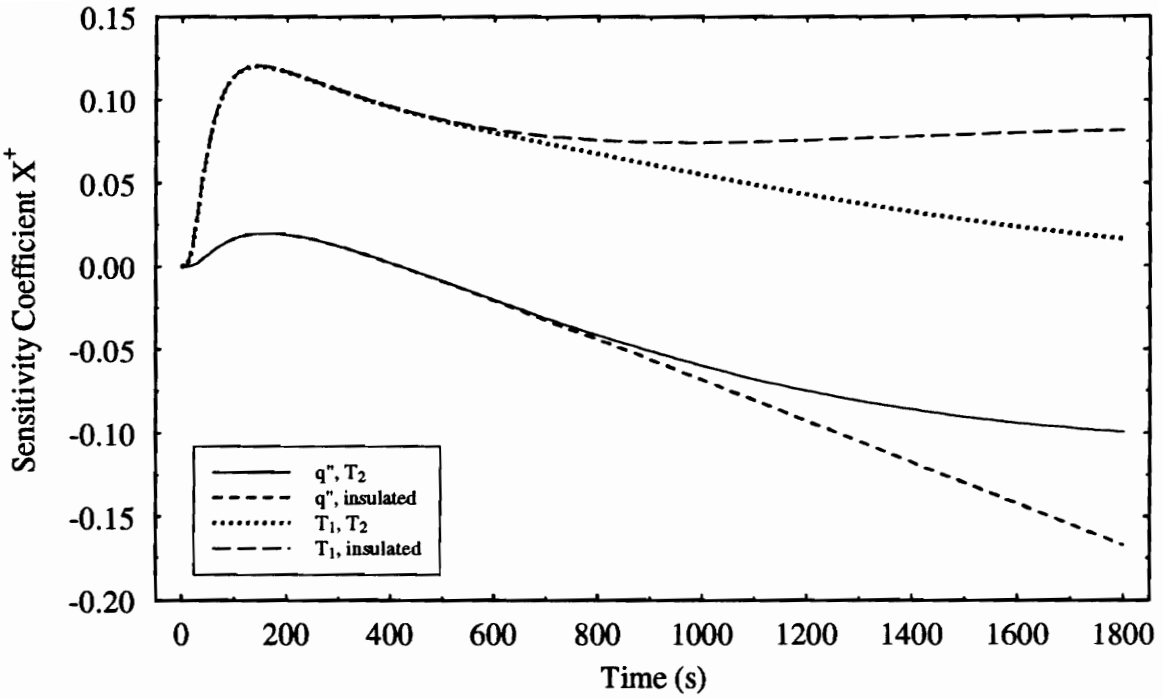

Figure 4.19 Nondimensional Diffusion Sensitivity Coefficients (X^+) at *x=(2D)/4* for Thermal Conductivity, *k*.

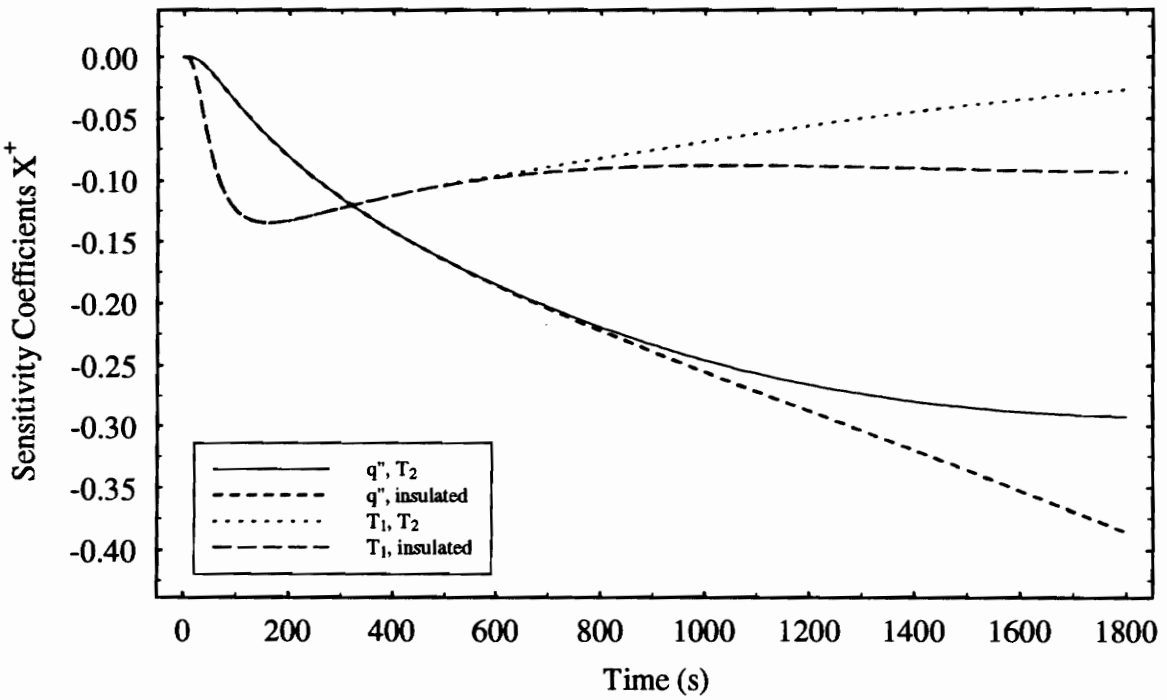

Figure 4.20 Nondimensional Diffusion Sensitivity Coefficients (X^+) at *x=(2D)/4* for Volumetric Heat Capacity, *c*.

maintain a one-dimensional setup. For a shorter time, the T_0, *insulated* case has a fairly high sensitivity coefficient value at the insulated surface at 479 s; however, the q'', T_D case reaches the same value at about 700s. For c, the T_0, *insulated* case gives the next best information at D (506 s) and $D/2$ (502 s). The same is true of β. Note that in all cases, except for c with q'', *insulated* boundaries, the highest value for any setup occurs at the heated surface, $x=0$.

Doubling the thickness to 2D resulted in the basic curve shapes remaining the same, but the maximum sensitivity coefficient being somewhat higher and occurring at a later time. As the curves are basically the same, only two are shown in Figure 4.19 and Figure 4.20 for k and c at (2D)/4.

All of the results here are dependent on the ability to create and maintain the experimental setups. Constant temperatures, especially those that are very high or very low, can be difficult to produce and maintain. It is easier to generate a large heat flux, and a larger heat flux would produce larger sensitivity coefficients, giving more information than a modest constant high temperature surface. The ability to place sensors nonobtrusively within the material is another concern. Placing sensors at locations other than the surface can change the nature of the material in the region of the sensor and introduce contact resistance. There is also the difficulty of knowing the position of the sensor in the material to a fair degree of accuracy. Doubling the thickness would allow easier placement in the middle of the sample and a higher sensitivity coefficient, but would also introduce contact resistance and require a longer experimental time.

Another important consideration for insulations is the ability to successfully produce

an insulated boundary. In most cases, the insulating material would have a thermal conductivity on the same order of magnitude as the specimen, making a realistic insulated boundary almost impossible to achieve. In fact, Copenhaver (1996) was unable to achieve a satisfactory insulated boundary condition on a relatively conductive honeycomb structure. The other ways to produce a reasonable insulated boundary would be to create a vacuum at the surface, which in most cases would not be feasible, to implement a more complicated guarded heater apparatus, or to create a symetrical situation. Note that a vacuum boundary would still allow radiation transfer and thus would preclude use of the diffusion solution anywhere close to the boundaries.

Overall, for insulative type materials with low thermal conductivities, the best experiment would have an applied heat flux on one boundary and a constant temperature on the other boundary. The highest possible heat flux and lowest possible constant temperature should be employed. Temperatures should be measured at the heated surface. Depending on the ability to maintain one-dimensional heat transfer for a long period of time, a thicker sample would provide more information, but a thinner sample may be more convenient and provide adequate information.

4.4 Transient Absorbing and Scattering

The one-dimensional experiment with an applied heat flux and constant temperature boundaries was investigated using the absorbing and scattering solution. The nominal

parameters used in the study were those for Styrofoam, but some deviation from these parameters is also investigated to gain some insight into the use of this experimental setup for other materials. Within the limitations of the experimental setup, the only parameters to optimize are the heating time, the experimental time, and the value of the heat flux.

The higher the heat flux, the greater the change in temperature and the greater the sensitivity coefficient, so the highest heat flux available would be best. However, as mentioned, another experimental constraint is the maximum serviceable temperature of the Styrofoam, which is 350 K. Equation (3.5) can be used to find the heat flux in steady-state conditions with a temperature of 350 K on one side and the constant room temperature on the other side. For the purposes of estimation, room temperature was considered 298 K (25°C). This results in a maximum heat flux of 100.0 W/m^2. The sensitivity coefficients for the properties are shown in Figure 4.21, given the nominal values and the nominal experimental parameters. Some variations on these parameters are presented in Figures 4.22 through 4.31 to gain insight into the general estimation problem for this type of experiment.

The nominal sensitivity coefficients reveal a significant amount of information for k, c, and a, but very little for σ_s, indicating it may be difficult to estimate. It also appears that a and σ_s are very correlated and k and a may be somewhat correlated. The sensitivity coefficients for the same material, but with scattering albedos of 0.5 and 0.8, are plotted in Figures 4.22 and 4.23. These plots reveal that as the percentage of scattering increases, the scattering coefficient has more information while the absorption coefficient has less, which is intuitive. Figure 4.22 also reveals quite clearly the correlation between the two, making

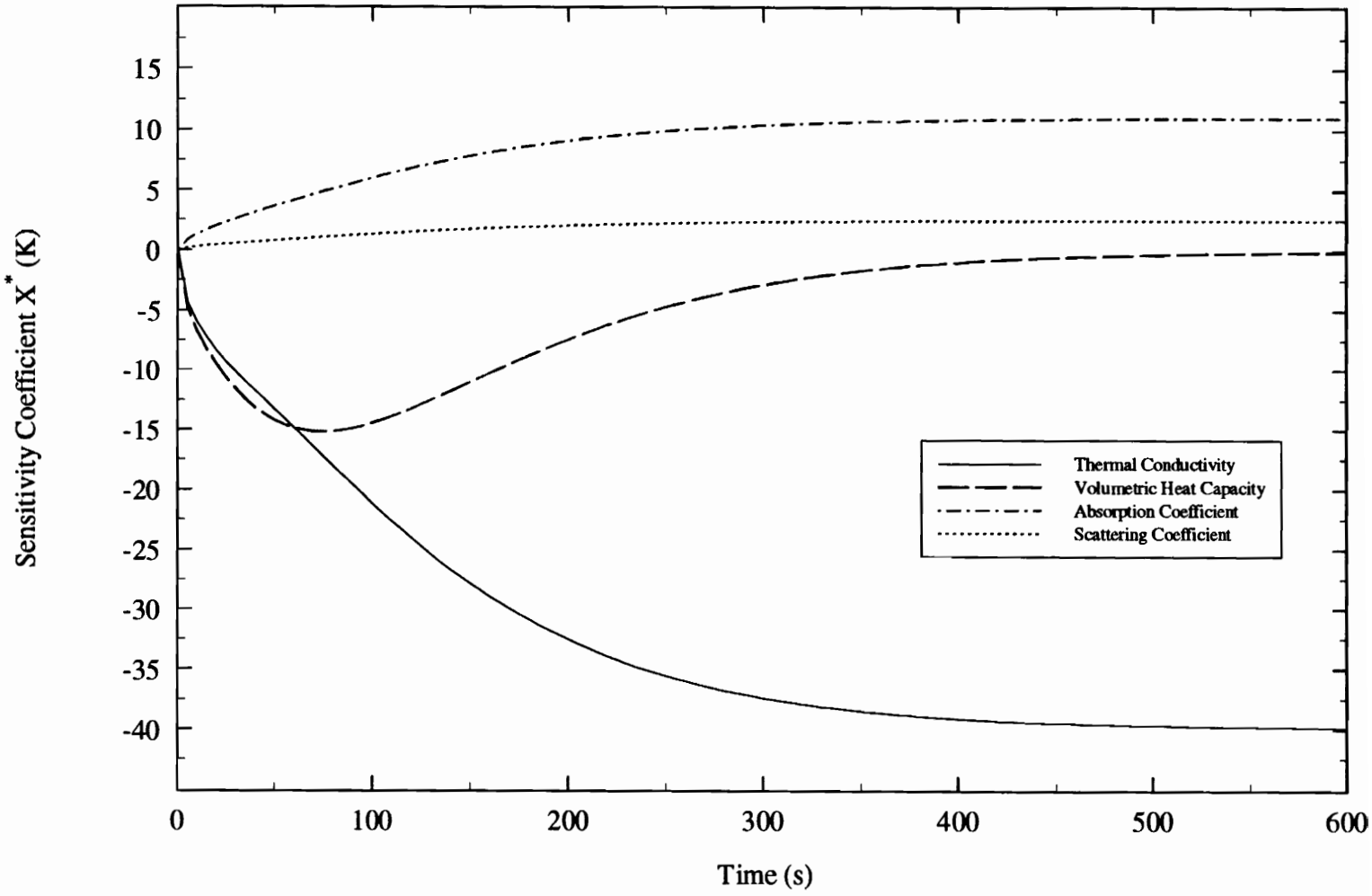

Figure 4.21 Normalized Sensitvity Coefficients (X*) for Nominal Styrofoam Properties Using Absorbing and Scattering Solution.

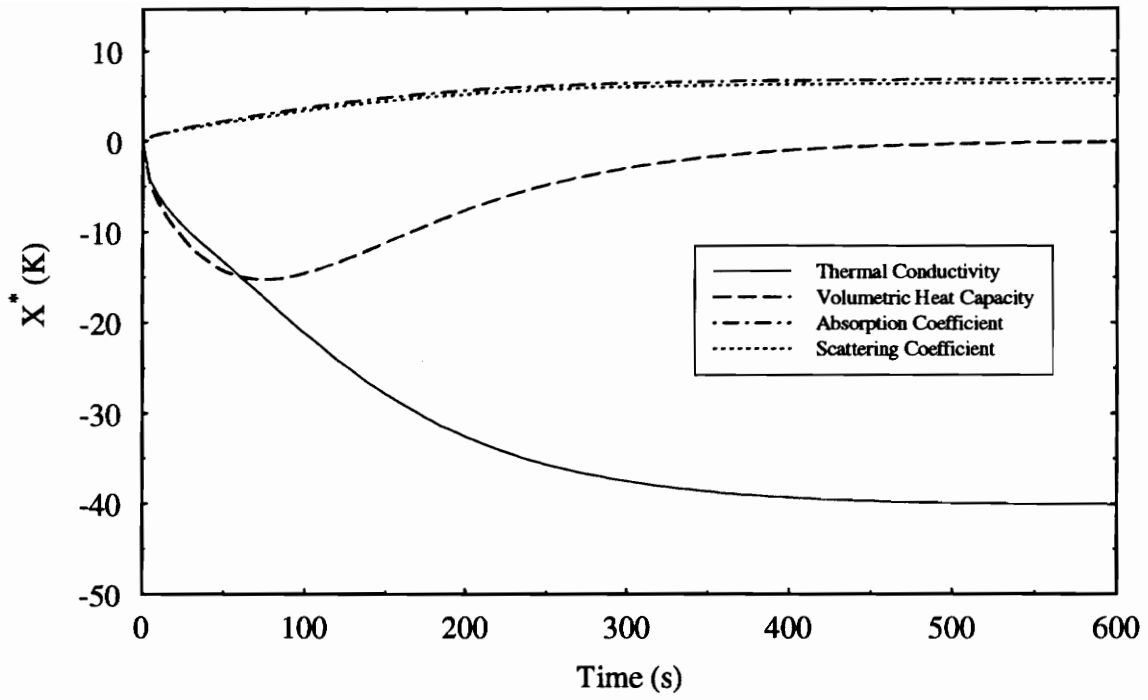

Figure 4.22 Normalized Sensitivity Coefficients (X*) for Nominal Styrofoam Parameters, Moderate Scattering Albedo, $\Omega = 0.5$.

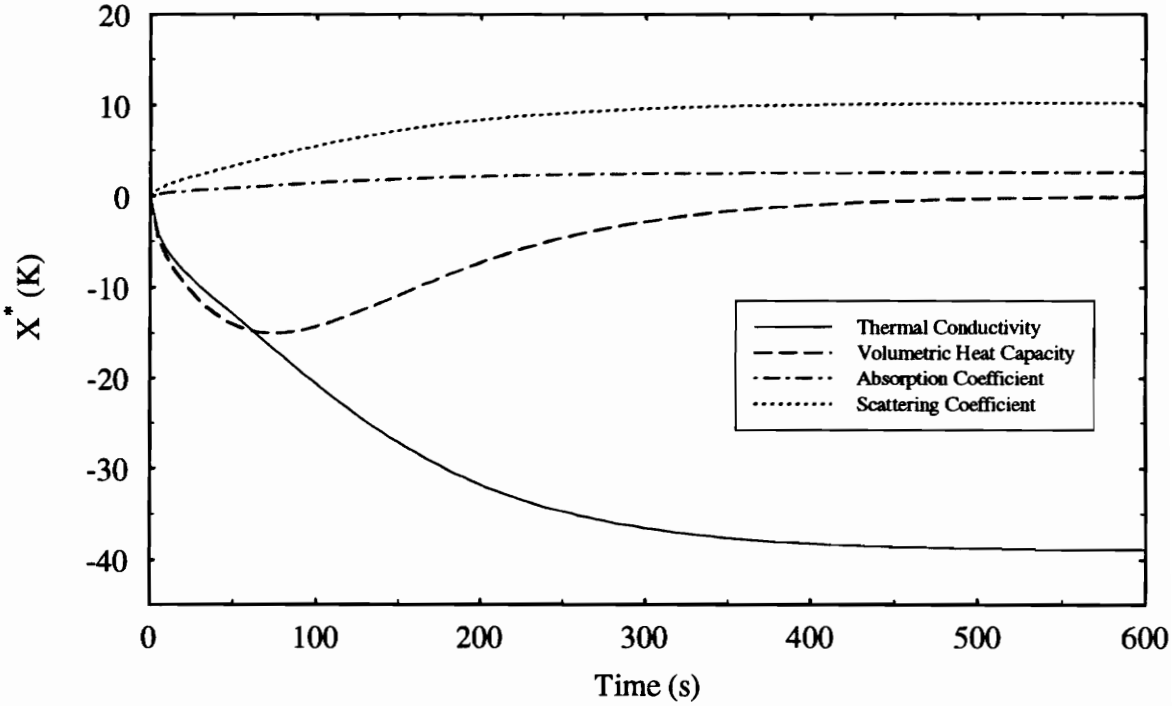

Figure 4.23 Normalized Sensitivity Coefficients (X*) for Nominal Styrofoam Parameters, High Scattering Albedo, $\Omega = 0.8$.

them very difficult to estimate together. Note that there is a slight difference in X_c^* and X_k^* for each case, but it is not significant.

Additional insight into the correlation between the absorption and scattering can be gained by computing sensitivity coefficients based on the scattering albedo and the extinction coefficient, two common quantities for radiation transfer in a medium. These parameters contain the same basic information, but written in a different form (the solution is exactly the same) using

$$\beta = (a + \sigma_s) \quad , \quad \Omega = \frac{\sigma_s}{a + \sigma_s} \, . \tag{4.5}$$

Note that the optical thickness is simply $\kappa_D = (a + \sigma_s)D$. The nominal sensitivity coefficients are plotted in Figure 4.24 and the same parameters, but with Ω=0.08, are shown in Figure 4.25. Very little information is available for the scattering albedo, even when scattering is high, and it is also nearly correlated with the extinction coefficient. The sensitivity coefficients reveal that for an optically thick medium, the major contribution of isotropic scattering is to the extinction of the radiation rather than to pure scattering effects. This suggests there is little to be gained by including the effects of isotropic scattering in an optically thick medium for this type of heat transfer and a simpler, purely absorbing model would be best.

Figures 4.26 and 4.27 show the results for a more optically thin case, $\kappa_D = 2.73$ (β = 150 m^{-1}). Figure 4.26 uses the absorption and scattering coefficients and it shows X^*_a and $X^*_{\sigma s}$, while on the same order as the nominal X^*_a and $X^*_{\sigma s}$, are much larger compared to X^*_k

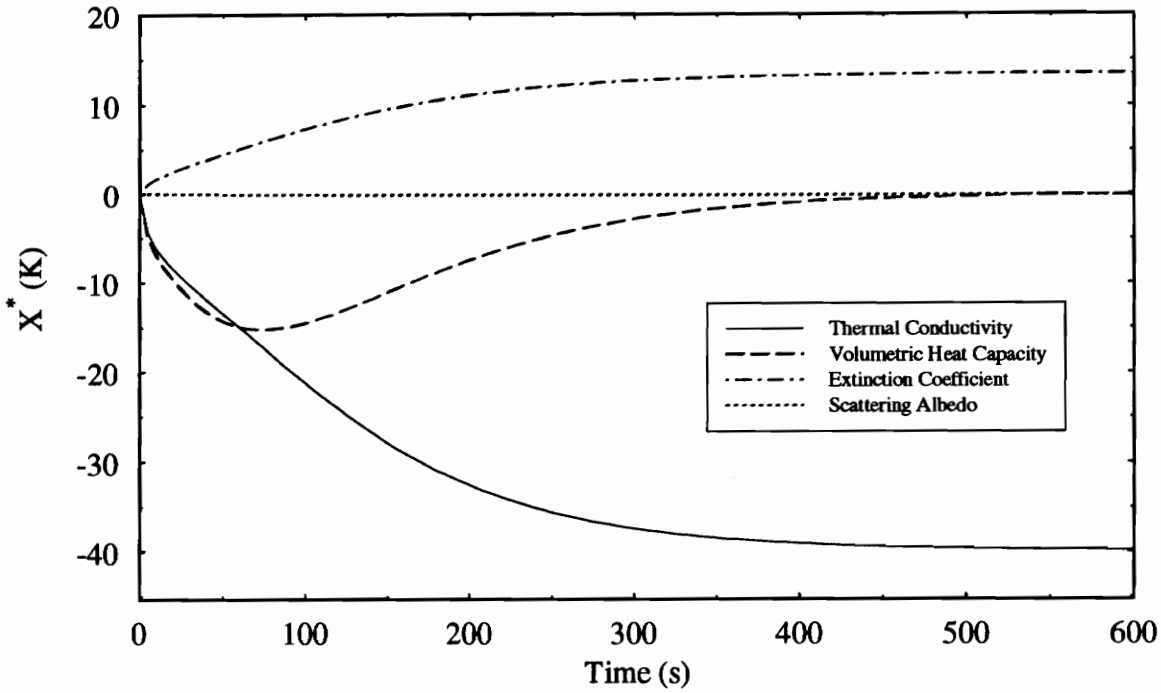

Figure 4.24 Normalized Sensitivity Coefficients Using Extinction Coefficient, β, and Scattering Albedo, Ω, and Nominal Styrofoam Parameters.

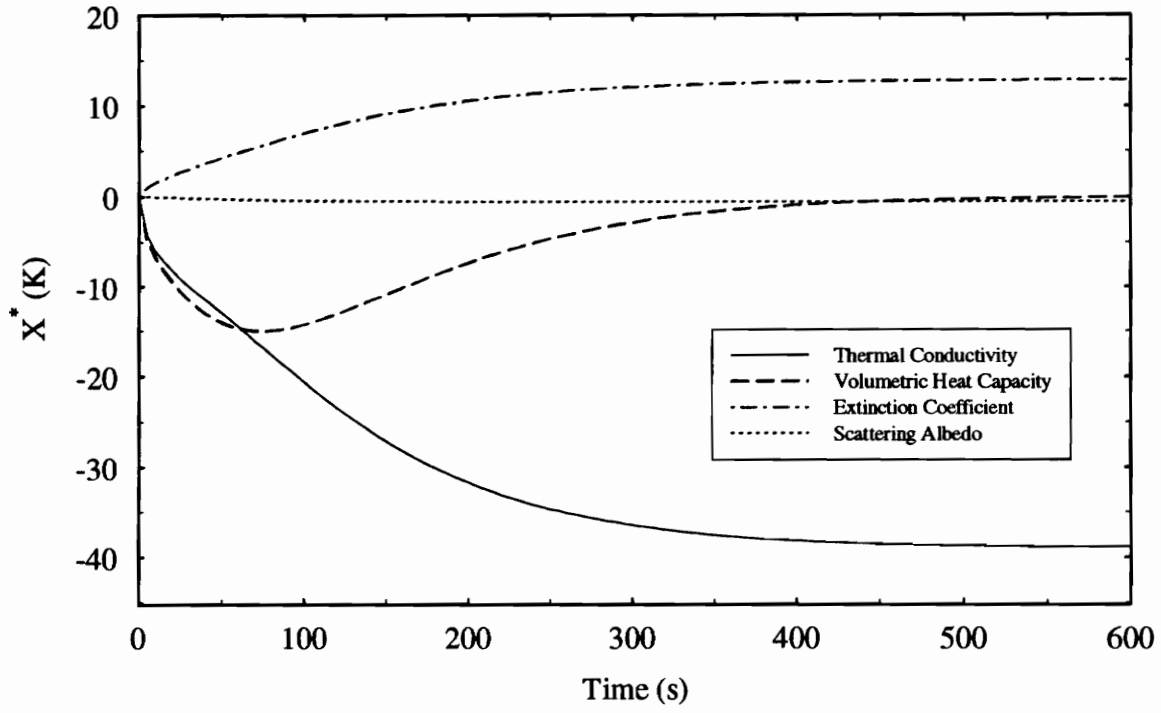

Figure 4.25 Normalized Sensitivity Coefficients Using Extinction Coefficient, β, and Scattering Albedo, Ω, and Nominal Styrofoam Parameters with Ω = 0.8.

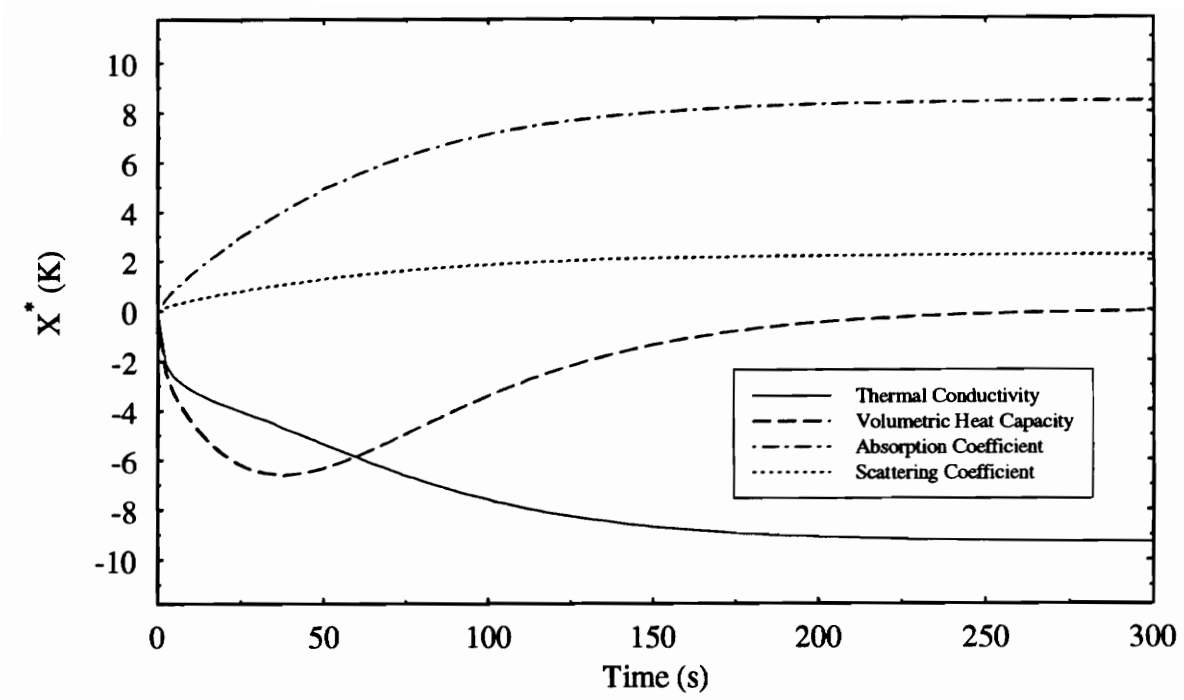

Figure 4.26 Normalized Sensitivity Coefficients (X*) for Optically Thin Case, Extinction Coefficient $\beta = 150\ m^{-1}$ ($\kappa_D = 2.73$).

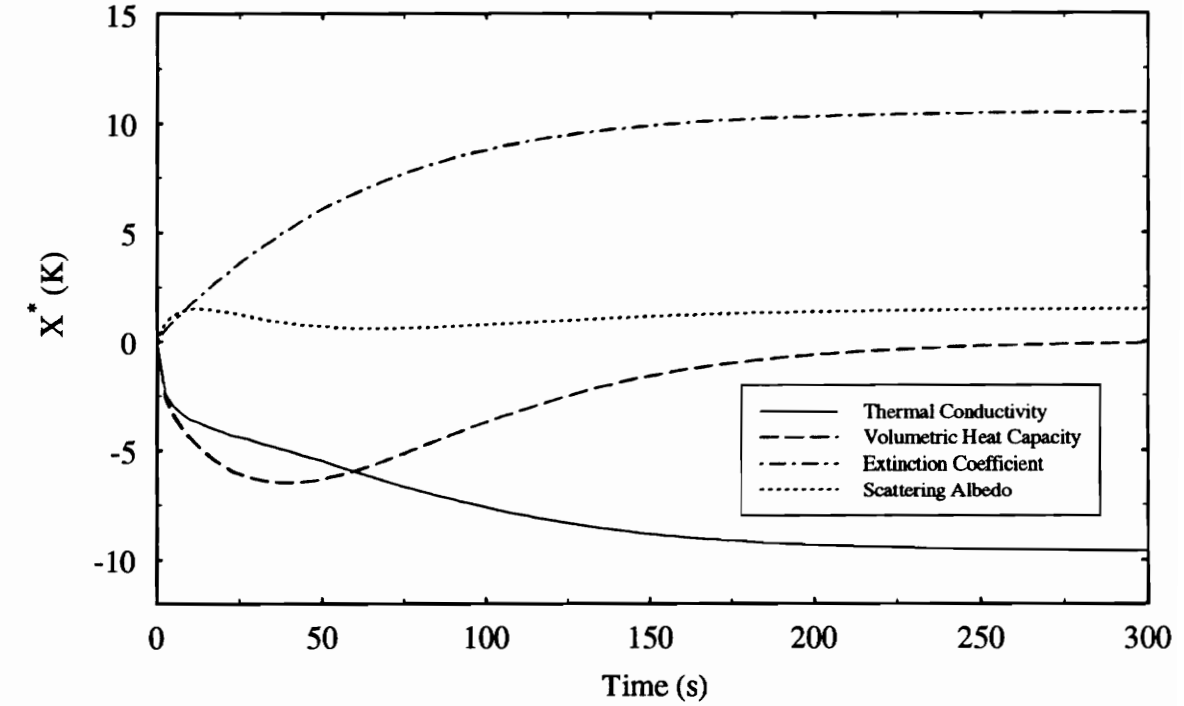

Figure 4.27 Normalized Sensitivity Coefficients (X*) for Optically Thin Case, Extinction Coefficient $\beta = 150\ m^{-1}$, High Scattering Albedo, $\Omega = 0.8$.

and X^*_c. Furthermore, relative to the absorption coefficient, the scattering coefficient is larger. Though the sensitivity coefficients are lower than those for the optically thick case, and occur at an earlier time, the temperature rise is also less; the steady-state temperature is only 324 K, about half the nominal value of 650 K. In this case, a heat flux about twice as large could be applied, resulting in reasonable values for all the parameters. The sensitivity coefficients for the extinction coefficient and the scattering albedo are shown in Figure 4.27 for the optically thin case with $\Omega=0.8$. The scattering albedo is again quite low and exhibits a slightly irregular behavior at the start of heating. Neglecting scattering for this optical thickness is a little more dubious, though it would still be difficult to estimate. If only a rough approximation were needed, it would be a reasonable assumption.

A difference in thickness of the sample is illustrated in Figures 4.28 and 4.29, plots of the sensitivity coefficients for $D_{nom}/2$ and $2D_{nom}$, respectively. The result is similar to that for the optically thin specimen; the D/2 produces similar curves, but with about half the maximum sensitivity coefficient value and with the maximum occurring at an earlier time. The steady-state temperature in this case is about 323 K. The same result is shown for a double thickness, but in reverse. In this case, care must be taken not to exceed the degradation point of the material. In fact, the solutions reaches 350 K at 143 s, which means, for Styrofoam, that the maximum sensitivity coefficient for k, a, and σ_s is less than that for a single thickness. However, the maximum value for X^*_c is significantly larger, even at 143 s, so if the nominal case did not provide enough information for c, increasing the thickness would be a means of gaining more information, but only for a loss in sensitivity of the other parameters. A material

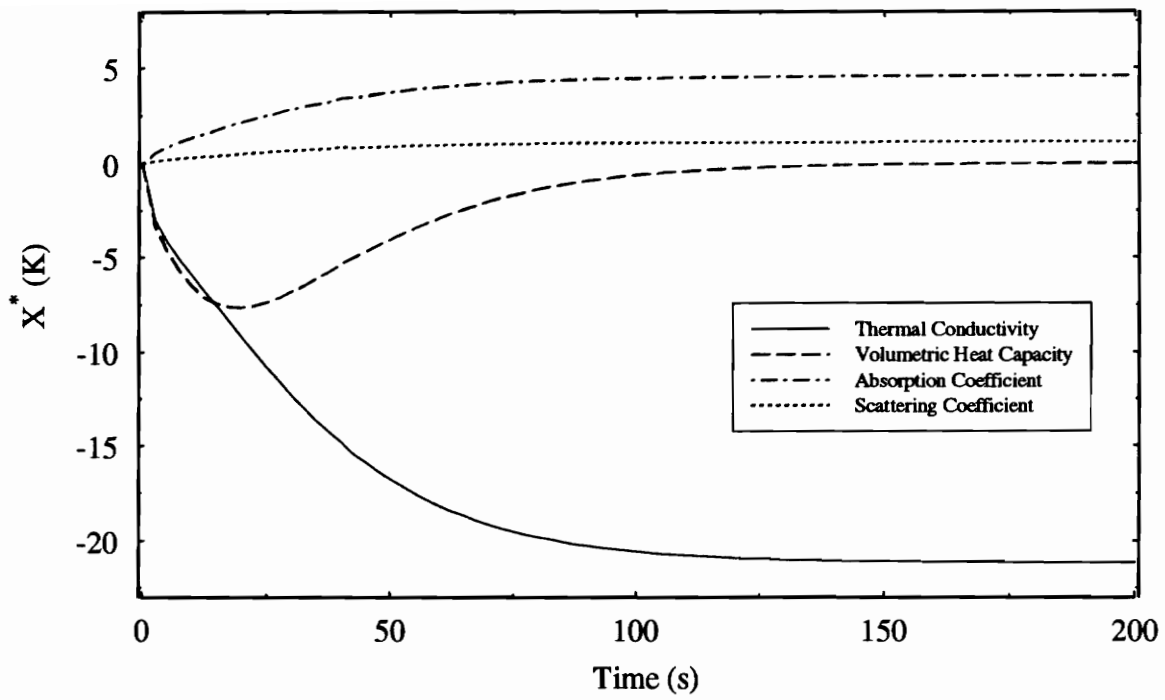

Figure 4.28 Normalized Sensitivity Coefficients (X*) for Nominal Styrofoam Parameters One Half Nominal Thickness (D/2).

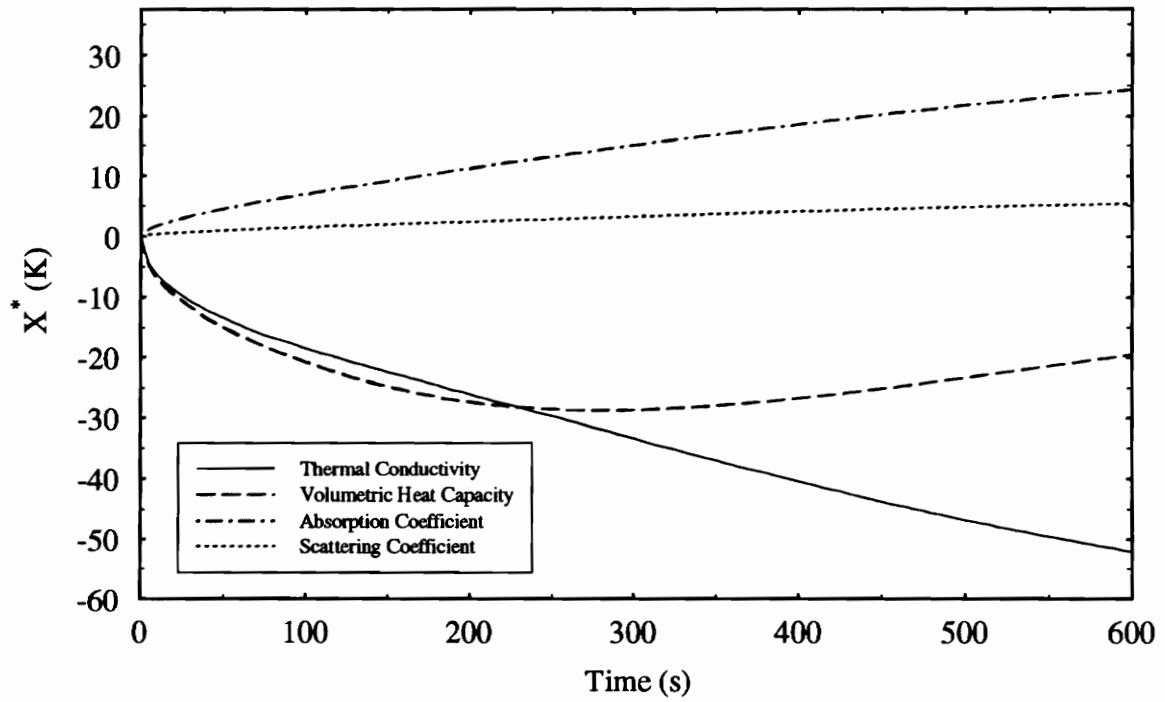

Figure 4.29 Normalized Sensitivity Coefficients (X*) for Nominal Styrofoam Parameters Double Nominal Thickness (2D).

with a higher maximum serviceable temperature would gain overall from an increase in thickness, though the experimental time would be longer.

Finally, it is worthwhile to note that in all cases the maximum sensitivity coefficient for the thermal conductivity and radiation parameters occurred at steady state. Thus, despite the advantages of transient experiments and their necessity for estimating heat capacity, a steady-state experiment will always provide the most information for estimating thermal conductivity and the scattering and absorption coefficients.

Due to the near linear dependence between the sensitivity coefficients for the radiation parameters and the thermal conductivity, avenues were explored to devise an experiment that reduced the correlation. As previously stated, there were not many experimental parameters that could be manipulated. It was decided, however, to explore the possibility of adding a reflective boundary at the heated surface in an attempt to reduce the linear dependence of the sensitivity coefficients, especially among the radiation parameters. The solution was implemented and the resulting sensitivity coefficients, including the sensitivity of the emissivity of the boundary, are shown in Figure 4.30 for the case of $\epsilon = 0.2$. The resulting curves are almost identical to the nominal values and the sensitivity of ϵ is almost zero. Thus, the solution is largely insensitive to the emissivity of the boundary, which not only prevents reducing the correlation , but makes it impossible to estimate ϵ if it was not well known.

The only variables to optimize for the transient experiment were the heating time and the length of the experiment. Generally, if heat capacity is being determined, the heat flux is stopped and data continue to be taken before steady state is reached. As can be seen quite

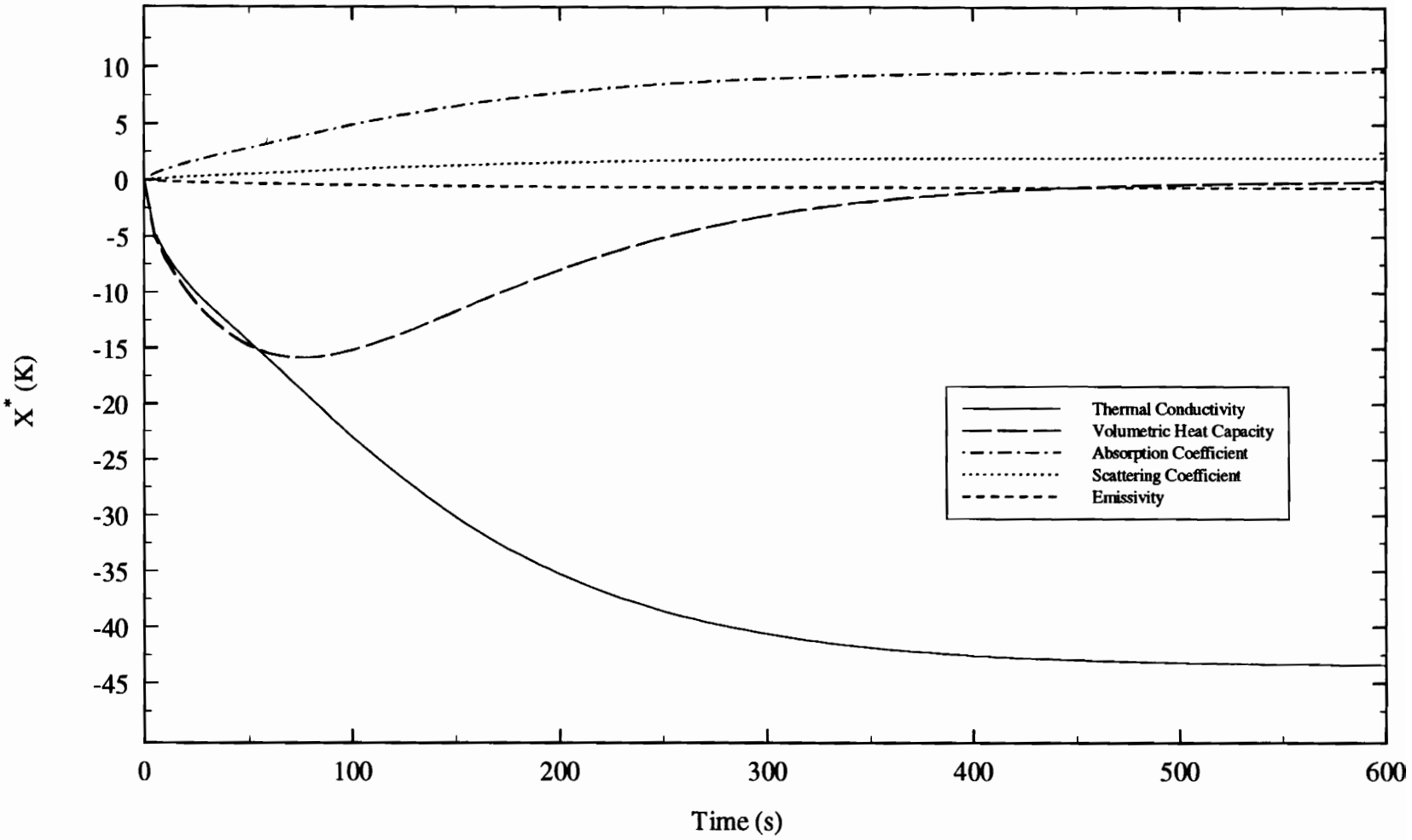

Figure 4.30 Normalized Sensitvity Coefficients (X*) for Nominal Styrofoam Values
Low Emissivity at Heated Surface: $\varepsilon = 0.02$.

clearly in Figure 4.21, the sensitivity coefficient for the volumetric heat capacity is zero at steady state. The termination of the heat flux and the resulting temperature changes produce additional information for heat capacity, as the sensitivity increases and the direction of the sensitivity coefficient changes, as illustrated in Figure 4.31. Note that if X^*_c had followed the same exact path as at the start of the experiment, no new information would be gained.

As there were only two experimental parameters to find and the properties of Styrofoam were not well known, it was decided to determine the heating and experiment times simply by examining the sensitivity coefficients. As the experiment approaches steady-state, the heat flux is stopped and data taken until the sensitivity coefficient for volumetric heat capacity decreases. Since the properties were not well known, this had the advantage of being implemented by simply watching the temperature measurements and terminating the power when they approached steady state. Furthermore, Figure 4.21 indicates that there is ample information for the estimates, with the exception of the scattering coefficient. Once a better idea of the properties was gained, a simple parametric optimization could be run to determine an even more optimum experiment and obtain the most accurate estimates.

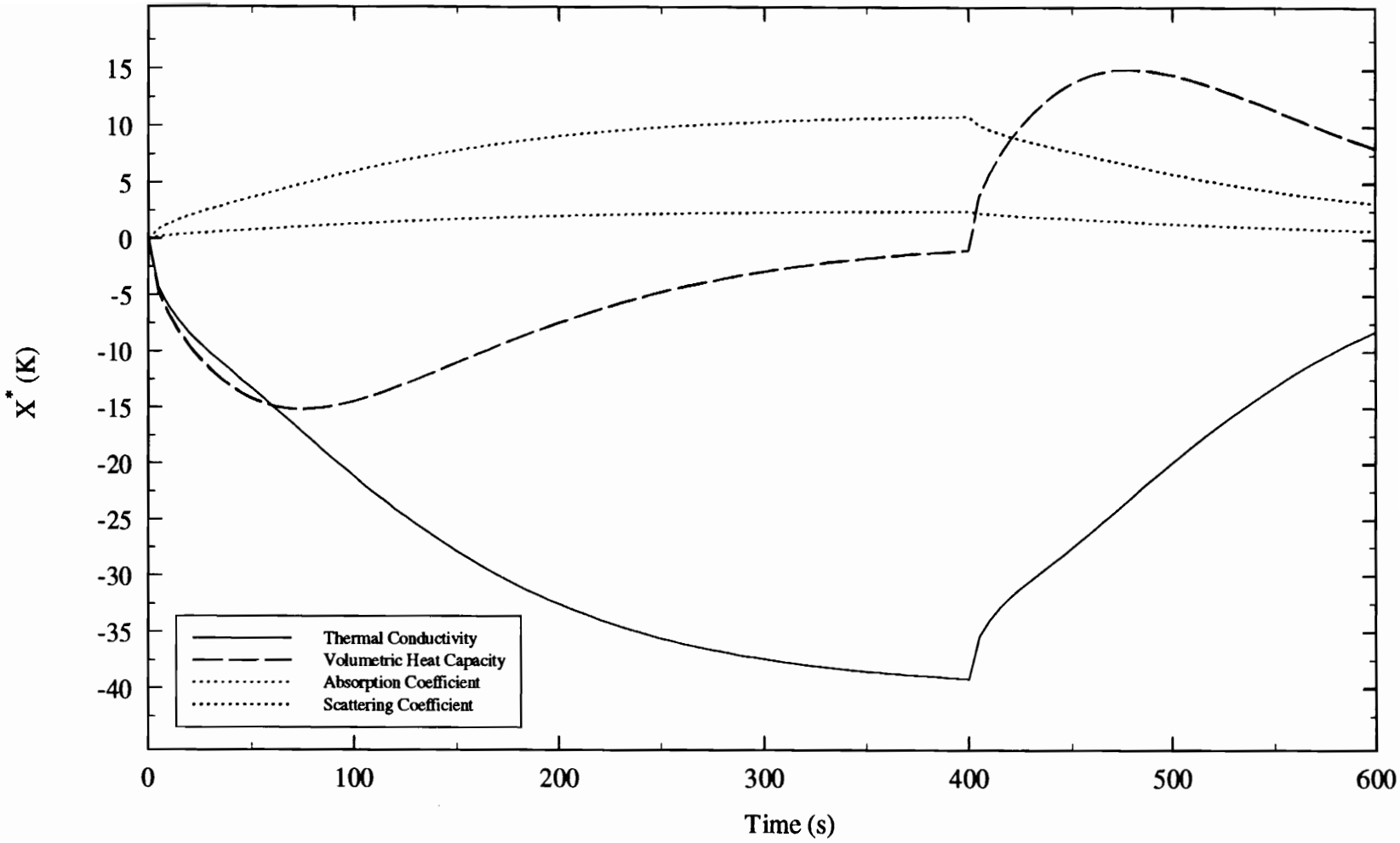

Figure 4.31 Normalized Sensitvity Coefficients (X*) for Nominal Styrofoam Properties Using Absorbing and Scattering Solution, Heat Flux Ends at 400 s.

Chapter 5

Experimental Methods

The experiment in this study consisted of a one-dimensional setup with an applied heat flux on one side of a Styrofoam sample and a constant temperature on the other side. Temperatures were recorded using a digital data acquisition system integrated with a personal computer.

5.1 Data Acquisition System

A detailed account of the particular data acquisition system utilized is given by Hanak (1995) and only a cursory review will be given here. The main purpose of the data acquisition system was to read in the thermocouple voltages, as well as the voltage and current used to power the heater. An overview of the setup is illustrated in Figure 5.1.

The thermocouples run from the experimental apparatus to an ice bath which provides a reference temperature for the thermocouples. Since thermocouples operate on the principle of a temperature-dependent voltage difference between different metals, the connection between the thermocouple metals (chromega™ and constantan) and the extension wire metal (copper) will induce an additional voltage. The constant temperature reference point allows

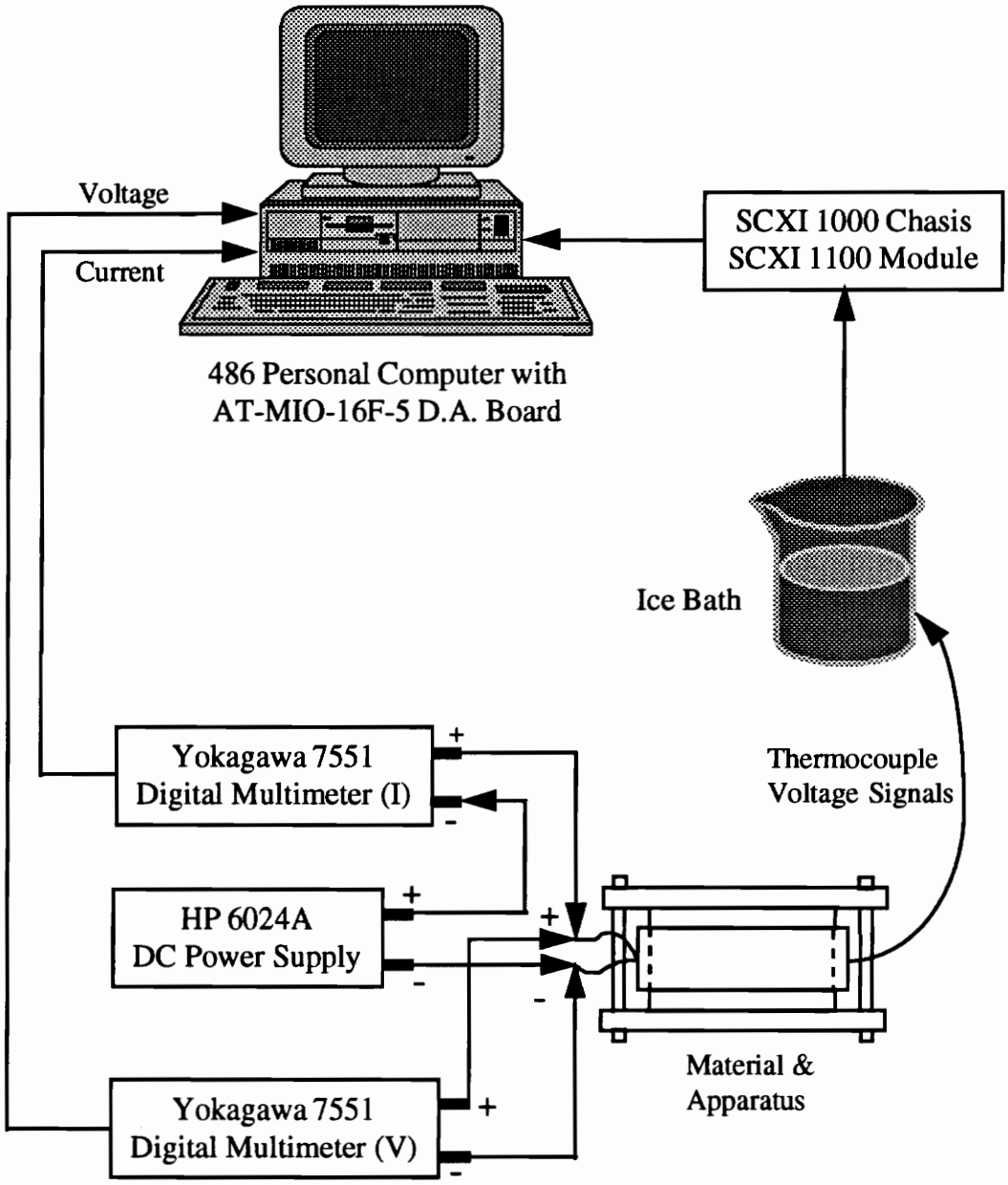

Figure 5.1 Data Acquisition System.

that voltage to be known and negated from the readings. The thermocouples are attached to the extension wires inside of oil-filled vials, which are used to keep water from the wires and to provide a more constant temperature. The extension wires lead into a National Instruments SCXI 1000 Chassis with a SCXI 1100 module. The chassis and module provide a noise-free environment where the thermocouple readings are amplified and multiplexed from thirty-two channels into eight. The SCXI 1100 module then sends the signals to a National Instruments AT-MIO-16F-5 data acquisition board. The AT-MIO-16F-5 is the heart of the system. It controls the timing, input and output operations, and receives the signals from the thermocouples and two multi-meters. The AT-MIO-16F-5 board is mounted in a 486 personal computer.

The heater is powered by an HP 6024A Autoranging DC Power Supply which can supply a maximum of 200 W. Two Yokogawa 7551 Digital Multimeters are used to measure the voltage and current supplied to the heater, which in turn is used to find the exact power supplied to the heater. One multimeter is placed in series with the power supply to measure current and the other is placed parallel to measure voltage. The two multimeters are connected to the AT-MIO-16F-5 through two RS-232 cables. To provide an immediate beginning and ending in power, power to the heater is controlled by connecting and disconnecting the negative of the power supply from the negative terminal of the multimeter. This also allows the power supply to be placed a considerable distance from the experimental setup, reducing the amount of electrical noise.

The AT-MIO-16F-5 data acquisition board, SCXI 1100 module, and multimeters are

controlled through National Instrument's Lab Windows programming environment. The C programming language is used with National Instruments library functions to control the AT-MIO-16F-5 and SCXI 100, read in the thermocouples and multimeters, convert the thermocouple voltages to temperatures, and output the information to both the monitor and the hard disk. A sample program can be found in Hanak (1995).

Since the numerical solutions required a time step of 0.5 s, the data acquisition system was set up to take data approximately every 0.5 s. The system does not take data in exact time increments; sometimes it might be 0.48 s, other times 0.53 s, etc. This required a slight modification to the solutions to allow varying time steps. This time increment resulted in approximately 2400 data points for a 1200 s run. Note that this is probably more data than the estimation procedure requires, but including all the points in the estimation results in little extra computational time.

5.1.1 Thermocouples

Thermocouples were chosen as the temperature measurement device because of their fast response time and their ability to measure temperatures at a point. The thermocouples used were ANSI standard Type E, composed of AWG 40 chromega™(+) and constantan(-) wire, manufactured by Omega Engineering, Inc. (part number TT-E-40). Type E thermocouples were selected because of their low conductivity and high sensitivity at low temperatures. They have the largest Seebeck coefficient, α, of standard thermocouples. The Seebeck coefficient determines the magnitude of the voltage difference through the equation

$$V = \alpha \Delta T. \quad (5.1)$$

The 40-gauge wire minimizes the contact resistance when the thermocouples are placed between the heater and the sample.

While the Type E thermocouples only have an accuracy of ±1.7°C, they have a precision of ±0.08°C, which is sufficient for temperature measurements in this study. The thermocouples were calibrated for each run by taking data for 90 s before the heater was turned on and obtaining a measurement of the ambient temperature using a Luxtron Flouroptic thermometer, which has an accuracy of ±0.1°C. As part of the postprocessing of the data, an offset for each thermocouple was determined using the first 90 s of data and the ambient temperature reading.

5.2 Experimental Apparatus and Assembly

The heat transfer equation emulated experimentally was one-dimensional combined conduction and radiation heat transfer between two black boundaries, with an applied heat flux on one side and a constant temperature on the other. The experimental setup to accomplish this is shown in Figure 5.2. The experiment consisted of a thin-film heater placed between two square Styrofoam samples, with the opposite sides of the samples placed in contact with aluminum plates which act as heat sinks to maintain those boundaries at room temperature. Both faces of each sample were painted black. The use of a symmetrical setup ensured that all the energy generated by the thin film heater entered the Styrofoam samples

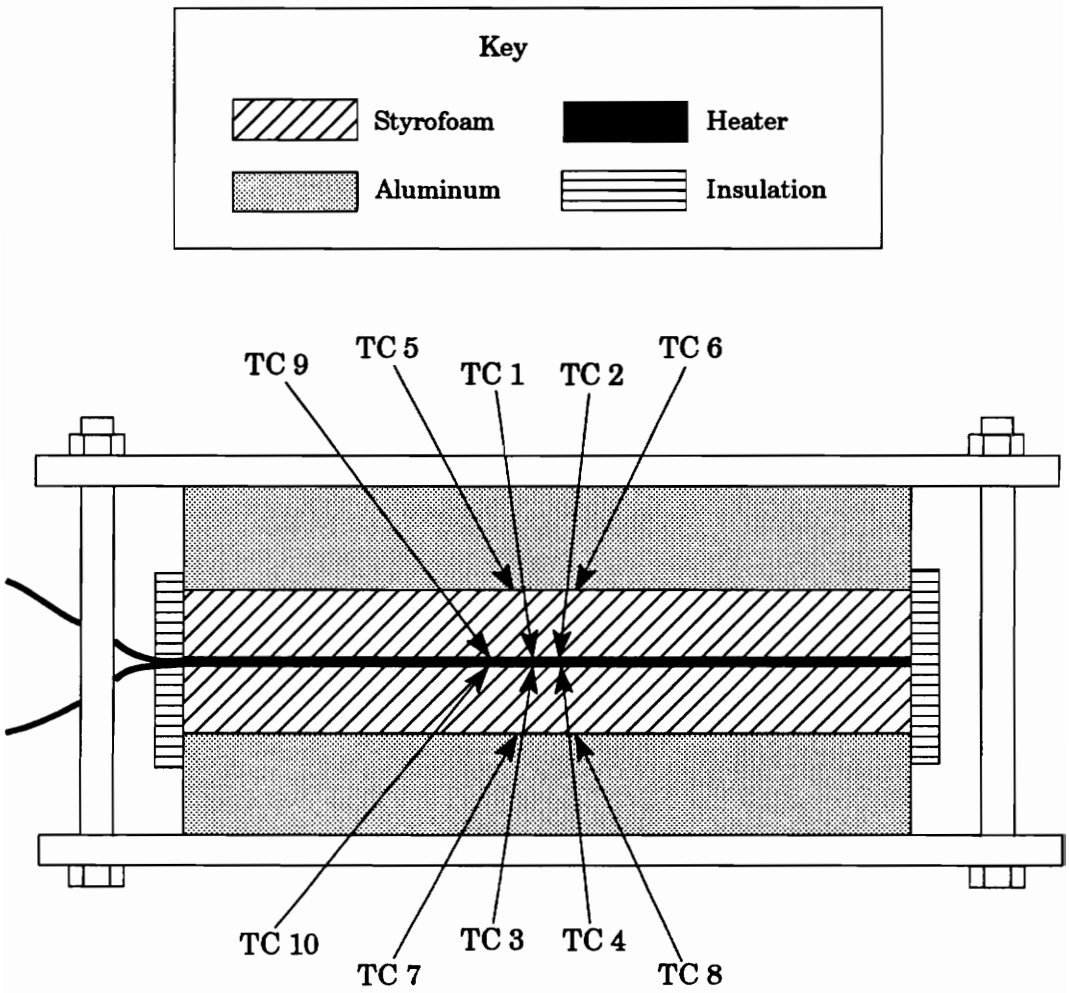

Figure 5.2 Experimental Apparatus.

and allows slight differences in samples to be averaged out.

The thin film heater is a standard Minco Products Inc. Thermofoil™ heater, which consists of a flat foil element laminated between two layers of flexible Kapton insulation (part no. HK5560R17.4L24A). The physical dimensions of the heater are 15.24 cm x 15.24 cm (6 in. × 6 in.) and 3.05 mm (0.012 in.) thick, which gives a surface area of 232.3 cm^2. However, the effective heating area is 95.5 percent of the physical area, or 221.8 cm^2. The effective heating area was used in calculating the heat flux. This particular heater was chosen for its size and for its low resistance, which helps to produce a more uniform heat flux. The flat foil element within the insulation is like a printed circuit board, as shown in Figure 5.3, and therefore does not cover the entire heater surface. This produces a nonuniform heat flux that can cause errors in the temperature measurements at the heated surface. Following Hanak (1995), one heated surface thermocouple was placed directly over the foil element and another was placed over the middle of a gap in the heating element, and the two were averaged to arrive at the correct temperature.

The surfaces of the Styrofoam needed to be painted black to simulate a black boundary. Initially, an attempt was made to spray paint the sheets, but the solvents in the paint dissolved the Styrofoam. This demonstrates one of the disadvantages of Styrofoam; it is very susceptible to chemical solvents and care must be taken in choosing paint, glue, or other liquids that come in contact with it. A flat poster paint was chosen instead and brushed onto the surfaces, which should provide an emissivity of at least 0.90. As the sensitivity study for the absorbing and scattering solution revealed, the temperature is fairly insensitive to the

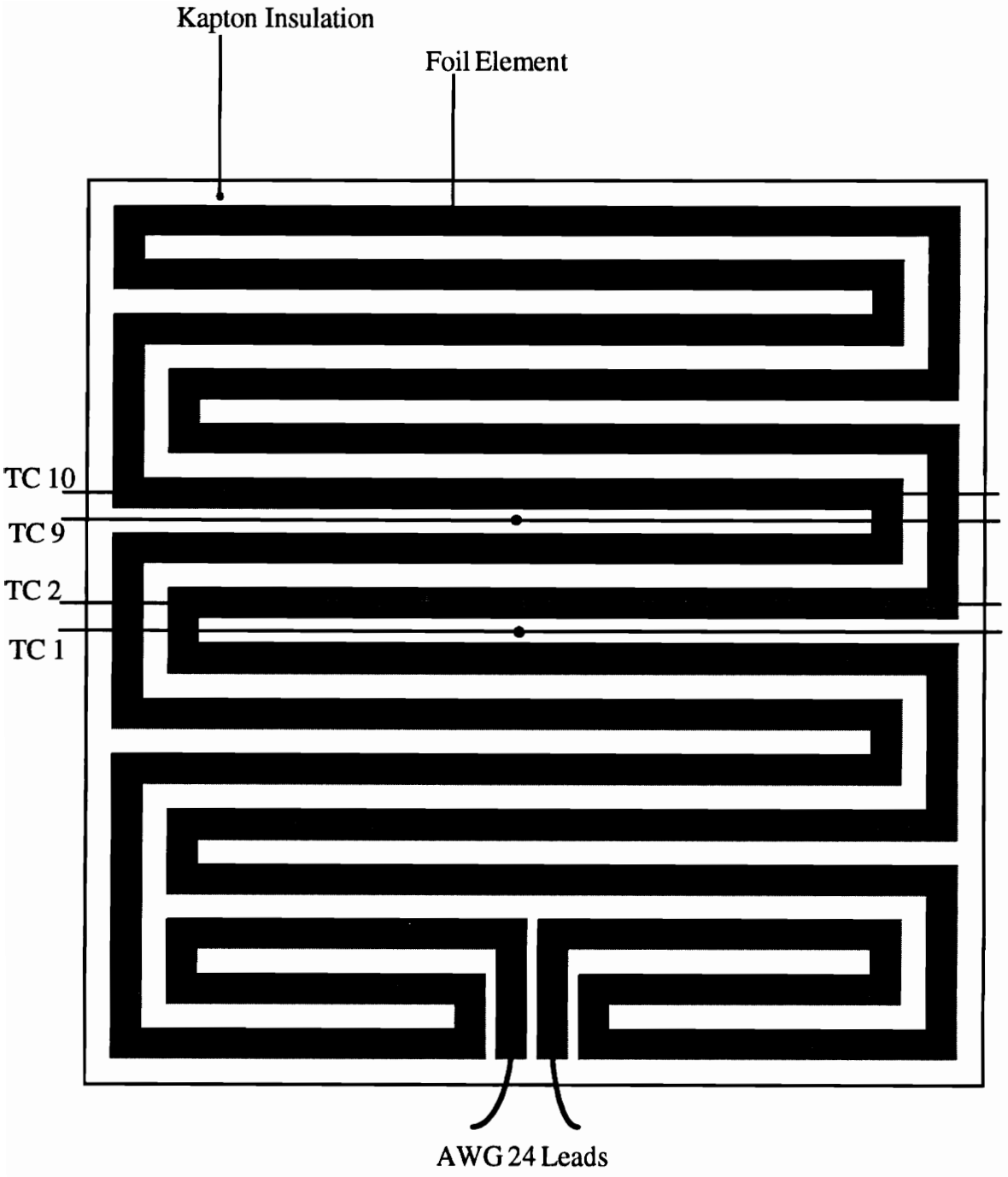

Figure 5.3 Diagram of the Thin Film Heater (Scale not Exact).

boundary emissivity and a value of at least 0.90 should suffice. Due to the thin-film heater's internally attached leads, a small notch had to be cut in one of the Styrofoam samples to provide room for the leads and allow the heater and Styrofoam surfaces to maintain good contact.

Typically, to maintain one-dimensional heat transfer in this type of setup, either a guarded hot plate apparatus would be used or insulation would be wrapped around the heater, sample material, and aluminum to prevent heat from flowing out the sides. This practice was followed in the setup, but largely to prevent heat loss from the heater and to minimize any convection along the edges by limiting air movement. Since Styrofoam is an insulating material, and a very effective one, the insulation would not facilitate one-dimensional heat transfer in this situation. The main method of ensuring one-dimensional heat transfer was to use a large length-to-thickness ratio of the sample material. The inability to insulate the sample is somewhat offset by the fact that the low thermal conductivity will also retard heat transfer in the lateral direction.

Since the length-to-thickness ratio is very important to the design of the experiment, an analysis was performed using a steady-state, three-dimensional finite-element model with a constant thermal conductivity. The boundary conditions were an applied heat flux of 150 W/m^2 at one surface, a constant temperature of 298 K at the other, and a convection heat transfer coefficient of 10 W/m^2 on the sides. A relatively high value of 0.04 W/m^2 was used for the thermal conductivity. The analysis revealed that a 15.24 cm (6 in.) square sample with a thickness of 1.815 cm had a negligible difference in temperature within a 1.0 cm square in

the center of the material on the heated side. This would be sufficient to model one-dimensional heat transfer for the experiment and 15.24 cm was the dimension chosen for the samples. The EAL program used in the analysis, *styconk3d.eal*, is listed in Appendix C.

The aluminum blocks were 1.905 cm (0.75 in.) thick, 15.24 cm square, and polished smooth on one side to ensure good contact with the Styrofoam. It was desired to have the aluminum fairly thin as the weight of the blocks could deform the Styrofoam. A finite element program, *styal.eal*, was written to check the sufficiency of 1.905 cm aluminum as a heat sink. The program is similar to those used in the steady-state sensitivity analysis and models the sample and aluminum together, with a 150 W/m^2 heat flux applied to the Styrofoam and a constant temperature on the far side of the aluminum. The thermal conductivity of the Styrofoam was variable, based on the diffusion solution for $\beta = 1500\ m^{-1}$. Within a 10 min. run, the temperature rise at the interface of the two materials was negligible, ensuring the aluminum thickness was adequate. The program is listed in Appendix D.

Two thermocouples were placed between the heater and each Styrofoam layer, for a total of four thermocouples to measure the temperature rise at $x=0$. The thermocouples were placed as close to the center of the layer as possible to ensure one-dimensional heat transfer was being measured. Two thermocouples were also placed between each Styrofoam layer and aluminum plate, opposite the heater thermocouples, to monitor the constant temperature boundary condition. Finally, two thermocouples were placed between the heater and the Styrofoam approximately 1.5 cm from the center, to gain an idea of how much heat was being transferred in a lateral direction. The thermocouples next to the heated surface were glued

to the heater itself using Borden Krazy Glue® and the thermocouples next to the aluminum blocks were glued to the Styrofoam using water based white glue.

To ensure good contact between the surfaces of the heater, aluminum, and Styrofoam, a thin layer of thermal paste was applied between each surface. The paste, Omegatherm® 210, manufactured by Omega Engineering Inc., is a highly conductive, smooth, silicon paste that reduces contact resistance between the surfaces. Before the paste was applied to the setup, some was spread on a scrap piece of Styrofoam to ensure it would not degrade the material; no effect was noticed. Care had to be taken in spreading the paste not to break the thermocouples.

Two layers of commercial pipe insulation, produced by Thermwell Inc., were wrapped around the assembly and held in place with rubber bands, which also kept the insulation against the aluminum and the Styrofoam. A small slit had to be cut halfway through the insulation for the heater leads.

The entire assembly was placed between two thin aluminum plates which had bolts running through holes in each corner and was used to hold the assembly together and provide good contact between the different layers. Only slight pressure could be applied, however, as the Styrofoam would deform if the bolts were excessively tightened. An unfused thermocouple wire was attached to the plates with electrical tape and connected to the junction box to act as a ground.

5.3 Temperature Measurement Procedure

The following procedure was followed to obtain the experimental temperature measurements use in the estimation:

Step 1 - The heater was connected to the DMMs and the power supply, DMMs, DMMs, and SCXI chassis turned on. The equipment was turned on for several hours before measurements were taken to allow the electronics to stabilize.

Step 2 - The negative lead of the ammeter DMM was connected to the negative lead of the heater, supplying power to the heater. The power supply was than adjusted to produce the desired wattage, as measured by the DMMs.

Step 3 - The setup was allowed to cool to ambient temperature, at least one hour. The ice bath was prepared and allowed to reach steady state (at least 30 min.).

Step 4 - Ambient air temperature was measured and the data acquisition program started.

Step 5 - After about 90 s of ambient temperature data, the negative lead of the ammeter DMM was connected to the negative lead of the heater, supplying power to the heater.

Step 6 - After the required amount of heating time, the heater was disconnected.

Step 7 - After the required experimental time, the data acquisition program was stopped.

Step 8 - The setup was left to cool and reach ambient conditions at least an hour and a half before another experiment was run.

Step 9 - The thermocouple temperatures were plotted to ensure the data acquisition correctly recorded the temperatures.

After the data were collected, they were post-processed to build a file that contained the time, the temperature at the heated surface, and the temperature at the constant temperature surface. The basic processing is described below:

Step 1 - Compute an average ambient temperature for each thermocouple based on the first 90 s of data. Determine the difference between that temperature

and the ambient temperature found using the Luxtron; add the difference to each thermocouple reading.

Step 2 - Average the four thermocouples at the heated surface and the four thermocouples at the constant temperature surface.

Step 3 - Determine the heating start time, end time, and average the wattage readings over the heated time. Compute the heat flux by dividing the watts by the *effective* area of the heater and halving the resulting value to account for the symmetric setup.

Step 4 - Adjust the time so that the beginning of heating is 0 s; discard the first 90 s of data.

Step 5 - Write the time, heated surface temperature, and far surface temperature to a file in column format. Also write the heating start and end times and the heat flux to the file.

The resulting data file is used as input for the estimation programs. The programs used for the calibration and the averaging, TC_CALIB.FOR and TC_AVG.FOR, are listed in Appendix F and Appendix G.

Chapter 6

Results and Discussion

Once the data were collected, they were reviewed and processed for use in the estimation procedures. The models were found to not quite represent the physics of the experimental setup due to the capacitance of the heater, but the solutions were modified to take this into account. Some additional, minor modifications were also included in the solutions to better represent the actual heat transfer.

The estimation procedure involved both a Box-Kanemasu analysis, which was found to be ineffective, and a genetic algorithm estimation, which does not suffer from the gradient problems of the Box-Kanemasu method. Correlation between the properties prevented their exact determination and also highlighted some difficulties in using the genetic algorithm as written. Modifications to the genetic algorithm and to the experimental setup were examined to reduce the correlation between the properties.

6.1 Analysis of Experimental Data

After the experiment was first conducted, the thermocouple data were examined to

check for anomalies or problems with the experimental setup. Analysis revealed that the boundary conditions were not ideal, but within the expected capabilities of the experimental setup. It was also found that the thermal behavior of the heater affected the temperature response of the Styrofoam. The effect of the heater was successfully analyzed and the solutions modified to account for both the heater and the non-ideal boundary conditions.

6.1.1 Thermal Grease Effects

After the first experiment was run, the data were preprocessed and plotted to check the results. The plotted data showed an unexpected and uncharacteristic linear shape compared to the theoretical curves shown in Figures 3.7 and 3.10; the plotted data are shown in Figure 6.1, with an expanded view of the starting time in Figure 6.2. The experimental curve is not only linear at the beginning, but the temperature increases at a much slower rate than predicted. Adjustment of the material properties (thermal conductivity, volumetric heat capacity, and extinction coefficient) could not produce the basic curve shape using the diffusion solution. Two approaches, one experimental and one analytical, were taken to determine whether the experiment or the analysis was defective. In both of these investigations, it was suspected that the thermal paste applied between the heater and the Styrofoam was the cause of this behavior.

First, the experimental setup was disassembled, the thermal paste was removed from one side of the heater, and a couple hundred seconds of data obtained. The resulting plot of the data was still fairly linear, but the temperature increased at a much faster rate. Next, the

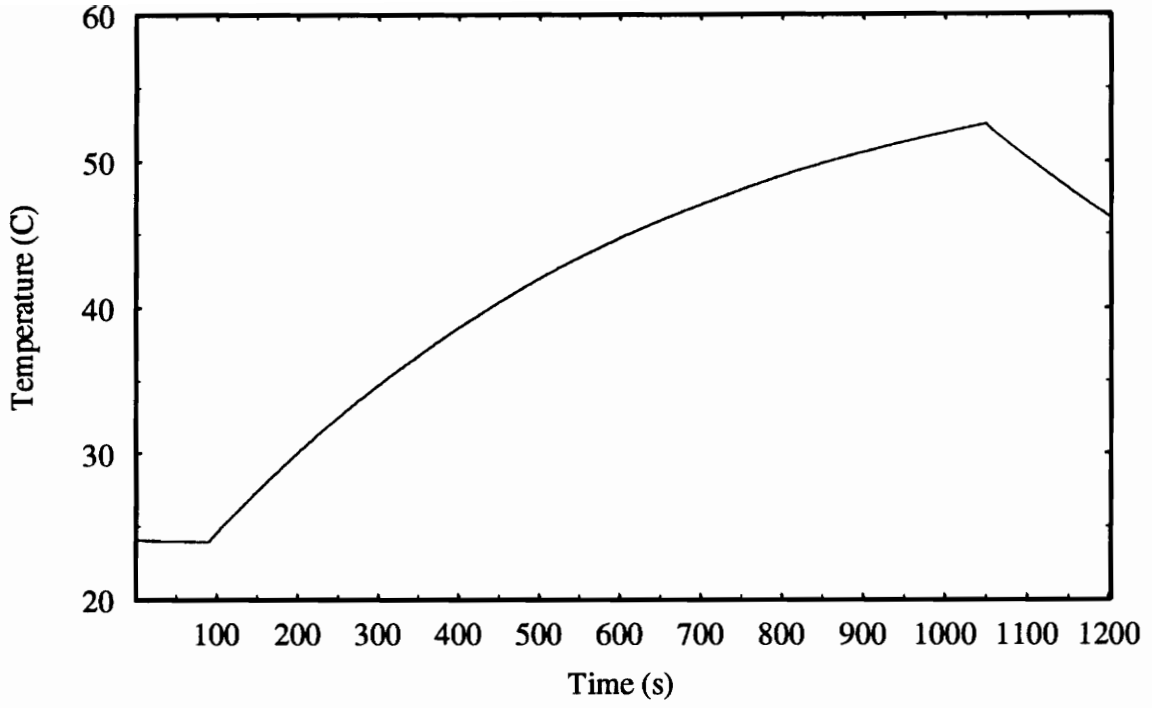

Figure 6.1 Original Experimental Temperature at Heated Surface of Styrofoam.

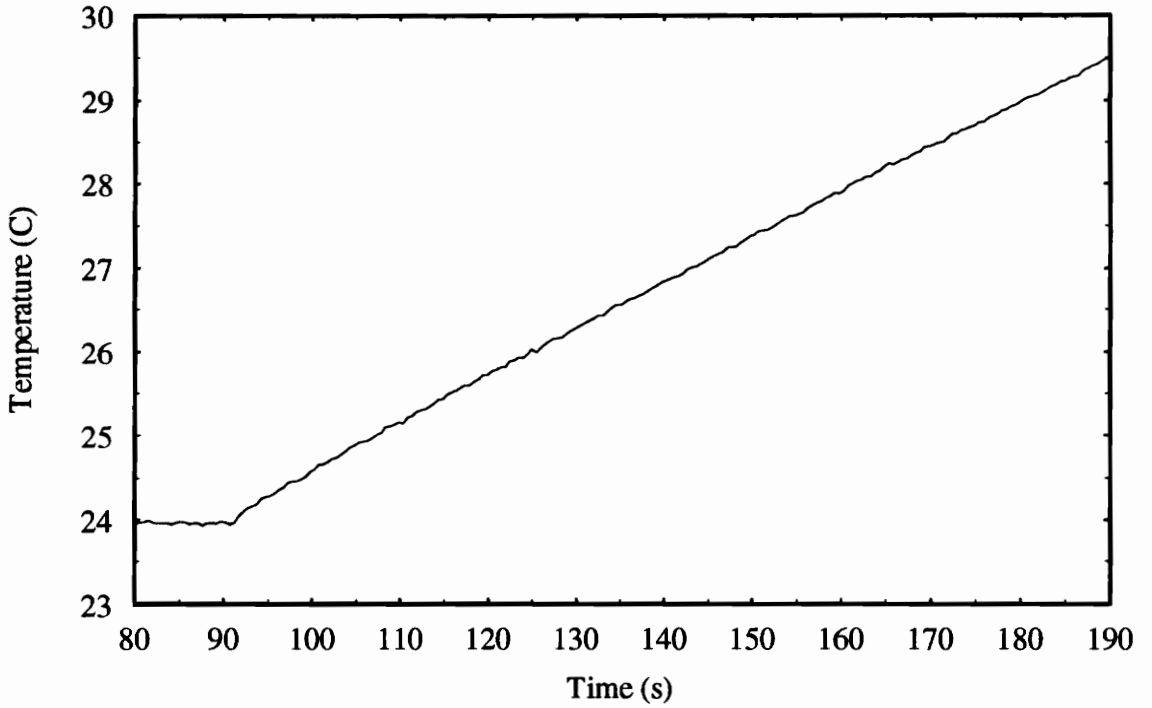

Figure 6.2 Original Experimental Temperature at Heated Surface of Styrofoam for First 100 s.

thermal paste was removed from the other side of the heater and the recorded data are shown in Figures 6.3 and 6.4. This data plot was much more curved and the temperature rose faster than in either previous case. The thermal had a great affect on the values of the temperature recorded.

Secondly, to investigate why the thermal paste would have such an effect, an analytical analysis was performed. A constant property, non-radiative medium was assumed for simplification. The curved nature of the predicted temperature rise at the surface can be determined by looking at the simplified case of a semi-infinite medium with an applied constant heat flux

$$T(0) = T_i + \frac{2q_0(\alpha t/\pi)^{1/2}}{k} = T_i + Ct^{1/2} . \qquad \textbf{(6.1)}$$

This clearly shows a temperature dependence to the ½ power of time, and though it is for a semi-infinite material, it indicates more of a curved shape for the radiation-conduction plot than is shown in Figure 6.2.

Since the thermal paste is in a thin layer and highly conductive, a lumped capacitance type model, where the temperature in the paste is treaded as uniform, was employed to investigate its effect. Considering a one-dimensional control volume around the thermal paste results in the following:

Energy in left side:

$$q_l'' = q_a'' \qquad \textbf{(6.2)}$$

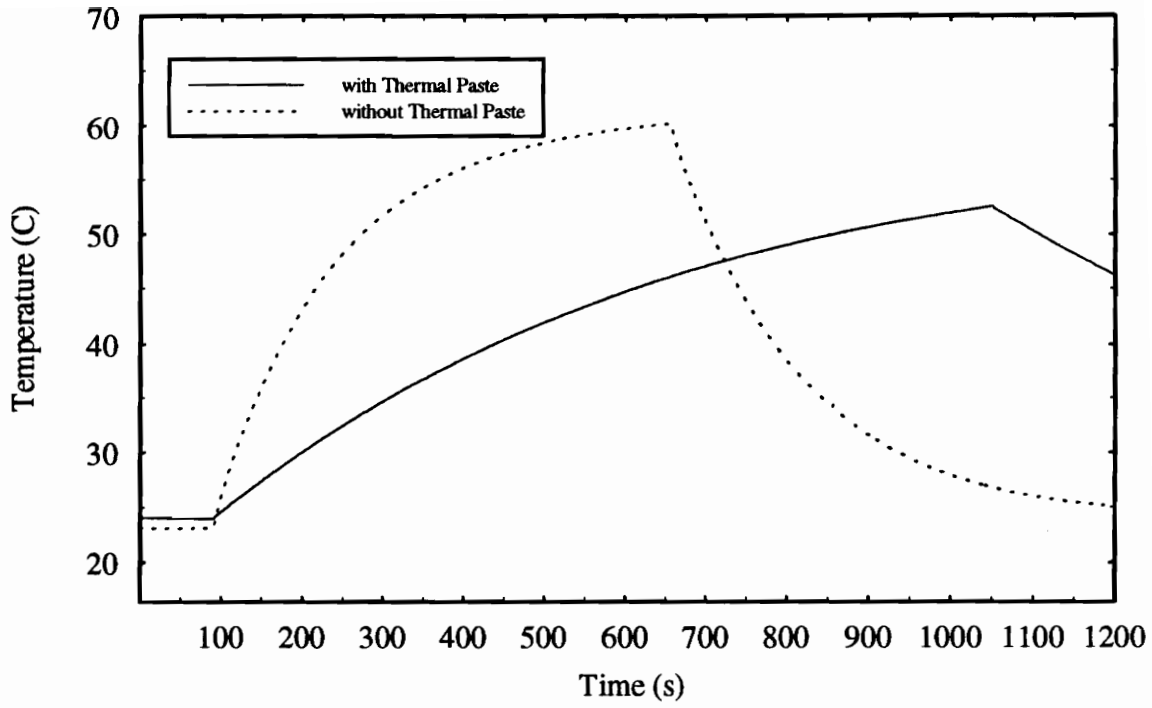

Figure 6.3 Experimental Temperature at Heated Surface of Styrofoam with and without Thermal Paste.

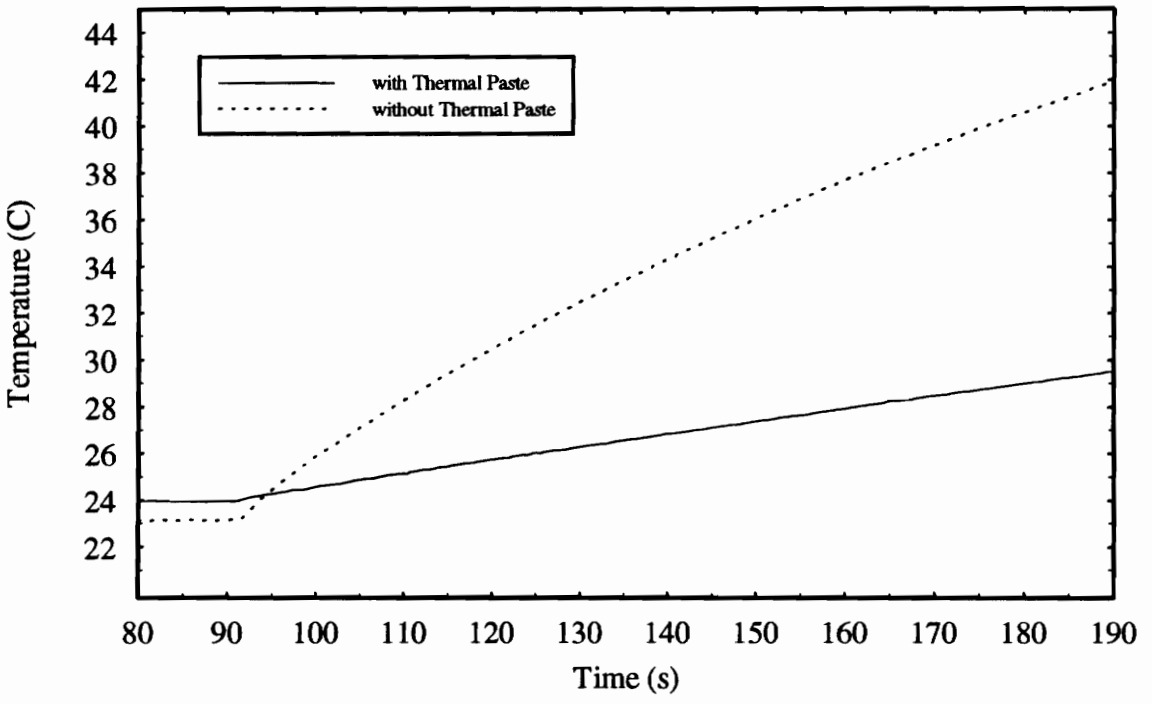

Figure 6.4 Experimental Temperature at Heated Surface of Styrofoam with and without Thermal Paste for First 100 s.

Energy out right side:

$$q_r'' = -k_2 \left. \frac{dT}{dx} \right|_2 \tag{6.3}$$

Rate of change of stored energy:

$$\Delta q = \rho c_p V \frac{dT}{dt} = \rho c_p A d \frac{dT}{dt} \tag{6.4}$$

Combining terms gives

$$q_a'' - \left(-k_2 \left. \frac{dT}{dx} \right|_2 \right) = \rho c_p d \frac{dT}{dt} \ . \tag{6.5}$$

For an insulating material, k_2 is small, and q''_r can be neglected compared to q_a''. This is an insulated boundary and leads to

$$\frac{dT}{dt} = \frac{q_a''}{\rho c_p d} \ . \tag{6.6}$$

The right-hand side is constant, so this can be integrated and the initial condition $T(0) = T_i$ applied, resulting in

$$T(t) = T_i + \frac{q_a''}{\rho c_p d} t = T_i + Ct \ . \tag{6.7}$$

Though an idealized derivation, this clearly shows a linear type relationship, as observed in Figure 6.2. Despite the thermal paste having a high conductivity and being a thin layer, the insulating sample helps to contain the energy in the layer, producing an erroneous temperature measurement.

As mentioned previously, due to the insulating characteristics of the sample material, the influence of any contact resistance should be negligible. Furthermore, the Styrofoam is deformable and will contact the heater and the thermocouples better than will other materials. The experimental setup was reassembled without thermal grease on either side of the heater surface. Since all the thermal grease could not be removed from the styrofoam and the samples suffered some degradation in tearing down the experiment, new samples were prepared. Also, the thermocouples at the heated surface were glued to the styrofoam rather than the heater.

6.1.2 Heater Capacitance Effects

Although the removal of the thermal paste produced better results, some preliminary estimation indicated that the model still did not accurately represent the experiment, as evidenced by Figure 6.5, which shows a predicted curve for a case that was relatively close to the data. Given that the difference between the predicted and measured data is still an issue of curvature at the beginning of heating, it was surmised that the heater may be acting as the thermal paste did, absorbing heat that would otherwise enter the insulation.

To analyze the effects of the heater on the temperature of the Styrofoam, the modeling of the heater was added to the numerical models. Data were available on the construction of the heater, which consists of foil elements, 0.001 in. of adhesive, and 0.002 in. of Kapton insulation. The maximum total thickness is 0.012 in. and the reported Kapton properties are listed in Table 6.1.

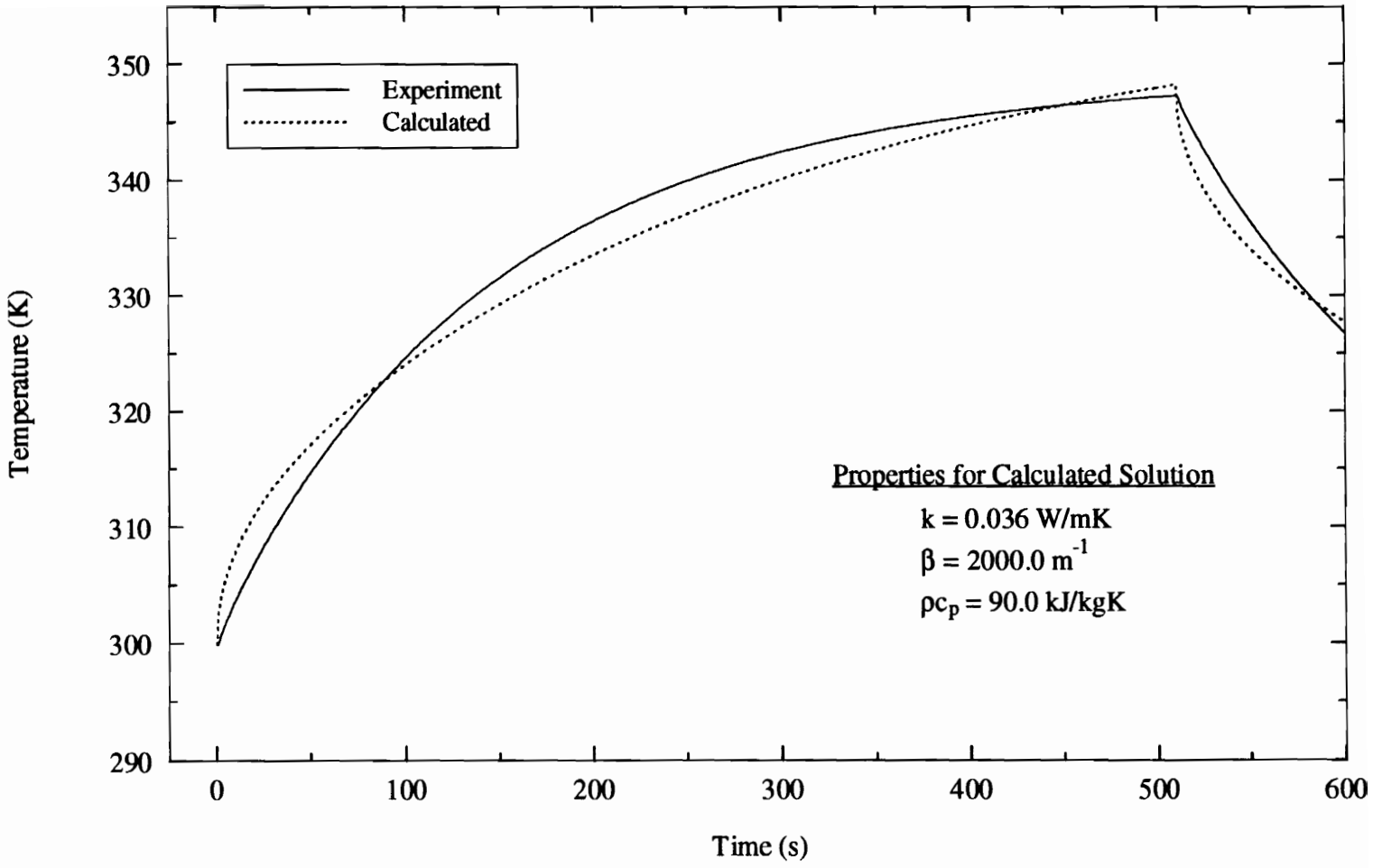

Figure 6.5 Experimental Temperature Rise Compared to Typical Calculated Diffusion Temperature Rise.

Table 6.1 Thermophysical Properties of Kapton.

Property	Value
Thermal Conductivity, k @ 296K	0.155 W/mK
Thermal Conductivity, k @ 348K	0.163 W/mK
Heat Capacity, c_p	1090 J/kgK
Density, ρ	1420 kg/m3

In the solution, the entire heater was assumed to be Kapton, the heater thickness was set at 0.152 mm (0.006 in.), representing half the heater due to symmetry, and the thermal conductivity was set at 0.160 W/mK. A comparison of numerical solutions at the heated surface with and without the heater is shown in Figure 6.6. The temperature rise at the beginning is slower and more linear and the steady state temperature occurs at a much later time, similar to the curve for the data shown in Figure 6.5.

The heater has a substantial impact on the solution due to the low thermal conductivity of the test material. However, this adds to the solution three new properties for the heater: thermal conductivity, k_h, volumetric heat capacity, c_h (ρc_p), and thickness, d_h. The reliability of the given Kapton properties is unknown and, furthermore, the heater was idealized as consisting entirely of Kapton, which it does not. Therefore, these properties should be estimated along with the Styrofoam properties. The problem can be simplified, however, by examining the sensitivity coefficients for the heater properties and realizing the heater may be viewed as a lumped capacitance system.

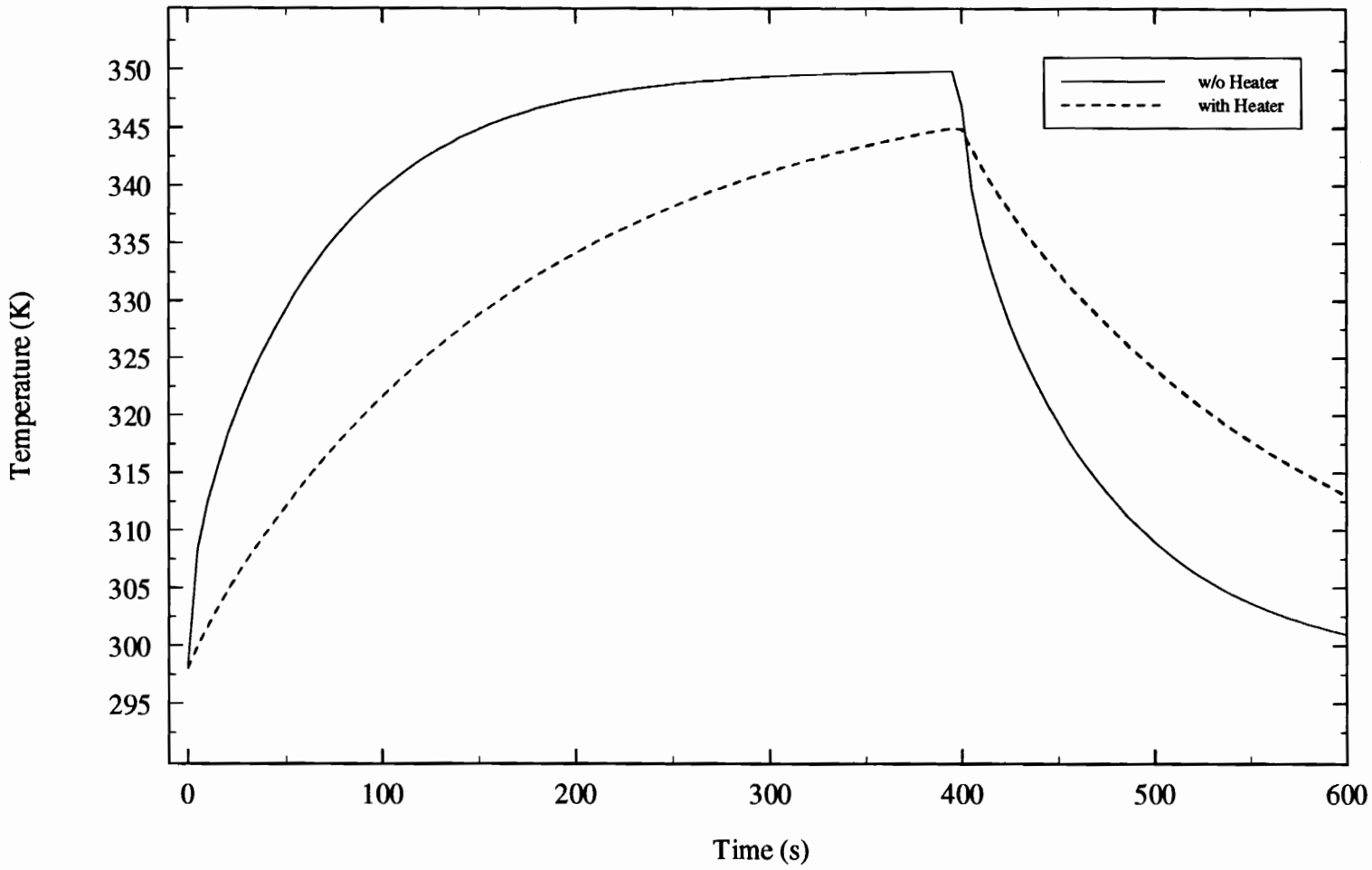

Figure 6.6 Comparison of Calculated Temperatures at Heated Surface with and without Heater Capacitance.

The sensitivity coefficients for all the properties using the diffusion solution, both with and without the heater, are plotted in Figures 6.7 and 6.8 and lead to the following observations. First, the thermal conductivity of the heater has little effect on the output and may be neglected. Secondly, the thickness and volumetric heat capacity of the Kapton are perfectly correlated. While this generally causes problems in estimation, in this case it is a great benefit, as one parameter can be fixed at an arbitrary value and only the other parameter estimated. These first two results are consistent with a lumped capacitance model. Thirdly, there is sufficient information to determine the value of the thickness or the volumetric heat capacity of the heater. Finally, the sensitivity coefficient for the Styrofoam volumetric heat capacity has been reduced due to the damping effect of the heater capacitance, and it appears to be somewhat correlated with the heater volumetric heat capacity.

The problem was reduced to finding the heat capacitance of the heater along with the Styrofoam properties. In the estimation, the thickness of the heater was arbitrarily set to 0.152 mm (0.006 in.) and the heater volumetric heat capacity became the fifth parameter to estimate.

6.1.3 Idealizations and Boundary Conditions

In order to determine the maximum heat flux that could be applied and to check the validity of a maximum serviceable temperature of 350 K, two test samples of Styrofoam were assembled with two thermocouples at the heated surface and subjected to various heat fluxes for various times. It was found that an applied heat flux of about 125-130 W/m^2 resulted in

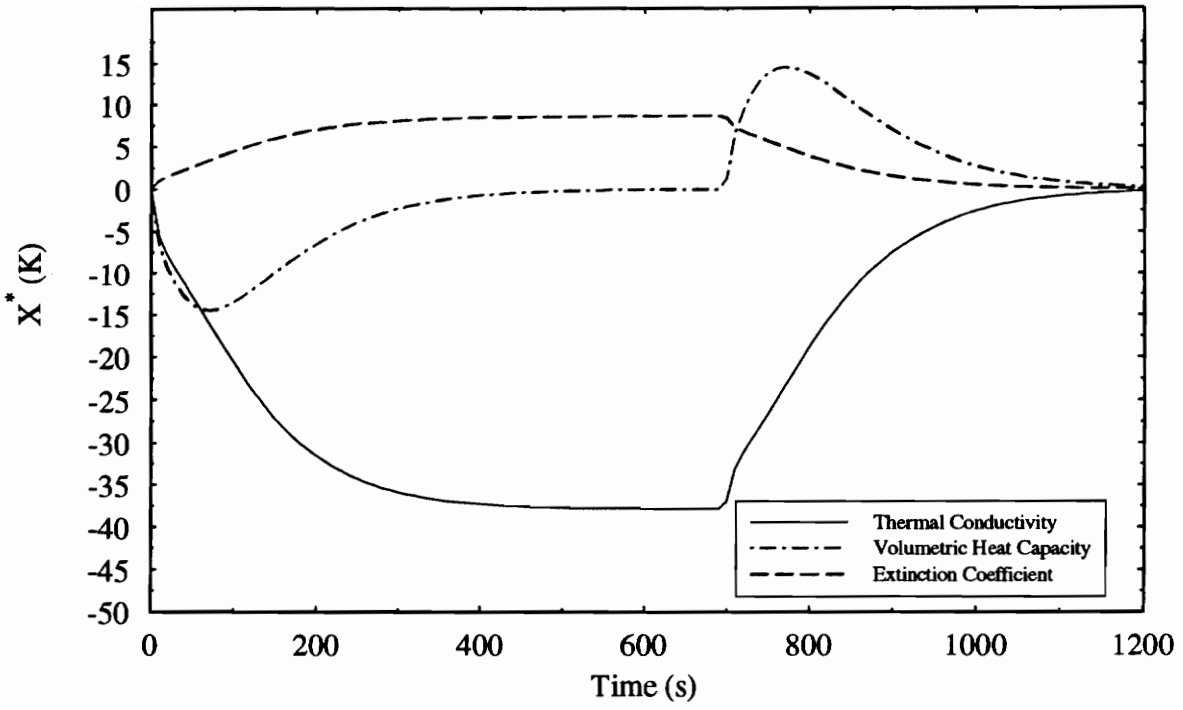

Figure 6.7 Diffusion Sensitivity Coefficients for Styrofoam at Heated Surface, Heater off at 700s.

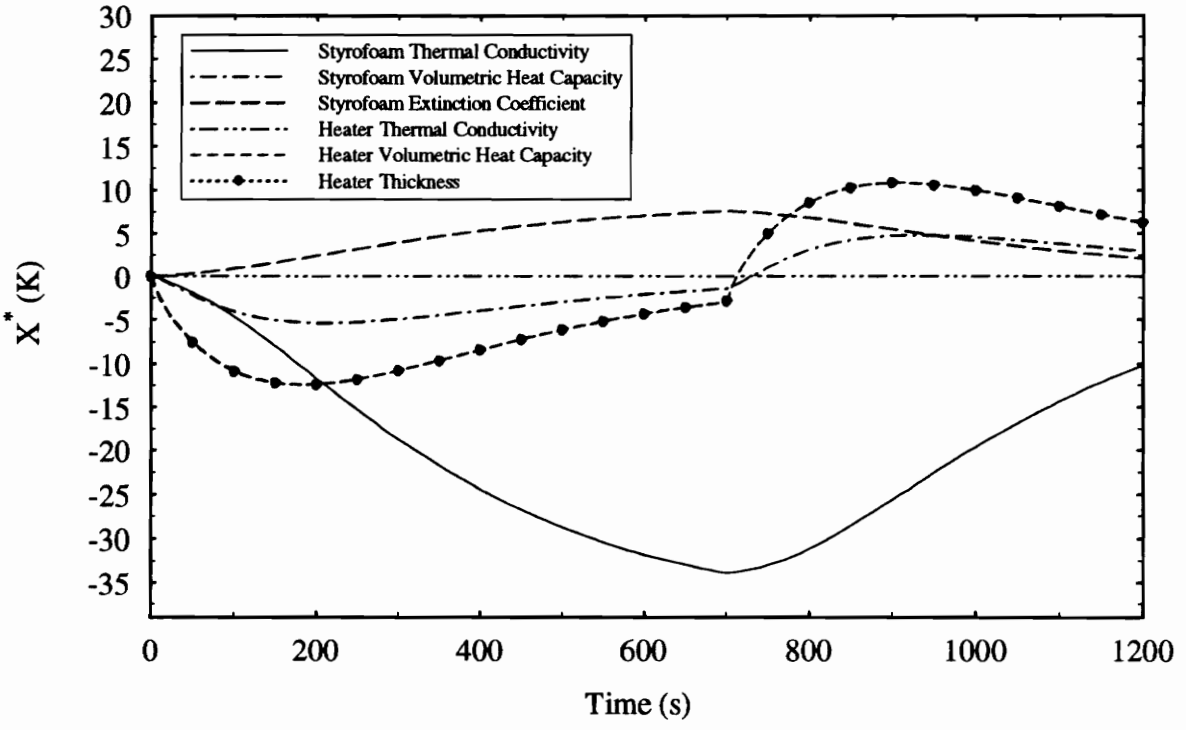

Figure 6.8 Diffusion Sensitivity Coefficients at Heated Surface, Including Heater Parameters Heater Off at 700s.

a steady state temperature close to 350 K. Furthermore, the Styrofoam suffered no degradation at 353 K for over 60 s. However, over several minutes, some flattening of high spots due to melting was noticed. A heat flux of 200 W/m^2 resulted in complete melting in the vicinity of the heater within 20 s after 350 K was reached. In the actual experiment, the maximum allowable temperature was considered to be 350 K and a heat flux of approximately 127 W/m^2 was applied.

The numerical solution for the heat transfer in the material was based on several idealizations and boundary conditions. The heat transfer is assumed to be one-dimensional, the heat flux is constant, and the temperature at $x=D$ is constant. The output from the data acquisition system can be used to check these assumptions.

As shown in Figure 5.2, thermocouples 5 and 6 were placed 1.5 cm from the heated surface to measure differences in temperature in the planar direction. Figures 6.9 and 6.10 are plots of the temperature at the heated surface for the averaged thermocouple pairs 1 and 2, 3 and 4, and 5 and 6 at both the start and end of heating. At the starting time, there is little difference; the difference that does exist at the very beginning is due to effects other than planar heat transfer, as evidenced by the fact that it disappears by 110 s. Towards the end of the heating time, there is a significant, but small, divergence between the center and off-center thermocouples. The difference at 420 s is only about 0.2°C and at 600 s about 0.3°C. Some variation in temperature was expected and given the time frame, the degree of the difference, and the temperature difference over time, the experimental setup achieved one-dimensional heat transfer for the experimental time period.

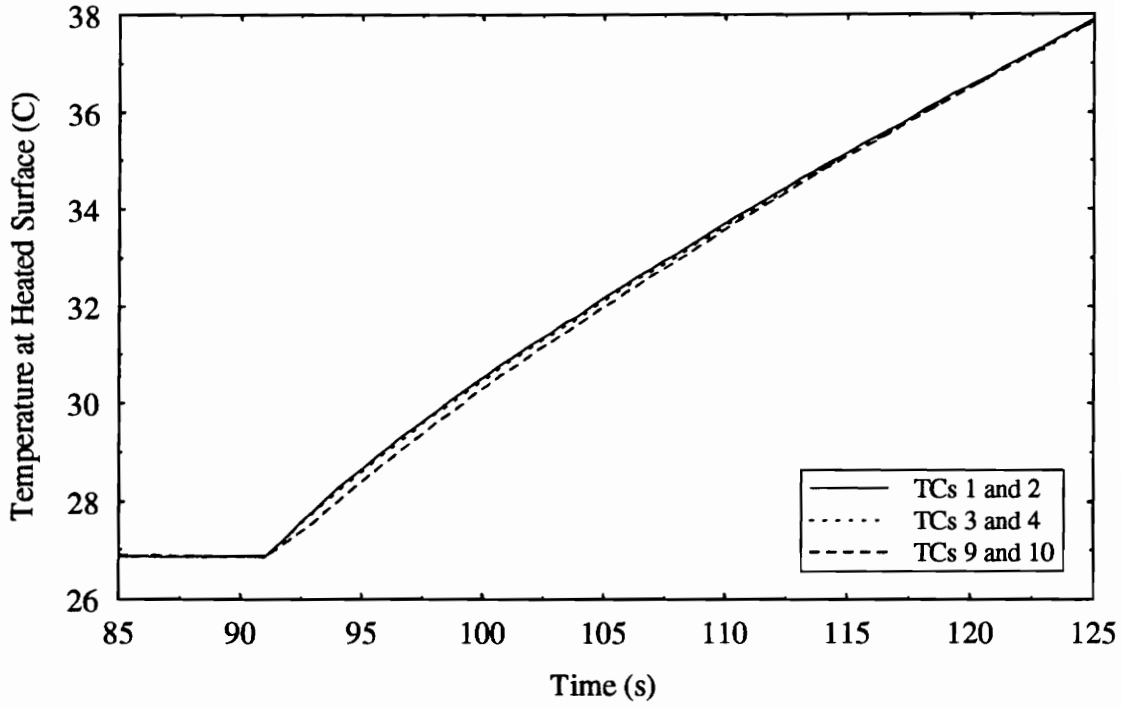

Figure 6.9 Heated Suface Thermocouple (TC) Temperatures at Start of Heating Time.

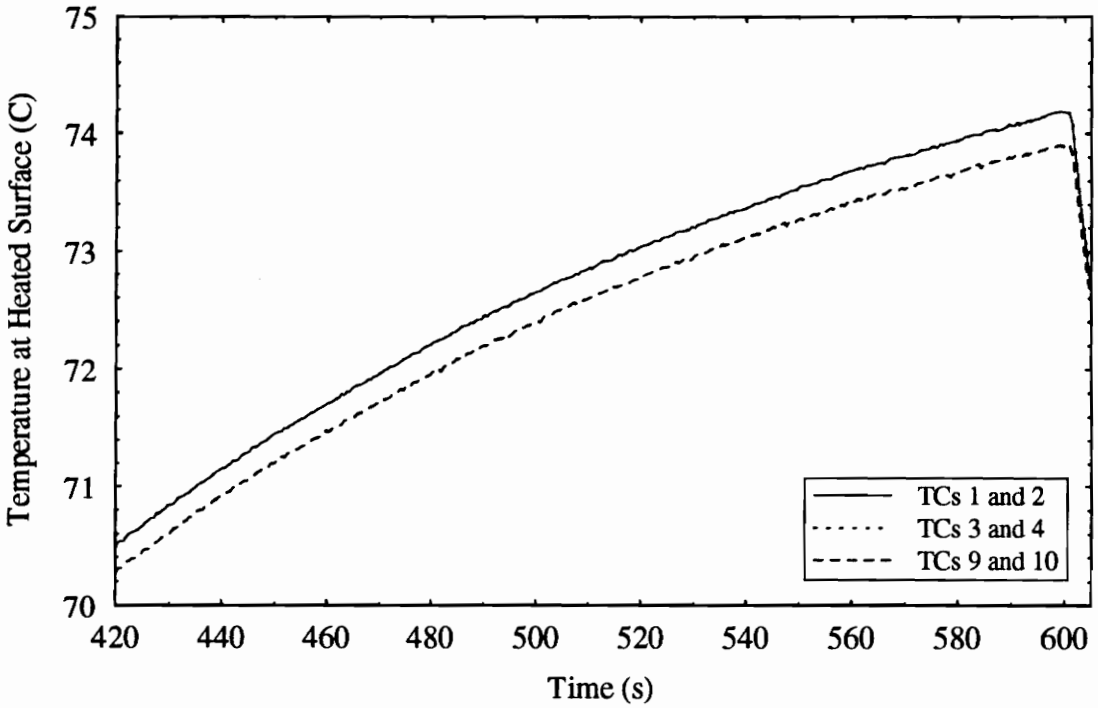

Figure 6.10 Heated Surface Thermocouple (TC) Temperatures at End of Heating Time.

Data from the four thermocouples at the constant temperature surface were plotted in Figure 6.11 and reveal that the temperature there is not quite constant. While it does not rise over 1.0°C, it does start to rise soon after heat is applied. Following Hanak (1995), the temperature history at $x=D$ was included as input to the numerical solution for added accuracy, as this is a trivial addition to the program. This boundary will now be referred to as the prescribed temperature boundary.

The power supply output, as shown in Figure 6.12, varies considerably, but within a very small range. A comparison of the numerical solutions computed with the heat flux history to solutions computed with constant heat fluxes, using both the highest and lowest values from the experiment, revealed mean residuals of about ±0.3°C. Though small, this difference is significant compared to the measurement precision and since a prescribed heat flux is also simple to add to the program, it was implemented in the solution.

6.1.4 Modifications of Solutions

Modifications needed to be made to the numerical solutions for the applied heat flux, prescribed temperature at $x=D$, and the addition of the heater. The modifications are basically the same for the diffusion and absorbing and scattering solutions.

The heat flux and temperature boundary are simply incorporated by reading the histories into arrays and replacing the constant values at each time step with the experimental value at that time.

The heater was modeled by adding points to the beginning of the mesh for the finite

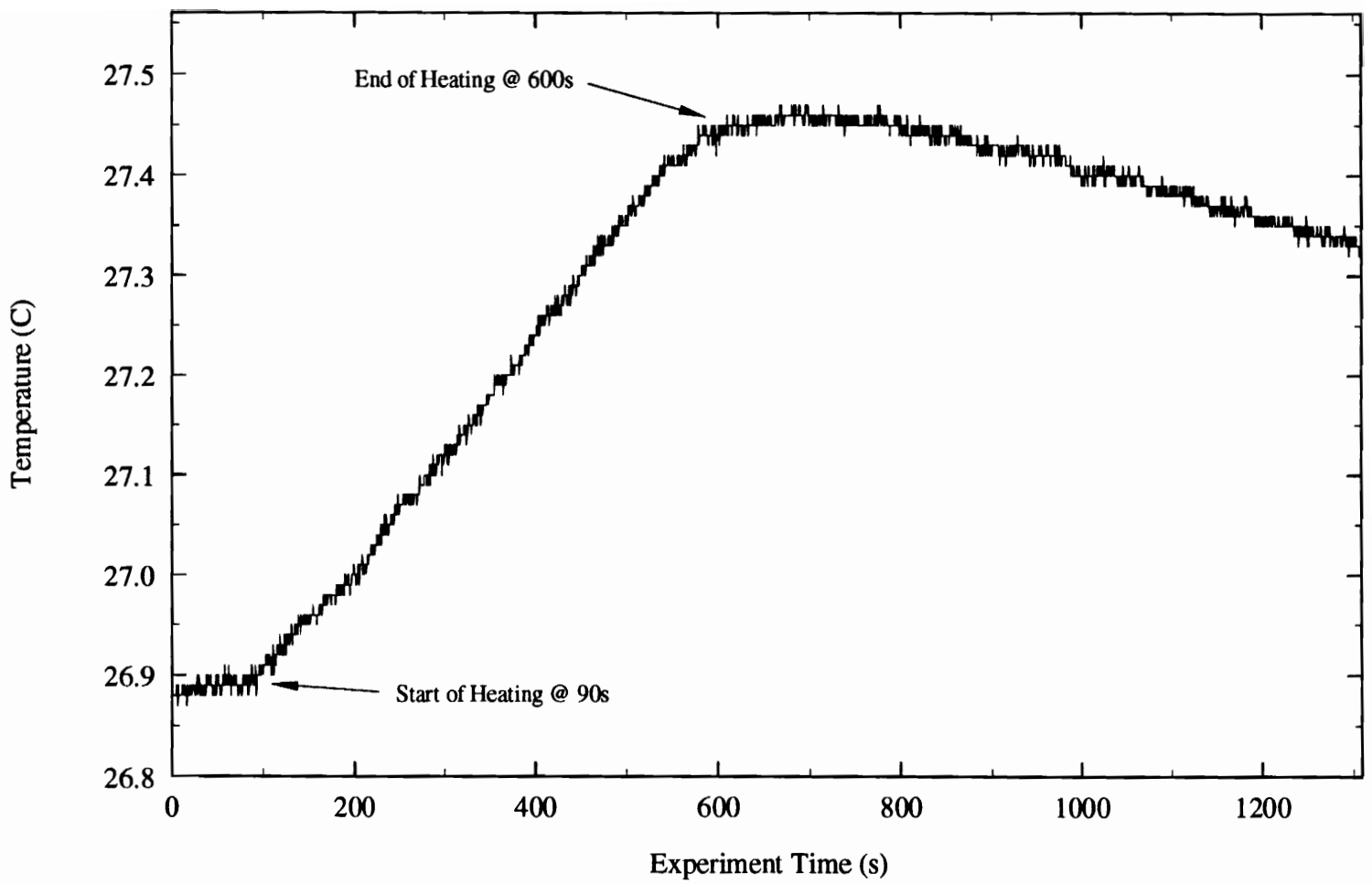

Figure 6.11 Variation in Temperature at the Prescribed Constant Temperature Boundary.

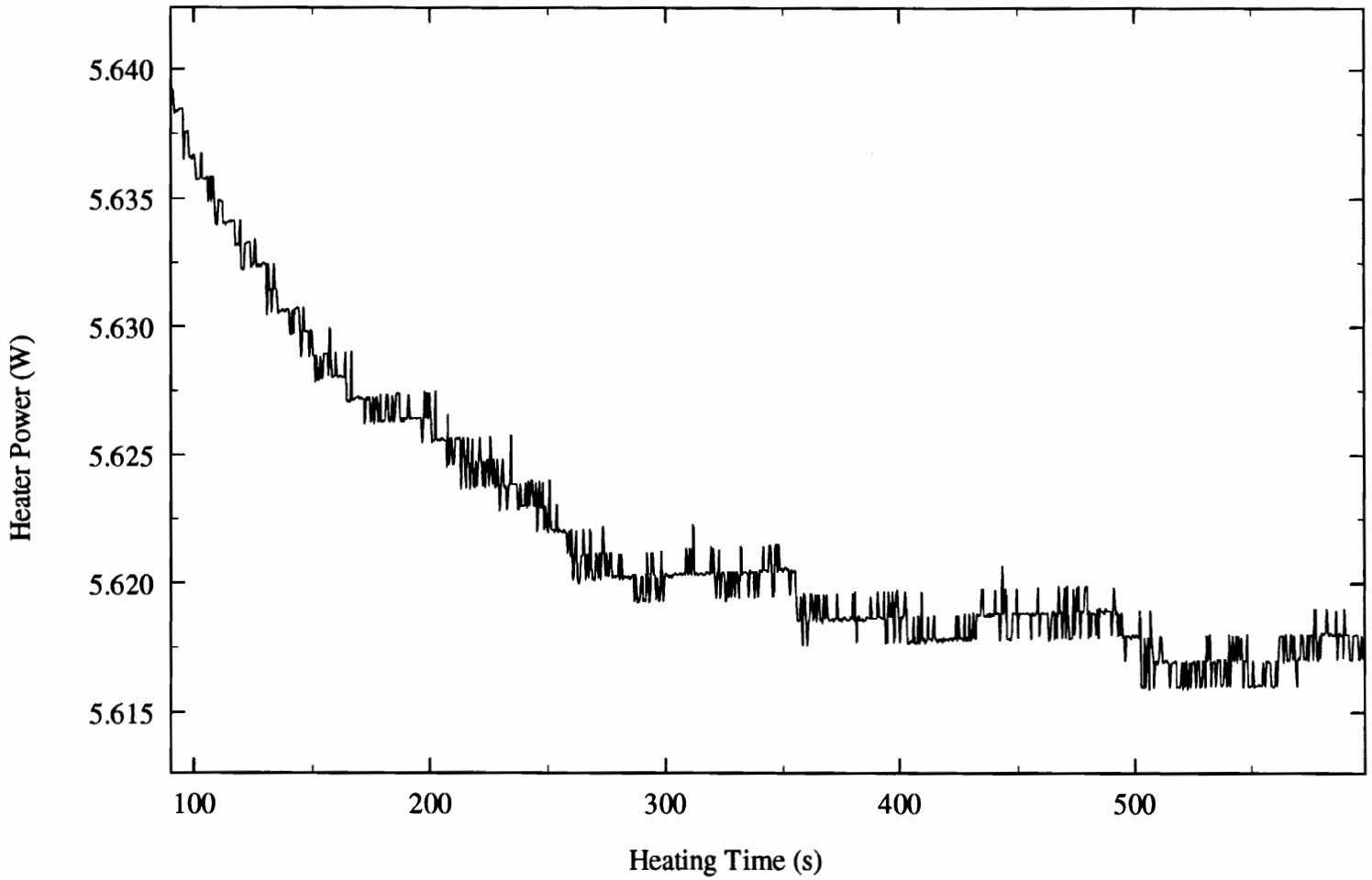

Figure 6.12 Variation in Heater Power over Time.

difference and assuming a heat flux applied to the heater surface. Six nodes were used to represent the heater. No extra quadrature points needed to be added to the radiation portion of the problem, as only conduction is present in the heater. This allowed the matrix for the heater to be built separately from the matrix for the material, and the two were combined only for solution of the temperatures by the Thomas algorithm. The temperatures output from the Thomas algorithm are then split into heater and material temperatures. This required the least reworking of the program and results in the coordinate system remaining the same, i.e. $\eta=0$ corresponds to the beginning of the Styrofoam.

The boundary with the heat flux is handled the same as the other solutions, though without the radiation term in the absorbing and scattering solution. The interface between the heater and the material required consideration of a control volume around the interface mesh point, illustrated in Figure 6.13. The temperature of the control volume is represented by the temperature at the interface mesh point and an energy balance leads to

$$q_{in} = -k_h \left.\frac{\partial T}{\partial x}\right|_h = -k_h \frac{(T_I - T_{I-1})}{\Delta x_h} , \qquad \textbf{(6.9)}$$

$$q_{out} = -k \left.\frac{\partial T}{\partial x}\right|_{Mat.} = -k \frac{(T_{I+1} - T_I)}{\Delta x} \quad where \quad k = k(T_I) , \qquad \textbf{(6.9)}$$

and

$$\Delta q = \left((\rho c_p)_h d_h + (\rho c_p) d\right)\frac{\partial T}{\partial t} = \left(c_h \frac{\Delta x_h}{2} + c\frac{\Delta x}{2} \right) \frac{(T_I^{p+1} - T_I^p)}{\Delta t} . \qquad \textbf{(6.11)}$$

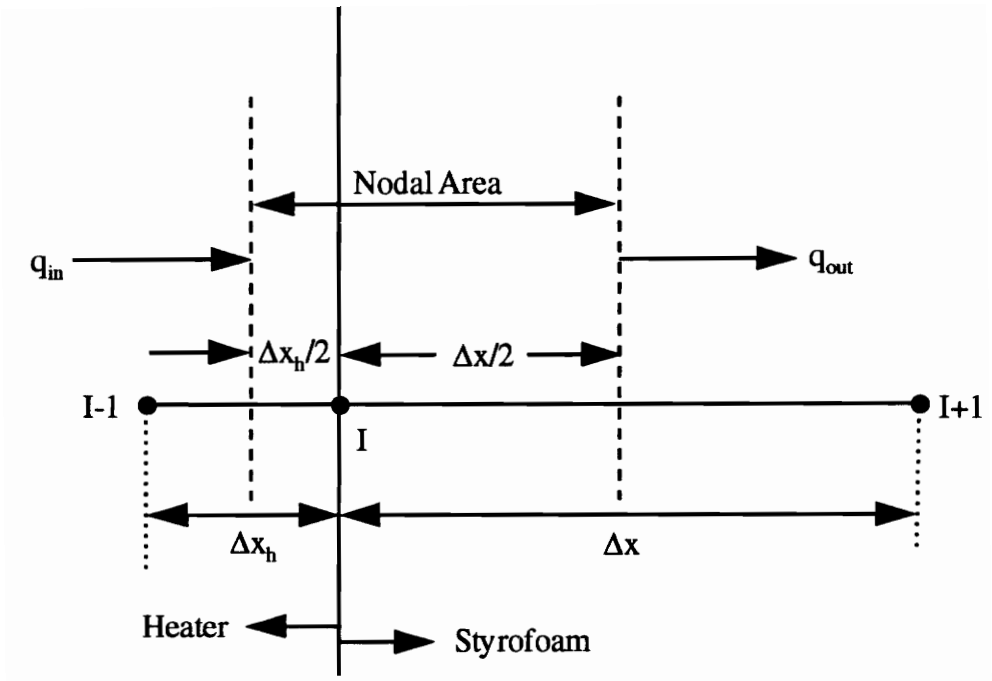

Figure 6.13 Control Volume for Discretized Heater/Styrofoam Interface Boundary Condition.

Combining equations and collecting terms leads to

$$-\frac{k_h}{\Delta x_h}T_{I-1}+\left(\frac{c_h\Delta x_h+c\Delta x}{2\Delta t}+\frac{k_h}{\Delta x_h}+\frac{k}{\Delta x}\right)T_I-\frac{k}{\Delta x}T_{I+1}=\left(\frac{c_h\Delta x_h+c\Delta x}{2\Delta t}\right)T_I^p \quad \textbf{(6.11)}$$

In the absorbing and scattering solution, the radiation heat flux at $\Delta x/2$, q_{ro} is included in the q_{out} term.

6.2 Application of Estimation Methods

Once the data were gathered, an estimation procedure was needed to find the property values. The modified Box-Kanemasu is a popular and relatively efficient method and was first used for the estimation. However, the sensitivity analysis revealed possible correlation between the thermal conductivity and the radiation coefficients, and the Box Kanemasu method has been demonstrated to fail on highly correlated parameters. This was the case with these parameters and the genetic algorithm was implemented with the hope of overcoming the correlation difficulties. The degree of correlation was too great, however, and could not be completely resolved even by using the genetic algorithm.

Four data sets were generated that had the same experimental parameters. Throughout most of the study, however, only one data set was used, as all the temperature histories were very close to one another. The purpose of four data sets is to compare confidence intervals for the actual estimates and so they are not necessary until actually reporting the estimates. The number of measurements in a data set can be used to calculate a root mean squared

(RMS) residual from the sum of squares

$$r_{RMS} = \sqrt{\frac{\sum_{i=1}^{n} (Y_i - \eta_{pi})^2}{n}} = \sqrt{\frac{S}{n}} . \qquad (6.13)$$

The RMS residual makes it easier to compare the "fitness" of parameters from data sets with different numbers of measurements.

6.2.1 Box-Kanemasu Estimation

The applicability of the modified Box-Kanemasu method for estimating the thermal conductivity, volumetric heat capacity, and absorption and scattering coefficients was investigated prior to running the experiment by using simulated data. The heater capacitance was not included in the simulated cases. A data set composed of temperatures at the heated surface was created for several hundred seconds using the scattering and absorbing solution with the nominal parameters. This is referred to as the exact data. A second data set was created by generating a random, normal distribution of errors with a standard deviation of 0.1°C and adding these to the exact solution to simulate the 0.08°C precision of the thermocouples. This is referred to as the simulated experimental data. Two sets of initial property values were tested.

Some results of the estimation are presented in Table 6.2. The Box-Kanemasu method did reasonably well with the exact data for thermal conductivity, but not as well for the other properties. The same was true of the simulated experimental data for the second set of initial

guesses, but for the first set β was made negative, which caused the program to stop. Furthermore, for initial guesses that were farther off than those presented below, the Box-Kanemasu method would not converge and would produce negative values for some of the properties. Note that there is no way to prevent this method from selecting negative parameters, even though they are physically meaningless.

Table 6.2 Box-Kanemasu Results for Simulated Data.

	k (W/mk)	c (kJ/m^{3}K)	a (m^{-1})	σ_s (m^{-1})
Actual value	0.02800	19.20	1500	300
Initial guess #1	0.03200	15.00	1000	700
Exact data	0.02743	18.70	817	800
Simulated experimental data	----------	----------	-------	-------
Initial guess #2	0.02500	24.00	900	400
Exact data	0.02746	18.74	1070	528
Simulated experimental data	0.02755	18.73	1090	519

The Box-Kanemasu method was also used for the actual experimental data and performed even worse for that case. This method was attempted for both the diffusion and the absorbing and scattering solutions and failed after the first iteration. Output from the program MBK.FOR indicated a large degree of correlation between k and β, as well as some correlation between c and c_h, which was expected from examination of the sensitivity

coefficients.

To gain a better idea of the property values for initial guesses and ranges, a semi-parametric study was performed using the modified Box-Kanemasu and the diffusion solution, as it is has a very short computational time. A Box-Kanemasu estimation was attempted using a fixed value for the extinction coefficient and estimating the other three parameters. Using a modest tolerance of 1.0×10^{-3}, convergence was obtained for the three parameters for several values of the extinction coefficient. In addition, an estimation was performed assuming no radiation transfer ($\beta = 0$). Some of the values, and the resulting sum of squares, are shown in Table 6.3 and the sum of squares is plotted for different βs in Figure 6.14.

Table 6.3 Thermal Properties for a Given β Using Box-Kanemasu.

β	k (W/mK)	c (kJ/m³K)	c_h (kJ/m³K)	S (n=2130)	r_{RMS} (°C)
No radiation	0.0464	26.1	1707	193.5	0.301
1825	0.0411	24.0	1787	142.4	0.259
1375	0.0393	23.4	1813	129.9	0.247
625	0.0307	20.0	1949	99.2	0.216
425	0.0234	17.0	2072	112.8	0.230

There appears to be a relatively well-defined minimum, though it must be realized that the difference between a sum of squares of 100 and 160 is quite small. Given these data, however, it was thought that the genetic algorithm would have no trouble finding the properties. Also, note that the *k* value of 0.0464 W/mK for no radiation provides a maximum

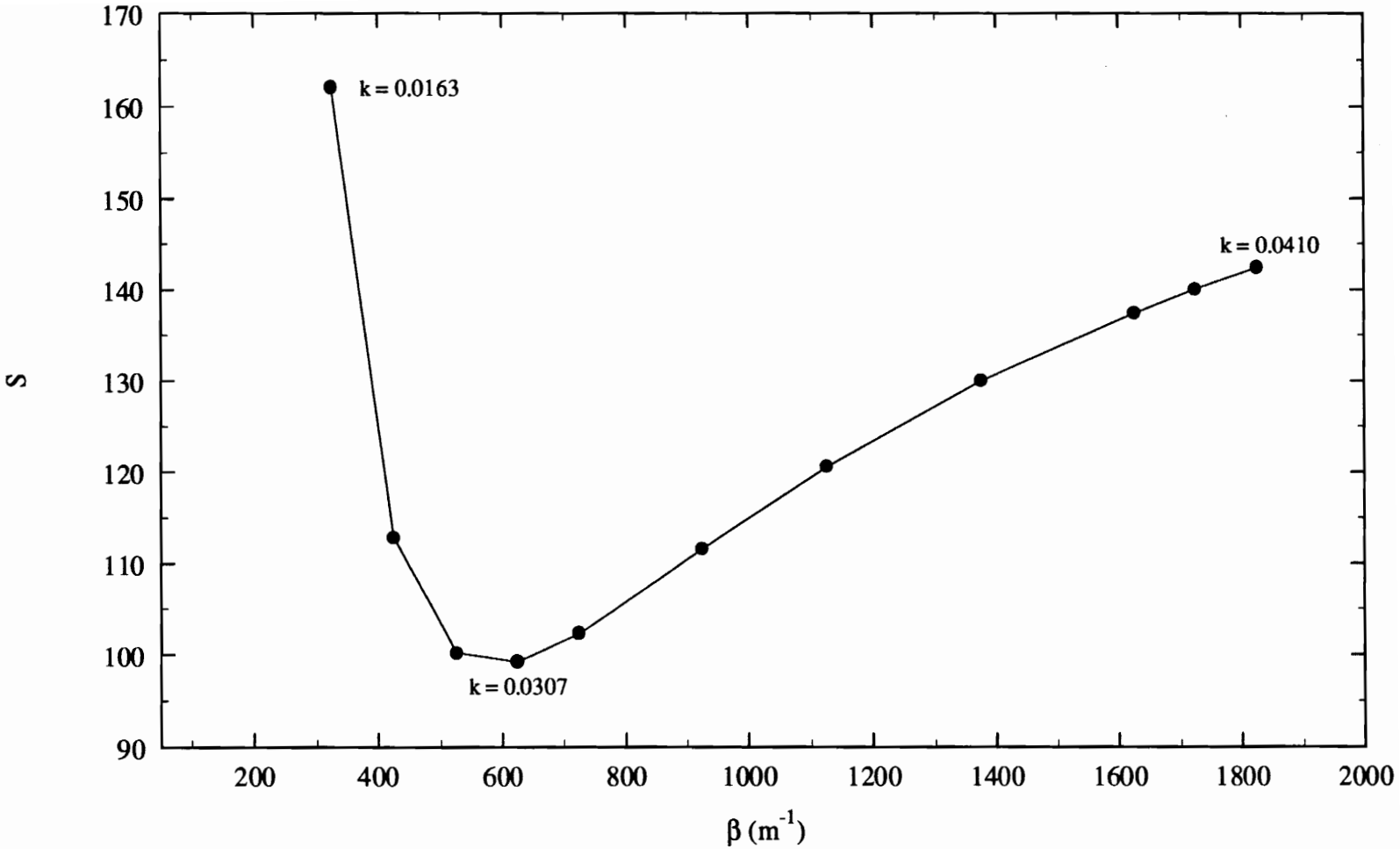

Figure 6.14 Sum of Squares as a Function of β Using Modified Box-Kanemasu to Estimate k, c, & c_h.

value for the thermal conductivity that can be used to narrow the ranges in the genetic algorithm.

6.2.2 Genetic Algorithm Estimation with Simulated Data

The genetic algorithm (GA), using the extended elitist strategy, was also first tested using the simulated data, both exact and with simulated errors of 0.1 °C. The algorithm was first run to narrow the parameter ranges; the initial parameter ranges were set fairly large, relative to how well the initial Styrofoam properties were known. The GA population was set at 50 and iterated for 20 generations. The initial and final ranges are listed in Table 6.4. The maximum range for k and c were greatly reduced, but the ranges for a and σ_s remained large, reflecting both the lower sensitivity coefficients and the parameter correlation.

Table 6.4 Initial and Final GA Ranges for Simulated Data, Absorbing and Scattering Solution.

	k (W/mK)		c (kJ/m³K)		a (m⁻¹)		σ_s (m⁻¹)	
	Min.	**Max.**	**Min.**	**Max.**	**Min.**	**Max.**	**Min.**	**Max.**
Initial	0.01	0.05	10	100	500	2000	150	600
Final	0.013	0.036	12.5	52.1	580	1900	188	568

Pop. size = 50, Gen. = 20

The GA was then used to estimate the parameters for both the exact and simulated experimental data. The program was run on a fairly powerful workstation, a Silicon Graphics

Power Challenge XL, but still took several days to complete for 20 generations with a population of 50. The results are presented in Table 6.5 for both cases.

Table 6.5 Genetic Algorithm Estimation Results for Simulated Data.

	k (W/mK)	c (kJ/m^{3}K)	a (m^{-1})	σ_s (m^{-1})	S (n=500)
Value	0.028	19.2	1200.0	300.0	-
Exact Data	0.028 ± 0.003	19.1 ± 0.3	1280.0 ± 670.0	323.0 ± 510.0	2.53×10^{-6}
Simulated Experimental Data	0.027 ± 0.003	19.2 ± 0.3	1040.0 ± 580.0	282.0 ± 483.0	7.48

Pop. size = 50, Gen. = 20

The values for the simulated thermal conductivity and volumetric heat capacity are quite good for both cases, though the confidence interval for the former is fairly large. The values for the radiation coefficients in the exact data case are relatively close, but note the large confidence intervals. Using the simulated experimental data, the absorption coefficient is significantly less than the actual value. The scattering coefficient is still close, but the confidence interval is almost one hundred percent. Note also that while the absorption coefficient is lower, so is the thermal conductivity. Both parameters describe the material's resistance to heat transfer; the lower the a or the higher the k, the more heat moves through the material. Therefore, the low value for a is compensated by the low value for k, which is why the sum of squares is very small, despite each parameter being significantly off. This highlights the problem with correlation for the estimation. However, given the relatively low

population size and the few generations, the genetic algorithm performed well. The actual estimation will require a larger population and more generations.

6.2.3 Genetic Algorithm Estimation with Diffusion Solution

Due to the length of the computational time for the absorbing and scattering solution, an initial GA run was performed with this solution for only two generations and a population of 15 to check that everything was working. The resulting range for k was narrow, but had larger values than expected, $k > 0.040$ W/mK. The corresponding values for the absorption and scattering were also large and indicated the algorithm may be missing the minimum area, given the values from the Box-Kanemasu analysis. It was decided to do some preliminary analysis using the diffusion solution, which would allow results from adjustment of the GA parameters within an hour because of its reduced computational time compared to the absorbing and scattering solution. The parameters to estimate were the thermal conductivity, Styrofoam volumetric heat capacity, extinction coefficient, and the heater volumetric heat capacity.

Two initial runs were made, the first with a population of 50 and the second with a population of 200, both for 20 generations. The resulting ranges and typical sum of squares values are shown in Table 6.6.

Table 6.6 Initial GA Diffusion Ranges.

		k (W/mK)	c (kJ/m³K)	β (m⁻¹)	c_h (kJ/m³K×10³)	S
Initial	Min.	0.0200	10.0	100	1.00	---
	Max.	0.1000	100.0	1000	3.00	
Pop. = 50	Min.	0.0436	26.4	3400	1.45	~ 225
	Max.	0.0451	32.1	6280	1.69	
Pop. = 200	Min.	0.0391	16.7	1330	1.53	~ 200
	Max.	0.0454	29.6	8990	2.11	

Gen. = 20

It is important to remember that the GA updated the parameter ranges each generation, based on the best values from the previous generation, so that even mutations will not introduce parameters outside those ranges. The purpose of the 200 population was to reduce the possibility of prematurely narrowing the ranges.

The resulting ranges for the two cases are quite different, but the sum of squares is similar. The number of points used was 2543, which results in a RMS residual of 0.28°C for *S=200*, which is quite close to the error in the thermocouples (0.1°C). However, it is not as good as the estimates from the Box-Kanemasu analysis, which are in turn most likely not the best overall values. The GA migrates towards the higher values of *k*, with a resulting higher range for β, even though the Box-Kanemasu analysis indicated good results for lower values of those parameters. The lower thermal conductivity range for the 200 population case is less than that for the 50 population case, but still high. These two runs also indicated a fair degree

of correlation between c and c_h, with a low value for one being compensated by a high value for the other. Nevertheless, the ranges for the two, especially the Styrofoam, are substantially reduced.

To investigate the lower values of thermal conductivity, another analysis was performed for a population of 50, with the initial range of k fixed between 0.028 and 0.038, and the results are in Table 6.7. The ranges of the other parameters remained the same.

Table 6.7 Diffusion Results for a Narrow k Range.

	k (W/mK)	c (kJ/m³K)	β (m⁻¹)	c_h (kJ/m³K ×10³)	S
Pop. = 50 Min.	0.0313	15.9	640	1.83	~ 150
Max.	0.0354	22.3	873	2.11	

Gen. = 20

This analysis revealed that lower values of k do indeed provide a lower sum of squares, though the S values are still relatively close to the $_s$ values for higher thermal conductivities. The resulting range for the extinction coefficient is also much lower. The ranges for the volumetric heat capacities are quite similar to those in the previous analysis.

It was surmised that the higher k values occur at some kind of local minimum and the GA was missing the global minimum, which occurs at a lower k value. Since the GA has been demonstrated to avoid such situations, it was desired to gain some idea of what the sum of squares function could look like to cause this behavior. A sum of squares surface plot was developed for different values of k and β, with c and c_h held at constant values of 19.2 kJ/m³K

and 1949.0 kJ/m^{3}K, respectively. The value of k was incremented by 0.0001 W/mK and the value of β by 25 m^{-1}. The function as a surface plot is pictured in Figures 6.15 and 6.16 and as a contour plot in Figure 6.17. Note that the contours on the contour plot are not equally spaced. It is important to remember that this plot is for a specific set of experimental parameters and is for specific values of c and c_h, and does not necessarily represent a global representation of the relationship between k and β. It does, however, provide some general insight into the problem.

These plots provide a clear picture of the correlation difficulty. First, note that for low k values combined with high β values and for very low β values, the S function is very large and those values clearly do not represent the actual properties. However, there is quite clearly a curved region where the S function is, relative to the other regions, very small and almost constant. Furthermore, at the low end of the thermal conductivity range, this region is a very narrow "valley", but as k increases this region expands into a large "plain". This explains the behavior of the genetic algorithm. The GA generates random populations of variables from the available ranges; ideally, the chosen values are evenly distributed over the entire range. In this case, however, the valley region is so narrow, and the plain region so large, that good S values almost never come from the lower k range, while many good S values are chosen from the higher k range. Furthermore, the range updating further reduces the probability of picking a low k by excluding the lower range from later generations. This suggests two means of improving the algorithm for this problem; choosing a very large population and eliminating the range updating procedure.

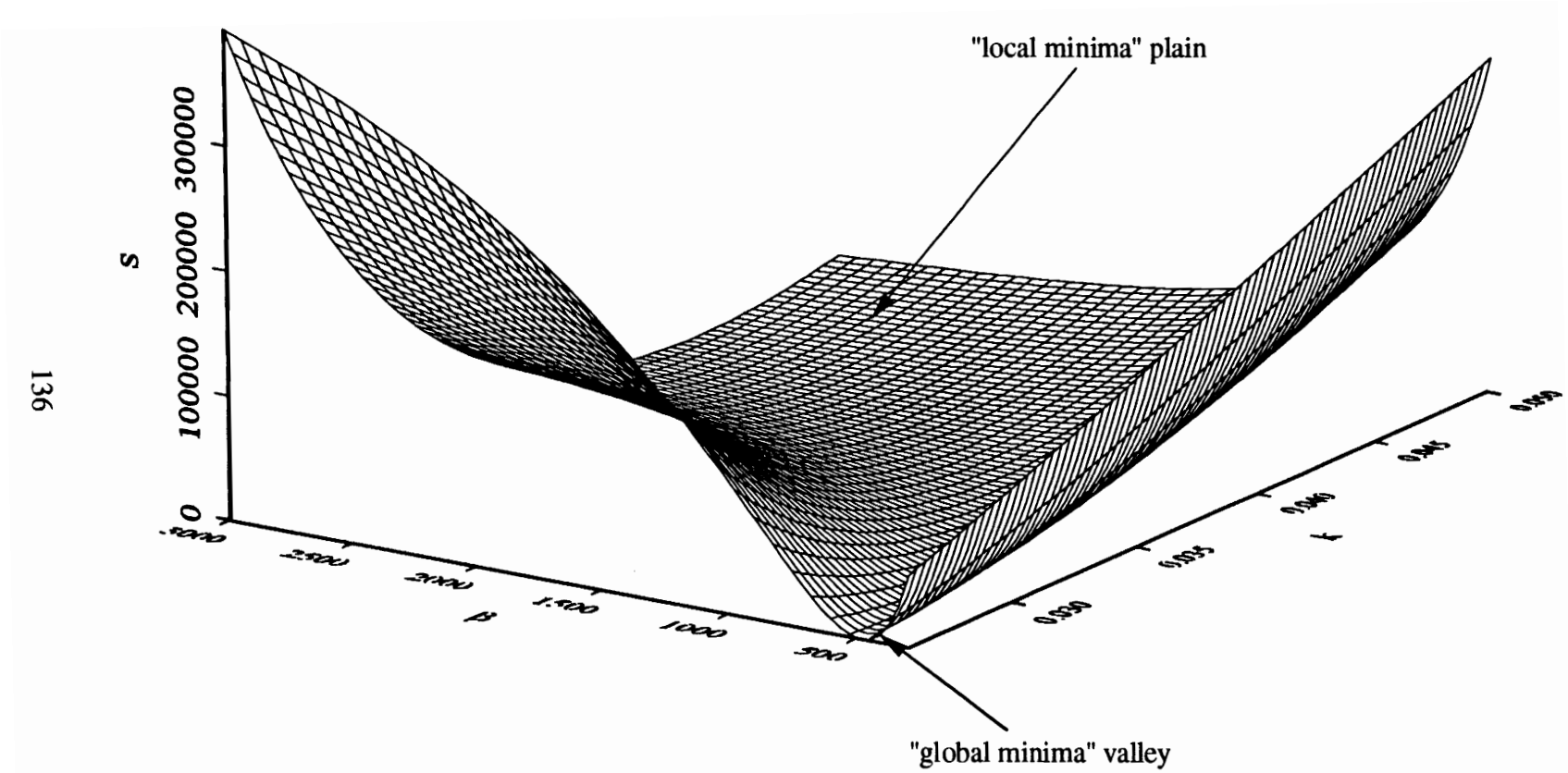

Figure 6.15 Diffusion Sum of Squares Function for k and β with c and c_h fixed.
c = 20.0 kJ/kgK c_h = 1949.0 kJ/kgK

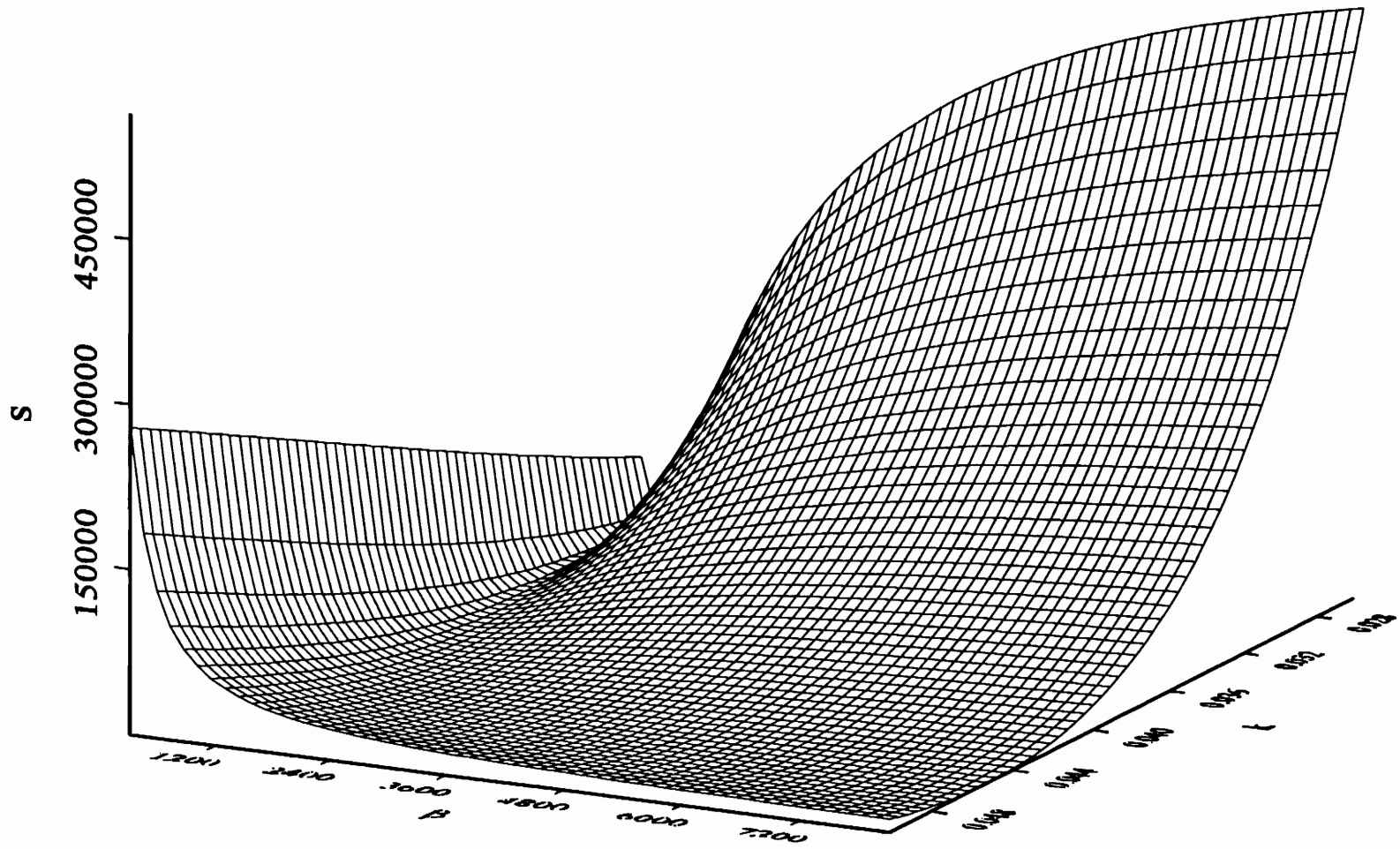

Figure 6.16 Diffusion Sum of Squares Function for k and β with c and c_h Fixed, Alternate View
c = 20.0 kJ/kgK c_h = 1949.0 kJ/kgK

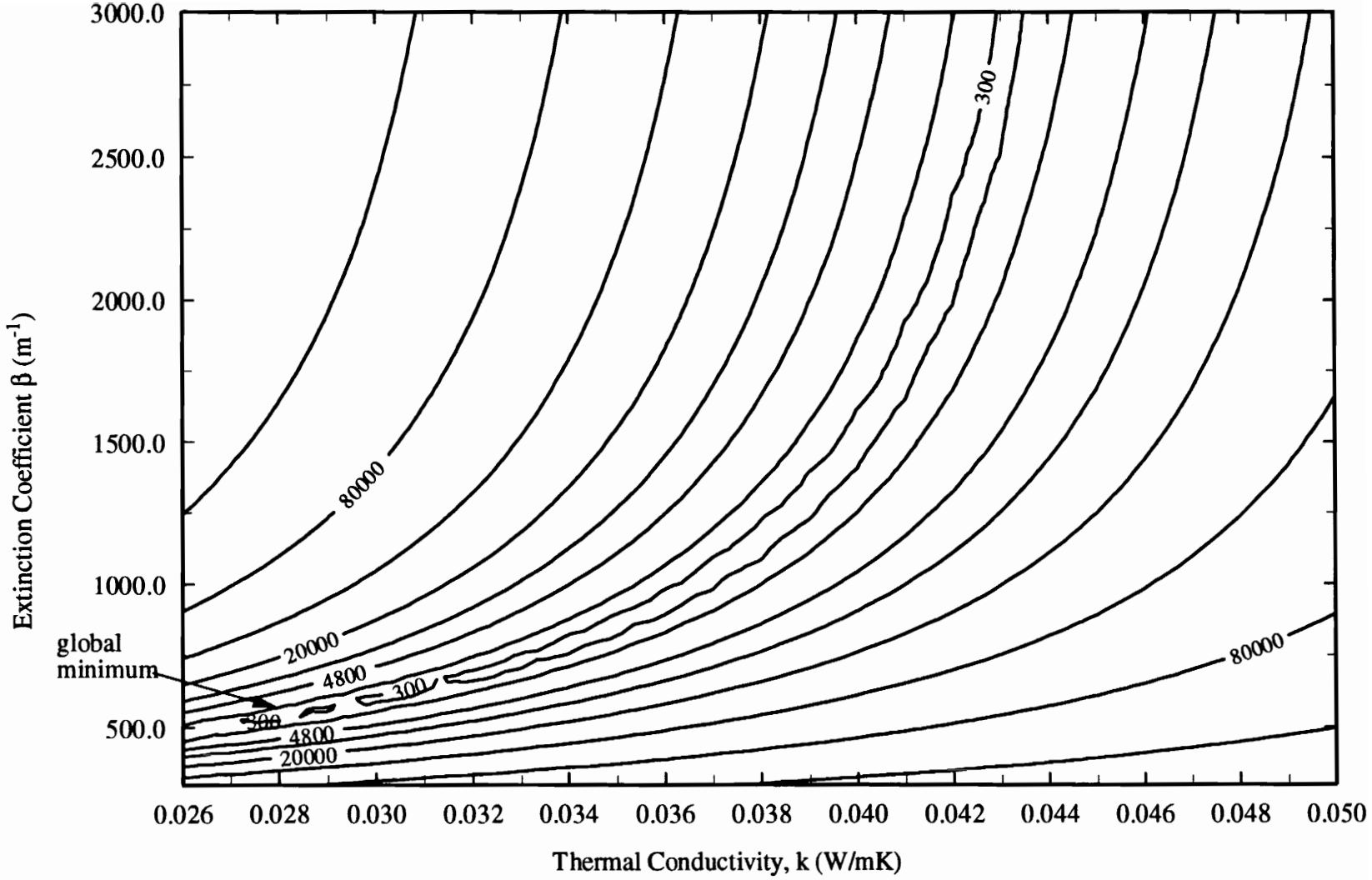

Figure 6.17 Contour Plot of Diffusion Sum of Squares Function for k and β with c and c_h Fixed
c = 20.0 kJ/kgK c_h = 1949.0 kJ/kgK

Another thing to note is the asymptotic nature of the minimum area as k increases. The value for β goes to infinity as k approaches 0.044 and beyond 0.044 S increases even for large β. This coincides with the resulting estimates from the Box-Kanemasu analysis assuming no radiation. That case gave a value for k of 0.0464 and the S plot confirms a limit for k around that value.

One question is whether or not there exists a minimum within the minimum band. The lowest S for each value of k is plotted in Figure 6.18 and reveals that a minimum does exist at the lower end of the k range, though it is very shallow. The oscillations in that area are due to the rough grid for β and the sensitivity of the solution to β. Even a small change in the extinction coefficient from the optimal value will produce a much larger sum of squares, on the order of the S at the other end of the range. The actual minimum S values occur at the lower end of the oscillations. Beyond $k=0.043$ W/mK, the sum of squares increases dramatically.

After reviewing the plotted S function, two different estimation procedures were performed. First, a set of 10 runs was made with a population of 50, 5 generations, and the original initial ranges. The data for each was exactly the same, with the exception of the random number seed for the GA program. This is similar to running a population of 5000. The results, in Table 6.8, show roughly the same k ranges for nine of the runs, but one run which had a much lower minimum value and a corresponding low value for β, verifying the need for a larger population for this problem.

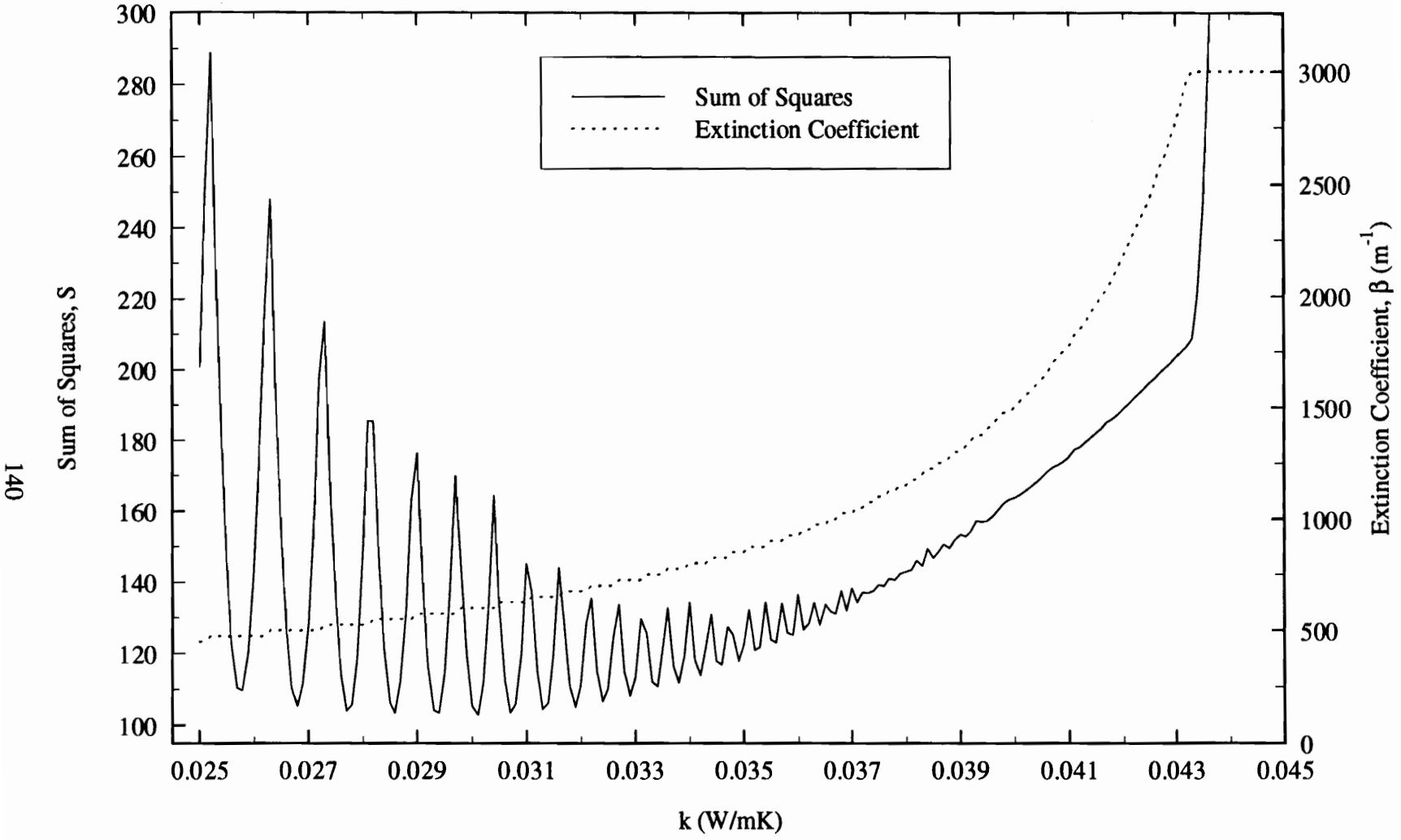

Figure 6.18 Minimum S, and Corresponding β, for Each k from Diffusion Sum of Squares Plot.

Table 6.8 Results of 10 Runs Using Exact Same Data.

Run	k (W/mK)		β (m^{-1})	
	Min.	Max.	Min.	Max.
1	0.0419	0.0455	2160	8110
2	0.0432	0.0458	2670	9160
3	0.0402	0.0444	1590	3900
4	0.0403	0.0456	1660	8980
5	0.0434	0.0460	4020	8760
6	**0.0344**	0.0465	**780**	9320
7	0.0414	0.0453	2030	8670
8	0.0433	0.0453	4010	7330
9	0.0423	0.0458	2200	9320
10	0.0441	0.0450	3790	8100

Pop. = 50, Gen. = 5

The second analysis consisted of dividing the thermal conductivity into "strips" of narrower ranges, Table 6.9, and performing the analysis for each strip with the other parameters retaining their original range. The ranges overlap slightly since the end ranges are less likely to be selected.

Table 6.9 Split *k* Ranges.

Strip	1	2	3	4	5
Min.	0.020	0.026	0.032	0.038	0.044
Max.	0.028	0.034	0.040	0.046	0.052

The results, in Table 6.10, coincide with the data plotted in Figure 6.17. The value for S_{best} represents the lowest sum of squares from the final population. The lower *k* range exhibits a lower *S* and represents the global minimum for this case, though the difference is slight.

Table 6.10 Resulting Ranges for Split *k* Initial Ranges.

Strip	k (W/mK)		c (kJ/m^{3}K)		β (m^{-1})		c_h (kJ/m^{3}K×10^3)		S_{best}
	min	max	min	max	min	max	min	max	
1	.0262	.0280	12.3	22.39	488	532	1.830	2.283	114.5
2	.0287	.0335	7.8	21.68	552	759	1.895	2.484	118.1
3	.0375	.0389	16.95	26.95	1110	1290	1.650	2.100	139.1
4	.0432	.0451	18.75	24.98	2950	7800	1.737	2.022	208.1
5	.0449	.0452	21.61	22.09	6160	7300	1.866	1.899	205.0

Pop. = 50, Gen. = 20

To check the use of a larger population and the effect of not updating the ranges, two more runs were made. One had a population of 800 and updated the ranges, while the other had a population of 800 and did not update the ranges. Ranges are given in Table 6.11 for

Table 6.11 Parameter Ranges for Diffusion with a Population of 800.

Run	k (W/mK)		c (kJ/m^{3}K)		β (m^{-1})		c_h (kJ/m^{3}K×10^3)	
	min	max	min	max	min	max	min	max
Initial	.0200	.0500	5.00	30.00	200	5000	1.00	3.00
Update: 100	.0306	.0449	8.82	29.97	603	4991	1.54	2.47
Update: 700	.0218	.0455	5.50	29.97	380	4991	1.44	2.64
No update: 100	.0233	.0449	9.40	29.97	422	4985	1.51	2.38
No update: 700	.0218	.0455	5.58	29.97	380	4991	1.48	2.63

Pop. = 800 Gen. = 10

the top 100 and top 700 values at the end of each run. Updating the ranges had little effect on the outcome after 10 generations for such a large population and not updating offered little advantage. In the top 100, the un-updated ranges produced a somewhat lower *k* and β range, but they are the same for the top 700. The ranges did not change much overall from the initial values, though the larger the population, the more generations must generally be used to narrow in on the estimates. After 10 generations, the lower *k* and β values are still available, but note that for the top 100 of the updated case, the lower ranges are much higher. In fact, the initial elitist population for both cases contained three values less than 0.030 W/mK in the top 50, but the final population for the updated case did not contain any less than 0.030 W/mK in the top 50 and only had two less than 0.040 W/mK, while the final population for the un-updated case had only two less than 0.040 W/mK. Since the higher thermal conductivity values represent a larger percentage of the "gene pool" used to create the parameter sets for subsequent generations, the effect of the parameters in the lower range is

diluted and the algorithm still tends to move towards the larger thermal conductivity and extinction coefficient values.

The procedure of separating the thermal conductivity range into several smaller ranges was repeated for the other three sets of data taken. The third and fourth data sets had data collected at approximately every 1.0s, rather than every 0.5s, which resulted in about half the number of measurements (around 1100). The solution was still computed at every 0.5s. The resulting ranges from all four sets were used to obtain the best estimates possible by performing two more GA analyses for each data set, the first with the narrowed ranges from the split k investigation and the second with narrowed ranges based on the first run. Each run had a population size of 50 and repeated for 20 generations. The results for the best values from each run are listed in Table 6.12. The top two parameter sets are listed for data sets two and four, because the resulting sum of squares for each were very close. Confidence intervals were unavailable for the second set of run number two.

The values are fairly close to one another, with the exception of the best in set four, but have relatively large confidence intervals, in the range of 5-25% of the stated values. The heater capacitance has the smallest confidence interval, on the order of 6%, and the extinction coefficient has the highest, on the order of 25%. There is also a difference between the first two and last two data sets, with the confidence intervals of the latter being larger than the former, indicating that even for 1100 measurements, additional measurements can help narrow the ranges.

The correlation does not allow a more certain estimate for the properties than presented

Table 6.12 Final Diffusion Estimates for Each Data Set.

	Data Set					
	1	2	2	3	4	4
	Best	Best	2nd Best	Best	Best	2nd Best
k (W/mK)	0.0306 ± 0.0038	0.0313 ± 0.0038	0.0299 ---	0.0311 ± 0.0053	0.0249 ± 0.0053	0.0275 ± 0.0052
c (kJ/m^3K)	20.9 ± 2.4	19.1 ± 2.6	18.7 ---	18.5 ± 3.7	19.7 ± 3.5	18.3 ± 3.7
β (m^{-1})	625 ± 150	638 ± 159	586 ---	639 ± 221	463 ± 116	532 ± 151
c_h (kJ/m^3K)	1.911 ± 0.107	1.971 ± 0.114	1.991 ---	2.011 ± 0.221	1.969 ± 0.154	2.024 ± 0.163
r_{RMS} (°C)	0.206	0.225	0.226	0.298	0.249	0.258

Pop. = 50, Gen. = 20

in Table 6.12. As an illustration, consider Figure 6.19, which is a plot of the average sum of squares for the parent population of each generation. The initial ranges were narrowed based on information in Table 6.12, except for the thermal conductivity, which was set between 0.022 and 0.032 W/mK. The GA was run with a population of 50 for 50 generations.

Ideally, the parent sum of squares will decrease from generation to generation, though it may increase a little for one or two generations due to the nature of the genetic algorithm. This behavior was observed for the examination of the narrowed thermal conductivity ranges, but Figure 6.19 clearly shows a non-convergent behavior due to the correlation, indicating that larger populations and more generations will not produce more decisive results.

6.2.4 Genetic Algorithm Estimation with Absorbing and Scattering Solution

The results of estimation using the diffusion solution indicate that the optical thickness of the Styrofoam, while not small, is not as large as previously believed. If the extinction coefficient is 500 m^{-1}, the resulting optical thickness is 9.1, and as seen in Figure 3.9, this will result in some difference between the diffusion solution and the more exact absorbing and scattering solution. Thus, it is important to examine the other solution as well.

It was decided to estimate κ_D and Ω instead of the absorption and scattering coefficients for two reasons. First, estimating optical thickness is the same as estimating the extinction coefficient, as D is known, and this will be easier to compare to the diffusion solution and will likely result in more accurate estimates of the extinction coefficient, though the accuracy of the scattering albedo will be small. Secondly, it is easier to assign a range to Ω and β than to

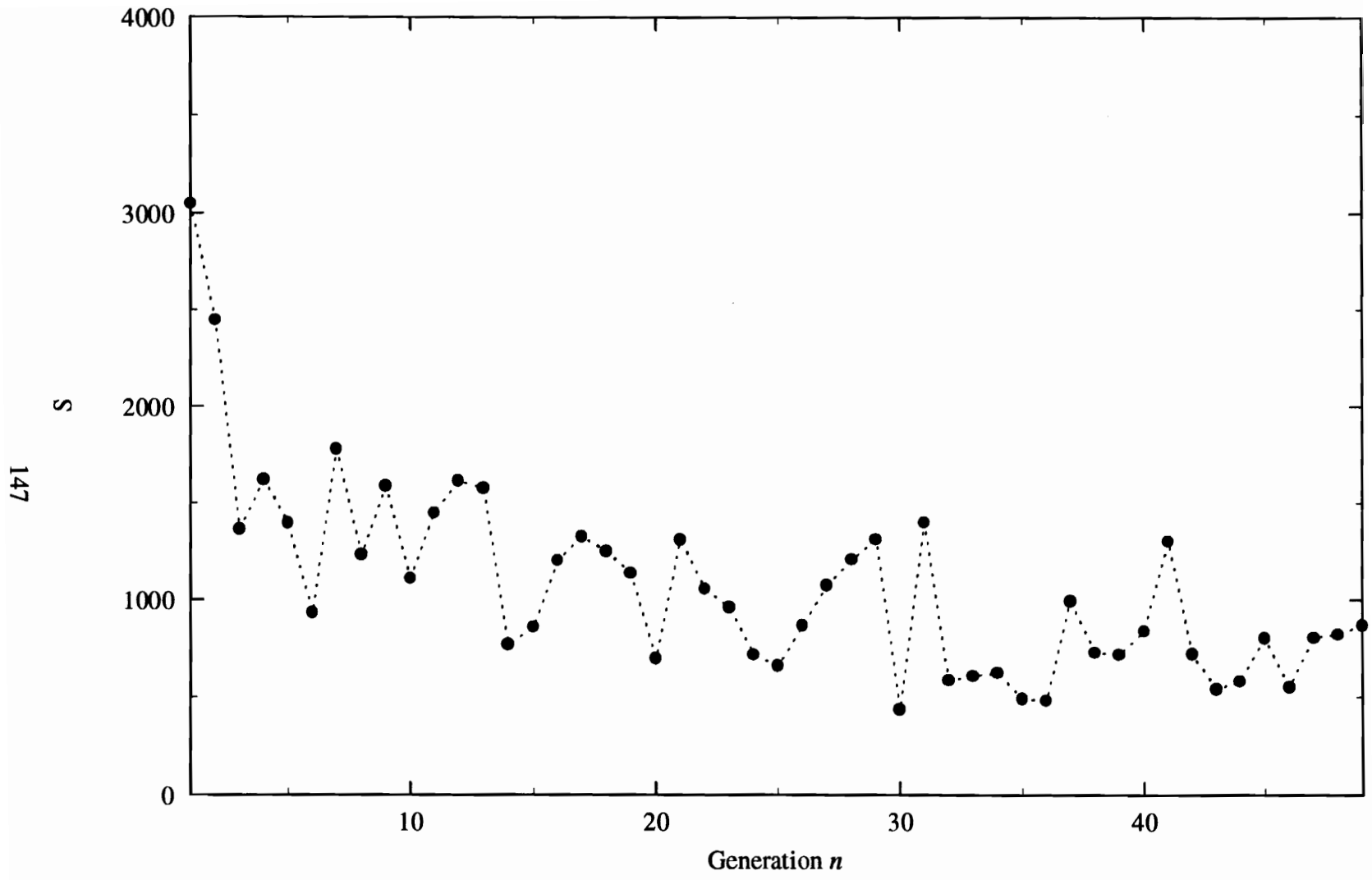

Figure 6.19 New Parent Population Sum of Squares for Diffusion Solution with Narrow Ranges.

a and σ_s. The range for Ω has to be between zero and one and the range for β will be similar to that for the diffusion solution. The other parameters, Styrofoam thermal conductivity and volumetric heat capcity and heater volumetric heat capacity, are the same for a total of five properties.

Also, several hundred seconds of data at the end of the experimental time were dropped, as the sensitivity coefficients at these times were relatively small and the solution time was critical. This resulted in 1457 observations, and consequently the sum of squares will not compare with the diffusion sum of squares. Instead, the RMS residual is reported, which can be directly compared with the diffusion RMS residual.

An initial GA run was made using large ranges, a population of 30, and 10 generations and the results are in Table 6.13. They indicate similar results as the diffusion case, though the range for k is relatively low. This is deceptive, however, as there was only one set of parameters with a k that low; the other 29 sets had a thermal conductivity of at least 0.0394 W/mK and an extinction coefficient of at least 1360 m^{-1}.

Table 6.13 Initial GA Ranges for Absorbing and Scattering.

		k (W/mK)	c (kJ/m³K)	β (m^{-1})	Ω	c_h (kJ/m³K)	r_{RMS} (°C)
Initial	Min.	0.0220	5.0	200	0.1	1.50×10^3	---
	Max.	0.0460	30.0	5000	1.0	2.50×10^3	
Final	Min.	0.0339	1634	766	0.48	1.88×10^3	~ 0.393
	Max.	0.0418	21.3	3370	0.89	2.11×10^3	

Pop. = 30, Gen. = 10

The next step was to analyze several strips, as in the diffusion case, and these results are in Table 6.14. The scattering albedo is not listed because the final range was almost equal to the initial range, which was to be expected given its low sensitivity. Only three initial thermal conductivity ranges were used: (0.022,0.030), (0.028,0.036), and (0.034,0.042). The results are similar to those for the diffusion case, with the lowest range having the best estimates, the middle range being relatively close, and the high range off quite a bit. The RMS residual is not quite as low as the diffusion case, but that is largely due to the low number of populations and generations.

Table 6.14 Final Ranges for Absorbing and Scattering Split Initial *k* Ranges.

Strip	k (W/mk)		c (kJ/m^{3}K)		β (m^{-1})		c_h (kJ/m^{3}K×10^3)		r_{RMS} (°C)
	min	max	min	max	min	max	min	max	
1	.0254	.0270	21.7	28.0	445	471	1.68	1.88	~ 0.32
2	.0330	.0338	22.8	25.9	721	816	1.73	1.85	~ 0.35
3	.0373	.0419	13.3	27.6	1080	2220	1.63	2.30	~ 0.51

Pop = 30, Gen. = 10

A final GA analysis with the absorbing and scattering solution was made where the ranges for thermal conductivity were not updated. The GA had a population of 50 and 20 generations and computation time was about one week. The final ranges and the best set of parameters are listed in Table 6.15. The first thing to note is that the residuals are not quite as good as those for the diffusion case. This is partly due to the lower population combined

with one more parameter, which increases the number of possible parameter sets. Secondly, the thermal conductivity and extinction coefficient are a little higher, while the volumetric heat capacity is lower (and consequently, the heater capacitance is higher). Again, the lower

Table 6.15 Final Results from Absorbing and Scattering Solution Using the GA without Updating the Range for *k*

	Min.	Max.	Best
k (W/mK)	0.0297	0.0358	0.0336 ± 0.0112
c (kJ/m³K)	17.03	27.26	18.34 ± 2.82
β (m^{-1})	541	897	724 ± 530
Ω	0.34	0.84	0.77 ± 1.09
c_h (kJ/m³K)	1.640	2.072	2.025 ± 0.134
r_{RMS} (°C)	~ 0.38		0.339

Pop. = 50 , Gen. = 20

population may contribute to this result. Furthermore, it may also have been better not to update the β range, as it is related to the thermal conductivity. The confidence intervals for the parameters, however, are large enough to include the diffusion values. The confidence intervals for *k* and β are much larger than the diffusion case because the property values are higher. As these two parameters increase, a deviation in the parameters will produce less of

a change in the sum of squares, as can be seen in Figures 5.15 through 5.17. Another reason for the difference between the two cases is the different solutions, so the two should not be expected to match exactly. The confidence interval for the scattering albedo, Ω, indicates there is not enough information for that property. The two volumetric heat capacities, c and c_h, have about the same confidence intervals as the diffusion case, which makes sense since their effect is the same in each solution. The absorbing and scattering estimates, as well as the best diffusion estimates, are shown in Figures 6.20 through 6.23 with their 95% confidence intervals.

6.3 Examination of Correlation for Diffusion Solution

A sample correlation matrix for the diffusion solution is shown below and the severe correlation between k and β, as well as correlation between c and c_h, can be seen clearly.

Table 6.16 Typical Approximate Diffusion Correlation Matrix.

	k	c	β	c_h
k	1.00000			
c	0.61372	1.00000		
β	0.99972	0.62158	1.00000	
c_h	-0.59638	-0.99509	-0.60434	1.00000

The analysis provides a good idea of the ranges, especially for β and c (as well as c_h), but the thermal conductivity still has a fairly large possible ranges. Note, however, that even though

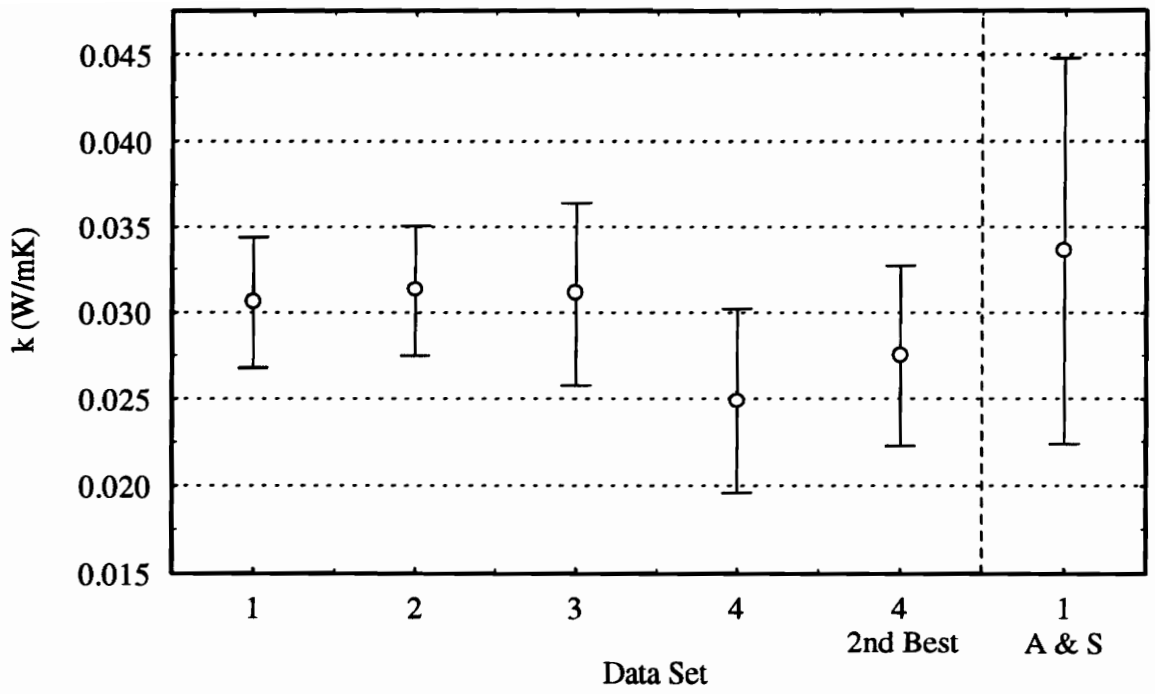

Figure 6.20 Confidence Intervals for Final Estimates of Thermal Conductivity, *k*, for Diffusion and Absorbing and Scattering (A & S) Solutions.

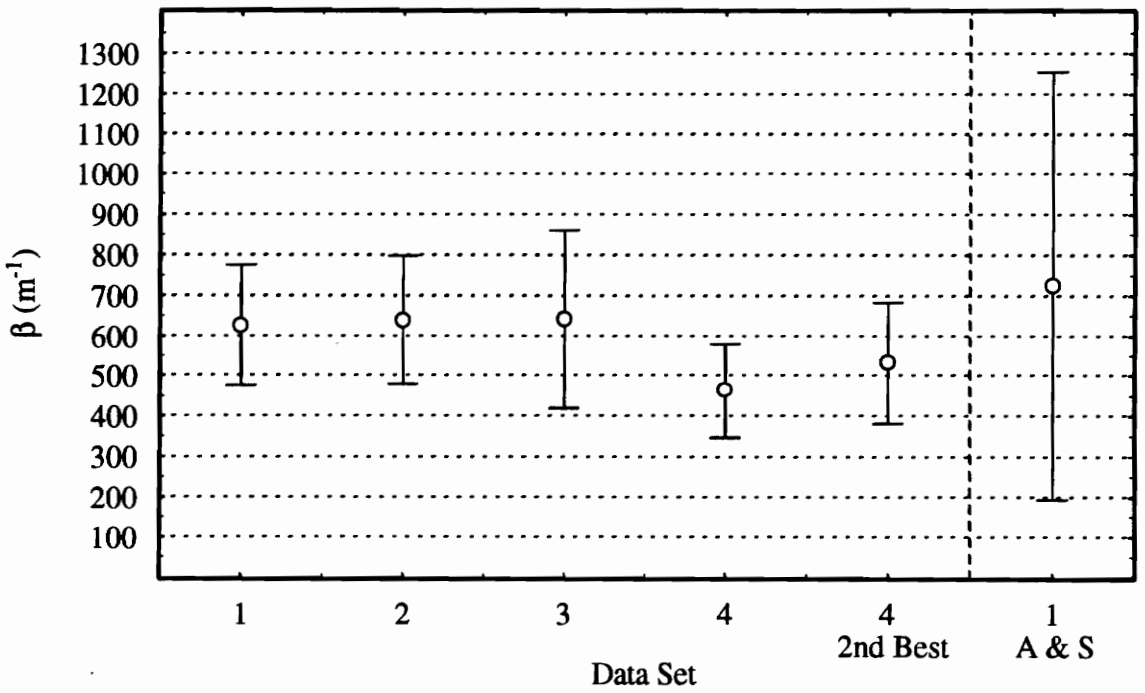

Figure 6.21 Confidence Intervals for Final Estimates of the Extinction Coefficient, β, for Diffusion and Absorbing and Scattering (A & S) Solutions.

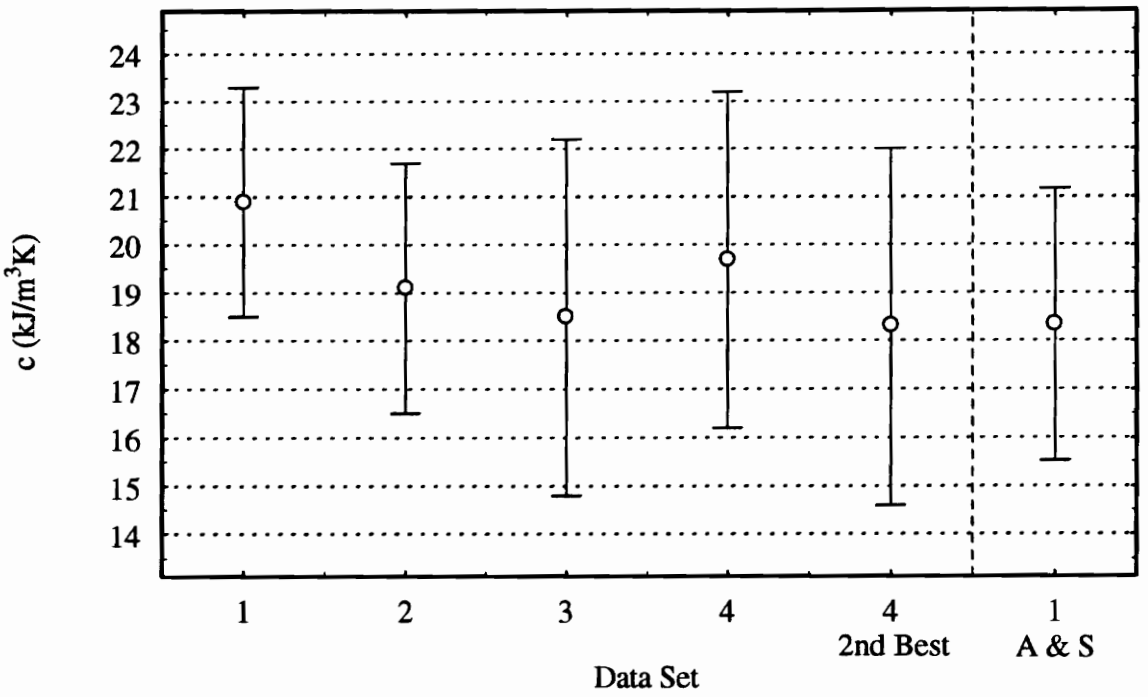

Figure 6.22 Confidence Intervals for Final Estimates of the Volumetric Heat Capacity, c, for Diffusion and Absorbing and Scattering (A & S) Solutions.

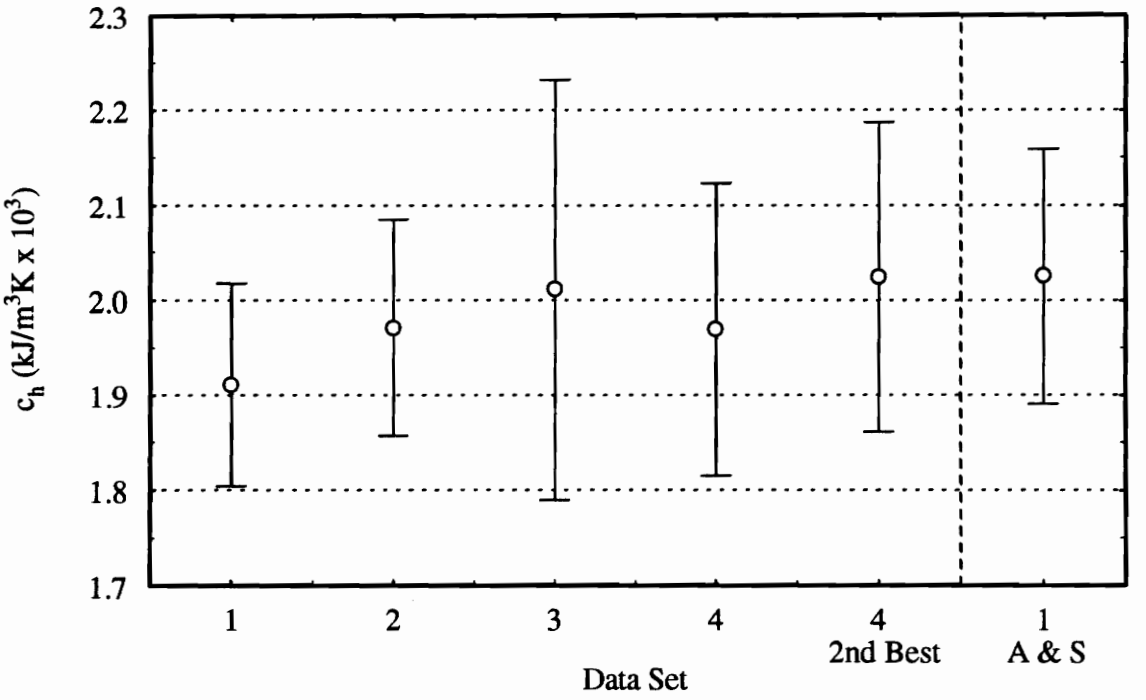

Figure 6.23 Confidence Intervals for Final Estimates of the Heater Volumetric Heat Capacity, c_h, for Diffusion and Absorbing and Scattering (A & S) Solutions.

k and β are correlated together, a much better idea of the extinction coefficient range is known. The reason can be ascertained by examining the S contour function in Figure 6.17, which shows that as the value of the thermal conductivity decreases, the allowable range for the extinction coefficient becomes much lower.

Given the high correlation between the thermal conductivity and extinction coefficient, the nominal values for Styrofoam from Incropera and DeWitt (1990) were revisited. There were a total of eight values given for the thermal conductivity of Styrofoam, each at a different temperature, from 200K to 300K. A curve fit was applied to this data based on the effective thermal conductivity formula of equation (3.10) and resulted in the following approximate values:

$$k = 0.022 \text{ W/mK} \qquad \beta = 430 \text{ m}^{-1}$$

While these are very inexact values, they nevertheless provide additional support for k and β being relatively low for Styrofoam. Note that the nominal value for the volumetric heat capacity, 19.2 kJ/kgK, is quite close to the estimates presented in Table 6.12.

If parameters are correlated, the sensitivity coefficient of one can be written as a constant times the sensitivity coefficient of the other, and therefore the ratio of the two sensitivity coefficients will be constant. Since the correlation was so great, the sensitivity coefficients were reexamined by plotting the ratio of X^*_k to X^*_β and X^*_c to $X^*_{c\,h}$, shown in Figure 6.24, to see if there was a region of low correlation. The parameters are significantly less correlated at the start of heating, and become very correlated as the experiment moves to steady state. However, as can be seen in Figure 6.7, the sensitivity coefficients are not very

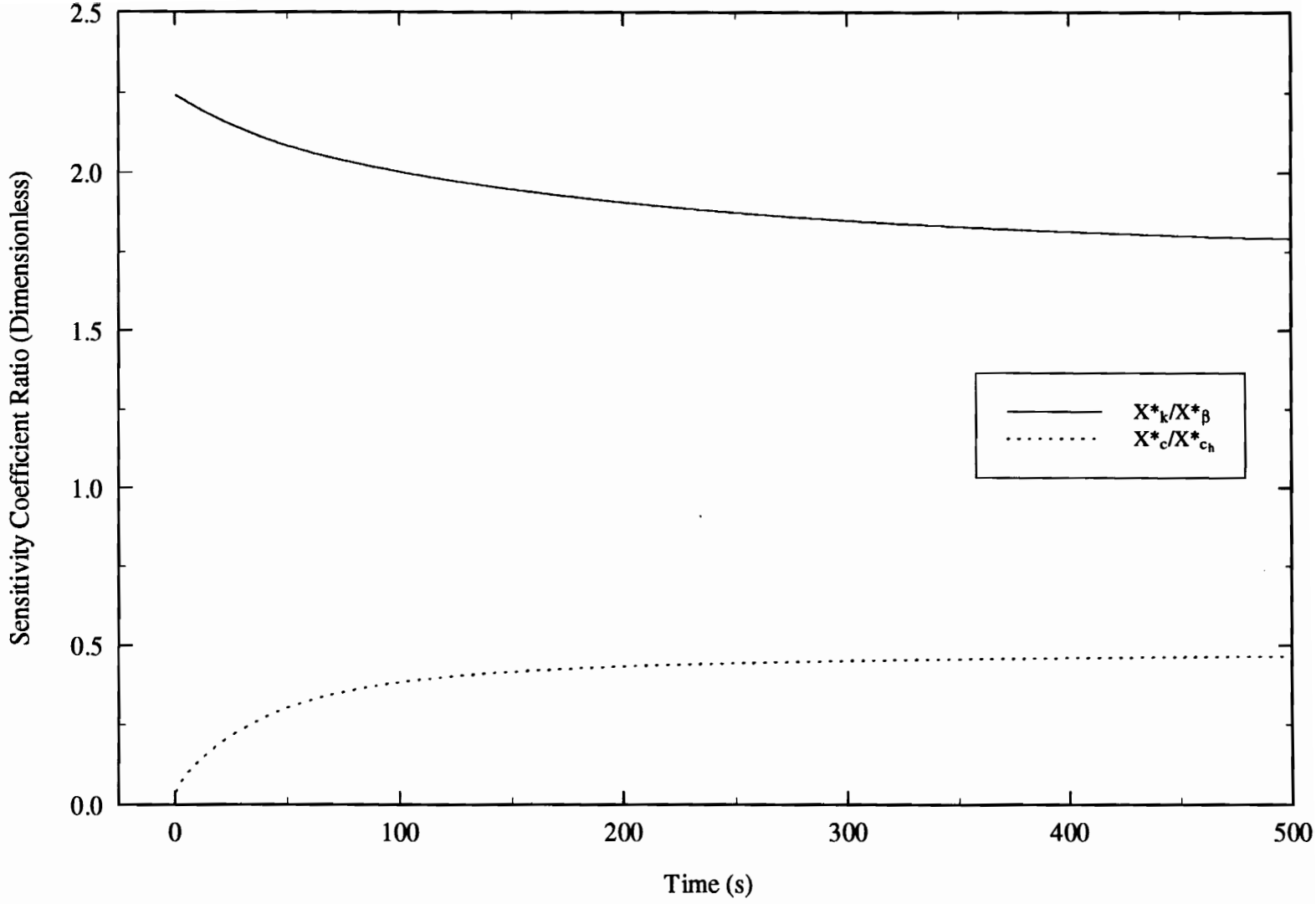

Figure 6.24 Ratio of Sensitivity Coeficients for k & β and c & c_h to Examine Correlation.

large in that time period and the thermal conductivity and volumetric heat capacity are also somewhat correlated in that region. On the other hand, if the experiment is only conducted for about a minute, a higher heat flux can be applied, which will result in higher sensitivity coefficients.

A new experiment was designed by using a parametric study that calculated the approximate correlation matrix using equation (3.63) and finding the least correlation among the parameters. The experimental parameters examined were the applied heat flux, the heating time, and the experiment time. The diffusion solution was used because of its speed, which allowed a large range of parameters to be examined. The analysis resulted in the choice of the following parameters: 450 W/m^2 heat flux, 50s of heating, and a total of 60s of experimental time. A new experiment was conducted and the resulting data used in an estimation using the genetic algorithm.

The GA was conducted with a population of 50 for 20 generations and resulted in the following best estimates:

Table 6.17 Best Estimates from Non-correlated Data.

Parameter	Value	C.I.
k (W/mK)	0.038	± 0.072
c (kJ/m^3K)	23.9	± 21.0
β (m^{-1})	770	± 4200
ch ($kJ/m^3K \times 10^3$)	1.86	± 0.22
r (°C)	0.195	---

Obviously, the estimates from this data are unusable, as the confidence intervals are so large. In fact, there were six sets of estimates with an RMS residual less than 0.21°C that included thermal conductivities of 0.028 and 0.041 W/mK and extinction coefficients of 770 and 1600 m^{-1}. This analysis highlights the importance of maximizing the sensitivity coefficients for parameter estimation.

The use of an alternate setup, with two constant temperature boundaries, was also briefly examined in regards to correlation. Figure 6.25 is a plot of the sensitivity coefficients for k and β at $x=D/4$ for two constant temperature boundaries, with the hot boundary at 350K and the cold boundary at 298K and ratio of the two sensitivity coefficients. This reveals the two are very uncorrelated for the transient portion of the experimental time. However, the maximum values of the sensitivity coefficients are on the same order as those used in the attempt to reduce correlation for the heat flux experiment and would not provide enough information to accurately estimate the properties.

6.4 Comparison of Models

Radiation has been shown to be a significant, in some cases dominant, mode of heat transfer in porous materials, including foams. The correlation between the thermal conductivity and the extinction coefficient poses a difficulty, however, in treating thermal property estimation for these materials. The correlation allows the incorrect assumption of

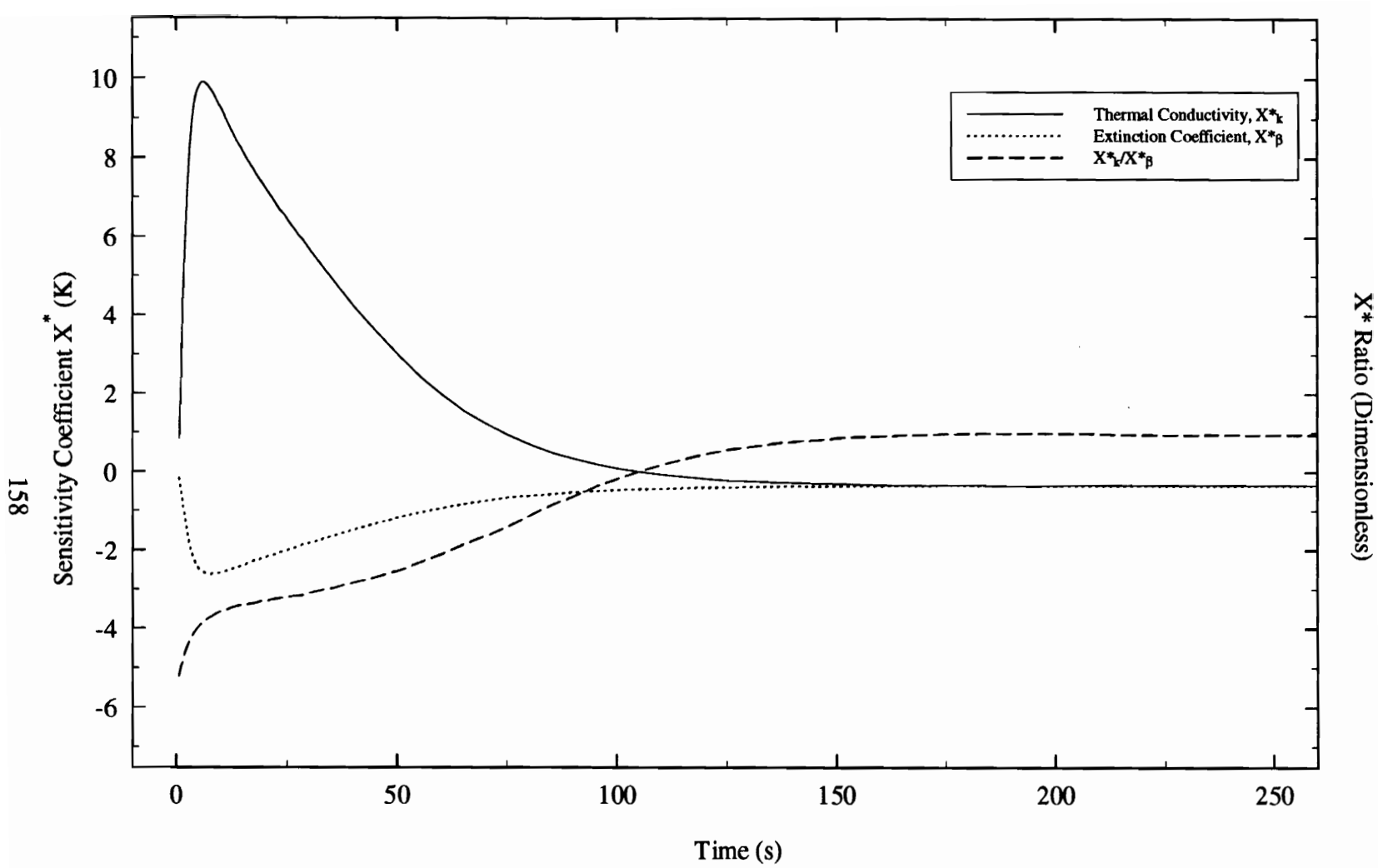

Figure 6.25 Plot of Normalized Sensitivity Coefficients (X*)and X^*_k/X^*_β Ratio for Experiment with Two Constant Temperature Boundaries.

no radiation to produce a reasonable estimate for a constant thermal conductivity. This thermal conductivity can be used to match the data, despite being an extremely inaccurate estimate. However, the use of that same property with different boundary conditions or in a different application could result in incorrect results. Even more importantly, the lack of knowledge concerning the radiation transfer would inhibit design of a better insulating system, as the radiation transfer could be reduced through the use of opacifiers or reflecting materials. Therefore, it is imperative that research is done on the type of material being studied and that there is a thorough knowledge of the heat transfer model being used.

In this case, a constant thermal conductivity was able to match the data within 0.30°C, though it was clearly not the correct value. The analysis revealed considerable radiation heat transfer within the Styrofoam. In fact, the material, while still considered optically thick, would benefit from a model that more accurately represents the physics of the problem than the diffusion solution. The inclusion of scattering is not necessary, as it has little effect on the solution for this case, and a purely absorbing solution would probably be adequate.

6.5 Residuals

The estimation procedure has been shown to match the data within an RMS residual of 0.20°C to 0.40°C. A comparison of the actual data to the calculated solution using the final set of diffusion properties from the first data set is shown in Figure 6.26 and demonstrates excellent agreement. However, the RMS residual is a mean value and in estimation the actual

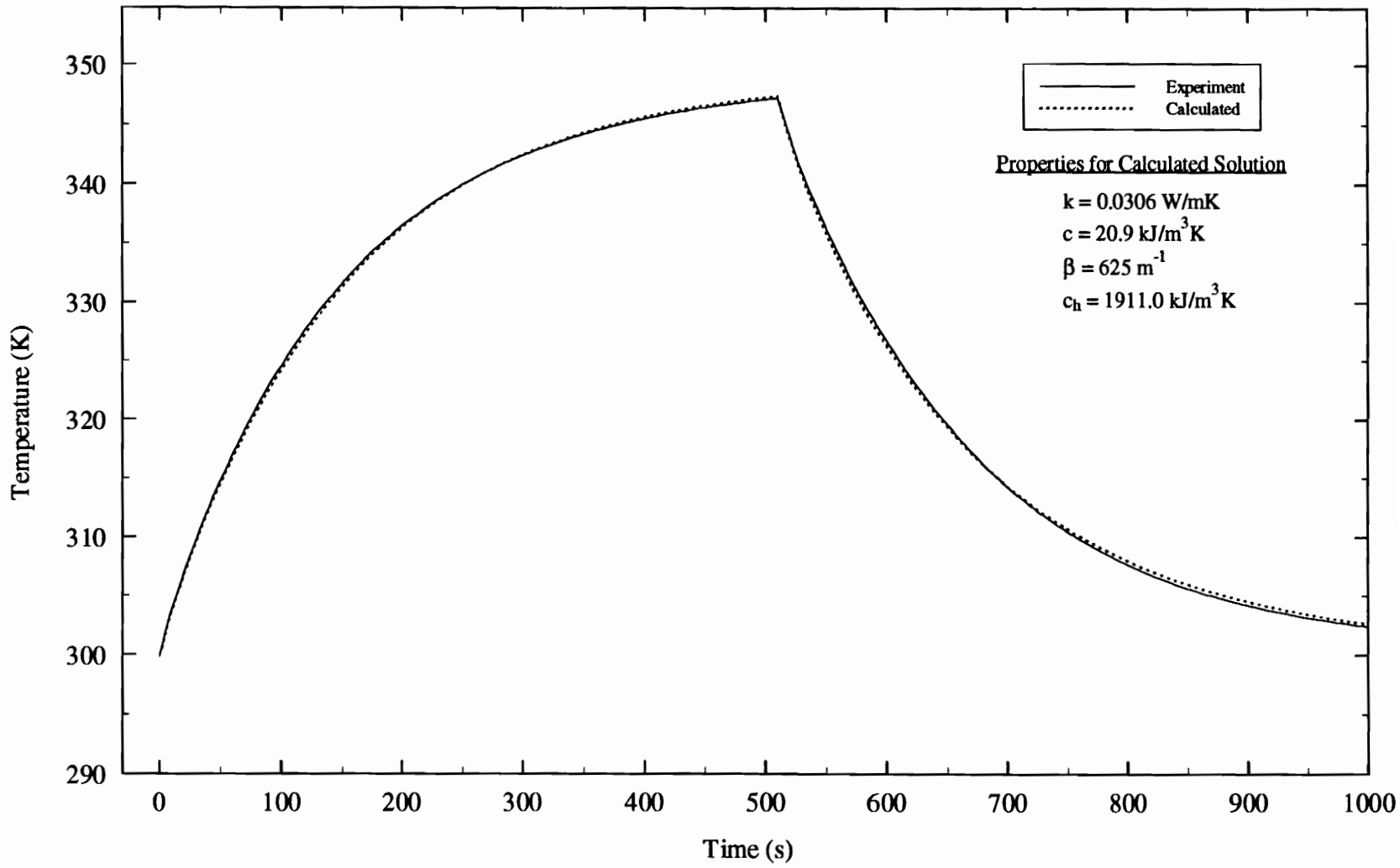

Figure 6.26 Comparison of Experimental Temperature at *x=0* to Temperature Calculated Using Diffusion Solution.

residuals are of importance as well.

The development of confidence intervals assumes zero mean, additive, normal errors in the measurements. One of the ways to check this is to plot the residuals, the difference between the measured and calculated values. If the errors meet the above criteria (are unbiased) and the estimates are close to the real properties, the residuals should be scattered zero in an approximate straight line with a root mean squared value close to the precision of the measurements. Residuals were plotted for two sets of parameters using the diffusion solution and one set of parameters using the absorbing and scattering solution, Figure 6.27. The residuals clearly show bias in the errors, as they all have a similar shape and are not linear about zero. Other residuals were plotted for different parameter sets and adjustments of some of the known parameters and all produced the same type of shape.

The residuals reveal why the RMS residual was never less than about 0.2°C, despite the measurement precision being within 0.08°C. It also contributes to non-convergence on a set of estimates. The residual shape most likely has to due with the heat capacity, since it increases at first, peaks and then decreases, and then starts to level off, until the heater is turned off, when it repeats the previous path. The total variation of the residuals is about 1.9% of the 50°C temperature rise, which is not large, but is significant. It is most probable that the heater is still not quite modeled correctly, which prevents the solution from matching the data any closer than is shown in Figure 6.27. Even if the parameters were uncorrelated, the model would have to be adjusted, or a more diffusive heater employed, to provide the most accurate estimates.

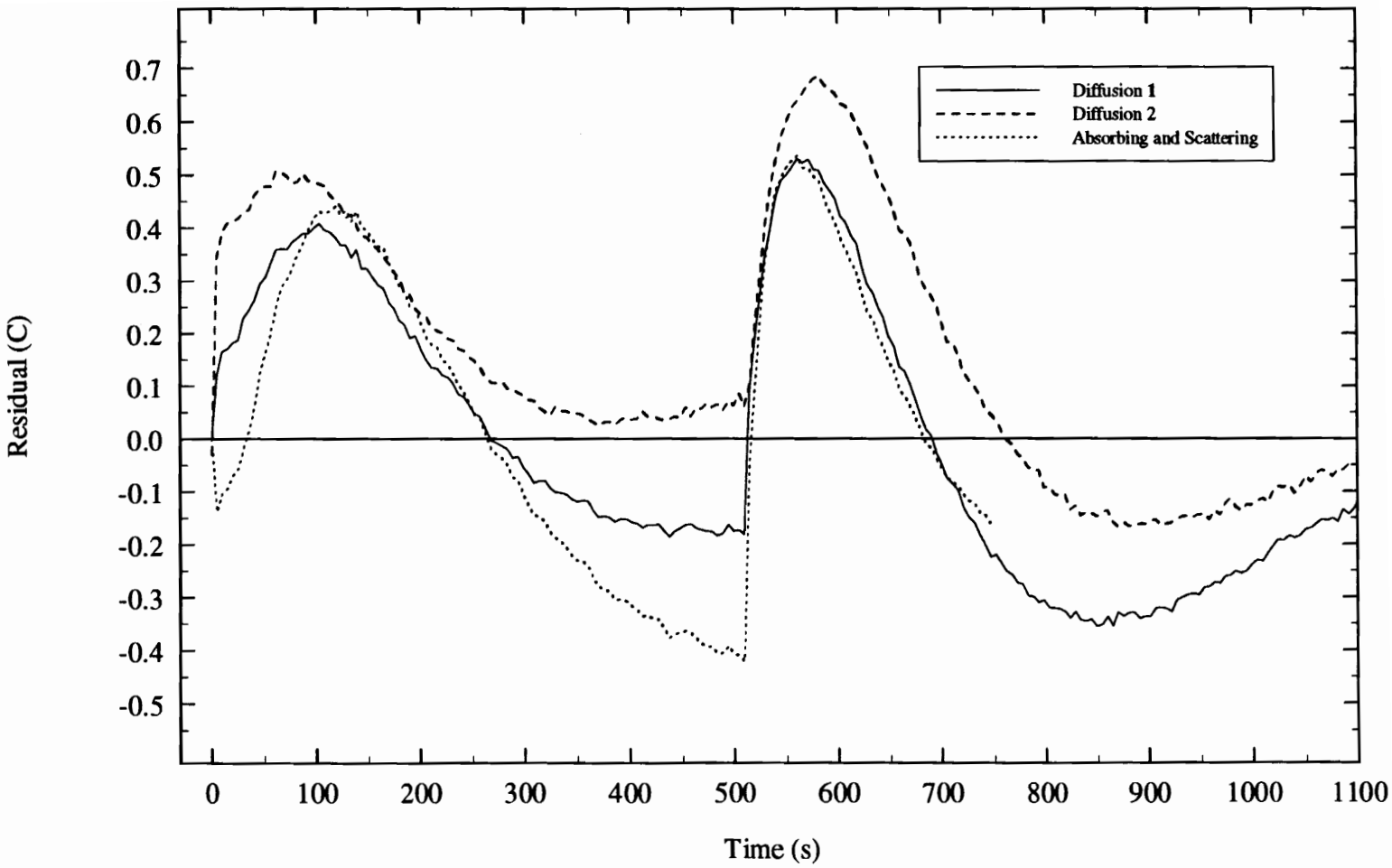

Figure 6.27 Residuals for 2 Diffusion and 1 Absorbing and Scattering Parameter Sets.

Chapter 7

Summary and Conclusions

Two solutions were developed for one-dimensional combined-mode conduction and radiation heat transfer in a gray, absorbing and isotropically scattering material. The approximate diffusion solution offers a great advantage in regards to computational time and is relatively accurate as an engineering approximation for optically thick materials; the absorbing and isotropically scattering solution may model the physics more accurately, but had the disadvantage of long CPU times for the solution.

Possible one-dimensional experimental setups for the determination of conductive and radiative properties were examined using the diffusion solution and a sensitivity analysis. Optimization of steady-state experiments was examined for the applied heat flux as the measured quantity. Transient diffusion optimization was conducted for a variety of boundary conditions and experimental parameters; a transient setup with heat flux and constant temperature boundaries was also examined using the absorbing and scattering solution.

The experimental setup successfully performed the function of collecting temperature data at the heated surface of a material for transient, one dimensional heat transfer involving conduction and radiation. The heater capacitance proved to be important due to the

insulating nature of the Styrofoam, and while it was unwanted, it was able to be modeled in the solution.

The Box-Kanemasu method failed to provide simultaneous estimates of all the properties, though it was used to gain an idea of property ranges by assuming a value for the extinction coefficient. The genetic algorithm was able to simultaneously estimate all properties for the problem, though the specific nature of the sum of squares function guided the estimation to the wrong ranges. Some adjustments of the genetic algorithm corrected this behavior and while the resulting estimates, especially the thermal conductivity and extinction coefficient, were not known with a great degree of certainty, a much better idea of the ranges was determined. Attempts to reduce the correlation between the thermal conductivity and extinction coefficient estimates were unsuccessful.

Four objectives were set forth in this study: to develop appropriate heat transfer models, to optimize experiments for estimation, to perform an experiment with Styrofoam, and to estimate the Styrofoam properties. The following are conclusions from this study concerning each objective.

7.1 Models and Assumptions

- The solutions were able to match the measured output of the experiment, though there was some bias in the solution due to incomplete modeling of the heater capacitance.

- The main contribution of scattering for optically thick materials is towards the attenuation of radiation, represented by the extinction coefficient. There does not appear to be much advantage in including isotropic scattering, as opposed to pure absorption, for this type of problem.

7.2 Experimental Setup

- The experimental setup and data acquisition system successfully gathered temperature data for a one-dimensional heat transfer experiment with a minimum of noise and error in the measurements.

- The proposed experimental setup resulted in correlation between the thermal conductivity and the extinction coefficient.

7.3 Experiment Optimization

- As would be expected, optimization revealed that the maximum achievable temperature is of prime importance in estimating conductive and radiative properties.

- Sensitivity analyses using the diffusion solution indicate that an experiment with an applied heat flux and constant temperature boundaries, with temperature measurements taken at the heated boundary, provides the best overall information for simultaneous thermal property estimation that includes basic radiation heat transfer.

- Investigation of sensitivity coefficients for the absorbing and scattering solution with the nominal Styrofoam parameters revealed that the absorption and scattering coefficients were strongly correlated, as well as those two parameters and the thermal conductivity.

- An experiment that is optimized to maximize the sensitivity coefficients is not necessarily the "best" experiment. The problem of correlation is a separate issue that should be examined.

7.4 Parameter Estimation

- The Box-Kanemasu does not perform well with most correlated parameters, has the disadvantages of having no constraints on the range of parameters, and requires a well defined sum of squares function. The genetic algorithm (GA) is a much more robust estimation method and can simultaneously

estimate five parameters, but can also be very time intensive computationally.

- For the determination of the initial parameter ranges, a large population should be used in the GA to avoid local minima.

- In the case of correlation and time intensive problems where very large populations are impractical, it is a good idea to divide the ranges of some of the parameters and perform the analysis for each smaller range.

- It may not be a good idea to update the parameter ranges for a small population. The larger the population, the less likely updating will prematurely narrow the parameter ranges.

- It can be stated decisively that radiation does contribute significantly to the heat transfer in the Styrofoam and the use of a constant thermal conductivity without radiation can be insufficient. While including isotropic scattering is more accurate, that accuracy may not be sufficient to enable the estimation of the scattering coefficient for the type of experiment considered here.

Chapter 8

Recommendations

This research provides many insights into the simultaneous estimation of combined-mode conduction and radiation properties in an insulative type material. Many suggestions can be made regarding the experiment, the estimation, and the use of the genetic algorithm.

8.1 Heat Transfer Models

The two heat transfer models considered adequately modeled the temperature, though the absorbing and scattering solution was more accurate. While the heat transfer models can be used for a variety of materials, there are a large group of materials, notably fibrous composites, that cannot accurately be described by these models due to anisotropic scattering. There is also the question of wavelength dependence for less gray materials. The following recommendations are made concerning the heat transfer models for estimation:

- Due to its simplicity and short computational time, the diffusion solution is recommended for any optically thick material, with the use of an adjusted mean scattering coefficient as mentioned in Caps et al. (1984) or Glicksman

et al. (1987) for anisotropically scattering media.

- Accounting for anisotropic scattering would be the single most important addition. The inclusion of scattering would be fairly straightforward by using a Legendere polynomial as was done by Thomas (1989) and by Neto and Özişik (1995) and solving the radiation equation using the P_N method. This would greatly increase the scope of the simultaneous thermal property estimation, though it would introduce many new parameters.

- A two-, or even three-dimensional model would allow much greater flexibility in designing an experiment and could help in reducing the correlation between the thermal conductivity and radiation estimates. This would be an especially simple matter for optically thick materials, as the effective thermal conductivity from the diffusion solution could be used in existing finite element languages, such as EAL.

- Reflective and refractive boundaries are commonly encountered, especially in layered materials, and would have to be modeled for accurate property determination. Simply including known reflectivities and indexes of refraction would not be difficult, but accurately estimating these properties may be problematic for the type of experiments considered here. Reasonable determination of these parameters would probably require spectral

measurements.

- The question of temperature and wavelength dependence is of significant concern, especially at higher temperatures. Unfortunately, such extensions would not only further complicate the solution, but would probably require detailed spectral analysis in order to accurately determine related radiative properties.

8.2 Experimental Setups

Though the experimental setup provided the temperature measurements necessary for this investigation, the following would improve the overall design:

- The most obvious improvement to the experimental setup would be a heater with a low capacitance and high thermal conductivity. An uninsulated heater such as the nichrome screen heater used by Tong et al. (1986) may be more appropriate. The thermal diffusivity of nichrome is 3.4×10^{-6} m^2/s, while the value for Kapton is 1.0×10^{-7} m^2/s. A low capacitance heater would allow a less complicated model and provide more information for the specific heat of the material.

- The ability to provide a lower constant temperature at one boundary and to start at a lower initial temperature would provide more information due to a larger temperature difference. This would be even more important for a material such as Styrofoam, which has a low maximum temperature.

8.3 Experiment Optimization

Analysis of the sensitivity coefficients and optimization based on sensitivity coefficients, whether through D-optimal criteria or genetic algorithms, provides adequate information for maximizing the experimental information and minimizing the confidence intervals of the estimates. The occurrence of correlation, however, is a common complication in simultaneous parameter estimation and is inherently an experimental optimization problem and not an estimation problem. Nevertheless, no methods or criteria exist for optimizing an experiment without correlation, other than basic parametric analyses. Simultaneous parameter estimation would greatly benefit from the development of a criterion for reducing the linear dependence of the sensitivity coefficients and incorporating this with a criterion based on maximizing the sensitivity coefficients, such as the D-optimal criterion, in a multi-objective optimization algorithm.

8.4 Parameter Estimation

The following are suggestions for the parameter estimation:

- Parameters should be checked carefully for correlation, with the best available nominal values, and, if possible, some idea of the sum of squares function for correlated parameters should be obtained, such as by graphing the function. Plotting the sum of squares can provide critical information on how the estimation algorithm will behave.

- The best alternative for estimating conductive and radiative properties might be to determine the extinction coefficient separately, as was done by Nicolau et al. (1994), using basic radiative with fairly simple spectrometer equipment. The resulting extinction coefficient could than be used to find the thermal conductivity and volumetric heat capacity using the heat flux experimental setup.

Several recommendations can be made regarding the specific estimation methods:

- The Box-Kanemasu method should be attempted for a time-intensive problem that does not present significant correlation between the parameters. By taking advantage of the sum of squares gradient, this method may be able to

narrow in on the optimum value very quickly.

- When the parameter ranges are not well known, it is a good practice to check the initial ranges for the genetic algorithm with a very large population and a fairly large parameter range. If two or more parameters in an estimation exhibit correlation, separate the parameter ranges into several smaller ranges. This can prevent overstepping the best parameter values can be faster than starting with a large population and a large number of generations.

- While the genetic algorithm will not fail to give estimates for correlated problems, the given estimates may not reflect the actual property values. If correlation is present, the results from any estimation algorithm must be carefully double checked.

Bibliography

Bard, Y., 1974, *Nonlinear Parameter Estimation*, Academic Press, New York.

Beck, J. V., 1969, "Determination of Optimum, Transient Experiments for Thermal Contact Conductance," *International Journal of Heat and Mass Transfer*, Vol. 12, pp. 621-633.

Beck, J. V. and K. J. Arnold, *Parameter Estimation in Engineering and Science*, John Wiley & Sons, New York, 1977.

Belegundu, A. D., D. V. Murthy, R.R. Salagame, and E. W. Constans, 1994, "Multi-Objective Optimization of Laminated Ceramic Composites Using Genetic Algorithms," *AIAA-94-4364-CP*, pp. 1015-1022.

Box, G. E. P. And H. Kanemasu, 1972, "Topics in Model Building, Part II, on Non-linear Least Squares," Technical Report No. 321, University of Wisconsin, Department of Statistics, Madison, Wisconsin.

Caps, R., A. Trunzer, D. Buttner, J Fricke, and H. Reiss, 1984, "Spectral Transmission and Reflection Properties of High Temperature Insulation Materials," *International Journal of Heat and Mass Transfer*, Vol. 27, No. 10, pp. 1865-1872.

Carroll, D. L., 1996, "Chemical Laser Modeling with Genetic Algorithms," *AIAA Journal*, Vol. 34, No. 2, pp. 338-346.

Copenhaver, D. C., 1996, *Thermal Characterization of Honeycomb Core Sandwich Structures*, M.S. Thesis, Department of Mechanical Engineering, Virginia Polytechnic Institute and State University, Blacksburg, VA.

Fadale, T. D., A. V. Nenarokomov, and A. F. Emery, 1995, "Uncertainties in Parameter Estimation: The Inverse Problem," *International Journal of Heat & Mass Transfer*, Vol. 38, No. 3, pp. 511-518.

Furuya, H. and R. T. Haftka, 1993, "Genetic Algorithms for Placing Actuators on Space Structures," *Proceedings of the Fifth International Conference on Genetic Algorithms*, Urbana, IL., pp. 536-542.

Garcia, S. and E.P. Scott, 1996, "Use of Genetic Algorithms in Optimal Experimental Designs," *Proceedings of the 2nd International Conference on Inverse Problems in Engineering: Theory and Practice*, Le Croisic, France.

Garcia, S., 1996, "Use of Genetic Algorithms in Experimental Design Optimization and Parameter Estimation," Proposal for Ph.D. Preliminary Examination, Department of Mechanical Engineering, Virginia Polytechnic Institute and State University, Blacksburg, VA.

Glicksman, L., M. Schuetz, and M. Sinofsky, 1987, "Radiation Heat Transfer in Foam Insulation," *International Journal of Heat & Mass Transfer*, Vol. 30, No. 1, pp. 187-197.

Goldberg, D.E., 1989, *Genetic Algorithms in Search, Optimization, and Machine Learning*, Addison-Wesley Publishing Co., Inc., Reading, MA.

Grossman, B., 1991, "Elementary Numerical Methods for Conduction Heat Transfer," Department of Aerospace & Ocean Engineering, Virginia Tech, Blacksburg, VA, version 1.01.

Hamaker, H. C., 1947, "Radiation and Heat Conduction in Light Scattering Materials," *Phillips Research Report*, Vol. 2, p. 55-67, 103-111.

Hanak, J. P., 1995, *Experimental Verification of Optimal Experimental Designs for the Estimation of Thermal Properties of Compositie Materials*, M.S. Thesis, Department of Mechanical Engineering, Virginia Polytechnic Institute and State University, Blacksburg, VA.

Hazzah, A. S. and J. V. Beck, 1970, "Unsteady Combined Conduction-Radiation Energy Transfer Using a Rigorous Differential Method," *International Journal of Heat and Mass Transfer*, Vol. 13, pp. 517-522.

Incropera, F. P. and D. P. DeWitt, *Fundamentals of Heat and Mass Transfer*, John Wiley, New York, 1990.

Larkin, B. K. and S. W. Churchill, 1959, "Heat Transfer by Radiation through Porous Insulations", *A.I.Ch.E. Journal*, Vol. 5, No. 4, pp. 467-474.

Lii, C. C. and M. N. Özişik, 1972, "Transient Radiation and Conduction in an Absorbing, Emitting, Scattering Slab with Reflective Boundaries," *International Journal of Heat and Mass Transfer*, Vol. 15, pp. 1175-1179.

Linford, R. M. F., R. J. Schmitt, and T. A. Hughes, 1974, "Radiative Contribution to the Thermal Conductivity of Fibrous Insulations," *Heat Transmission Measurements in Thermal Insulations*, ASTM STP 544, pp. 68-84.

Loh, M. H. And J. V. Beck, 1991, "Simultaneous Estimation of Two Thermal Conductivity Components from Transient Two-Dimensional Experiments," ASME Paper No. 91-WA/HT-11 ASME, NY.

Mann, D., R. E. Field, and R. Viskanta, 1992, "Determination of Specific Heat and True Thermal Conductivity of Glass from Dynamic Temperature Data," *Wärme-und Stoffübertragung* 27, pp. 225-231.

Moncman, D. A., 1994, *Optimal Experimental Designs for the Estimation of Thermal Properties of Composite Materials*, M.S. Thesis, Department of Mechanical Engineering, Virginia Polytechnic Institute and Syate University, Blacksburg, VA.

Nicolau, V. P., M. Raynaud, and J. F. Sacadura, 1994, "Spectral Radiative Properties Identification of Fiber Insulating Materials," *International Journal of Heat & Mass Transfer*, Vol. 37, Suppl. 1, pp. 311-324.

Özişik, M. N., *Radiative Transfer and Interaction with Conduction and Convection*, Wiley, New York, NY, 1973.

Press, W. H., et al., *Numerical Recipes in FORTRAN*, 2nd ed., Cambridge University Press, Cambridge, 1992.

Scheutz, M. A. and L. R. Glicksman, 1984, "A Basic Study of Heat Transfer Through Foam Insulation," *Jounal of Cellular Plastics*, March/April 1984, pp. 114-121.

Siegel, R. and J. R. Howell, *Thermal Radiation Heat Transfer*, 3rd ed., McGraw-Hill, New York, 1992.

Siegel, R., 1992, "Finite Difference Solution for Transient Cooling of a Radiating-Conducting Semitransparent Layer," *Journal of Thermophysics*, vol. 6, pp. 77-3

Siewert, C. E. and J. R. Thomas, Jr., 1991, "A Computational Method for Solving a Class of Coupled Conductive-Radiative Heat Transfer Problems," *Journal of Quant. Spectrosc. Radiat. Transfer*, Vol. 45, No. 5, pp. 273-281.

Silva, A. J. and M. N. Özişik, 1995, "An Inverse Problem of Simultaneous Estimation of Radiation Phase Function, Albedo, and Optical Thickness," *Journal of Quant. Spectrosc. Radiat. Transfer*, Vol. 4, No. 4, pp. 397-409.

Skochdopole, Richard. E., 1961, "The Thermal Conductivity of Foamed Plastics," *Chemical Engineering Progress*, Vol. 57, No. 10, pp. 55-59.

Taktak, R., E. P. Scott, and J. V. Beck, 1991, "Optimal Experimental Designs for Estimating the Thermal Properties of Composite Materials," Proceedings of the 3rd ASME/JSME Thermal Engineering Joint Conference, ASME, Vol. 3, pp. 481-488.

Thomas, J. R., Jr., 1989, "Modelling of Transient Tests to Determine Thermal Properties of Fiberglass Insulations," *Thermal Conductivity 20*, D. H. Hasselman and J. R. Thomas, Jr., eds., pp. 13-19.

Tong, T.W., D. L. McElroy, and D. W. Yarbrough, 1986, "Analysis of Transient Heat Transfer Measurements on Porous Thermal Insulations," *Proceedings of The Eigth International Heat Transfer Conference*, Vol. 2, pp. 703-708.

Tsai, C-F. and G. Nixon, 1986, "Transient Temperature Distribution of a Multilayer Composite Wall with Effects of Internal Thermal Radiation and Conduction," *Numerical Heat Transfer*, Vol. 10 , pp 95-101.

Valenzuela, J. A. and L. R. Glicksman, 1981, "Thermal Resistance and Aging of Rigid Urethane Foam Insulation," *Proceedings of the DOE-ORNL Workshop on Mathematical Modeling of Roofs*, Conf-811179, pp. 261-262.

Viskanta, R. and R. J. Grosh, 1962, "Heat Transfer by Simultaneous Conduction and Radiation in an Absorbing Medium," *Journal of Heat Transfer*, vol. 84, no. 1, pp. 63-72.

Viskanta, R., 1965, "Heat Transfer by Conduction and Radiation in Absorbing and Scattering Materials," *Journal of Heat Transfer*, vol. 87, no. 1, pp. 143-150.

Appendix A

FORTRAN Diffusion Model Program: HCVK.FOR

```
c HCVK.FOR: Heat Conduction Variable K (Diffusion Solution)
c           - includes heater
c           - inputs experimental data: time, t(D), heat flux
c Actual temperature solution is in a SUBROUTINE format.
c Returns dimensionAL temperature (Kelvin)
c
c Input:  HCVK2.IN, contains solution parameters, based on RC.IN
c         Experimental input file: same format as for MBK.FOR
c Output: HCVK2.OUT
c
c 1 refers to heater (k1, c1, xmax1, etc.)
c 2 (or no #) refers to the material (k2, c2, xmax2, etc.)
c

      DOUBLE PRECISION k1,k2,c1,c2,beta,tbegin,tend,dp,dt,tdimen
      DOUBLE PRECISION tprnt,temp1,temp2,tempi,tempr,htflux,qend
      DOUBLE PRECISION thick1,thick2,ext,toler
      DOUBLE PRECISION time(3001),t(3001),tbc(3001),qa(3001)
      INTEGER i,pmax,n1,n2,outfmt,maxl
      CHARACTER ifile*12
      COMMON/hccon/n1,n2,tempi,temp2,tempr,htflux,qend,thick2,toler,
     1       outfmt,k2,c2,beta,k1,c1,thick1

* Read in solution parameter data from input file
      OPEN(UNIT=11,FILE='hcvk2.in',STATUS='OLD')
      READ(11,5) n1,n2,outfmt,maxl,toler
    5 FORMAT(4(/,9X,I4),/,9X,G12.6)
      READ(11,15)tbegin,tend,dt,tprnt,temp1,temp2,tempi,tempr,
     1           htflux,qend,thick2,beta,k2,c2,thick1,k1,c1
   15 FORMAT(17(/,9X,G12.6))
      CLOSE(11)

* Get name of experimental file and read in time, t(D), and heat
* flux.Determine number of time steps, pmax.
      WRITE(*,*) 'Enter experimental file: '
      READ(*,'(A12)') ifile

      OPEN(UNIT=12,FILE=ifile,STATUS='OLD')
      DO 10 i = 1,3001
        READ(12,25,END=30) time(i), tbc(i), qa(i)
   10 CONTINUE
```

```
   25 FORMAT(1X,F7.2,8X,1X,F7.2,1X,F8.3)
   30 pmax = i-1

* Open output file
      OPEN(UNIT=11,FILE='hcvk2.out',STATUS='UNKNOWN')

* k = k + cT^3, where c=beta
      beta = (16.d0*5.67d-08)/(3.d0*beta)

* Temperature solution subroutine
      CALL hc(time,t,pmax,tbc,qa)

* Write output to output file
      DO 20 i = 1,pmax
        WRITE(11,'(1X,F7.2,1X,F7.2)') time(i),t(i)
   20 CONTINUE
      CLOSE(11)

      STOP
      END



      SUBROUTINE hc(time,thc,pmax,tbc,qa)

      DOUBLE PRECISION ti,t1,t2,toler,rho1,cp1,dx1,tbc(3001)
      DOUBLE PRECISION xmax,dx2,dt,k1,k2,beta,vhc1,vhc2,dtprnt
      DOUBLE PRECISION t(101),tnew(101),a(101),b(101),c(101),d(101)
      DOUBLE PRECISION told(101),tsum,fop,fom,q0,tref,xmax1,xmax2
      DOUBLE PRECISION xpos,time(3001),thc(3001),qend,htflux
      DOUBLE PRECISION qa(3001),xdim,kt,t1(6),told1(6),tnew1(6)
      INTEGER n,n1,n2,nmax,p,pmax,outfmt
      COMMON dx2,dt
      COMMON/hccon/n1,nmax,ti,t2,tref,htflux,qend,xmax2,toler,
     1       outfmt,k2,vhc2,beta,k1,vhc1,xmax1
      DATA fop,fom/0.d0,0.d0/

      dx1 = xmax1/DBLE(n1-1)
      dx2 = xmax2/DBLE(n2-1)

* Provide initial temperatue solution for both heater and material
* temperature arrays.
      DO 10 n=1,n1
        t1(n) = ti
        tnew1(n) = ti
        told1(n) = ti
   10 CONTINUE
      DO 11 n=1,nmax
        t(n) = ti
        tnew(n) = ti
        told(n) = ti
   11 CONTINUE

* Output initial temperature.
      thc(1) = tnew(outfmt)

* Start time loop.
```

```
      DO 20 p=2,pmax

* Define time increment for each time step, as experimental times
* are not consistent.
        dt = time(p) - time(p-1)
        q0 = qa(p)

        DO 80 n=1,n1
          t1(n) = tnew1(n)
   80   CONTINUE
        DO 81 n=1,nmax
          t(n) = tnew(n)
   81   CONTINUE

* Return point for each iteration; fix temperatures at x=D.
   50   DO 30 n = 1,n1
          told1(n) = tnew1(n)
   30   CONTINUE
        DO 31 n = 1,nmax
          told(n) = tnew(n)
   31   CONTINUE
        tnew(nmax) = tbc(p)
        told(nmax) = tnew(nmax)

* Define matrix elements for heater; implement heat flux at
* heater surface.
        c1 = vhc1*dx1**2/(k1*dt)
        DO 41 n=2,n1-1
          a(n) = -1.d0
          b(n) = 2.d0 + c1
          c(n) = -1.d0
          d(n) = c1*t1(n)
   41   CONTINUE
        b(2) = b(2) + a(2)
        d(2) = d(2) - a(2)*q0*dx1/k1

* Define matrix elements for interface.
        c1 = (dx1*vhc1 + dx2*vhc2)/(2.d0*dt)
        a(n1) = -k1/dx1
        b(n1) = k1/dx1 + kt(tnew1(n1),k2,beta)/dx2 + c1
        c(n1) = -kt(tnew1(n1),k2,beta)/dx2
        d(n1) = c1*t(n1)

* NOTE: t1(n1) = tnew(1)

* Define matrix for material.  CALCFO calculated Fourier number
* for variable k (thermal conductivity).
        im = 0
        DO 40 n=1,nmax-2
          nm = im + 1
          CALL calcfo(tnew(n-1),tnew(n),tnew(n+1),
     1                fom,fop,k2,beta,vhc2)
          a(nm) = -fom
          b(nm) = (1.d00 + fom + fop)
          c(nm) = -fop
          d(nm) = t(n)
   40   CONTINUE
```

```
         nm = nm + 1
         CALL calcfo(tnew(nmax-2),tnew(nmax-1),tnew(nmax),
     2         fom,fop,k2,beta,vhc2)
         a(nm1) = -fom
         b(nm) = (1.d0 + fom + fop)
         c(nm) = 0.d0
         d(nm) = t(nmax-1) + fop*t(nmax)

*  Solve matrix using Thomas' algorithm; find t(0) based on heat
*  flux
         CALL tridag(2,n1+nmax-2,107,a,b,c,d,tsolve)
         tsolve(1) = tsolve(2) + q0*dx1/k1

*  Split TSOLVE into the two temperature matrices/arrays
         DO 45 n=1,n1
           tnew1(n) = tsolve(n)
      45 CONTINUE
         nm = 0
         DO 46 n=n1+1,n1+nmax-1
           nm = nm + 1
           tnew(nm) = tsolve(n)
      46 CONTINUE

*  Determine if solution needs to be iterated
         tsum = ABS(tnew(1) - told(1))/told(1)
         IF (tsum .GT. toler) GOTO 50

*  Output temperature
         thc(p) = tnew(outfmt)

    20 CONTINUE

       RETURN
       END



*  Implements Thomas' Algorithm for solving a tri-diagonal matrix
       SUBROUTINE tridag(if,l,is,a,b,c,d,v)
       IMPLICIT DOUBLE PRECISION(a-h,o-z)
       DIMENSION a(is),b(is),c(is),d(is),v(is),beta(2000)
       DIMENSION gamma(2000)
       beta(if) = b(if)
       gamma(if) = d(if)/beta(if)
       ifp1 = if+1

       DO 10 i=ifp1,l
         beta(i)=b(i)-a(i)*c(i-1)/beta(i-1)
         gamma(i)=(d(i)-a(i)*gamma(i-1))/beta(i)
    10 CONTINUE

       v(l)=gamma(l)
       last=l-if
       DO 20 k=1,last
         i=l-k
         v(i)=gamma(i)-c(i)*v(i+1)/beta(i)
    20 CONTINUE
```

```
      RETURN
      END


* Calculates a Fourier number
      SUBROUTINE calcfo(tm,t,tp,fom,fop,k,beta,vhc)
        DOUBLE PRECISION tm,t,tp,fop,fom,dx,dt,t2,k2,cp2,k,vhc
        DOUBLE PRECISION kt,beta
        COMMON dx,dt

          t2 = (t + tp)/2.d0
          k2 = kt(t2,k,beta)
          cp2 = vhc
          fop = (k2*dt)/(cp2*dx**2)
          t2 = (tm + t)/2.d0
          k2 = kt(t2,k,beta)
          cp2 = vhc
          fom = (k2*dt)/(cp2*dx**2)

      RETURN
      END


* Calculates the effective thermal conductivity
      FUNCTION kt(t,k,beta)
        DOUBLE PRECISION kt,t,k,beta,vhc,dx,dt
        COMMON dx,dt

        kt = k + beta*t**3

      RETURN
      END
```

The following is a sample input file, HCVK2.IN

```
* Read in program parameters 1st (Integers I4, Reals G12.6)
n1      = 6             Number of nodes; dX = 1./REAL(m-1)
n2      = 51            Number of integration points
outfmt  = 1             Output format; must be a value between [0,m]
maxl    = 15            Maximum iterations for non-linearity
toler   = 1.0D-04       (Tnew - Told)/Told < toler
* Read in problem parameters 2nd
mint    = 0.d0          If not 0., requires an input temp. dist.(hcvktd.in)
maxt    = 1300.0d0      Maximum time (s)
dt      = 0.5d0         Time step (s)
tprnt   = 0.5d0         Time step to print output for outfmt = 0 (s)
temp1   = 0.0d0         Temperature on left side (K)
temp2   = 299.9d0       Temperature on right side (K)
tempi   = 299.9d0       Initial temperature (K)
tempr   = 350.0d0       Reference temperature used in t = T/Tr
htflux  = 126.9d0       Heat Flux applied on left side (W/m^2)
qend    = 510.42d0      Time to stop heat flux (s)
thick   = 0.01815d0     Thickness of material, D (m)
absorb  = 300.d0        Absorption coefficient, a (1/m)
scat    = 166.8d0       Scattering coefficient, sigma sub s (1/m)
cond    = 0.026872d0    Thermal conductivity, k (W/mK)
vhtcap  = 23548.d0      Volumetric Heat Capacity, rho*cp (J/Km^3)
h_thic  = 15.2D-05      Thickness of Heater (m)
h_k     = 0.16d0        Thermal Conductivity of heater (W/mK)
h_vhc   = 1824700.d0    Volumetric Heat Capacity of Heater (J/Km^3)
```

Appendix B

FORTRAN Conduction and Radiation Program: RCB.FOR

```
C RCB.FOR: RCB (includes emissivity as a parameter) in subroutine
C          format.
C ** Note: RCB returns dimensionAL temperature **
C
c Jerome H. Guynn
c 100V Randolph Hall, Mechanical Engineering Dept.
c Virginia Tech, Blacksburg, VA 24061
c
c Solution of the 1-D, transient, combined conduction and radiation heat
c transfer in a gray absorbing-emitting and isotropically scattering
c medium between black, diffuse walls.  The is basically the problem in
c section 16-4.2 in Siegal and Howell, eqs. 16:16-18, with the addition
c of the time change term (Eq. 16-8).  A finite-difference aglorithm is
c used for the x-gradient & time and the radiation source equation, an
c inhomogeneous Freedholm equation of the 2nd kind, is solved using the
c Nystrom method, with modification due to the singularity in E(1,0). An
c iterative process is required since the temperature and radiation
c equations are coupled.  The iterative process may require an
c under-relaxation factor in certain situations.

c N.R.: Numerical Recipes in FORTRAN, 2nd ed. Press, William H., et. al.
c       Cambridge University Press, Cambridge, 1992.

c SUBROUTINES:
c   fred2   Solves Freedholm eq. of the 2nd kind; from N.R.
c           w/modifications
c   spline  Computes y' for cubic spline interpolation; from N.R.
c   gauleg  Guass-Legendre quadrature rule; from N.R.
c   ludcmp  LU decomposition; from N.R.
c   lubksb  LU back-substitution; from N.R.
c   tridag  Thomas algorithm for solving tri-diagonal matrices
c FUNCTIONS
c   splint  Cubic spline interpolation; from N.R.
c   e       Computes exponential integral functions; from N.R.
c   ak      Function used by fred2; computes Kernel
c   g       Function used by fred2; computes non-homogeneous term

      DOUBLE PRECISION tbase(3001),tsub(3001),sc(5,3001),p(5),p2(5),time
      DOUBLE PRECISION tmin,tmax,tprnt,temp1,temp2,tempi,htflux,qend
      DOUBLE PRECISION scat,cond,vhtcap,emis,toler,dt,thick,absorb
```

```
      INTEGER i,j,k,kmax,mm,nn,maxl,outfmt
      COMMON/RCCON/mm,nn,outfmt,maxl,toler,z,tmin,tmax,dt,tprnt,
     1          temp2,tempi,tempr,htflux,qend,thick

      WRITE(*,*) ' RCB running...'

c All the parameters are contained in an input file, RC.IN; this allows
c parameters to be changed without recompiling.  The input file contains
c descriptions of the parameters.

      OPEN(UNIT=11,FILE='rc.in',STATUS='OLD')
      READ(11,5) mm,nn,outfmt,maxl,toler,z
    5 FORMAT(4(/,9X,I4),2(/,9X,G12.6))
      READ(11,15) tmin,tmax,dt,tprnt,temp1,temp2,tempi,tempr,htflux,
     1    qend,thick,p(3),p(4),p(1),p(2),p(5)
   15 FORMAT(16(/,9X,G12.6))
      CLOSE(11)

* P(2) is the volumetric heat capacity, which is in terms of kJ
      p(2) = 1000.d0*p(2)
      kmax = INT((tmax-tmin)/dt) + 1

      CALL rcb(p(1),p(2),p(3),p(4),p(5),tbase)

      OPEN(UNIT=12,FILE='rc.out',STATUS='UNKNOWN')
      DO 40 k=1,kmax
        time = DBLE(k-1)*dt
        WRITE(12,25) time,tbase(k)
   40 CONTINUE
   25 FORMAT(1X,F7.2,1(1X,E12.6))
      CLOSE(12)
      WRITE(*,*) ' DONE'

      STOP
      END



      SUBROUTINE rcb(cond,vhtcap,absorb,scat,emisp,tsub)

      DOUBLE PRECISION t(101),tnew(101),a(101),b(101),c(101),d(101)
      DOUBLE PRECISION isol(101),w(101),xgq(101),y2(101),told(101)
      DOUBLE PRECISION ti,t1,t2,Nr,kd,dx,toler,yp1,ypn,omega,dt,time,x
      DOUBLE PRECISION integ,qr0,qflux,qterm,alpha,tmin,tmax,tprnt,temp1
      DOUBLE PRECISION tempi,htflux,qend,thick,absorb,scat,cond,vhtcap
      DOUBLE PRECISION irad(101),tsub(3001),temp2,emis,emisp,splint,e
      INTEGER i,m,mm,n,nn,l,maxl,outfmt,p
      EXTERNAL g,ak
      COMMON/RCCON/mm,nn,outfmt,maxl,toler,z,tmin,tmax,dt,tprnt,
     1          temp2,tempi,tempr,htflux,qend,thick
      COMMON kd,dx,omega,t1,t2,Nr,m,n,told,emis


c Non-dimensional variables are calculated from the input parameters;
c these variables are explained in the notes.  SB is the Stefan-Boltzman
c constant.  Note that T1 is not used in this program; I have kept it
c from the constant temperature boundaries case for archival purposes.
```

```
c Also note that dx = x/D, a non-dimensional quantity.
      m = mm
      n = nn
      emis = emisp
      sb = 5.67d-08
      t2 = temp2/tempr
      t1 = temp1/tempr
      ti = tempi/tempr
      qflux = htflux/(sb*tempr**4)
      omega = scat/(scat + absorb)
      Nr = cond/(4.d0*sb*absorb*thick**2*tempr**3)
      kd = (absorb + scat)*thick
      tau = vhtcap/(4.d0*absorb*sb*tempr**3)
      alpha = 4.d0*Nr*(1-omega)*kd
      dx = 1./DBLE(m-1)

c YP1 & YPN are used by the SPLINE subroutine.
      yp1 = 1.0d30
      ypn = 1.0d30

c The output file, RC.OUT, is opened.  Several of the dimensionaless
c variables are output for analysis
*      OPEN(UNIT=11,FILE='rcb.out',STATUS='UNKNOWN')
*      WRITE(11,25) t2,ti,dx,qflux,tau,omega,Nr,kd
*   25 FORMAT(1X,'t2 = ',F6.4, ' ti = ',F6.4,' dx = ',F7.5,' qflux = ',
*     2       F8.5,' tau = ',F7.4,/,1X,'Omega = ',F5.3,' Nr = ',F9.4,
*     3       ' kd = ',F7.3,/)

c OUTFMT determines the type of output.  If 0, the output is the temp.
c at every x point in the medium at the time intervals determined by
c TPRNT.  If not 0, OUTFMT should be a value between 1 and m; the output
c is the temperature at x(OUTFMT) at every computed time step.  If
OUTFMT
c is not in the range [0,m], it is set to 1 (temperature at x = 0).
c In either case, the temperature distribution across the layer for the
c final time is output so it can be used to start another solution.
     IF (outfmt .NE. 0) THEN
       WRITE(*,35) outfmt
       outfmt = 1
     ELSE
       x = DBLE(outfmt-1)*dx
       WRITE(11,45) x
     ENDIF
   35 FORMAT(/,1X,'Invalid outfmt: ',I4,'; outfmt set to 1')
   45 FORMAT(1X,'Temperature output is at x = ',F7.3,/)

c TMIN is the start time; if it is non-zero, than the program will read
c in a temperature distribution from RCTD.IN for time = TMIN.  This
c input distribution must have the same x-points (m) as the the current
c run.
c If TMIN is 0, all values of T(i) are initialized to TI.
     IF (tmin .NE. 0.) THEN
       OPEN(UNIT=11,FILE='rctd.in',STATUS='OLD')
       DO 10 i=1,m
         READ(11,55) t(i)
   10  CONTINUE
   55  FORMAT(12X,F8.5)
```

```
         CLOSE(11)
      ELSE
         DO 20 i=1,m
           t(i) = ti
   20    CONTINUE
      ENDIF

c The following loop serves 2 purposes; 1) output the initial
temperature
c distribution and 2) initialize all arrays
      DO 30 i=1,m
         x = DBLE(i-1)*dx
         told(i) = t(i)
         tnew(i) = t(i)
         irad(i) = 0.d0
   30 CONTINUE
   65 FORMAT(/,2X,'Time is: ',F6.2)
   75 FORMAT(3X,F6.4,3X,F7.5)

c This is the start of the time loop; since the temperature distribution
c at TMIN is known, the 1st solution to find is at TMIN+DT.
      p = 1
      tsub(p) = t(outfmt)*tempr
      DO 200 time=(tmin+dt),tmax,dt

c Check to see if heat flux is still applied; reset the iteration
counter,
c L, to 1, and write the current TIME to the screen. The TIME is output
c to the screen to give the user and idea how the program is
progressing.
       IF (time .EQ. qend) qflux = 0.d0
       l = 1
       p = p + 1
       WRITE(*,*) 'time: ',time

c This is the returning point for a new iteration
  100   CONTINUE

c FRED2 solves the dimensionaless radiation source function; solution is
c in ISOL for the points in XQG
c NOTE: In the original FRED2 subroutine, N was the 1st parametr passed;
c   however, N is in the COMMON statement, so it is not necessary to
c   include it in the parameter list.
     CALL fred2(0.d0,1.d0,xgq,isol,w,g,ak)

c SPLINE finds y', for the radiation source, stored in Y2, for use in a
c cubic spline interpolation
     CALL spline(xgq,isol,n,yp1,ypn,y2)

c The radiation source function is found at the mesh points using cubic
c spline interpolation of ISOL at XGQ.
       DO 50 i=1,m
         x = DBLE(i-1)*dx
         irad(i) = splint(xgq,isol,y2,n,x)
   50 CONTINUE

c The Finite Difference matrix is setup; C1 and C2 are groupings of
```

```
c parameters.  T(m) is maintained at t2.  Note the T(i) in D is the
c temperature at i for the previous time step, while TOLD(i) in D
c is the temperature at i for the previous iteration: TOLD(i) changes
c for each iteration, T(i) DOES NOT (it changes for each time step).
      c1 = tau*dx**2/(Nr*dt)
      c2 = dx**2/(Nr*omega)
      qterm = dx*(qflux)/alpha
      t(m) = t2
      tnew(m) = t2

       DO 60 i = 2,m-1
         a(i) = -1.d0
         b(i) = 2.d0 + c1
         c(i) = -1.d0
         d(i) = c1*t(i) + c2*(irad(i) - told(i)**4)
   60 CONTINUE

      b(2) = b(2) + 4.d0/3.d0*a(2)
      c(2) = c(2) - a(2)/3.d0
      d(2) = d(2) - a(2)*2.d0/3.d0*qterm
      d(m-1) = d(m-1) - c(m-1)*t(m)

c The resulting matrix is tri-diagonal and is solved using the Thomas
c algorithm. A 2nd order one-sided difference is utilized at the heat
c flux boundary; this results in T(i) {TNEW(i)} being computed after the
c matrix is solved.
       CALL tridag(2,m-1,101,a,b,c,d,tnew)
       tnew(1) = 4.d0/3.d0*tnew(2) - tnew(3)/3.d0 + 2.d0/3.d0*qterm

c The convergence criteria is checked at the boundary, T(1), since this
c is where the temperature is changing the most; it was found that this
c gave identical results to satisfying the criteria for every T.  If the
c convergence criteria is not met, the temperature is updated using the
c new temperataures and the solution is recomputed.  The temperatue is
c updated using an under-relaxation factor, Z.  The more radiation
c contributes to the heat transfer, the lower the Z factor.  The exact
c value is a matter of trial and error.
       ctoler = ABS((tnew(1) - told(1))/told(1))
       IF ((ctoler .LT. toler .AND. l .GT. 2) .OR. l .GT. maxl) GOTO 70
        DO 80 i=1,m
          told(i) = told(i) + z*(tnew(i)-told(i))
   80  CONTINUE
*      WRITE(*,*) l,ctoler
       l = l + 1
       GOTO 100

c TNEW is the final temperature distribution for this time step; the
c solution is stored in T for use in the next time step.
   70   DO 90 i=1,m
           t(i) = tnew(i)
   90   CONTINUE

        tsub(p) = tnew(outfmt)*tempr
        IF (tsub(p) .GT. 350. .AND. tsub(p) .LT. 350.5) THEN
          write(*,*) time, tsub(p)
        ENDIF
```

```
  200 CONTINUE

      RETURN
      END


c FRED2 came from N.R., but has been modified to subtract off the
c singularity at E(1,0).
      SUBROUTINE fred2(a,b,t,f,w,g,ak)
     INTEGER n,NMAX
     DOUBLE PRECISION a,b,f(n),t(n),w(n),g,ak,kd,dx,omega,t1,t2,Nr
     DOUBLE PRECISION tp1,tpn,told(101),e,splint,temp
     PARAMETER (NMAX=200)

     INTEGER i,j,indx(NMAX)
     DOUBLE PRECISION d,omk(NMAX,NMAX),tp2(NMAX),tx(NMAX),emis
     COMMON kd,dx,omega,t1,t2,Nr,m,n,told,emis

     IF (n .GT. NMAX) PAUSE 'Increase NMAX in fred2'
     CALL gauleg(a,b,t,w,n)

c YP1 & YPN are used by the SPLINE subroutine.
c SPLINE finds y', for the radiation source, stored in Y2, for use in a
c cubic spline interpolation
      DO 30 i=1,m
        tx(i) = DBLE(i-1)*dx
   30 CONTINUE
      tp1 = 1.0d30
      tpn = 1.0d30
      CALL spline(tx,told,m,tp1,tpn,tp2)

       DO 10 i=1,n
         omkii = 0.d0
         DO 20 j=1,n
           IF (i .NE. j) THEN
             omk(i,j) = -w(j)*ak(t(i),t(j))
             omkii = omkii - omk(i,j)
           ENDIF
   20    CONTINUE
         rr = 2.d0*(1.d0-emis)*E(2,kd*t(i))*( E(3,0.d0)-E(3,kd) )
         r = omega/2.d0*(rr - E(2,kd*(b-t(i))) - E(2,kd*(t(i)-a)) +
     1         2.d0*E(2,0.d0))
         omk(i,i) = 1.d0 + omkii - r

         temp = splint(tx,told,tp2,m,t(i))

         f(i) = g(t(i),temp)
   10 CONTINUE

      CALL ludcmp(omk,n,NMAX,indx,d)
      CALL lubksb(omk,n,NMAX,indx,f)

      RETURN
      END


      FUNCTION ak(x,u)
```

```
      DOUBLE PRECISION ak,x,u,kd,dx,omega,t1,t2,Nr,told(101),e
      DOUBLE PRECISION lambda,emis
      INTEGER m,n
      COMMON kd,dx,omega,t1,t2,Nr,m,n,told,emis

      lambda = kd*omega/2.d0
      ak = lambda*( 2.d0*(1.d0-emis)*E(2,kd*x)*E(2,kd*u) +
     1       E(1,kd*ABS(u-x)) )

      RETURN
      END


      FUNCTION g(x,tx)
        DOUBLE PRECISION g,x,kd,dx,omega,t1,t2,Nr,told(101),tx,emis,e
        INTEGER m,n,j
        COMMON kd,dx,omega,t1,t2,Nr,m,n,told,emis

        g = (1.d0-omega)*tx**4 + omega/2.d0*( emis*told(1)**4*E(2,kd*x)
     1       + told(m)**4*( 2.d0*(1.d0-emis)*E(2,kd*x)*E(3,kd)
     2       + E(2,kd*(1.d0-x)) ) )

      RETURN
      END


c The following FUNCTION evaluates the Exponential Integral Functions
c using series represenations and a convergence criteria (EPS).
      FUNCTION E(n,x)
      INTEGER n,MAXIT
      DOUBLE PRECISION E,x,EPS,FPMIN,EULER
      PARAMETER (MAXIT=100,EPS=1.d-7,FPMIN=1.d-30,EULER=.5772156649)
      INTEGER i,ii,nm1
      DOUBLE PRECISION a,b,c,d,del,fact,h,psi

      nm1 = n - 1
      IF (n .LT. 0 .OR. x .LT. 0.d0 .OR. (x .EQ. 0.d0 .AND.
     1      n .EQ. 0 )) THEN
        PAUSE 'bad arguments in En(x)'
      ELSEIF (x .EQ. 0.d0 .AND. n .EQ. 1) THEN
        E = 1.d0
        WRITE(*,*) 'E(1,0) called; results invalid'
      ELSEIF (n .EQ. 0) THEN
        E = EXP(-x)/x
      ELSEIF (x .EQ. 0.d0) THEN
        E = 1.d0/nm1
      ELSEIF (x .GT. 1.d0) THEN
        b = x+n
        c = 1.d0/FPMIN
        d = 1.d0/b
        h = d
        DO 10 i=1,MAXIT
          a = -1*(nm1+i)
          b = b + 2.d0
          d = 1.d0/(a*d+b)
          c = b+a/c
          del = c*d
```

```
      h = h*del
      IF (ABS(del-1.d0) .LT. EPS) THEN
        E = h*EXP(-x)
        RETURN
      ENDIF
10     CONTINUE
    PAUSE 'continued fraction failed in En(x)'
  ELSE
    IF (nm1 .NE. 0) THEN
      E = 1.d0/nm1
    ELSE
      E = -LOG(x)-EULER
    ENDIF
    fact = 1.d0
    DO 20 i=1,MAXIT
      fact = -fact*x/DBLE(i)
      IF (i .NE. nm1) THEN
        del = -fact/DBLE(i-nm1)
      ELSE
        psi = -EULER
        DO 30 ii=1,nm1
   psi = psi + 1.d0/ii
30          CONTINUE
        del = fact*(-LOG(x) + psi)
      ENDIF
      E = E + del
      IF (ABS(del) .LT. abs(E)*EPS) RETURN
20     CONTINUE
    PAUSE 'series failed in En(x)'
  ENDIF

    RETURN
    END


  SUBROUTINE tridag(if,l,is,a,b,c,d,v)
  IMPLICIT DOUBLE PRECISION(a-h,o-z)
  DIMENSION a(is),b(is),c(is),d(is),v(is),beta(2000),gamma(2000)
  beta(if) = b(if)
  gamma(if) = d(if)/beta(if)
  ifp1 = if+1

  DO 10 i=ifp1,l
    beta(i)=b(i)-a(i)*c(i-1)/beta(i-1)
    gamma(i)=(d(i)-a(i)*gamma(i-1))/beta(i)
10    CONTINUE

  v(l)=gamma(l)
  last=l-if
  DO 20 k=1,last
    i=l-k
    v(i)=gamma(i)-c(i)*v(i+1)/beta(i)
20    CONTINUE

    RETURN
    END
```

```
      SUBROUTINE ludcmp(a,n,np,indx,d)
      INTEGER n,np,indx(n),NMAX
      DOUBLE PRECISION d,a(np,np),TINY
      PARAMETER (NMAX=500,TINY=1.0e-20)
      INTEGER i,imax,j,k
      DOUBLE PRECISION aamax,dum,sum,vv(NMAX)

      d = 1.d0
      DO 10 i=1,n
        aamax = 0.d0
        DO 20 j=1,n
          IF (ABS(a(i,j)) .GT. aamax) aamax = abs(a(i,j))
20        CONTINUE
        IF (aamax .EQ. 0.d0) PAUSE 'singular matrix in ludcmp'
        vv(i) = 1.d0/aamax
10      CONTINUE

      DO 30 j=1,n
        DO 40 i=1,j-1
          sum = a(i,j)
          DO 50 k=1,i-1
            sum = sum - a(i,k)*a(k,j)
50          CONTINUE
          a(i,j) = sum
40        CONTINUE
        aamax = 0.d0
        DO 60 i=j,n
          sum = a(i,j)
          DO 70 k=1,j-1
            sum = sum - a(i,k)*a(k,j)
70          CONTINUE
          a(i,j) = sum
          dum = vv(i)*ABS(sum)
          IF (dum .GE. aamax) THEN
            imax = i
            aamax = dum
          ENDIF
60        CONTINUE
        IF (j .NE. imax) THEN
          DO 80 k=1,n
            dum = a(imax,k)
            a(imax,k) = a(j,k)
            a(j,k) = dum
80          CONTINUE
          d = -d
          vv(imax) = vv(j)
        ENDIF
        indx(j) = imax
        IF (a(j,j) .EQ. 0.d0) a(j,j) = TINY
        IF (j .NE. n) THEN
          dum = 1.d0/a(j,j)
          DO 90 i=j+1,n
            a(i,j) = a(i,j)*dum
90          CONTINUE
        ENDIF
30      CONTINUE
```

```
      RETURN
      END


      SUBROUTINE lubksb(a,n,np,indx,b)
      INTEGER n,np,indx(n)
      DOUBLE PRECISION a(np,np),b(n)
      INTEGER i,ii,j,ll
      DOUBLE PRECISION sum

        ii = 0
        DO 10 i=1,n
          ll = indx(i)
          sum = b(ll)
          b(ll) = b(i)
          IF (ii .NE. 0) THEN
          DO 20 j=ii,i-1
            sum = sum - a(i,j)*b(j)
 20         CONTINUE
        ELSEIF (sum .NE. 0.) THEN
          ii = i
        ENDIF
        b(i) = sum
 10     CONTINUE

      DO 30 i=n,1,-1
        sum = b(i)
        DO 40 j=i+1,n
          sum = sum - a(i,j)*b(j)
 40       CONTINUE
        b(i) = sum/a(i,i)
 30     CONTINUE

        RETURN
        END


      SUBROUTINE gauleg(x1,x2,x,w,n)
      INTEGER n
      DOUBLE PRECISION x1,x2,x(n),w(n)
      DOUBLE PRECISION EPS
      PARAMETER (EPS=3.1d-14)
      INTEGER i,j,m
      DOUBLE PRECISION p1,p2,p3,pp,xl,xm,z,z1

      m = (n+1)/2
      xm = 0.5d0*(x2+x1)
      xl = 0.5d0*(x2-x1)
      DO 10 i=1,m
        z = COS(ACOS(-1.d0)*(DBLE(i)-.25d0)/(DBLE(n)+.5d0))
100       CONTINUE
        p1 = 1.d0
        p2 = 0.d0
        DO 20 j=1,n
          p3 = p2
          p2 = p1
          p1 = ((2.d0*DBLE(j)-1.d0)*z*p2-(DBLE(j)-1.d0)*p3)/DBLE(j)
```

```
20      CONTINUE
        pp = DBLE(n)*(z*p1-p2)/(z*z-1.d0)
        z1 = z
        z = z1 - p1/pp
        IF (ABS(z-z1) .GT. EPS) GOTO 100
          x(i) = xm - xl*z
          x(n+1-i) = xm + xl*z
          w(i) = 2.d0*xl/((1.d0 - z*z)*pp*pp)
          w(n+1-i) = w(i)
10      CONTINUE

      RETURN
      END


      SUBROUTINE spline(x,y,n,yp1,ypn,y2)
      INTEGER n,NMAX
      DOUBLE PRECISION yp1,ypn,x(n),y(n),y2(n)
      PARAMETER (NMAX=500)
      INTEGER i,k
      DOUBLE PRECISION p,qn,sig,un,u(NMAX)
      IF (yp1 .GT. .99d30) THEN
        y2(1) = 0.d0
        u(1) = 0.d0
      ELSE
        y2(1) = -0.5d0
        u(1) = (3.d0/(x(2)-x(1)))*((y(2)-y(1))/(x(2)-x(1))-yp1)
      ENDIF
      DO 10 i=2,n-1
        sig = (x(i)-x(i-1))/(x(i+1)-x(i-1))
        p = sig*y2(i-1)+2.d0
        y2(i) = (sig-1.)/p
        u(i) = (6.d0*((y(i+1)-y(i))/(x(i+1)-x(i))-(y(i)-y(i-1))
     1            /(x(i)-x(i-1)))/(x(i+1)-x(i-1))-sig*u(i-1))/p
10    CONTINUE
      IF (ypn .GT. .99d30) THEN
        qn = 0.d0
        un = 0.d0
      ELSE
        qn = 0.5d0
        un = (3.d0/(x(n)-x(n-1)))*(ypn-(y(n)-y(N-1))/(x(n)-x(n-1)))
      ENDIF
      y2(n) = (un-qn*u(N-1))/(qn*y2(n-1)+1.)
      DO 20 k=n-1,1,-1
        y2(k) = y2(k)*y2(k+1)+u(k)
20    CONTINUE
      RETURN
      END


      FUNCTION splint(xa,ya,y2a,n,x)
      INTEGER n
      DOUBLE PRECISION splint,x,xa(n),y2a(n),ya(n)
      INTEGER k,khi,klo
      DOUBLE PRECISION a,b,h
      klo = 1
      khi = n
```

```
10    IF (khi - klo .GT. 1) THEN
      k = (khi + klo)/2
      IF (xa(k) .GT. x) THEN
        khi = k
      ELSE
        klo = k
      ENDIF
      GOTO 10
    ENDIF
    h = xa(khi)-xa(klo)
    IF (h .EQ. 0.d0) PAUSE 'bad xa input in splint'
    a = (xa(khi)-x)/h
    b = (x-xa(klo))/h
    splint = a*ya(klo) + b*ya(khi) +
     1           ((a**3-a)*y2a(klo)+(b**3-b)*y2a(khi))*(h**2)/6.d0
      RETURN
      END
```

The following is a sample nput file, RC.IN

```
* Read in program parameters 1st (Integers I4, Reals G12.6)
m       = 81          Number of nodes; dX = 1./REAL(m-1)
n       = 43          Number of integration points
outfmt  = 1           Output format; must be a value between [0,m]
maxl    = 15          Maximum iterations for non-linearity
toler   = 1.0E-04     (Tnew - Told)/Told < toler
z       = 0.5         Under-relax. factor: tnew = told + z*(tnew - told)
* Read in problem parameters 2nd
mint    = 0.0         If not 0., requires an input temp. dist. (rctd.in)
maxt    = 600.0       Maximum time (s)
dt      = 0.5         Time step (s)
tprnt   = 1.0         Time step to print output for outfmt = 0 (s)
temp1   = 0.0         Temperature on left side (K)
temp2   = 298.0       Temperature on right side (K)
tempi   = 298.0       Initial temperature (K)
tempr   = 350.0       Reference temperature used in t = T/Tr
htflux  = 100.0       Heat Flux applied on left side (W/m^2)
qend    = 2000.0      Time to stop heat flux (s)
thick   = 0.01815     Thickness of material, D (m)
absorb  = 1200.0      Absorption coefficient, a (1/m)
scat    = 300.0       Scattering coefficient, sigma sub s (1/m)
cond    = 0.028       Thermal conductivity, k (W/mK)
vhtcap  = 19.2        Volumetric Heat Capacity, rho*cp (kJ/Km^3)
emis    = 1.0         Emissivity at x=0 (reflectivit = 1 - emis)
```

Appendix C

EAL 3-D Constant Thermal Conductivity Program: styconk3d.eal

```
$styconk3d.eal: Styrofoam, constant k, 3d
$
*XQT U1
*CM=200000
$
*RACM=0
$
!F=0.666667
$
!TI=298.0                $ Ambient Temperature
!D = 1.815/100.          $ Thickness
!L = 15.24/100./2.       $ 1/2 Length of side (square sample,
                           $symmetry)
!Q = 150.0               $ Applied heat flux, per area
!H = 10.0                $ Convection heat transfer coefficient
$
!DX = L/10.
!x2 = DX
!x3 = 2.*DX
!x4 = 3.*DX
!x5 = 4.*DX
!x6 = 5.*DX
!x7 = 6.*DX
!x8 = 7.*DX
!x9 = 8.*DX
!x10 = 9.*DX
!x11 = 10.*DX
$
*XQT TAB
START 605
JLOC
   1  0.     0.     0.     0.     "L"     0.    11   1   5
  11  0.     0.     "D"    0.     "L"     "D"
  56  "x2"   0.     0.     "x2"   "L"     0.    11   1   5
  11  "x2"   0.     "D"    "x2"   "L"     "D"
 111  "x3"   0.     0.     "x3"   "L"     0.    11   1   5
  11  "x3"   0.     "D"    "x3"   "L"     "D"
 166  "x4"   0.     0.     "x4"   "L"     0.    11   1   5
  11  "x4"   0.     "D"    "x4"   "L"     "D"
 221  "x5"   0.     0.     "x5"   "L"     0.    11   1   5
  11  "x5"   0.     "D"    "x5"   "L"     "D"
```

```
 276   "x6"    0.     0.     "x6"    "L"      0.    11    1    5
  11   "x6"    0.     "D"    "x6"    "L"      "D"
 331   "x7"    0.     0.     "x7"    "L"      0.    11    1    5
  11   "x7"    0.     "D"    "x7"    "L"      "D"
 386   "x8"    0.     0.     "x8"    "L"      0.    11    1    5
  11   "x8"    0.     "D"    "x8"    "L"      "D"
 441   "x9"    0.     0.     "x9"    "L"      0.    11    1    5
  11   "x9"    0.     "D"    "x9"    "L"      "D"
 496   "x10"   0.     0.     "x10"   "L"      0.    11    1    5
  11   "x10"   0.     "D"    "x10"   "L"      "D"
 551   "x11"   0.     0.     "x11"   "L"      0.    11    1    5
  11   "x11"   0.     "D"    "x11"   "L"      "D"
$
*XQT AUS
$
$TABLE(NI=9,NJ=1): COND PROP 1: I=2 3 4 5 6: J=1:    16.0 1210.0      .04
.04 .04
TABLE(NI=9,NJ=1): COND PROP 1: I=4 5 6:     J=1:    .04  .04  .04
TABLE(NI=9,NJ=1): COND PROP 2: I=4 5 6:     J=1:    0.0  0.0  0.0
TABLE(NI=2,NJ=1): CONV PROP 1: I=2:         J=1:    1.+5
TABLE(NI=2,NJ=1): CONV PROP 2: I=2:         J=1:    "H"
TABLE(NI=1,NJ=100): CTEM C41 1:              J=1,100: "TI"
TABLE(NI=1,NJ=80): CTEM C41 2:               J=1,80: "TI"
$TABLE(NI=1,NJ=160): CTEM C41 2:              J=1,160: "TI"
TABLE(NI=1,NJ=100): SOUR K41 1:              J=1,100: "Q"
TABLE(NI=1,NJ=1): K THIC:                   J=1:    1.
$
*XQT ELD
RESET NUTED=1
$
C41: GROUP 1: NMAT 1:    1   56   57    2   1  10  10   0
     GROUP 2: NMAT 2:    1   12   13    2   1   0  10   4
                         1   56   67   12   1  10   0   4
$                      561  572  571  560   1  10   4
$                      561  506  517  572   1  10   4
K41:          NMAT 2:   45  100  101   46   1  10  10
K81:          NMAT 1:    1   10   10    4  55   1  11  0  1
*XQT TGEO
*XQT SSTA
$*XQT TRTB
$RESET T1="TIMI" T2="TIMF" DT="DELT" PRINT=0 MXNDT=100000 PTV=0.00001
BETA="F"
$TEMP="TI"
$TSAVE="TRPT"
$KTIME="DELT"
*XQT DCU
$PRINT 1 TRAN TEMP 1 1
PRINT 1 STAT TEMP
*XQT DCU
PRINT 1 COND PROP 1
PRINT 1 COND PROP 2
PRINT 1 CTEM C41 1
PRINT 1 CTEM C41 2
PRINT 1 SOUR K41 1
PRINT 1 K THIC
TOC 1
```

Appendix D

EAL 1-D Variable *k*, Aluminum B.C. Program: styal.eal

```
$ styal.eal: Styrofoam & Aluminum
$ Jerome H. Guynn, based on a program by Greg Walker
$
$ Program produces temperature output for the following problem:
$  1-D heat transfer through a 2-layer slab of thickness 2L with a
$  constant heat flux on one boundary and a constant temperature
$  on the other boundary.  Density and heat capacity are constant,
$  but the thermal conductivity is temperature dependent.
$
$            ->|          |          |        Material starts at some
$ Heat Flux ->|  x->     |          | T1     initial temperature Ti=T1.
$            ->|          |          |
$             x=0        x=L        x=2L
$
$ Units are SI.
$
$ This version has 60 (40/20) elements, L = 1.905 cm, and runs
$ for 10 min.
$
$*********************************************************************
*XQT U1
*CM=200000
$
$*********************************************************************
$
$  Subroutine VARB - defines variables used in the program
$                    NOTE: Variable names can only be four
$                          letters long!
$*********************************************************************
$
*(29 VARB DEFI) VARB
$
$  Set RACM = 0 to use Fortran logic in all subroutines
*RACM = 0
$
!L=0.01815              $Thickness of the slab (m)
!L2=0.01905
!LT=L+L2
!NE=40                  $Number of elements for styrofoam
!NN=NE+1                $Number of styrofoam nodes
!NA=20                  $Number of elements for aluminum
```

```
!NNA=NE+NA+1          $Total number of nodes
!N1=1                 $Beginning node
$
$ Define initial temperature, initial and final time, time step
$ for  transient solution, total heating time, and heat flux
$ value.
$
!TI=298.0              $Initial temperature (K)
!T1=298.0              $Temperature at "end boundary" (K)
!HF=150.0              $Heat flux (W/m^2)
!TIMI=0.0              $Initial (starting) time (sec)
!TIMF=600.0            $Final (stopping) time (sec)
!DELT=0.5             $Time step for transient solution (sec)
!TRPT=30.0             $Time interval to record temperatures; used by
TSAVE
$                       in TRTB (sec)
$
$ Following is the calculation of the number of temperatures recorded
$
!NTMP=(TIMF-TIMI)/TRPT
!NRPT=IFIX(NTMP+0.001)+1
$
!COU=TIMF-TIMI           $Length of time for experiment
!COU=COU/DELT            $Number of time steps used in taking temp. meas.
!NTS=IFIX(COU+0.0001)    $Number of time steps must be an integer
!NTS=NTS+1               $Total number of times from TIMI to TIMF
$
!NVE=51                  $Number of variable property entries
$
$ Define scheme (C-N Implicit Galerkin Explicit)
$
!F=0.666667     $Defines Galerkin explicit
$
*RETURN
*VARB
$
$*********************************************************************
$
$  Subroutine NODE - defines the nodal positions
$
$*********************************************************************
$
*(29 NODE GENE)NODE
*XQT TAB
START "NNA"      $ Define the total number of nodes
JLOC            $ Give the location of the nodes (set up the mesh)
$
$ In the next statement, FORMAT=1 specifies rectangular
$ coordinates; N1 is the number to start the node locations at (in
$ this case, 1); 0,0,0 are the coordinates of N1; L,0,0 are the
$ coordinates for the end of the slab; NN is the number of nodes
$ in the x direction.
$
FORMAT = 1: "N1", 0., 0., 0., "LT", 0., 0., 61
*RETURN
*NODE
$
```

```
$*********************************************************************
$
$  Subroutine ELEM - defines the element connectivity
$
$*********************************************************************
$
*(29 ELEM DEFI)ELMT
*XQT ELD
$
$  Define K21 elements
$  K21 signifies a conductive, 2 node element.
$
RESET NUTED=1
 K21
$
 GROUP = 1          $Group 1; for the source element
 NMAT = 1           $Material 1; for the source element
!J1=N1              $J1 is first node in model
!J2=N1              $J2 same as J1 b/c Source Elem. has zero length
 "J1" "J2"
$
 GROUP = 2          $Group 2; actual insulation
 NMAT = 2           $Material 2; actual insulation
!J1=N1              $J1 is first node in model
!J2=N1+1            $J2 is second node
$ "J1" "J2", 1, "NE"
 1 2 1 40
$
 GROUP = 3          $Group 3; aluminum
 NMAT = 3           $Material 3; aluminum
!J1=NN
!J2=J1+1
$ "J1" "J2", 1, "NA"
 41 42 1 20
*RETURN
*ELMT
$
$*********************************************************************
$
$  Subroutine TABL - Defines the thickness of the elements
$
$*********************************************************************
$
*(29 TABL GENE)TABL
*XQT AUS
TABLE(NI=1,NJ=1): K AREA: J=1: 1.   $The area of K21 elements
$
*RETURN
*TABL
$
$*********************************************************************
$
$  Subroutine UPDA - Updates thermal property values
$
$*********************************************************************
$
*(29 TABL UPDA) UPDA
```

```
*XQT AUS
$
$ Define tables for Source Elem. properties, which are zero.
$
 TABLE(NI=9,NJ=1): COND PROP 1: I=3,4: J=1: 0.,0.
 TABLE(NI=1,NJ=1): SOUR K21 1     $: I=1: J=1: "HF"
 BLOCK 1
 J=1: "HF"
 BLOCK 2
 J=1: "HF"
 TABLE(NI=1,NJ=2): SOUR TIME: I=1: J=1,2: "TIMI", "TIMF"
$
$ Place variable property data, which has been read into MATL PROP
$ table, into the COND PROP 2 table.
$
 DEFINE C = 2 MATL PROP
 TABLE(NI=9,NJ="NVE"): COND PROP 2
 TRANSFER(SOURCE=C,DSKIP=5,ILIM=4,JLIM="NVE",OPER=XSUM)
$
$ Define the properties for aluminum
$
 TABLE(NI=9,NJ=1): COND PROP 3: I=2,3,4: J=1: 2700.,  850.,  160.
$
$  Table TEMP NODE contains the node numbers that are to be
$  held at constant temp.  APPL TEMP contains the actual temps.
$  used.  The "J" value ties the 2 tables together i.e. N1 has
$  temp T1, NN has temp. T2.  Each Block corresponds to a time in
$  TEMP TIME i.e. BLOCK 2 has the temps for time TIMF (TEMP TIME
$  J=2).  EAL interpolates between values for temps. not in TEMP
$  TIME.  Since, for this program, temps. are constant, they are
$  given only for initial and final times.
$
$  Need to convert INTEGER node numbers to FLOATING point for the
$  tables
$
!FNNA=FLOAT(NNA)
 TABLE(NJ=1): TEMP NODE
 J=1: "FNNA"
 TABLE(NJ=1): APPL TEMP
 BLOCK 1
 J=1: "T1"
 BLOCK 2
 J=1: "T1"
 TABLE(NJ=2): TEMP TIME
 J=1: "TIMI"
 J=2: "TIMF"
$
*XQT DCU
$
$ Print tables for error checking and verification
$
 PRINT 1 SOUR TIME
 PRINT 1 SOUR K21
 PRINT 1 COND PROP 1
 PRINT 1 TEMP TIME
 PRINT 1 APPL TEMP
 PRINT 1 COND PROP 2
```

```
*RETURN
*UPDA
$
$*********************************************************************
$
*(29 BILD TS) XXXX
$
$  Bring surface temperature data from TRAN TEMP multi-block data
$  set using XSUM and TRANSFER.
$
$*********************************************************************
$
$ Temperatures are printed out for all points at intervals defined
$ by TRPT (30 s in this case).
$
*XQT DCU
PRINT 1 TRAN TEMP 1 1
$
*RETURN
*XXXX
$
$
$*********************************************************************
$
$  Subroutine TRAN - Solves direct problem using TRTB processor
$
$*********************************************************************
$
*(29 TRAN ANAL)TRAN
*DCALL(29 NODE GENE) $Generate the nodes used in the mesh
*DCALL(29 TABL GENE) $Generate tables needed in analysis
*DCALL(29 TABL UPDA) $Update the thermal properties (estimates)
*DCALL(29 ELEM DEFI) $Defines the elements (Cond.,Conv., Heat Source,
etc
$
*XQT TGEO      $ Element goemetry processor; it computes local
               $ coordinates and performs element geometry checks.
               $ The user MUST execute TGEO after each execution of
               $ ELD.
$
*XQT TRTB             $Transient analysis processor
 RESET T1="TIMI" T2="TIMF" DT="DELT" PRINT=0 MXNDT=100000
PTV=0.00001 BETA="F"
 TEMP="TI"
 TSAVE="TRPT"
 KTIME="DELT"
$
*DCALL (29 BILD TS)
$
*RETURN
*TRAN
$
$*********************************************************************
$
$  Main program
$
$*********************************************************************
```

```
$
*DCALL (29 VARB DEFI)
*XQT AUS
$
$ Read in variable property data, number of entries "NVE"
$
*TF OPEN 2'vprc.dat
 TABLE(NI=4,NJ="NVE"):  2 MATL PROP: I=1,2,3,4
*TF READ 2
*TF CLOSE 2
*XQT DCU
 PRINT 2 MATL PROP
$
*DCALL (29 TRAN ANAL)
*XQT EXIT
```

Appendix E

FORTRAN Modified Box-Kanemasu Program: MBK.FOR

```
c MBK.FOR: Modified Box-Kanemasu for Diffusion Solution
c   Modification of a program by Sandrine Garcia
c
c Variable Thermal Conductivity Solution (HCVK)
c 4 Parametrers:
c    Thermal conductivity
c    Volumetric heat capacity
c    Extinction Coefficient of Styrofoam
c    Volumetric heat capacity of heater
c Constant Std. Dev. (sigma2)
c Ordinary Least Squares
c DOES NOT INCLUDE VARIABLE HEAT FLUX
c
c * NOTE: All page references are to: Beck, J.V. and K.J. Arnold
c         "Parameter Estimation in Engineering and Science",
c         John Wiley and Sons, New York, 1977.
c
c  Name of the main variables used in this code
c   Integers:
c    Np : number of parameters to estimate
c    maxT : number of data
c    iterk : iteration number
c    lastk : maximum number of iterations
C
c   Reals:
c    sigma(maxT) : standard deviation of Y(maxT)
c    ETA : calculated dependent variable
c    Y(maxT) : measured dependent variable
c    T(maxT) : Temperature/independent variable
c    mubeta(Np) : prior info
c    varbeta(Np) : prior info
c    RES : [Y(maxT)-ETA]
c    XT(Np) : sensitivity coefficients
c    bSeq(Np) : new sequential parameter estimate
c    bBK(Np) : modified and final parameter estimate from B-K part
c    binitk(Np) : initial parameter estimate for each iterk
c    P(Np,Np) : P matrix
c    R(Np,Np) : correlation matrix
c
c  - Matrix Inversion Lemma method variables -
c    a{i}(Np) =XT{i}(Np)*P{i-1}(Np,Np)
```

```
c     delta =sigma(maxT)**2+XT(Np)*a(Np)
c     valueK(Np) =a(Np)/delta
c     valueH =RES-XT(Np)*[bSeq(Np)-bBK(Np)]
c
c   - Modified Box Kanemasu method variables -
c     S0: sum of squares for bBK (=present par. values=final BK)
c          estimates from previous iterk); =(RES/sigma(maxT))**2
c     Salpha: sum of squares for bBK obtained using alpha to
c               modify the G step-size(=B-K parameter values);
c               Salpha decreases towards a positive constant and
c               should be less than S0
c     XTX(Np,Np) =[XT(Np)*XT(Np)]/sigma(maxT)**2
c     XTY(Np) =[XT(Np)*RES]/sigma(maxT)**2
c     sumg(Np) =[XT(Np)*RES]/sigma(maxT)**2
c     alpha: used to modify bBK; initially 1.0
c     AA: used to calculate h; =1.1
c     deltab =bBK(Np)obtained using alpha-boldBK(Np)
c     G: the slope of sum of squares vs. h; =deltab*sumg(Np);
c        G should always be positive and approach zero at
c        convergence
c     sumch : right side in inequality 5 to check (see p366);
c             =S0-alpha*G*(2-1/AA)
c     h: scalar interpolation factor; fraction of the Gauss
c        step-size given by the Box-Kanemasu method
c     change: used to determine when all parameters stop varying
c     ratio: determines when the change in the parameter estimates
c            is insignifiant
c     criter: criterion used to determine when the iterative
c             procedure is negligible; =0.0001
c     epsden: small value added to the previous estimate to
c              determine ratio; =1d-30
C#####################################################################
      integer iterT,Np,maxT,iterk,lastk,change,endit
      REAL mubeta(4),varbeta(4),Y(2200),sigma2,T(2200),tbc(2200),
     +             ETA(2200),RES,bSeq(4),bBK(4),binitk(4),P(4,4),C(4,4),
     +             det,r(4,4),a(4),delta,valueK(4),valueH,
     +             XT(4,2200),XTX(4,4),XTY(4),S0,Salpha,sumg(4),alpha,
     +             AA,deltab,G,sumch,h,ratio,criter,epsden
C
      COMMON/ESTITERK/bBK
      COMMON/MEAS/Y,sigma2,T,maxT,Np,mubeta,varbeta,tbc
      COMMON/CST/lastk,criter,epsden
C
      write(*,*) 'Enter maximum iteration: '
      read(*,*) endit
      open(unit=98,file='mbk.out')
C
C   Set the constants
      call const
C
C   Read Y (simulated measured T)
C   Initialize bBK(Np): mubeta for MAP/initial guess for ML or OLS
      call init
C
C
---------------------------------------------------------------------
C   PART 1: GAUSS METHOD
```

```
C     It estimates the parameters using the Matrix Inversion Lemma (MIL)
C   based on the Gauss method.
C     The sequential process always begin here, obtaining estimates
C   for bSeq(i) and calculating S0.
C     The estimated parameters are then modified in the next section of
C   the program using the Modified Box-Kanemasu Method.
C
      iterk=0
1     iterk=iterk+1
      IF (iterk .GT. endit) GOTO 1000
C   START ITERATION ON ESTIMATION PROCESS (SEQUENTIAL+BK)
      write(98,*)
      write(98,*)
      write(98,*)'iterk= ',iterk
C
C   Initialization
C     In the MAP estimation the starting value of bSeq equal mubeta
C   and the starting P(0) matrix is varbeta for each iteration.
C     In the ML and OLS estimation the starting value of bSeq equal the
C   initial parameter estimate; bSeq will then change for every iterk
C   (becoming the modified BK estimate from the previous iterk). The
C   starting P(0) matrix is selected to have relatively large diagonal
C   terms for each iteration.
C     Set XTX and XTY sums and sumg equal to zero

      DO 10 i=1,Np
      XTY(i)=0.0
      sumg(i)=0.0
C   for MAP:
ccc         bSeq(i)=mubeta(i)
ccc         binitk(i)=mubeta(i)
C   for ML or OLS:
      bSeq(i)=bBK(i)
      binitk(i)=bBK(i)
      DO 20 j=1,Np
         XTX(i,j)=0.0
         P(i,j)=0.0
         P(i,i)=varbeta(i)
   20    CONTINUE
   10  CONTINUE
C
      S0=0.0
C    Inverse the P matrix

      CALL invert(P,C)

       write(98,*)'Sequential estimates of the parameters given below'
       write(98,*)'(these est. are found using the Gauss Method)'
       write(98,'(/,''iterT'',5x,''ETA'',5x,''RES'',6x,''bSeq(1)'',
     +  2x,''bSeq(2)'',3X,''bSeq(3)'',5X,''bSeq(4)'')')

      CALL hcvk(bbk(1),bbk(2),bbk(3),bbk(4),t,eta,maxT,tbc)
      call sens(ETA,XT)
      DO 51 iterT=1,maxT
C
C   Calculate S0 (used in BK)
      RES = Y(iterT)-ETA(iterT)
```

```
C  MAP estimator
*         do i=1,Np
*            do j=1,Np
*               S0=S0+(mubeta(i)-bSeq(i))*(mubeta(j)-bSeq(j))*C(i,j)
*            enddo
*         enddo
C  ML or OLS estimator
      S0=S0+RES**2/sigma2
C
C  Calculate XTX, XTY and sumg (used in BK)
      DO 30 i=1,Np
         XTY(i)=XTY(i)+XT(i,iterT)*RES/sigma2
         sumg(i) = sumg(i) + XT(i,iterT)*RES/sigma2
*            DO 31 j=1,Np
C  Note that the 2nd term is for the Map estimator
*               sumg(i)=sumg(i)+XT(i,iterT)*RES/sigma2
*     +                          +C(i,j)*(mubeta(j)-bBK(j))
*               XTX(i,j)=XTX(i,j)+XT(i,iterT)*XT(j,iterT)/sigma2
*   31         CONTINUE
   30    CONTINUE
C
C  See p392: use the scalar equations in the order given in the
C  MIL method
      DO 40 i=1,Np
         a(i)=0.0
   40    CONTINUE
      DO 50 i=1,Np
         DO 60 j=1,Np
            a(i)=a(i)+XT(j,iterT)*P(i,j)
   60       CONTINUE
   50    CONTINUE
C
      delta=0.0
      DO 70 i=1,Np
         delta=delta+XT(i,iterT)*a(i)
   70    CONTINUE
      delta=sigma2+delta
C
      DO 80 i=1,Np
         valueK(i)=a(i)/delta
   80    CONTINUE
C
      valueH=0.0
      DO 90 i=1,Np
         valueH=valueH+XT(i,iterT)*(bSeq(i)-bBK(i))
   90    CONTINUE
      valueH=RES-valueH
C
      DO 100 i=1,Np
         bSeq(i)=bSeq(i)+valueK(i)*valueH
  100    CONTINUE
C
      DO 110 i=1,Np
         DO 120 j=1,Np
            P(i,j)=P(i,j)-valueK(i)*a(j)
  120       CONTINUE
  110    CONTINUE
```

```
c  Make P symmetrical
      DO 130 i=2,Np
         ii=i-1
         DO 140 j=1,ii
            P(j,i)=P(i,j)
  140       CONTINUE
  130    CONTINUE
C
C  DONE WITH GAUSS CALCULATIONS
c  Print results
       write(98,17)iterT,ETA(iterT),RES,(bSeq(k),k=1,Np)
ccc          ENDIF
C
51    CONTINUE
17    format(I4,2E11.5,4F9.4)
C
C  Determine the correlation matrix
C    The diagonal terms of the correlation matrix are all unity and the
off
C  -diagonal terms must be in the interval [-1,1]. Whenever all the off
C  -diagonal terms exceed 0.9 in magnitude, the estimates are highly
C  correlated and tend to be inaccurate
      DO 150 i=1,Np
      DO 160 j=1,i
         r(i,j)=P(i,j)/sqrt(P(i,i)*P(j,j))
  160    CONTINUE
  150 CONTINUE
C  Print out the P and correlation matrices
      write(98,'(/,''The P matrix is'')')
      DO 170 i=1,Np
      write(98,'(4D15.7)') (P(i,j),j=1,Np)
  170 CONTINUE
      write(98,'(/,''The correlation matrix is'')')
      DO 180 i=1,Np
      write(98,'(4E15.7)') (r(i,j),j=1,i)
  180 CONTINUE
C
      write(98,*)
      write(98,*)'The final sequential estimates will now be modified'
      write(98,*)'using the Box-Kanemasu method'
      write(*,*)'END BASIC LOOP'
C
C
------------------------------------------------------------------------
C  PART 2: MODIFIED BOX-KANEMASU METHOD
C    It uses the direction provided by the Gauss Method but modifies the
C  step size by introducing a scalar interpolation factor (h).
C
      AA=1.10
      alpha=2.0
    2 alpha=alpha/2.0
C
C  Calculate the parameters using the modified step-size; the gauss
step-
C  size is obtained from the sequential procedure and modified with
alpha.
      DO 190 i=1,Np
```

```
      bBK(i)=binitk(i)+alpha*(bSeq(i)-binitk(i))
  190 CONTINUE
C
C    Note that deltab is the step size obtained using the estimate
calculated
C  above with alpha.
C    G is calculated from (7.6.8a) p364
C
      G=0.0
      DO 200 i=1,Np
      deltab=bBK(i)-binitk(i)
      G=G+deltab*sumg(i)
  200 CONTINUE
      if (G.lt.0.0) then
      write(98,*)'G < 0 !'
      G = 0.0
      DO 210 i=1,Np
        deltab = bBK(i) - binitk(i)
        G = G + deltab*sumg(i)
        write(98,*) 'G: ',G,'  deltab: ',deltab,'  sumg: ',sumg(i)
  210    CONTINUE
      go to 1000
      endif
C
C  Calculate the new sum of squares based on the modified parameters
with
C  alpha
      Salpha=0.0

C   Inverse the P matrix
      CALL invert(P,C)

      CALL hcvk(bbk(1),bbk(2),bbk(3),bbk(4),t,eta,maxT,tbc)
      DO 52 iterT=1,maxT
      RES=Y(iterT)-ETA(iterT)
C  MAP estimator
*         do i=1,Np
*            do j=1,Np
*             Salpha=Salpha+(mubeta(i)-bBK(i))*(mubeta(j)-bBK(j))*C(i,j)
*            enddo
*         enddo
C  ML or OLS estimator
      Salpha=Salpha+RES**2/sigma2
52    CONTINUE
C
      if (Salpha.gt.S0) then
      if (alpha.le.0.010) then
         write(98,*)'alpha is too small !'
         write(98,'(''alpha = '',F12.6,2x,''Salpha = '',E15.6,
     +                2x,''S0 = '',E15.6)')alpha,Salpha,S0
         go to 1000
      else
         go to 2
      endif
      endif
C
      sumch=S0-alpha*G*(2.0-1.0/AA)
```

```
       if (Salpha.ge.sumch) then
      h=(alpha**2)*G/(Salpha-S0+2.0*alpha*G)
       else
      h=alpha*AA
       endif
C
C    Calculate the final parameter estimates using h.
C    Also calculate ratio; if it is less than criter, then the change in
C  the estimated parameters is insignifiant and the iterative process is
C  terminated. Change is used to determine when all parameters stop
varying
       change=0
       DO 220 i=1,Np
      bBK(i)=binitk(i)+h*(bSeq(i)-binitk(i))
      ratio=abs((bBK(i)-binitk(i))/(binitk(i)+epsden))
      if (ratio.le.criter) change=change+1
  220 CONTINUE
C
c  Print out the calculated values for h, G, S0 and Salpha
      write(*,1300)
      write(98,1300)
1300  format(5x,'iterk',10x,'h',13x,'G',12x,'S0',11x,'Salpha')
      write(*,1301)iterk,h,G,S0,Salpha
      write(98,1301)iterk,h,G,S0,Salpha
1301  format(I8,4E14.6,/)
C
c  Print out the final parameter estimates
      write(98,*)'The final parameter estimates for this iteration are'
      write(98,'(10x,''bBK('',i1,'') ='',E16.6)') (i,bBK(i),i=1,Np)
      write(*,'(10x,''bBK('',i1,'') ='',E16.6)') (i,bBK(i),i=1,Np)
C
c ---------------------- end the B-K modification
------------------------
C
      if (Np.gt.change.and.iterk.le.lastk) goto 1
      write(98,*) '  Parameters converged.'
C
C  Compute the 95% CI and CR
      S0=0.0
      CALL hcvk(bbk(1),bbk(2),bbk(3),bbk(4),t,eta,maxT,tbc)
      DO 53 iterT=1,maxT
*         call model(iterT,T,ETA)
     RES=Y(iterT)-ETA(iterT)
*C  Map estimator
*         do i=1,Np
*            do j=1,Np
*               S0=S0+(mubeta(i)-bBK(i))*(mubeta(j)-bBK(j))*C(i,j)
*            enddo
*         enddo
*C  ML or OLS  estimator
     S0=S0+RES**2/sigma2
53    CONTINUE
      call CICR(Np,S0,P,C,maxT)
C
1000  close(98)
      close(99)
      STOP 'BOX-KANEMESU ESTIMATION DONE'
```

```
      END
CCCCCCCCCCCCCCCCCCCCCCCCCCCCCCCCCCCCCCCCCCCCCCCCCCCCCCCCCCCCCCCCCCCCCCCCCCCCCCC

      subroutine const
C
      integer lastk
      REAL criter,epsden
C
      COMMON/CST/lastk,criter,epsden
C
      criter=1.E-3
      epsden=1.E-30
      lastk=100
C
C     output title :
      write(*,*)' Gauss w/Box-Kanemasu Modification running ...'
      write(98,*)'Sequential modified BK method'
      write(98,*)'Non linear problem, OLD'
      write(98,*)'criter=',criter
C
      return
      end
CCCCCCCCCCCCCCCCCCCCCCCCCCCCCCCCCCCCCCCCCCCCCCCCCCCCCCCCCCCCCCCCCCCCCCCCCCCCCCC
      subroutine init
C
      integer maxT,Np
      REAL Y(2200), sigma2,T(2200),bBK(4),mubeta(4),
     +                varbeta(4),s,scale(4),tbc(2200)
C
      COMMON/ESTITERK/bBK
      COMMON/MEAS/Y,sigma2,T,maxT,Np,mubeta,varbeta,tbc
C

c COMMON block RCCON contains values that are passed to the
c conduction-radiation subroutine, RCT1D.
      DOUBLE PRECISION toler,tmin,tmax,dt,tprnt,temp1,temp2,tempi
      DOUBLE PRECISION htflux,qend,thick,vhc1,xmax1,k1,tempr,beta
      REAL absorb,scat,cond,vhtcap
      INTEGER n1,n2,outfmt,maxl,p,pmax
      COMMON/HCCON/n1,n2,outfmt,maxl,toler,tprnt,temp1,temp2,tempi,
     1             tempr,htflux,qend,thick,scale,vhc1,xmax1,k1

c The following code reads parameter values and run information from
c an input file, HCVK2.IN.  Most of these variables are listed in the
c HCCON COMMON block. Descriptions of the variables are given in the
c input file.

      OPEN(UNIT=11,FILE='hcvk2.in',STATUS='OLD')
      READ(11,5) n1,n2,outfmt,maxl,toler
    5 FORMAT(4(/,9X,I4),1(/,9X,G12.6))
      READ(11,15) tmin,tmax,dt,tprnt,temp1,temp2,tempi,tempr,htflux,
     1    qend,thick,beta,cond,vhtcap,xmax1,k1,vhc1,s
   15 FORMAT(18(/,9X,G12.6))
      CLOSE(11)

      Np = 4
```

```
c Scale values to same order of magnitude (1.0)
      bbk(1) = cond
      bbk(2) = vhtcap
      bbk(3) = beta
      bbk(4) = vhc1

      DO 20 i=1,Np
     DO 30 j = -5,10
       temp = bbk(i)/10.**j
       IF (temp .LT. 10.0) THEN
         scale(i) = 10.**j
         write(*,*) 'scale: ',i,' = ',scale(i)
         GOTO 40
       ENDIF
  30    CONTINUE
     write(*,*) 'Parameter: ',i,'unscalable between -5 and 10.'
     scale(i) = 1.0
  40    bbk(i) = bbk(i)/scale(i)
  20  CONTINUE
      sigma2 = s**2

C OLS estimator (no knowledge about the errors)
C ML or OLS estimator (no prior info)
C T(i): time,  Y(i): temperature
      open(unit=1,file='mbk.in')
      DO 50 i=1,maxT
     read(1,'(3(1X,F7.2))',END=60) T(i), Y(i), tbc(i)
   50 CONTINUE
   60 maxT = i-1
      DO 70 i=1,Np
     mubeta(i) = 0.0
     varbeta(i) = 10.0E+5
   70 CONTINUE
      close(1)
C
      return
      end
ccccccccccccccccccccccccccccccccccccccccccccccccccccccccccccccccccccccccc

      subroutine sens(ETA,XT)
C
      integer maxT,Np
      REAL Y(2200), sigma2,T(2200),bBK(4),mubeta(4),
     +                 varbeta(4),tbc(2200)
      integer i,j
      REAL ts(2200),XT(4,2200),ETA(2200),dp
      real p(4)
C
      COMMON/ESTITERK/bBK
      COMMON/MEAS/Y,sigma2,T,maxT,Np,mubeta,varbeta,tbc
C
*      open(unit=99,file='junk',status='unknown')
      DO 10 i=1,Np
     DO 20 j=1,Np
       IF (i .EQ. j) THEN
         dp = 0.02*bbk(j)
         p(j) = dp + bbk(j)
```

```
        ELSE
          p(j) = bbk(j)
        ENDIF
   20   CONTINUE
      write(*,'(2X,A4,I1)') 'SC: ',i
      CALL hcvk(p(1),p(2),p(3),p(4),t,ts,maxT,tbc)
*          write(99,*) 'Parameter: ',i
      DO 30 j = 1,maxT
        XT(i,j) = (ts(j) - eta(j))/dp
*             WRITE(99,'(3(1X,F8.3))') t(j),eta(j),ts(j)
   30   CONTINUE
   10 CONTINUE
*       write(99,*) 'sc'
*       DO 59 i=1,maxT
*         WRITE(99,'(1X,F8.2,3(1X,E11.5))') t(i),xt(1,i),xt(2,i),xt(3,i)
*    59 CONTINUE
*       CLOSE(99)

C
      return
      end
cccccccccccccccccccccccccccccccccccccccccccccccccccccccccccccccccccccccc

      subroutine CICR(Np,R,P,C,maxT)
C
      integer Np,maxT
      REAL R,CI(4),P(4,4),C(4,4),det,lambda(4),e(4,4),
     +                 coord1(4),coord2(4)
C
C Computation of the 95% CI
      DO 10 k=1,Np
     CI(k)=1.96*sqrt(P(k,k)*R/REAL(maxT-Np))
   10 CONTINUE
C
C Computation of the 95% CR
C   Compute the eigenvalues of the C matrices
c       lambda(1)=0.50*(C(1,1)+C(2,2)-sqrt((C(1,1)+
c      + C(2,2))**2-4.0*(C(1,1)*C(2,2)-C(1,2)**2)))
c       lambda(4)=0.50*(C(1,1)+C(2,2)+sqrt((C(1,1)+
c      + C(2,2))**2-4.0*(C(1,1)*C(2,2)-C(1,2)**2)))
C
C   Compute the matrices e1 and e2
c       e(2,1)=1.0/sqrt(1.0+C(1,2)**2/(C(1,1)-lambda(1))**2)
c       e(1,1)=-C(1,2)*e(2,1)/(C(1,1)-lambda(1))
c       e(1,2)=1.0/sqrt(1.0+C(1,2)**2/(C(2,2)-lambda(4))**2)
c       e(2,2)=-C(1,2)*e(1,2)/(C(2,2)-lambda(2))
C
C   Compute the coord (b-beta)max/min of the ellipses
c       DO 20 i=1,Np
c         coord1(i)=2.4470*abs(e(1,i)/sqrt(lambda(i)))
c         coord2(i)=2.4470*abs(e(2,i)/sqrt(lambda(i)))
c   20 CONTINUE
C
C OUTPUT
      write(98,*)
      write(98,*)'Sum of squares of res and  95% CI:'
      write(98,*)'R       CI(A2)       CI(E2)'
```

```
      write(98,101)R,CI(1),CI(2)
      write(98,*)
      write(98,*)'Coordinates of the 95% CR (b-beta)max/min:'
      write(98,*)'CRA2max    CRA2min     CRE2max       CRE2min'
c      write(98,102)coord1(1),coord1(2),coord2(1),coord2(2)
101   format(3(E10.3,3x))
102   format(4(E15.5))
C
      return
      end
CCCCCCCCCCCCCCCCCCCCCCCCCCCCCCCCCCCCCCCCCCCCCCCCCCCCCCCCCCCCCCCCCCCCCCCCCCCCCCC
    SUBROUTINE invert(ai,b)
     REAL ai(4,4),a(4,4),b(4,4),d
     INTEGER i,j,n,indx(4)

     n = 4

     DO 10 i=1,n
       DO 20 j=1,n
         b(i,j) = 0.
         a(i,j) = ai(i,j)
   20      CONTINUE
       b(i,i) = 1.
   10   CONTINUE
     CALL ludcmp(a,indx,d)
     DO 30 j=1,n
       CALL lubksb(a,indx,b(1,j))
   30   CONTINUE

     RETURN
     END

*************************************************************************

     SUBROUTINE ludcmp(a,indx,d)
     INTEGER n,np,indx(4),NMAX
     REAL d,a(4,4),TINY
     PARAMETER (NMAX=500,TINY=1.0e-20)
     INTEGER i,imax,j,k
     REAL aamax,dum,sum,vv(NMAX)

     n = 4
     np = 4

     d = 1.
     DO 10 i=1,n
       aamax = 0.
       DO 20 j=1,n
         IF (ABS(a(i,j)) .GT. aamax) aamax = abs(a(i,j))
   20      CONTINUE
       IF (aamax .EQ. 0.) PAUSE 'singular matrix in ludcmp'
       vv(i) = 1./aamax
   10   CONTINUE

     DO 30 j=1,n
       DO 40 i=1,j-1
         sum = a(i,j)
```

```
        DO 50 k=1,i-1
          sum = sum - a(i,k)*a(k,j)
50        CONTINUE
        a(i,j) = sum
40      CONTINUE
      aamax = 0.
      DO 60 i=j,n
        sum = a(i,j)
        DO 70 k=1,j-1
          sum = sum - a(i,k)*a(k,j)
70        CONTINUE
        a(i,j) = sum
        dum = vv(i)*ABS(sum)
        IF (dum .GE. aamax) THEN
          imax = i
          aamax = dum
        ENDIF
60      CONTINUE
      IF (j .NE. imax) THEN
        DO 80 k=1,n
          dum = a(imax,k)
          a(imax,k) = a(j,k)
          a(j,k) = dum
80        CONTINUE
        d = -d
        vv(imax) = vv(j)
      ENDIF
      indx(j) = imax
      IF (a(j,j) .EQ. 0.) a(j,j) = TINY
      IF (j .NE. n) THEN
        dum = 1./a(j,j)
        DO 90 i=j+1,n
          a(i,j) = a(i,j)*dum
90        CONTINUE
      ENDIF
30    CONTINUE

      RETURN
      END

*************************************************************************

      SUBROUTINE lubksb(a,indx,b)
      INTEGER n,np,indx(4)
      REAL a(4,4),b(4)
      INTEGER i,ii,j,ll
      REAL sum

        n = 4
        np = 4

        ii = 0
        DO 10 i=1,n
          ll = indx(i)
          sum = b(ll)
          b(ll) = b(i)
          IF (ii .NE. 0) THEN
```

```
        DO 20 j=ii,i-1
          sum = sum - a(i,j)*b(j)
20        CONTINUE
      ELSEIF (sum .NE. 0.) THEN
        ii = i
      ENDIF
      b(i) = sum
10    CONTINUE

    DO 30 i=n,1,-1
      sum = b(i)
      DO 40 j=i+1,n
        sum = sum - a(i,j)*b(j)
40      CONTINUE
      b(i) = sum/a(i,i)
30    CONTINUE

      RETURN
      END

*****************************************************************************
      SUBROUTINE hcvk(p1,p2,p3,p4,time,thc,pmax,tbc)

      DOUBLE PRECISION ti,t1,t2,toler,rho1,cp1,dx1,ar
      DOUBLE PRECISION xmax,dx2,dt,k1,k2,beta,vhc1,vhc2,tprnt
      DOUBLE PRECISION t(101),tnew(101),a(101),b(101),c(101)
      DOUBLE PRECISION told(101),tsum,fop,fom,q0,tref,xmax1,xmax2
      DOUBLE PRECISION xpos,qend,htflux,xdim,kt,d(101)
      REAL p1,p2,p3,p4,scale(4),time(1201),thc(1201),tbc(1201)
      INTEGER n,n1,n2,nmax,p,pmax,outfmt,pprnt,maxl
      COMMON dx2,dt
      COMMON/HCCON/n1,n2,outfmt,maxl,toler,tprnt,t1,t2,ti,tref,
     1             htflux,qend,xmax2,scale,vhc1,xmax1,k1
      DATA fop,fom/0.d0,0.d0/

      k2 = DBLE(p1*scale(1))
      vhc2 = DBLE(p2*scale(2))
      ar = DBLE(p3*scale(3))
      vhc1 = DBLE(p4*scale(4))
      IF (k2 .LT. 0.d0 .OR. vhc2 .LT. 0.d0 .OR. ar .LT. 0.d0 .OR.
     2    vhc1 .LT. 0.d0) THEN
        WRITE(*,*) 'NEGATIVE PARAMETER ENCOUNTERED!'
        STOP
      ENDIF
      beta = (16.d0*5.67d-08)/(3.d0*ar)
      q0 = htflux

      dx1 = xmax1/DBLE(n1-1)
      dx2 = xmax2/DBLE(n2-1)
      nmax = n1 + n2 - 1
      pprnt = 0

      DO 10 n=1,nmax
        t(n) = ti
        tnew(n) = ti
        told(n) = ti
 10   CONTINUE
```

```
      thc(1) = REAL(tnew(outfmt))

      DO 20 p=2,pmax

         dt = DBLE(time(p) - time(p-1))
         IF (DBLE(time(p)) .GE. qend) q0 = 0.d0
         tnew(nmax) = DBLE(tbc(p))

         DO 80 n=1,nmax
           t(n) = tnew(n)
80       CONTINUE

50       DO 30 n = 1,nmax
           told(n) = tnew(n)
30       CONTINUE

         c1 = vhc1*dx1**2/(k1*dt)
         DO 41 n=2,n1-1
           a(n) = -1.d0
           b(n) = 2.d0 + c1
           c(n) = -1.d0
           d(n) = c1*t(n)
41       CONTINUE
         b(2) = b(2) + a(2)
         d(2) = d(2) - a(2)*q0*dx1/k1

         c1 = (dx1*vhc1 + dx2*vhc2)/(2.d0*dt)
         a(n1) = -k1/dx1
         b(n1) = k1/dx1 + kt(tnew(n1),k2,beta)/dx2 + c1
         c(n1) = -kt(tnew(n1),k2,beta)/dx2
         d(n1) = c1*t(n1)

         DO 40 n=n1+1,nmax-2
           CALL calcfo(tnew(n-1),tnew(n),tnew(n+1),
     3        fom,fop,k2,beta,vhc2)
           a(n) = -fom
           b(n) = (1.d00 + fom + fop)
           c(n) = -fop
           d(n) = t(n)
40       CONTINUE
         CALL calcfo(tnew(nmax-2),tnew(nmax-1),tnew(nmax),
     4       fom,fop,k2,beta,vhc2)
         a(nmax-1) = -fom
         b(nmax-1) = (1.d0 + fom + fop)
         c(nmax-1) = 0.d0
         d(nmax-1) = t(nmax-1) + fop*t(nmax)

         CALL tridag(2,nmax-1,101,a,b,c,d,tnew)
         tnew(1) = tnew(2) + q0*dx1/k1

         tsum = ABS(tnew(6) - told(6))/told(6)
         IF (tsum .GT. toler) GOTO 50

         thc(p) = REAL(tnew(outfmt))

20    CONTINUE
```

```
      RETURN
      END


      SUBROUTINE tridag(if,l,is,a,b,c,d,v)
      IMPLICIT DOUBLE PRECISION(a-h,o-z)
      DIMENSION a(is),b(is),c(is),d(is),v(is)
       DIMENSION beta(2000),gamma(2000)
      beta(if) = b(if)
      gamma(if) = d(if)/beta(if)
      ifp1 = if+1

      DO 10 i=ifp1,l
         beta(i)=b(i)-a(i)*c(i-1)/beta(i-1)
         gamma(i)=(d(i)-a(i)*gamma(i-1))/beta(i)
10    CONTINUE

      v(l)=gamma(l)
      last=l-if
      DO 20 k=1,last
         I=l-k
         v(i)=gamma(i)-c(i)*v(i+1)/beta(i)
20    CONTINUE

      RETURN
      END


      SUBROUTINE calcfo(tm,t,tp,fom,fop,k,beta,vhc)
         DOUBLE PRECISION tm,t,tp,fop,fom,dx,dt,t2,k2,cp2,k,vhc
         DOUBLE PRECISION beta,kt
         COMMON dx,dt

         t2 = (t + tp)/2.d0
         k2 = kt(t2,k,beta)
         cp2 = vhc
         fop = (k2*dt)/(cp2*dx**2)
         t2 = (tm + t)/2.d0
         k2 = kt(t2,k,beta)
         cp2 = vhc
         fom = (k2*dt)/(cp2*dx**2)

      RETURN
      END


      FUNCTION kt(t,k,beta)
        DOUBLE PRECISION kt,t,k,beta,vhc,dx,dt
         COMMON dx,dt

         kt = k + beta*t**3

      RETURN
      END
```

Appendix F

FORTRAN Thermocouple Calibration Program: TC_CALIB.FOR

```
* TC_CALIB.FOR: Post-processing program to "calibrate" TCs
* Input and Output are user supplied
*   Input:  TC file from data acquisition program STYRO.C
*           Ambient Temperature
*   Output: File with "calibrated" Tcs and heat flux history

      REAL time(3001),tc(10,3001),tcmean(10),watt(3001)
      REAL ta,temp,area
      INTEGER i,j,k,itimea,iqend,maxi
      CHARACTER*12 ifile,ofile

* Note: Skips 10th column (ground) and reads in 11th (TC 10)
* NTC: Number of Tcs
* AREA: Effective area of heater: 6" x 6" Minco heater
      ntc = 10
      area = 0.955*(0.1524)**2
      itimea = 0

* Need to input the input file name, the output file name, and the
* ambient/initial temperature.
      WRITE(*,*) 'Enter input file:'
      READ(*,'(A12)') ifile
      WRITE(*,*) 'Enter output file:'
      READ(*,'(A12)') ofile
      WRITE(*,*) 'Enter ambient temperature:'
      READ(*,'(G12.6)') ta

      DO 9 j=1,ntc
        tcmean(j) = 0.0
    9 CONTINUE

* Reads the input and determines when the heater was turned on
      OPEN(UNIT=11,FILE=ifile,STATUS='OLD')
      READ(11,*)
      k = 0
      DO 10 i=1,3001
        READ(11,5,END=20) time(i),(tc(j,i),j=1,ntc),watt(i)
        IF (watt(i) .GT. 0.001 .AND. itimea .EQ. 0) THEN
          itimea = i-1
        ENDIF
   10 CONTINUE
```

```
    5 FORMAT(F7.2,1X,9(1X,F8.3),9X,1X,F8.3,24X,F12.6)
   20 maxi = i - 1
      CLOSE(11)

* Determine the mean TC reading over the time before power
* was supplied
      DO 30 i=1,itimea
        DO 40 j=1,ntc
          tcmean(j) = tcmean(j) + tc(j,i)
   40   CONTINUE
   30 CONTINUE
      DO 50 j=1,ntc
       tcmean(j) = tcmean(j)/REAL(itimea)
   50 CONTINUE

* Write the output, offsetting each TC according to the mean
* temperature determined in the previous section.
      OPEN(UNIT=12,FILE=ofile,STATUS='UNKNOWN')
      WRITE(12,15) 0.0,ta,ta,ta,ta,ta,ta,ta,ta,ta,ta
      DO 60 i=1,maxi
        DO 70 j=1,ntc
          tc(j,i) = tc(j,i) + (ta - tcmean(j))
   70   CONTINUE
        WRITE(12,15) time(i),(tc(j,i),j=1,ntc),watt(i)/area/2.
   60 CONTINUE
   15 FORMAT(1X,F7.2,10(1X,F7.3),2X,F6.2)

      CLOSE(12)
      STOP
      END
```

Appendix G

FORTRAN Thermocouple Averaging Program: TC_AVG.FOR

```
c TC_AVG.FOR: Program to average 8 TC voltages for estimation
c             1-4, heated surface; 5-8, "constant" temp. surface
c             Also rescales time so that t=0 is the begining of
c             heating and converts degree C to degree K
c             Outputs heat flux history as well
c User supplied Input and Output files:
c    Input:  TC file from TC_CALIB.FOR
c    Output: Temperature file for use in MBK
c

      REAL time,temp1,temp2,value(8),watt
      INTEGER j,ntc,go
      CHARACTER*12 ifile,ofile

* NTC: Number of ThermoCouples
      ntc = 8
      go = 0

* Open Input and Output files
      WRITE(*,*) 'Enter input file:'
      READ(*,'(A12)') ifile
      WRITE(*,*) 'Enter output file:'
      READ(*,'(A12)') ofile
      OPEN(UNIT=11,FILE=ifile,STATUS='OLD')
      OPEN(UNIT=12,FILE=ofile,STATUS='UNKNOWN')

* Read Input file until EOF encountered, determine heating start
* time, average Tcs 1-4 and 5-8, and output results.
      DO 10 i=1,3001
        READ(11,5,END=20) time,(value(j),j=1,ntc),watt
        IF (i .EQ. 1) THEN
          WRITE(12,15) time,value(1)+273.0,value(5)+273.0,watt
        ELSEIF (watt .GE. 0.01 .OR. go .EQ. 1) THEN
          go = 1
          temp1 = 0.
          temp2 = 0.
          DO 30 j=1,4
            temp1 = temp1 + value(j)
            temp2 = temp2 + value(j+4)
   30     CONTINUE
          temp1 = temp1/4 + 273.0
```

```
        temp2 = temp2/4 + 273.0
        WRITE(12,15) (time-qstart), temp1, temp2, watt
      ELSE
        qstart = time
      ENDIF
10  CONTINUE
20  CLOSE(11)
    CLOSE(12)
 5  FORMAT(1X,F7.2,8(1X,F7.3),18X,F6.2)
15  FORMAT(4(1X,F7.2))

    STOP
    END
```

Vita

The author, Jerome H. Guynn, was born on June 22, 1969 in Westminster, Maryland. He spend most of his life in Carroll County, Maryland and graduated from South Carroll High School in May, 1997. He began his engineering studies at Virginia Polytechnic Institute and State University in August 1987. While at Virginia Tech, he spend 3 years co-oping with CACI, Inc. in Fairfax, VA and on August 10, 1991, married Elizabeth Curl. He received the Bachelor of Science degree in Aerospace Engineering from Virginia Tech in May, 1992 and went to work full time for CACI, Inc. in Arlington, VA. In January of 1995, he returned to Virginia Tech and began a masters program in Mechanical Engineering under the direction of Dr. Elaine P. Scott. Upon completion of this Thesis, he will have fulfilled the requirements for the Master of Science degree in Mechanical Engineering on the 24th of July, 1996. He currently plans to continue his engineering career with a job in industry.